

UNCLASSIFIED

AD NUMBER
AD108104
NEW LIMITATION CHANGE
TO Approved for public release, distribution unlimited
FROM Distribution authorized to DoD only; Administrative/Operational Use; APR 1956. Other requests shall be referred to Bureau of Aeronautics, Department of the Navy, Washington, DC 20350. Pre-dates formal DoD distribution statements. Treat as DoD only.
AUTHORITY
NAVAIR ltr dtd 22 Apr 1980

THIS PAGE IS UNCLASSIFIED

UNCLASSIFIED

AD108104

Armed Services Technical Information Agency

Reproduced by

DOCUMENT SERVICE CENTER

KNOTT BUILDING, DAYTON, 2, OHIO

This document is the property of the United States Government. It is furnished for the duration of the contract and shall be returned when no longer required, or upon recall by ASTIA to the following address: Armed Services Technical Information Agency, Document Service Center, Knott Building, Dayton 2, Ohio.

NOTICE: WHEN GOVERNMENT OR OTHER DRAWINGS, SPECIFICATIONS OR OTHER DATA ARE USED FOR ANY PURPOSE OTHER THAN IN CONNECTION WITH A DEFINITELY RELATED GOVERNMENT PROCUREMENT OPERATION, THE U. S. GOVERNMENT THEREBY INCURS NO RESPONSIBILITY, NOR ANY OBLIGATION WHATSOEVER; AND THE FACT THAT THE GOVERNMENT MAY HAVE FORMULATED, FURNISHED, OR IN ANY WAY SUPPLIED THE SAID DRAWINGS, SPECIFICATIONS, OR OTHER DATA IS NOT TO BE REGARDED BY IMPLICATION OR OTHERWISE AS IN ANY MANNER LICENSING THE HOLDER OR ANY OTHER PERSON OR CORPORATION, OR CONVEYING ANY RIGHTS OR PERMISSION TO MANUFACTURE, USE OR SELL, ANY PATENTED INVENTION THAT MAY IN ANY WAY BE RELATED THERETO.

UNCLASSIFIED

BU AER REPORT AE-61-4-VI

**AUTOMATIC FLIGHT CONTROL SYSTEMS
FOR
PILOTED AIRCRAFT**



FC


BASIC VOLUME PREPARED BY
NORTHROP AIRCRAFT INC.

FOR

BUREAU OF AERONAUTICS NAVY DEPARTMENT

Final Report (1) Phase Itr Aer-TD-416/349
OF 24 SEP 1956

**BU AER REPORT
AE-61-4 VI
APRIL 1956**



**AUTOMATIC FLIGHT
CONTROL SYSTEMS
FOR
PILOTED AIRCRAFT**

**BASIC VOLUME
WRITTEN AND EDITED BY
FLIGHT CONTROL SYSTEMS DEPARTMENT
NORTHROP AIRCRAFT INC.**

**CONTRIBUTIONS TO VOLUME
BY OTHER AUTHORS
ARE NOTED IN INDIVIDUAL
SECTIONS IN ACCORDANCE WITH
IMPORTANT NOTE
ON FOLLOWING PAGE**

**PREPARATION OF VOLUME SPONSORED BY
BUREAU OF AERONAUTICS
NAVY DEPARTMENT**

IMPORTANT NOTE

This volume was written by and for engineers and scientists who are concerned with the analysis and synthesis of piloted aircraft flight control systems. The Bureau of Aeronautics undertook the sponsorship of this project when it became apparent that many significant advances were being made in this extremely technical field and that the presentation and dissemination of information concerning such advances would be of benefit to the Services, to the airframe companies, and to the individuals concerned.

A contract for collecting, codifying, and presenting this scattered material was awarded to Northrop Aircraft, Inc., and the present basic volume represents the results of these efforts.

The need for such a volume as this is obvious to those working in the field. It is equally apparent that the rapid changes and refinements in the techniques used make it essential that new material be added as it becomes available. The best way of maintaining and improving the usefulness of this volume is therefore by frequent revisions to keep it as complete and as up-to-date as possible.

For these reasons, the Bureau of Aeronautics solicits suggestions for revisions and additions from those who make use of the volume. In some cases, these suggestions might be simply that the wording of a paragraph be changed for clarification; in other cases, whole sections outlining new techniques might be submitted.

Each suggestion will be acknowledged and will receive careful study. For those which are approved, revision pages will be prepared and distributed. Each of these will contain notations as necessary to give full credit to the person and organization responsible.

This cooperation on the part of the readers of this volume is vital. Suggestions forwarded to the Chief, Bureau of Aeronautics (Attention AE-61), Washington 25, D. C., will be most welcome.

PREFACE

This volume, "Automatic Flight Control Systems for Piloted Aircraft," is the sixth in a series written under BuAer Contract NOas 51-514 (c) on the general subject of the analysis and synthesis of piloted aircraft flight control systems. The preceding five volumes are listed below.

BuAer Report

AE-61-4 I	Methods of Analysis and Synthesis of Piloted Aircraft Flight Control Systems
AE-61-4 II	Dynamics of the Airframe
AE-61-4 III	The Human Pilot
AE-61-4 IV	The Hydraulic System
AE-61-4 V	The Artificial Feel System

Volumes I through IV of the above list are concerned with methods of constructing and manipulating mathematical models of the various components of automatic flight control systems. The methods used are based on the transfer function concept. Volume I deals with general techniques which are applicable to any problem in servomechanisms or automatic control. Volume II is concerned specifically with the airframe and was written to provide the flight control designer with the basic knowledge of rigid body airframe dynamics bearing directly on aircraft control system design. The characteristics of the human pilot which are important to the design of flight control systems are covered in Volume III, and transfer functions are presented for those human pilot characteristics for which such representation is realistic. Mathematical models

of typical aircraft hydraulic surface control systems are developed in Volume IV. Volume V is the first in the series to be devoted to design methods; it presents the fundamental concepts underlying the design of the artificial feel system.

Like Volume V, the present volume (Volume VI) is devoted primarily to design. Its purpose is to present methods for designing automatic flight control systems. A large portion of the volume is based on actual experience at Northrop Aircraft, Inc., particularly Chapters III and IV which deal specifically with design procedures. Section 3 of Chapter III traces the actual design of a stability augments which is currently in operational use.

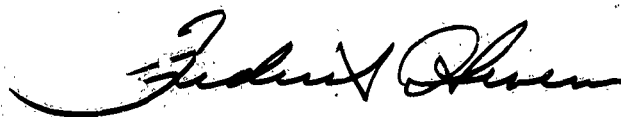
This volume is written for the college graduate who has had some training in systems engineering. It is assumed that the reader is familiar with the material covered in the other five volumes. However, where necessary, certain aspects of the material previously presented are reviewed.

The history of the development of automatic aircraft control is briefly described in Chapter I, along with a discussion of the general functions performed by present day automatic flight control systems. The basic components of automatic flight control systems are described in Chapter II, and where possible, their transfer functions are derived. In Chapter III, a design procedure is recommended and its use is illustrated by an example. The manual is concluded with Chapter IV, in which the systems engineering concept is discussed along with some other useful design considerations.

Special mention should be made of the following people for their help and cooperation: Budd Stone for his work in drawing the figures, Mary Lou Coburn for transcribing the equations and Edna Garcia for typing the manuscript.

AUTHOR

K.G.Hart



F. Stevens, Chief
Guidance & Controls

EDITORIAL BOARD

16 May 1956

D.D.Miles
J.E.Moser
R.M.Pitts, Jr.
R.E.Trudel
E.C.Wirth

TABLE OF CONTENTS

PREFACE	iv
CHAPTER I AUTOMATIC FLIGHT CONTROL SYSTEMS, PAST AND PRESENT . . .	I-1
Section 1 History	I-1
Section 2 Automatic Flight Control Systems of Today	I-5
CHAPTER II COMPONENTS OF AUTOMATIC FLIGHT CONTROL SYSTEMS	II-1
Section 1 Introduction	II-1
Section 2 The Airframe	II-2
(a) The Complete Airframe Equations of Motion	II-4
(b) The Perturbation Equations	II-22
(c) Longitudinal Motions	II-32
(d) Lateral Motions	II-44
(e) Airframe Motions in Transonic Flight	II-57
(f) The Equivalent Stability Derivative Approach	II-60
Section 3 The Human Pilot	II-75
Section 4 The Surface Control System	II-79
Section 5 Sensors	II-92
(a) The Gyroscope	II-93
(b) Accelerometers	II-105
(c) Local Flow Direction Detectors	II-113
(d) Local Flow Magnitude Detectors	II-114
(e) Pressure Altitude Sensors	II-116
(f) Summary	II-116
Section 6 The System Controller	II-118
Section 7 Controller Actuators	II-119

CHAPTER III	DESIGN METHODS	III-1
Section 1	Introduction	III-1
Section 2	System Design Procedure	III-1
(a)	Preliminary Analysis	III-1
(b)	Analysis and Synthesis	III-5
(c)	Prototype Systems	III-12
(d)	Testing Prototype Systems	III-13
(e)	Design of Production Components	III-27
(f)	Testing Production Systems	III-27
Section 3	An Example Design Problem	III-31
(a)	Preliminary Analysis	III-31
(b)	Analysis and Synthesis	III-32
(c)	Analog Computer Studies	III-86
CHAPTER IV	SYSTEMS ENGINEERING AND OTHER DESIGN CONSIDERATIONS .	IV-1
Section 1	Introduction	IV-1
Section 2	Systems Engineering	IV-1
Section 3	Functional Mechanization	IV-3
Section 4	Other Design Considerations	IV-5
BIBLIOGRAPHY		
APPENDIX	Equations of the Gyroscope	A-1
(a)	Law of the Gyro Element	A-1
(b)	Rate Gyro Indications	A-8
(c)	Vertical Gyro Indications	A-17
(d)	Directional Gyro Indications	A-44

INDEX

CHAPTER I
PAST AND PRESENT
AUTOMATIC FLIGHT CONTROL SYSTEMS

SECTION 1 - HISTORY

The first formal records of an attempt to control an aircraft automatically are those describing the early work of Elmer Sperry. His first attempts were made in 1910, only seven years after the Wright brothers' first flight. Mr. Sperry's original device was called a "gyro stabilizer" and its function was to keep the airplane in level flight. It consisted of a large rotor with its spin axis aligned with the yaw axis of the airplane. The rotor was driven by a belt from the engine. Mr. Sperry felt that the rotor, which was attached rigidly to the airframe, would resist unwanted rolling and pitching tendencies. This device was never flown, however.

During the two years following 1910 Sperry designed and built a gyro stabilizer which contained the basic elements that were used in all autopilots for the following thirty years. The gyro stabilizer of 1912 used gyros only to establish a substantially horizontal plane in the airplane and to generate signals to operate servos driving the ailerons and elevator. Provision was made for the pilot to give flight commands by using his controls to introduce signals between the servos and the geometrical references provided by the gyros. The first flight of the gyro stabilizer was made in 1912, and additional development work was carried out in 1913. In 1914, Mr. Sperry's son Lawrence won a

safety prize of 50,000 francs offered by the Aero Club of France for the most stable airplane. The winning demonstration, which took place in Paris, consisted of a low altitude flight down the Seine in a Curtiss flying boat with the gyro stabilizer installed. As the airplane approached the judges' stand, the French mechanic climbed out on the wing while Sperry stood up in the cockpit and raised his hands above his head.

Sperry's objective in developing the gyro stabilizer was to provide an accessory which would make the airplane a more practical device. This was considered necessary for the early airplanes because their stability was so marginal that it was only with extreme and continuous alertness that the human pilot was able to keep them in the air. However, during the war years of 1915 to 1920, a great deal was learned about building inherent stability into the airframe. For this reason the autopilot was no longer needed to provide stability, since the human pilot could provide adequate control. This condition existed through World War II.

However, by the late 1920's airplane performance had improved to the point where the duration of flight and range were so great that pilot fatigue became an element for consideration. The usefulness of the autopilot in providing pilot relief during long hours of flight was first demonstrated publicly by Wiley Post in his solo flight around the world in 1933. In this flight, Post used the prototype of an autopilot manufactured by the Sperry Gyroscope Company. The use of the autopilot for this flight attracted a considerable amount of publicity at a time when the commercial airlines were beginning their rapid expansion because it was in this same year that the United States Commerce

Department gave the airlines permission to fly passengers under instrument conditions. In the following year (1934), the first commercial airline installation of an autopilot was made in the Boeing 247. Between 1934 and 1940 the autopilot was widely used in both commercial and military aircraft.

Prior to World War II, most of the autopilots were early versions of the Sperry autopilot. Their primary function was to hold the airplane "still" while the human pilot performed other duties. Physically they consisted of air-driven gyros with the gyro gimbals operating air valves. The resulting air signal was used to operate the pilot valve on a hydraulic cylinder which in turn applied torque to the control surface. A schematic diagram of the elevator channel of the Sperry autopilot of 1936 is shown in Figure I-1.

The first all-electric autopilots were developed in 1941 and one version was used in many of the bombing type airplanes of this era in combination with the Norden bombsight to provide automatic control of the airplane during bombing runs. This combination was used very successfully throughout World War II. With the exception of the bombsight tie-in, the autopilot was still essentially a pilot relief device, although coordinated turns could be accomplished by means of a single knob, and a miniature "formation stick" was provided to allow easier maneuvering. Heading reference was obtained from a free gyro which necessitated frequent resetting to compensate for gyro drift. Manual synchronization of the gyro pickoffs

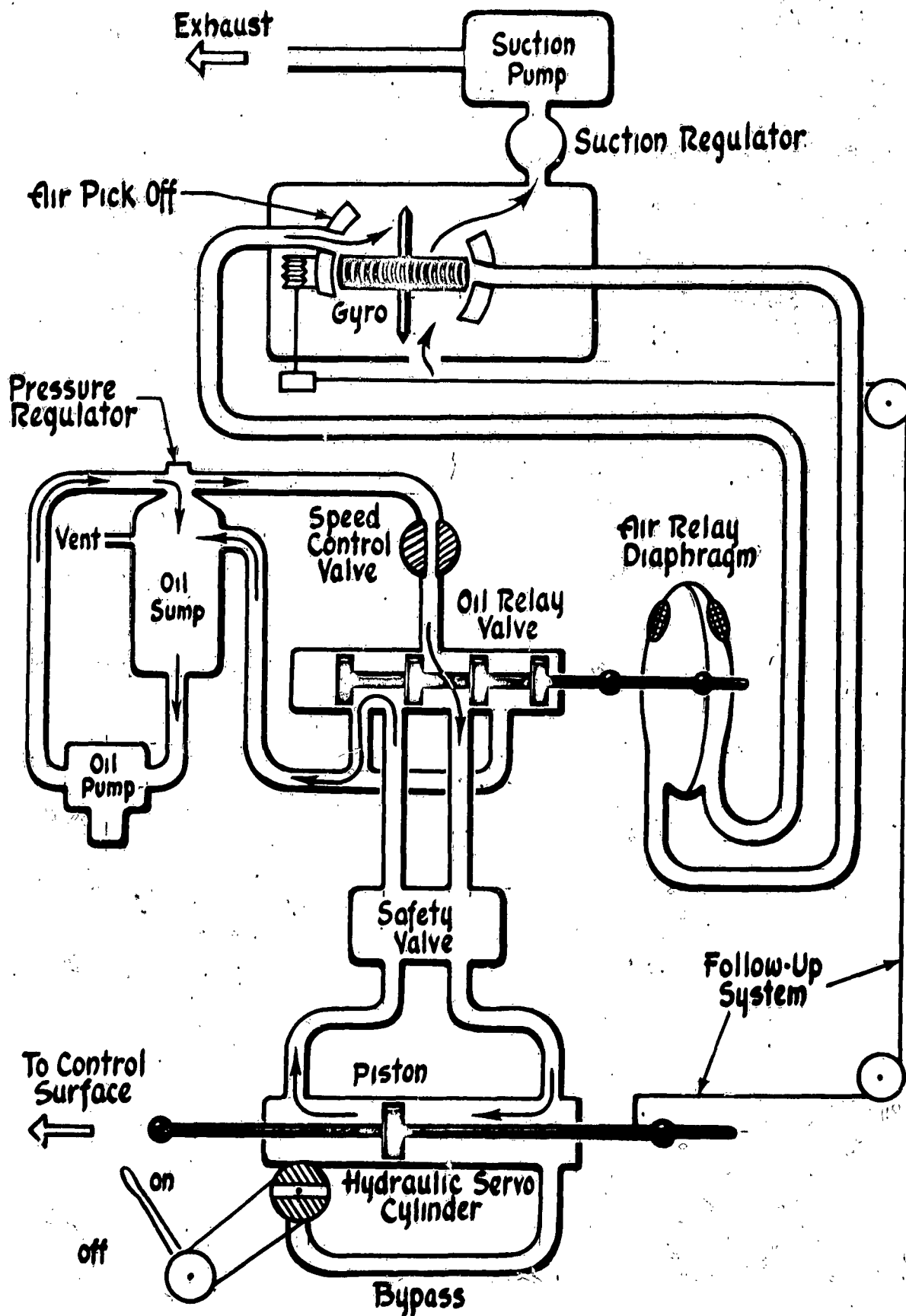


Figure I-1 Early Sperry Autopilot

was required prior to engagement, and autopilot parameter adjustment knobs were available to the pilot in the cockpit. In fact, the number of adjustments which the human pilot was required to make to insure proper flight control constituted one of the major disadvantages of autopilots of this era.

The first autopilot to provide automatic synchronization of the signal pickoffs was produced in 1943. This same autopilot was also the first to provide a magnetic heading reference. The altitude control function was added in the following year, and automatic landing approach equipment was used successfully in the late 1940's. With the exception of the refinement of components, the basic relief autopilot of today uses essentially the same mechanization as those of the 1940's.

SECTION 2 - AUTOMATIC FLIGHT CONTROL SYSTEMS OF TODAY

As mentioned in the previous section, automatic control was considered useful on the very early airplanes because of their poor stability. However, much was learned about designing inherently stable airframes during World War I so that autopilots were no longer needed to improve stability. This situation existed throughout World War II.

The war emergency brought about a tremendous increase in military airplane design effort which resulted in airplanes with greatly improved speed and altitude capabilities. This trend has continued since the war and has been greatly accelerated through the use of jet propulsion. The

tremendous increase in airplane performance since 1940 has been accompanied by a continual increase in control surface hinge moment requirements and a continual decrease in airframe inherent stability. Early attempts to reduce the control stick forces which accompanied the increased surface hinge moments consisted of such aerodynamic devices as aerodynamic surface balance, servo tabs, spring tabs, etc. As aircraft speeds continued to increase, however, it was found necessary to provide hydraulic power to aid the pilot in moving the control surfaces. Early versions of hydraulic boost systems aided the pilot by providing only a portion of the required hinge moment. However, as the dynamic pressures encountered in flight continued to increase and control surface centers of pressure moved aft due to the effects of supersonic flow, it was found necessary to increase the portion of the hinge moment supplied by the hydraulic boost system, and most present transonic airplanes require that 100 percent of the surface hinge moment be supplied by the hydraulic system. The pilot in such systems merely provides the function of positioning the control surface through the hydraulic system. However, since pilots have been trained to fly by the physical association of control force with airframe response, the introduction of artificial force producing devices has become necessary for such systems. Two of the volumes in this series have been devoted to the problems created by the increased surface hinge moment; Volume IV covers the design of hydraulic surface actuating systems and Volume V the design of the artificial feel system.

As in the case of the increased surface hinge moment, the reduced airframe stability was handled successfully during World War II by aerodynamic means, but by the late 1940's it was found that aerodynamic methods were no longer adequate for those airplanes whose maximum speeds were approaching the velocity of sound. The reduction in airframe inherent stability which has accompanied the improved performance stems from several sources. Among these are:

- (a) increased speed resulting in wider variation of aerodynamic characteristics
- (b) increased altitude
- (c) smaller wings - higher wing loading
- (d) reduced effective aspect ratios and redistribution of airplane weight components increasing the importance of inertia factors
- (e) variations of the aerodynamic parameters in the transonic range
- (f) increase in flexibility of airplane structure.

The deterioration in airplane stability which has accompanied the above changes is manifested by an increase in the airframe natural frequencies, a decrease in airframe damping and deterioration of airframe static stability. This trend has continued to the present and there is no indication that future airframe designs will show an improvement.

One of the several modes of airframe motion which have been affected by the deterioration in stability is the so called dutch roll oscillation which is characterized by a combined rolling, yawing, and sideslipping motion. Although the dutch roll damping is almost always positive, it is often so low that continuous oscillations occur in flight due to frequent excitation by gusts and control inputs. Continuous dutch roll is not only uncomfortable to both the pilot and crew, but is in the case of a military airplane an impediment to the accomplishment of its mission. Tactical military airplanes must be capable of flying a smooth flight path for gunnery or rocket firing, bombing or photography. It is therefore necessary that any erratic airframe motion that cannot be controlled by the pilot be controlled by some other method. The only presently known method of accomplishing the desired stabilization on contemporary airplanes is by means of automatic control.

Automatic control devices for improving airframe stability have been labelled variously in the past as stabilizers, dampers, autopilots and stability augmenters. The latter term will be used throughout this report. Stability augmenters operate almost universally by sensing one or more of the airframe motions and then moving a control surface to oppose the airframe motion. This can best be visualized by reference to Figure I-2, which shows the block diagram of a yaw stability augmentser. Such a device serves the purpose of increasing the damping of the airframe dutch roll mode of oscillation. In practice, the rate of yaw is sensed by the rate

gyro. The rate gyro output signal then consists of a voltage proportional to the rate of yaw. This signal is amplified and shifted in phase as necessary by the control unit, and the resulting signal is used to operate the servo actuator. The servo actuator, in turn produces rudder motion proportional to the control unit output signal and phased to oppose the rate of yaw.

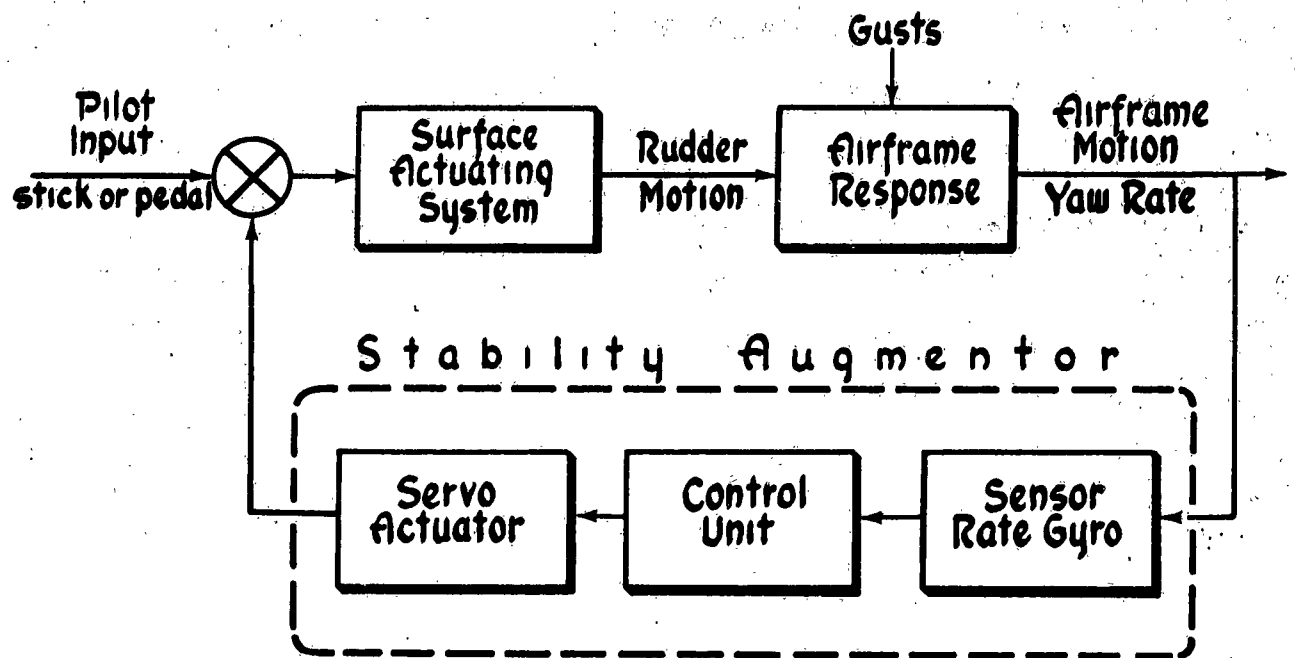


Figure I-2 Block Diagram of Airframe Control Loop with Stability Augmentor

The function fulfilled by the stability augmentor of Figure I-2 is only one of the manifold uses to which the various systems and subsystems of automatic flight control systems are put. Among the additional functions of automatic flight control systems are:

- (a) Pilot fatigue relief
- (b) Maneuvering control
- (c) Automatic navigation
- (d) Automatic tracking
- (e) Automatic take off and landing

Before concluding this chapter, one additional comment should be made. Through years of usage, the term "automatic pilot" has to a great many people, implied a device which performs only the function listed as item (a) above. This definition applies quite well to most of the automatic control devices discussed in Section 1 of this chapter. As discussed above, however, present day automatic flight control systems perform many functions in addition to pilot fatigue relief. For this reason, the term "autopilot" has been used quite sparingly in the discussions which follow.

CHAPTER II

COMPONENTS OF AUTOMATIC FLIGHT CONTROL SYSTEMS

SECTION 1 - INTRODUCTION

In Chapter I, only a general discussion of automatic flight control systems was given and no attempt was made to give specific details about any particular system or component. This chapter presents a somewhat detailed discussion of the components that are commonly used in automatic flight control systems. The components to be discussed are shown in the block diagram of Figure II-1. Most systems contain examples of all the blocks shown in the diagram.

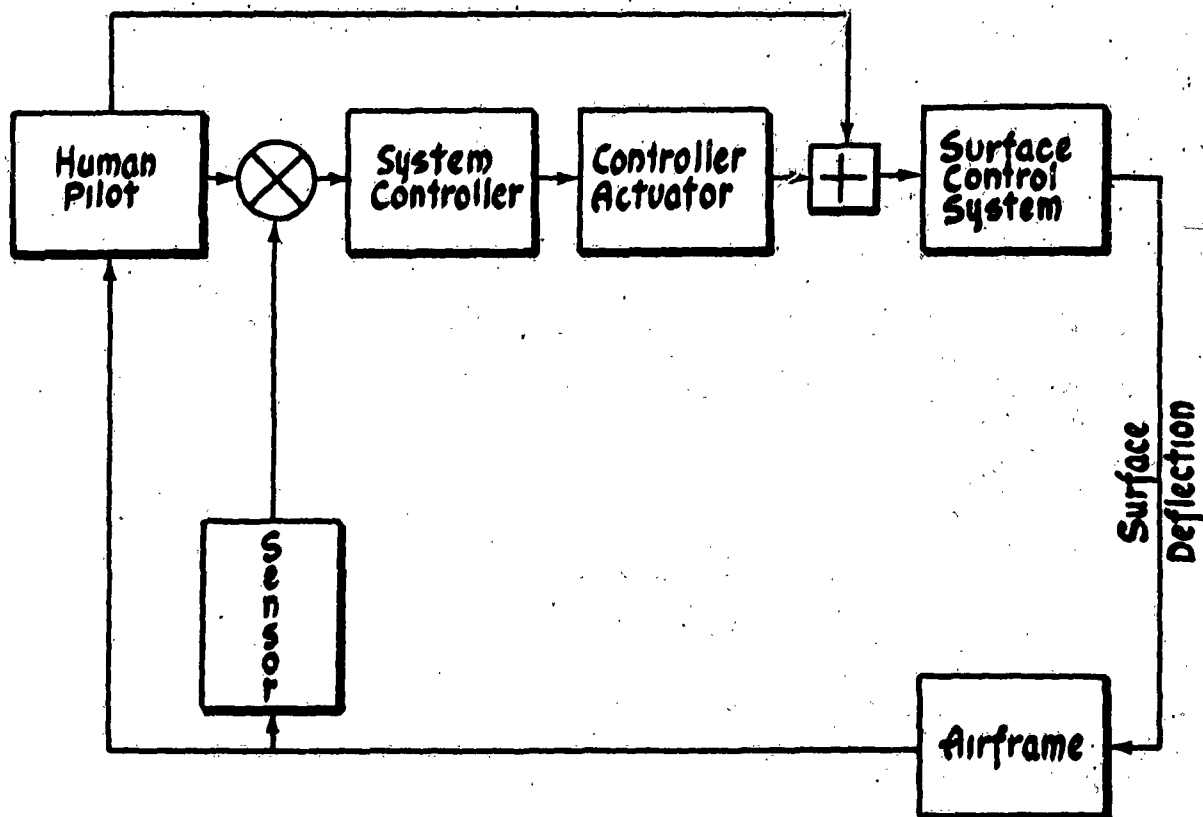


Figure II-1 Generic Block Diagram of an Automatic Flight Control System II-1

Section 2

The components shown in the figure will be discussed in the following order:

1. Airframe
2. Human Pilot
3. Surface Control Systems
4. Sensors
5. Controllers
6. Actuators

SECTION 2 - THE AIRFRAME

The problem of designing an automatic flight control system resolves itself into that of building a mechanism capable of controlling the motions of an airframe. This procedure is greatly facilitated when the motions of the airframe are represented by a mathematical model. The equations which represent the mathematical model of the airframe can be derived by equating the aerodynamic forces and moments acting on the airframe to the craft reactions according to Newton's laws. Since the airframe has six degrees of freedom in space, six nonlinear simultaneous differential equations are required to provide complete representation of airframe motion. Three additional equations are required to describe the airframe orientation with respect to the earth. In this section, these nine equations are presented and their application is discussed.

It has been customary in the past, when studying airframe dynamics, to assume that the airframe motion consists of small perturbations about some steady flight condition. This assumption permits considerable simplification of the airframe equations of motion. As a result of this simplification, the six nonlinear differential equations reduce to two independent sets of three linear simultaneous differential equations. These equations have been called the "airframe perturbation equations." The simplification provided by the above assumption greatly facilitates the manipulation of the airframe

mathematical model because the resulting equations are linear and therefore subject to the many powerful analytical techniques involving the use of transfer functions. In addition, relatively simple equipment can be used for analog computer studies.

These equations are used very extensively when studying airframe dynamics in conjunction with the design of automatic flight control equipment, and the bulk of the material contained in this manual is based on the use of the airframe perturbation equations.

Comparison of analog computer results, obtained using the perturbation equations, with flight test results has often verified the accuracy of such representation, especially when the airframe disturbances from the steady flight condition are relatively small. However, when studying the dynamics of an airframe during maneuvers involving large changes in airframe attitude, it may be necessary to utilize the complete six degree of freedom equations, especially for those airframe configurations which exhibit strong inertial coupling between longitudinal and lateral modes of motion. This characteristic is becoming increasingly important, in view of present airframe design trends toward shorter wings, thus concentrating the airframe mass near the fuselage. In the airframe equations of motion, this trend causes the inertia coupling parameter* $\frac{I_y - I_x}{I_z}$ to become larger. This parameter approaches unity for configurations having low inertia in roll relative to pitch and yaw. For fighters of World War II, this parameter was of the order of 0.3 to 0.4.**

*See Equations (II-13).

**Ordway B. Gates, Jr., Joseph Weil, and C.H. Woodling, "Effect of Automatic Stabilization on Sideslip and Angle of Attack Disturbance in Rolling Maneuvers," NACA RM L55E25b, 1955. (Confidential)

Section 2

In the initial stages of design of an aircraft control system, the airframe may be considered an alterable element. Airframe parameters such as control surface effectiveness and tail size as well as requirements for split or separate surfaces for automatic control may be influenced by control system objectives and requirements during the preliminary design stage. Studies for establishing those airframe characteristics which are influenced by the automatic control system can be made on the analog computer utilizing the airframe equations of motion and equations representing some portion of the control system, such as a stability augments. However, many design parameters affecting the airframe performance are fixed by considerations other than control, such as landing speed and maximum weight. In addition, because of production requirements for lead time, the final airframe exterior configurations must be completely established very early relative to other components of the control system. These considerations make it necessary to regard the airframe as an unalterable element very early in the design stage. For the purpose of convenience in the discussion that follows, it will be assumed that initial studies have been completed, and the airframe will be considered an unalterable element.

(a) THE COMPLETE AIRFRAME EQUATIONS OF MOTION

The form of the airframe equations of motion depend somewhat on the axis system along and about which the force and moment equations are written. Many systems are in common use and convenience usually dictates the form which is best for a particular application. Table I lists the axis systems which are commonly used. All of those listed are right hand orthogonal systems with the origin at the airframe center of gravity, the z axis in the plane of symmetry and positive downward, the x axis positive forward, and the y axis positive to the right.

System	Description
Stability Axes	The x axis is in the plane of symmetry, aligned with the projection of the relative wind in the plane of symmetry for the steady flight condition. The y axis is perpendicular to the plane of symmetry. Axes remain fixed to the airframe in this position throughout any subsequent maneuver.
Principal Axes	These are the same as stability axes except that the x axis is aligned with the airframe principal axis.
Body Axes	These are the same as principal axes and stability axes except that the x axis is aligned with some convenient longitudinal reference line, such as the fuselage reference line or wing cord line.
Wind Axes	The x axis is always aligned with the relative wind; however, the z axis remains in the plane of symmetry. The y axis is perpendicular to the x and z axes.
Wind Stability Axes	The x and z axes always remain in the plane of symmetry; however, the x axis moves in such a way that it is always aligned with the projection of the relative wind in the plane of symmetry.

Table II-1. Airframe Axis Systems

The first three sets of axes listed in Table II-1 are fixed to the airframe. The choice of axis system to be preferred for any given problem usually depends upon the form of the available stability derivative data. Some engineers prefer to use principal axes since the cross product of inertia is thus eliminated; however, stability derivative data are seldom obtained with respect to this axis system. In the past, most aerodynamic

Section 2

data have been presented with respect to stability axes, and for this reason, this axis system has probably been more popular than any other. Present trends, especially for the presentation of supersonic aerodynamic data, are toward the use of body axes. As indicated in Table II-1, the x-body axis is usually aligned with the fuselage reference line. This simplifies the bookkeeping somewhat since all aerodynamic data are referred to a fixed axis system.

In the wind axis system, the lift, drag, and velocity need not be resolved into components, since the x axis is always parallel to the drag vector and the z axis is at all times parallel to the lift. However, the moments and products of inertia vary with angles of attack and sideslip. One way of avoiding the latter complication is to write the force equation along wind axes and the moment equations about stability axes.* It is of course necessary to relate the two axis systems.

As the name implies, the wind stability axis system is, in some respects, a combination of the stability and wind axis systems. In this case the lift is always along the z axis, but the drag vector may deviate from the x axis by the sideslip angle β . As in the case of the wind axes, the moments and products of inertia vary with angle of attack unless the moment equations are written about axes fixed to the airframe.

*J.T. Van Meter, Dynamic Response of Interceptor Airplanes to Turn Commands, TACP Report 10, MIT, August 1954.

The derivation which follows is valid for any of the first three sets of axis systems described in Table II-1, or for any right hand orthogonal axis system in which the origin is at the airframe cg, the xz plane is a plane of symmetry, the positive x axis lies more or less along the flight path and the z axis is positive downward. Axes attached rigidly to the airframe are chosen over wind axes because most stability derivative data are presented with reference to either stability or body axes and because computer results are somewhat easier to interpret when angular and linear velocities are referenced to the same axes.

The complete derivation of the airframe perturbation equations has been carried out in Reference 9. In that derivation, the equations are linearized prior to the expansion of the aerodynamic forces and moments, and for this reason, the complete equations are not presented there in a form suitable for immediate application. The early portion of the derivation of Reference 9, is, however, valid for the derivation of the complete equations. Although this portion of the procedure is straightforward, it is rather lengthy, and for this reason will not be repeated here. The steps which are omitted consist of obtaining expressions for the components of the linear and angular acceleration of a rigid body. The resulting expressions are presented as Equations (II-25) of Reference 9, and are given below as Equations (II-1).

Section 2

$$\sum F_x = m(\dot{U} + QW - RV)$$

$$\sum F_y = m(\dot{V} + RU - PW)$$

$$\sum F_z = m(\dot{W} + PV - QU)$$

(II-1)

$$\sum L = \dot{P}I_x - I_{xz}(\dot{R} + QP) + QR(I_z - I_y)$$

$$\sum M = \dot{Q}I_y - I_{xz}(R^2 - P^2) + PR(I_x - I_z)$$

$$\sum N = \dot{R}I_z - I_{xz}(\dot{P} - QR) + PQ(I_y - I_x)$$

Equations (II-1) are based on the following assumptions:

1. The airframe is a rigid body.
2. The earth is assumed to be fixed in space and the earth's atmosphere is assumed to be fixed with respect to the earth.
3. The mass of the airframe is constant during any dynamic analysis.
4. The xz plane is a plane of symmetry and therefore $I_{xy} = I_{yz} = 0$.

In Equations (II-1), the letters $U, V, W, P, Q,$ and R represent total velocities along and about the x, y, and z axes respectively; m is the mass of the airframe; $F_x, F_y,$ and F_z are the externally applied forces along the x, y, and z axes; and $L, M,$ and N are the externally applied moments. The moments of inertia about the x, y, and z axes are given by $I_x, I_y,$ and I_z ; and the cross product of inertia is given by I_{xz} .

The externally applied forces and moments consist of aerodynamic, gravitational, and thrust forces and moments.

Then

$$\begin{aligned} \sum F_x &= F_{xAERO} + F_{xG} + F_{xT} \\ (II-2) \quad \sum F_y &= F_{yAERO} + F_{yG} + F_{yT} \\ \sum F_z &= F_{zAERO} + F_{zG} + F_{zT} \\ \sum L &= L_{AERO} + L_G + L_T \\ \sum M &= M_{AERO} + M_G + M_T \\ \sum N &= N_{AERO} + N_G + N_T \end{aligned}$$

If the origin of the chosen axis system is at the airframe cg, and if the thrust line lies in the plane of symmetry (xz plane), several of the terms in (II-2) are equal to zero.

$$(II-3) \quad F_{yT} = L_T = N_T = L_G = M_G = N_G = 0$$

Then Equations (II-2) can be reduced to Equations (II-4).

$$\begin{aligned} \sum F_x &= F_{xAERO} + F_{xG} + F_{xT} \\ \sum F_y &= F_{yAERO} + F_{yG} \\ (II-4) \quad \sum F_z &= F_{zAERO} + F_{zG} + F_{zT} \\ \sum L &= L_{AERO} \\ \sum M &= M_{AERO} + M_T \\ \sum N &= N_{AERO} \end{aligned}$$

Section 2

Each of the terms on the right side of Equations (II-4) will now be expanded in terms which can be utilized to form the complete airframe equations of motion.

To express the forces along the x, y, and z axes due to gravity, the two angles Φ and Θ are utilized. These angles are defined in Figure II-2. Figure II-2 also shows the angle Ψ which is used to define airframe heading. The angles Φ , Θ , and Ψ are called "Euler angles" and are used to relate the airframe axes to earth-bound axes. In Figure II-2, the angle Φ is the angle between the airframe y axis and the horizontal plane, measured in a plane perpendicular to the airframe x axis; the angle Θ is measured vertically between the airframe x axis and the horizontal plane; and the angle Ψ is the angle between an arbitrary reference line in the horizontal plane and the projection of the airframe x axis in the horizontal plane. By direct resolution from Figure II-2, the gravity forces along the airframe axes are found to be

$$\begin{aligned} F_{Y_G} &= -W_x \sin \Theta \\ (II-5) \quad F_{Y_G} &= W_x \cos \Theta \sin \Phi \\ F_{Z_G} &= W_x \cos \Theta \cos \Phi \end{aligned}$$

where W_x is the airframe weight.

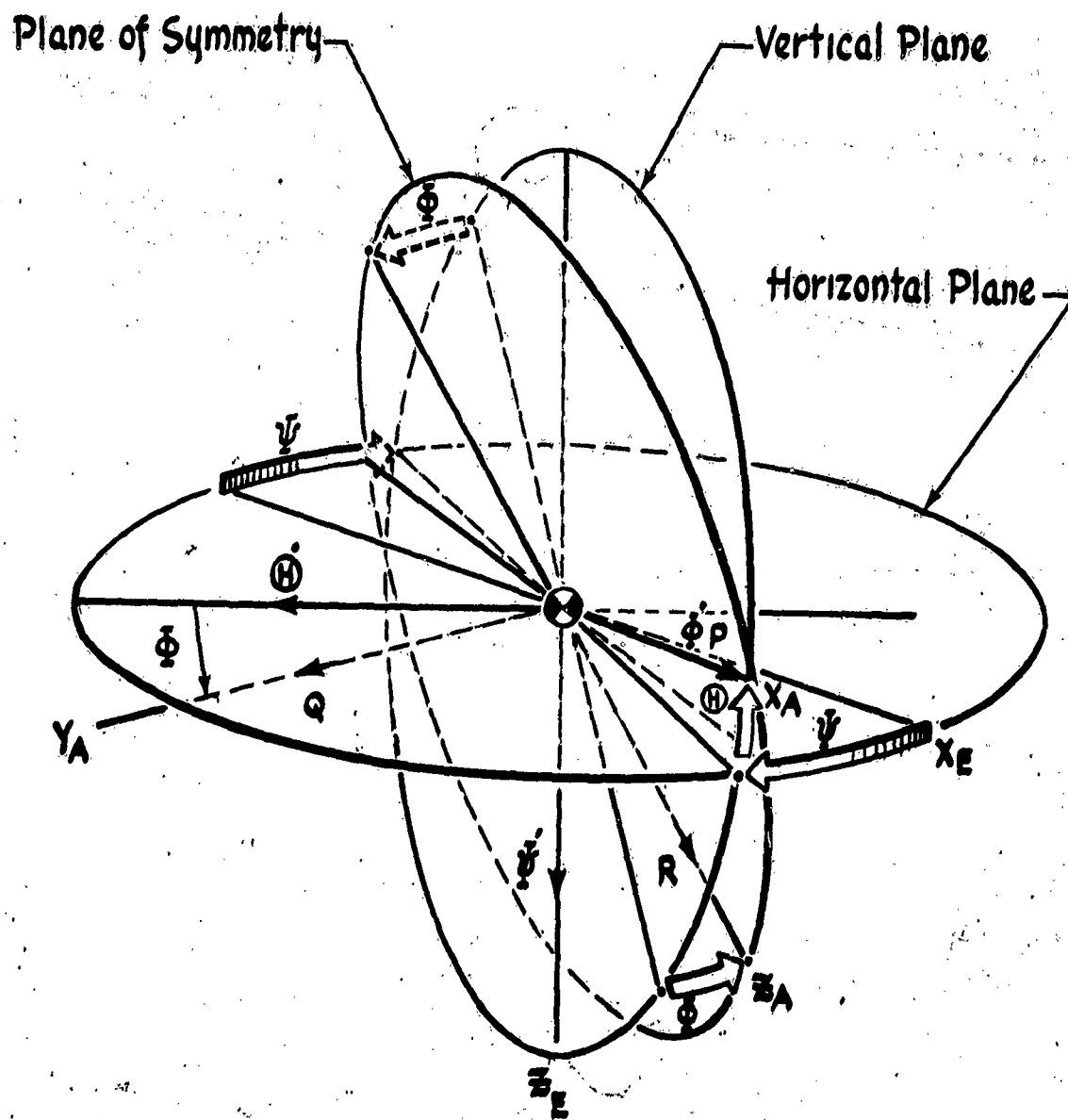


Figure II-2 Euler Angles

Section 2

The thrust forces and moments are expanded with the aid of Figure II-3. If the magnitude of the thrust along the thrust line is designated by T ,

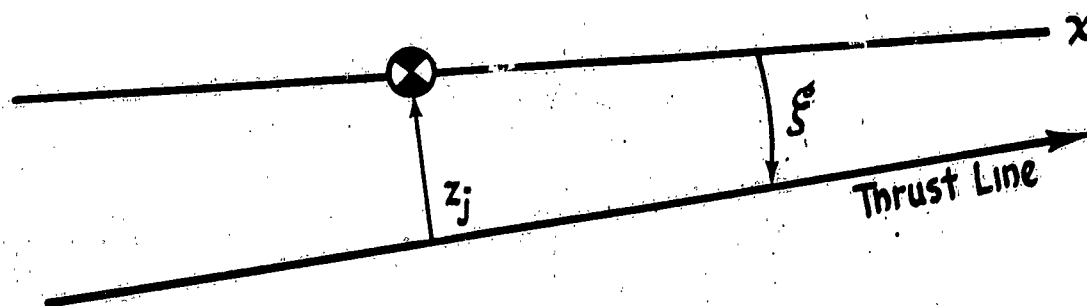


Figure II-3 Thrust Relationships

the thrust components can be written as

$$\begin{aligned}
 F_{x_T} &= T \cos \epsilon \\
 F_{z_T} &= -T \sin \epsilon \\
 M_T &= T z_j
 \end{aligned}
 \tag{II-6}$$

If it is assumed that the thrust is a function of only the variables U and δ_{TAM} (engine rotational velocity), Equations (II-6) become

$$\begin{aligned}
 F_{x_T} &= [T(U) + T(\delta_{TAM})] \cos \epsilon \\
 F_{z_T} &= -[T(U) + T(\delta_{TAM})] \sin \epsilon \\
 M_T &= [T(U) + T(\delta_{TAM})] z_j
 \end{aligned}
 \tag{II-7}$$

The aerodynamic forces and moments can be expressed functionally as shown in Equation (II-8).

$$(II-8) \quad F_{AERO} = F(U, V, W, P, Q, R, \Delta_A, \Delta_E, \Delta_R, \Delta_F, \Delta_B)$$

where Δ_A = aileron deflection
 Δ_E = elevator deflection
 Δ_R = rudder deflection
 Δ_F = flap deflection
 Δ_B = speed brake deflection

and the functional notation indicates the force is a function of the indicated variables and their derivatives.

Before the complete equations are written, however, several simplifications can be made. Since it has been assumed that the xz plane is a plane of symmetry, all terms which represent the functional relationship between the longitudinal forces and moments (X , Z , and M) and the lateral variables P and R can be dropped from the equations because the quantities are not functionally related. The same condition exists for those terms which represent the functional relationship between the lateral forces and moments (Y , N , and Y) and the longitudinal variable Q . In addition, it is assumed that the flow is quasi-steady. This assumption eliminates all time derivatives arising from acceleration of the air mass except the \dot{W} term which is retained in the pitching moment equation to account for the effect of downwash lag. It is further assumed that the drag caused by Δ_A and Δ_R is negligible. With these simplifications, the functional relationships are expressed as:

Section 2

(II-9)

$$\Sigma F_{xAERO} = X(U, V, W, Q, \Delta_E, \Delta_F, \Delta_B)$$

$$\Sigma F_{yAERO} = Y(U, V, W, P, R, \Delta_A, \Delta_R)$$

$$\Sigma F_{zAERO} = Z(U, V, W, Q, \Delta_E, \Delta_F, \Delta_B)$$

$$\Sigma L_{AERO} = L(U, V, W, P, R, \Delta_A, \Delta_R)$$

$$\Sigma M_{AERO} = M(U, V, W, W, Q, \Delta_E, \Delta_F, \Delta_B)$$

$$\Sigma N_{AERO} = N(U, V, W, P, R, \Delta_A, \Delta_R)$$

Although mathematically rigorous methods exist for separating the variables of (II-9), the resulting equations cannot easily be mechanized on an analog computer. This situation exists because the forces and moments cannot in general be represented as the sum of the forces and moments due to each of the variables individually, since the force or moment due to one variable is a function of many of the other variables. For example, the L moment due to V is a function of U and W . Experience has shown, however, that many of these effects are small and that useful results can be obtained if the functional relationships shown in Equation (II-9) are separated as shown in Equations (II-10).

$$\sum F_{XAERO} = X(U) + X(W)_U + X(V)_{U,W} + X(Q)_U + X(\Delta E)_U \\ + X(\Delta F)_U + X(\Delta B)_U$$

$$\sum F_{YAERO} = Y(V)_{U,W} + Y(P)_{U,W} + Y(R)_{U,W} + Y(\Delta A)_{U,W} + Y(\Delta R)_{U,W}$$

$$\sum F_{ZAERO} = Z(U) + Z(W)_U + Z(V)_{U,W} + Z(Q)_{U,W} + Z(\Delta E)_U \\ + Z(\Delta F)_U + Z(\Delta B)_U$$

(II-10)

$$\sum L_{AERO} = L(V)_{U,W} + L(P)_U + L(R)_{U,W} + L(\Delta A)_U + L(\Delta R)_{U,W}$$

$$\sum M_{AERO} = M(U) + M(W)_U + M(\dot{W})_U + M(Q)_U + M(V)_{U,W} \\ + M(\Delta E)_U + M(\Delta F)_U + M(\Delta B)_U$$

$$\sum N_{AERO} = N(V)_{U,W} + N(P)_{U,W} + N(R)_{U,W} + N(\Delta A)_{U,W} + N(\Delta R)_{U,W}$$

In the above equations, symbols of the form $L(V)_{U,W}$ indicate that the rolling moment due to V is a function of U and W . Data representing these relationships will usually be presented in nondimensional form as families of curves, as shown in Figure II-4.

Section 2

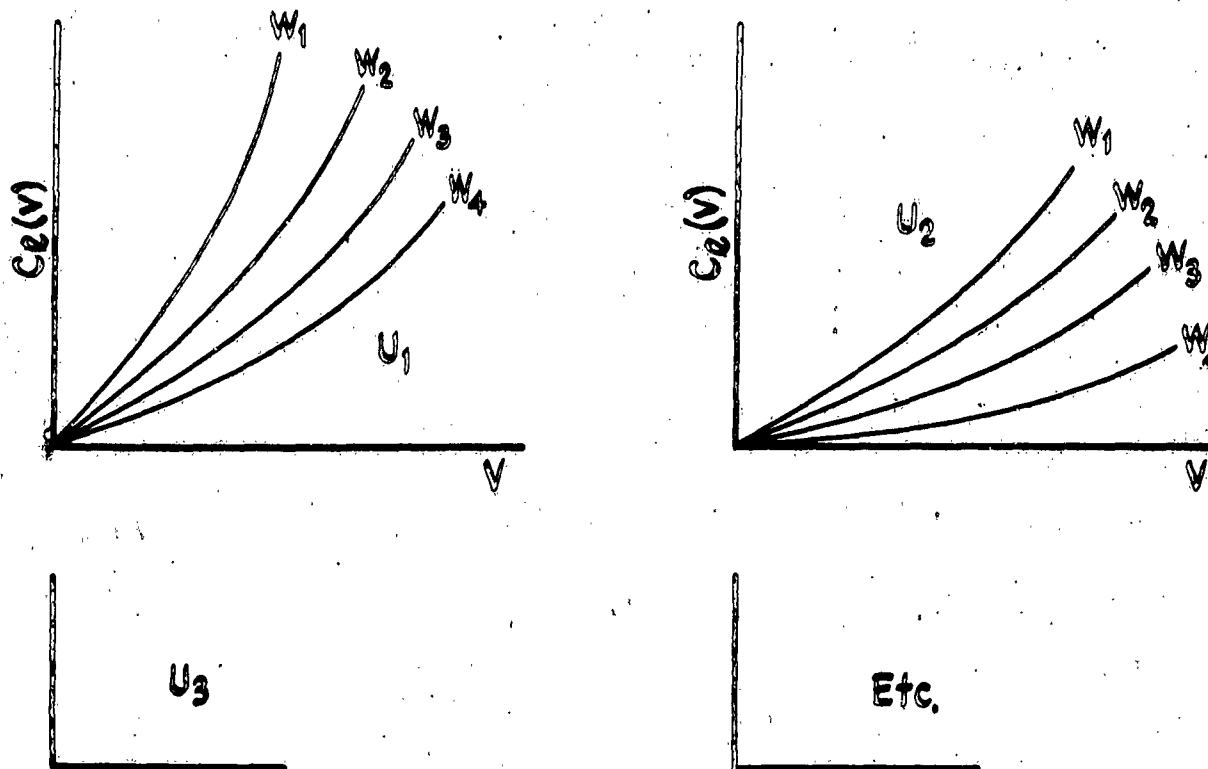


Figure II-4 Typical Presentation of Aerodynamic Data

In Figure II-4,

$$(II-11) \quad C_L(V) = \frac{L(V)^*}{qSb}$$

To simplify the presentation of aerodynamic data, curves such as those of Figure II-4 are usually plotted as a function of β and α rather than V and W . Reference to Figure II-5 shows that β and α are given by Equation (II-12).

*A more complete discussion of dimensional and nondimensional coefficients is given in Reference 9.

$$\beta = \tan^{-1} \frac{v}{u} \cong \frac{v}{u}$$

(II-12)

$$\alpha = \tan^{-1} \frac{w}{u} \cong \frac{w}{u}$$

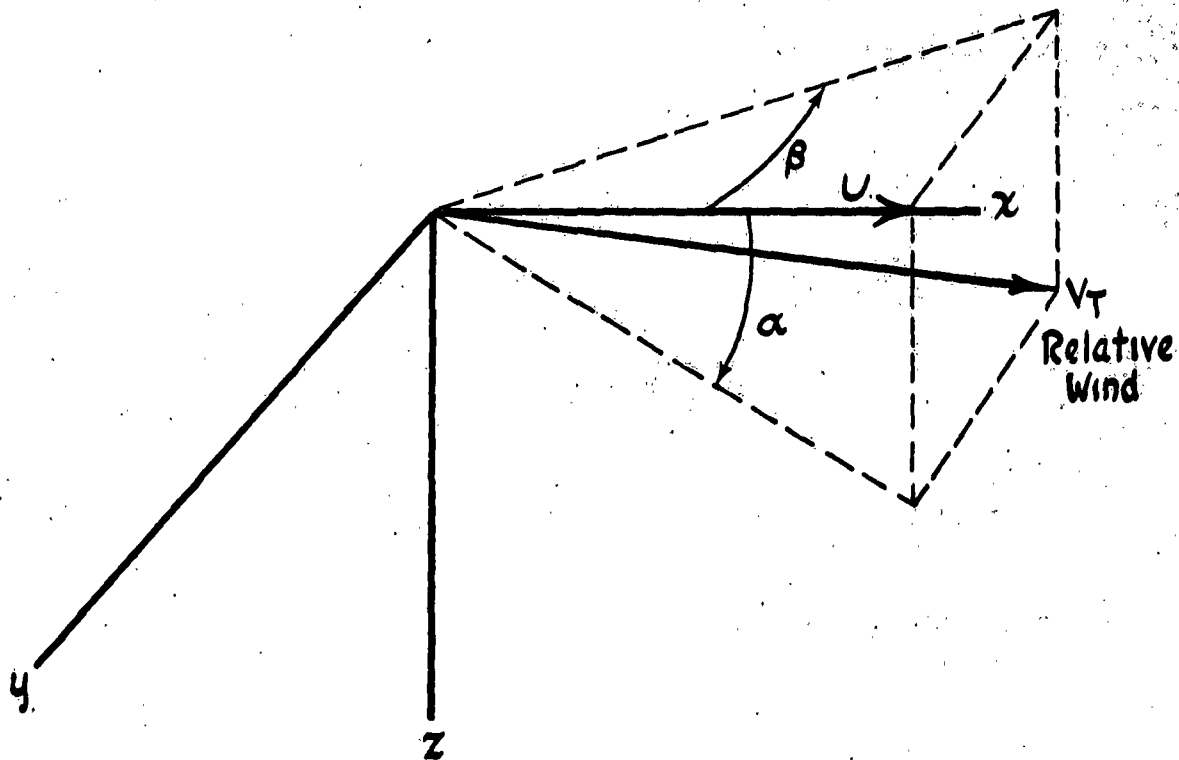


Figure II-5 Angles of Attack and Sideslip

The approximations of Equations (II-12) are quite accurate for small values of β and α and are in error by less than 10% for angles up to 30 degrees.

Aerodynamic data defining the other terms in Equations (II-10) would be presented by curves similar to those of Figure II-4. It is evident that for any particular airframe and flight condition, the determination of each

Section 2

of the terms in Equations (II-10) becomes an individual problem. Each term is investigated to determine how elaborate its mechanization should be to provide acceptable accuracy.

When Equations (II-4), (II-5), (II-7), and (II-10) are combined with Equations (II-1), the result is

$$(II-13) \quad \dot{U} = -QW + RV + \frac{1}{m} [X(U) + X(W)_U + X(V)_{U,W} + X(Q)_U + X(\Delta E)_U \\ + X(\Delta F)_U + X(\Delta B)_U + T(U) \cos \xi + T(\Delta rpm) \cos \xi - W_e \sin \theta]$$

$$\dot{V} = -RU + PW + \frac{1}{m} [Y(V)_{U,W} + Y(P)_{U,W} + Y(R)_{U,W} + Y(\Delta A)_{U,W} \\ + Y(\Delta E)_{U,W} + W_e \cos \theta \sin \phi]$$

$$\dot{W} = -PV + QU + \frac{1}{m} [Z(U) + Z(W)_U + Z(V)_{U,W} + Z(Q)_{U,W} + Z(\Delta E)_U \\ + Z(\Delta F)_U + Z(\Delta B)_U + T(U) \sin \xi + T(\Delta rpm) \sin \xi + W_e \cos \theta \cos \phi]$$

$$\dot{P} = \frac{1}{I_x} [I_{xz} (R + QP) - QR(I_z - I_y) + L(V)_{U,W} + L(P)_{U,W} + L(R)_{U,W} \\ + L(\Delta A)_U + L(\Delta R)_{U,W}]$$

$$\dot{Q} = \frac{1}{I_y} [I_{xz} (R^2 - P^2) - PR(I_x - I_z) + M(U) + M(W)_U + M(\dot{W})_U \\ + M(Q)_U + M(V)_{U,W} + M(\Delta E)_U + M(\Delta F)_U + M(\Delta B)_U \\ + T(U) z_j + T(\Delta rpm) z_j]$$

$$\dot{R} = \frac{1}{I_z} [I_{xz} (P - QR) - PQ(I_y - I_x) + N(V)_{U,W} + N(P)_{U,W} \\ + N(R)_{U,W} + N(\Delta A)_{U,W} + N(\Delta R)_{U,W}]$$

Since Equations (II-13) are composed of eight variables but only six equations, two additional equations are required before a simultaneous solution can be made. These two additional equations are needed to relate the airframe attitude angles Φ and Θ to the airframe angular velocities P , Q , and R . These equations, plus the equation relating the heading angle Ψ to the airframe angular velocities, can be written from an inspection of Figure II-2.

$$(II-14) \quad \begin{aligned} \dot{\Phi} &= P + \tan \Theta (Q \sin \Phi + R \cos \Phi) \\ \dot{\Theta} &= Q \cos \Phi - R \sin \Phi \\ \dot{\Psi} &= \frac{R \cos \Phi + Q \sin \Phi}{\cos \Theta} \end{aligned}$$

Equations (II-13) and (II-14) make up the complete airframe equations of motion, and they can be mechanized on an analog computer in the form shown. It will be noted that the equations are nonlinear, and therefore nonlinear computing elements are required to perform function multiplication and function generation. The equations are valid for any attitude or configuration for which aerodynamic data can be obtained, except for $\Theta = \pm 90$ degrees, at which attitude the Euler angles Φ and Ψ are undefined, as is evident from their definitions and from Equations (II-14).

As mentioned previously, Equations (II-13) and (II-14) are valid for any of the first three sets of axis systems defined in Table II-1. In the discussion accompanying that table, it was noted that some simplification

Section 2

is effected if the principal axes are chosen since this eliminates the cross products of inertia, and thus the terms multiplied by I_{xz} in Equations (II-13) are eliminated. Further, since the fuselage reference line often lies very close to the principal x axis, the cross product of inertia is sometimes negligible for this axis orientation also. However, if stability axes are chosen, it will be necessary to retain I_{xz} for most flight conditions.

For a specific airframe, it will be possible to reduce many of the aerodynamic terms in Equations (II-13) to the form of the conventional dimensional stability derivatives. For example, if the term $X(u)_w$ is a linear function of u and does not vary significantly with w for the ranges of u and w anticipated for a specific problem, then $X(u)_w$ can be replaced in the equation by

$$(II-15)^* \quad X(u)_w = \frac{\partial X}{\partial u} u + X(u_0)$$

Dividing the partial derivative by m gives the conventional stability derivative,

$$(II-16) \quad \frac{1}{m} \frac{\partial X}{\partial u} = X_u$$

When the complete equations are applied to a specific airframe, it will often be found that many of the nonlinear terms are negligible. One investigator,

*Where the zero subscript indicates the initial value and the lower case letter indicates deviations therefrom.

Triplett,* has found that the terms QR and R^2 were unimportant for rolling maneuvers involving roll angles up to 100 degrees. Two other investigators, Sherman and Sternfield,** using equations referenced to principal axes, found that the terms RV and QR were negligible, that the terms PV , PR , and PQ were small but could not be neglected, and that the term PW was very important for turning maneuvers involving roll angles up to 90 degrees and load factors up to 5 g's. Sherman and Sternfield also found that the nonlinear variations of $M(W)$, $N(V)_W$, $L(V)_W$, $L(P)$, and $N(P)$ were important. Both investigations were concerned with an advanced design interceptor.

Other simplifications can often be made when a specific problem or maneuver is being investigated. For example, since the airframe heading Ψ does not contribute to the solution of airframe equations, the Euler equation for $\dot{\Psi}$ need not be mechanized unless the airframe heading Ψ is required for use in a heading controller mechanization or for some similar purpose. If the maneuver being investigated is primarily rolling, it may be possible to neglect the Euler angle Θ , or to approximate $\sin \Theta$ by Θ and $\cos \Theta$ by unity. If only small speed changes are anticipated, it is often possible to eliminate the X force equation, thus reducing the problem to five degrees of freedom.

*William C. Triplett, "Considerations Involved in the Design of a Roll Angle Computer for a Bank-to-turn Interceptor," paper presented at the NACA Conference on Stability and Control of Aircraft, Moffett Field, California, March 29-30, 1955.

**Windsor L. Sherman and Leonard Sternfield, "Some Results of a Study Performed on the Typhoon Computer," paper presented at the NACA Conference on Stability and Control of Aircraft, Moffett Field, California, March 29-30, 1955.

Section 2

One method for determining the required complexity for an analog computer simulation consists of first solving the complete equations on IBM equipment. The equations are then simplified by dropping the nonlinear terms, one term at a time, until the maximum permissible error has been introduced.

If IBM equipment is not available, the required complexity can still be determined for those cases where a specific maneuver is being investigated for which flight test results exist. In this case one begins with the perturbation equations and the nonlinear effects are then added one at a time until the analog results show acceptable correlation with flight test results.

(b) THE PERTURBATION EQUATIONS

The airframe perturbation equations can be derived directly from Equations (II-13) and (II-14) by means of two additional assumptions and a change of variables. The first assumption is:

Assumption 6

The disturbances from the steady flight condition are assumed to be small enough that the products and squares of the changes in velocities are negligible in comparison to the changes themselves. Also the disturbance angles are assumed to be small enough that the sines of these angles may be set equal to the angles and the cosines may be set equal to unity. It is further assumed that products of these angles are also approximately zero and can be neglected.

Application of Assumption 6 is simplified if a change of variable is made. Let each of the total variables of Equations (II-13) and (II-14) be represented as the sum of the steady state value and the disturbed value. Then

$$\begin{array}{ll}
 U = U_0 + u & \bar{\Phi} = \bar{\Phi}_0 + \phi \\
 V = V_0 + v & \bar{\Psi} = \bar{\Psi}_0 + \psi \\
 W = W_0 + w & \bar{\Psi} = \bar{\Psi}_0 + \psi \\
 \text{(II-17)} & \Delta F = \Delta F_0 + \delta F \\
 P = P_0 + p & \Delta B = \Delta B_0 + \delta B \\
 Q = Q_0 + q & \Delta A = \Delta A_0 + \delta A \\
 R = R_0 + r & \Delta E = \Delta E_0 + \delta E \\
 & \Delta R = \Delta R_0 + \delta R
 \end{array}$$

where the zero subscript indicates the steady flight value and the lower case letters indicate deviations therefrom.

As a result of the above change of variables, all the aerodynamic quantities in Equations (II-13) can be represented by the sum of two terms, one representing the value of the aerodynamic quantity in the initial flight condition and the other term representing the change in the quantity due to perturbed airframe motion. Since the perturbed airframe motion is small, this quantity can be represented by the "slope" of the aerodynamic quantity at the steady flight condition, multiplied by the change in the airframe variable.

Section 2

For example, the expression $X(W)_U$ becomes $X(W_0) + \frac{dX}{dW} W$

Constant terms such as $X(W_0)$ can be eliminated by means of an additional assumption.

Assumption 7

It is assumed that in the steady flight condition, all accelerations are equal to zero (i.e., $\dot{U}_0 = \dot{V}_0 = \dot{W}_0 = \dot{P}_0 = \dot{Q}_0 = \dot{R}_0 = 0$).

As a result of Assumption 7, the left sides of Equations (II-13) are equal to zero for the steady flight condition. Therefore the algebraic sum of all the constant terms appearing on the right sides of Equations (II-13) must be equal to zero and are therefore dropped from the equations.

Utilizing Assumptions 6 and 7 and Equations (II-17), it is possible to write Equations (II-13) and (II-14) as

$$(II-18) \quad \begin{aligned} \dot{U} = & -Q_0 W - W_0 Q + R_0 U + V_0 R + \frac{1}{m} \left[\frac{dX}{dU} U + \frac{dX}{dW} W + \frac{dX}{dV} V \right. \\ & + \frac{dX}{d\delta} \delta + \frac{dX}{d\epsilon} \epsilon + \frac{dX}{dF} F + \frac{dX}{d\theta} \theta + \frac{dT}{dU} U \cos \xi \\ & \left. + \frac{dT}{d\Gamma} \Gamma \sin \xi - W_x \theta \cos \theta_0 \right] \end{aligned}$$

$$\begin{aligned} \dot{V} = & -R_0 U - U_0 R + P_0 W + W_0 P + \frac{1}{m} \left[\frac{dY}{dV} V + \frac{dY}{dP} P + \frac{dY}{dT} T \right. \\ & \left. + \frac{dY}{dA} A + \frac{dY}{dR} R + W_x (\phi \cos \theta_0 \cos \xi_0 - \theta \sin \theta_0 \sin \xi_0) \right] \end{aligned}$$

$$\dot{w} = -P_0 \dot{\psi} - V_0 \dot{\rho} + Q_0 \dot{u} + U_0 \dot{g} + \frac{1}{m} \left[\frac{\partial Z}{\partial u} u + \frac{\partial Z}{\partial w} w + \frac{\partial Z}{\partial g} g + \frac{\partial Z}{\partial v} v \right. \\ \left. + \frac{\partial Z}{\partial \delta E} \delta E + \frac{\partial Z}{\partial \delta F} \delta F + \frac{\partial Z}{\partial \delta B} \delta B + \frac{\partial T}{\partial u} u \sin \xi + \frac{\partial T}{\partial r_{PM}} r_{PM} \sin \xi \right. \\ \left. - W_x (\dot{\phi} \cos \Theta_0 \sin \Phi_0 + \dot{\theta} \sin \Theta_0 \cos \Phi_0) \right]$$

$$\dot{p} = \frac{1}{I_x} \left[I_{xz} (\dot{\gamma} + Q_0 \rho + P_0 g) - (Q_0 \tau + R_0 g) (I_z - I_y) + \frac{\partial L}{\partial v} v + \frac{\partial L}{\partial \rho} \rho \right. \\ \left. + \frac{\partial L}{\partial \tau} \tau + \frac{\partial L}{\partial \delta A} \delta A + \frac{\partial L}{\partial \delta R} \delta R \right]$$

$$\dot{q} = \frac{1}{I_y} \left[\frac{1}{I_{xz}} (2R_0 \tau - 2P_0 g) - (P_0 \tau + R_0 g) (I_x - I_z) + \frac{\partial M}{\partial u} u + \frac{\partial M}{\partial w} w \right. \\ \left. + \frac{\partial M}{\partial \dot{w}} \dot{w} + \frac{\partial M}{\partial g} g + \frac{\partial M}{\partial v} v + \frac{\partial M}{\partial \delta E} \delta E + \frac{\partial M}{\partial \delta F} \delta F + \frac{\partial M}{\partial \delta B} \delta B \right. \\ \left. + \frac{\partial T}{\partial u} u z_j + \frac{\partial T}{\partial r_{PM}} r_{PM} z_j \right]$$

$$\dot{r} = \frac{1}{I_z} \left[-I_{xz} (\dot{\rho} - P_0 \tau - R_0 g) - (P_0 g + Q_0 \rho) (I_y - I_x) + \frac{\partial N}{\partial v} v \right. \\ \left. + \frac{\partial N}{\partial \rho} \rho + \frac{\partial N}{\partial \tau} \tau + \frac{\partial N}{\partial \delta A} \delta A + \frac{\partial N}{\partial \delta R} \delta R \right]$$

$$\dot{\phi} = \dot{\rho} + \theta (\dot{\Phi}_0 \cos \Theta_0) + \dot{\psi} (\sin \Theta_0)$$

$$\dot{\theta} = \dot{g} \cos \Phi_0 + \dot{\gamma} \sin \Phi_0 - \dot{\phi} (\dot{\Phi}_0 \cos \Theta_0)$$

$$\dot{\psi} = \frac{\theta (\dot{\Phi}_0 \sin \Theta_0) + \dot{\phi} (\Theta_0) + \dot{\gamma} \cos \Phi_0 + \dot{g} \sin \Phi_0}{\cos \Theta_0}$$

Section 2

Equations (II-18) are quite general and can be used to study the motions of an airframe disturbed by a small amount from some initial flight condition. The initial flight condition can be any combination of airframe angular and linear velocities (within the limitations of Assumption 7) and any attitude as long as $(H) \neq \pm 90$ degrees, and as long as the perturbed velocities u, v, w, p, q, r and the perturbed Euler angles ϕ and θ are kept small. It will be noted that Equations (II-18) are linear.

As shown, Equations (II-18) are much more complicated than usually required. Most airframe studies using the perturbation equations are not adversely affected through the use of an additional assumption:

Assumption 8

It is assumed that the initial flight condition consists of wings-level flight at constant altitude and zero sideslip angle. This results in $V_0 = P_0 = Q_0 = R_0 = \dot{\phi}_0 = \dot{\theta}_0 = \dot{\psi}_0 = \dot{\psi}_0 = 0$

By means of Assumption 8, Equations (II-18) are reduced to those of (II-19).

$$\dot{u} = -W_0 q + \frac{1}{m} \left[\frac{dX}{du} u + \frac{dX}{dw} w + \frac{dX}{dv} v + \frac{dX}{d\delta} \delta + \frac{dX}{d\epsilon} \epsilon + \frac{dX}{d\phi} \phi + \frac{dX}{d\theta} \theta + \frac{dT}{du} u \cos \xi + \frac{dT}{d\delta} \delta \sin \xi - W_x \theta \cos (H_0) \right]$$

$$(II-19) \quad \dot{v} = -U_0 r + W_0 p + \frac{1}{m} \left[\frac{dY}{dv} v + \frac{dY}{d\phi} \phi + \frac{dY}{d\theta} \theta + \frac{dY}{d\delta} \delta + \frac{dY}{d\epsilon} \epsilon + \frac{dY}{d\psi} \psi + W_x \phi \cos (H_0) \right]$$

$$\dot{w} = U_0 q + \frac{1}{m} \left[\frac{dZ}{dw} w + \frac{dZ}{d\delta} \delta + \frac{dZ}{d\epsilon} \epsilon + \frac{dZ}{d\psi} \psi + \frac{dZ}{d\phi} \phi + \frac{dZ}{d\theta} \theta + \frac{dT}{d\delta} \delta \sin \xi + \frac{dT}{d\epsilon} \epsilon \cos \xi - W_x \theta \sin (H_0) \right]$$

(II-19)
CONT.

Section 2

$$\dot{p} = \frac{1}{I_x} \left[I_{xz} \dot{r} + \frac{\partial L}{\partial v} v + \frac{\partial L}{\partial p} p + \frac{\partial L}{\partial r} r + \frac{\partial L}{\partial \delta_A} \delta_A + \frac{\partial L}{\partial \delta_R} \delta_R \right]$$

$$\dot{q} = \frac{1}{I_y} \left[\frac{\partial M_u}{\partial u} u + \frac{\partial M_w}{\partial w} w + \frac{\partial M_{\dot{w}}}{\partial \dot{w}} \dot{w} + \frac{\partial M_q}{\partial q} q + \frac{\partial M_v}{\partial v} v + \frac{\partial M}{\partial \delta_E} \delta_E \right]$$

$$+ \frac{\partial M}{\partial \delta_F} \delta_F + \frac{\partial M}{\partial \delta_B} \delta_B + \frac{\partial T_u}{\partial u} z_j + \frac{\partial T}{\partial \delta_{TAM}} \delta_{TAM} z_j \Big]$$

$$\dot{r} = \frac{1}{I_z} \left[I_{xz} \dot{p} + \frac{\partial N}{\partial v} v + \frac{\partial N}{\partial p} p + \frac{\partial N}{\partial r} r + \frac{\partial N}{\partial \delta_A} \delta_A \right]$$

$$+ \frac{\partial N}{\partial \delta_R} \delta_R \Big]$$

$$\dot{\phi} = \dot{p} + \psi \sin \Theta_0$$

$$\dot{\Theta} = \dot{q}$$

$$\dot{\psi} = \dot{r} / \cos \Theta_0$$

In Equations (II-19), the terms $\frac{\partial X}{\partial v}$, $\frac{\partial Z}{\partial v}$, and $\frac{\partial N}{\partial v}$ are set equal to zero by the following reasoning: Since the airframe has been assumed symmetrical about the xz plane, the above partial derivatives are even functions and have the general form shown in Figure II-6.

Section 2

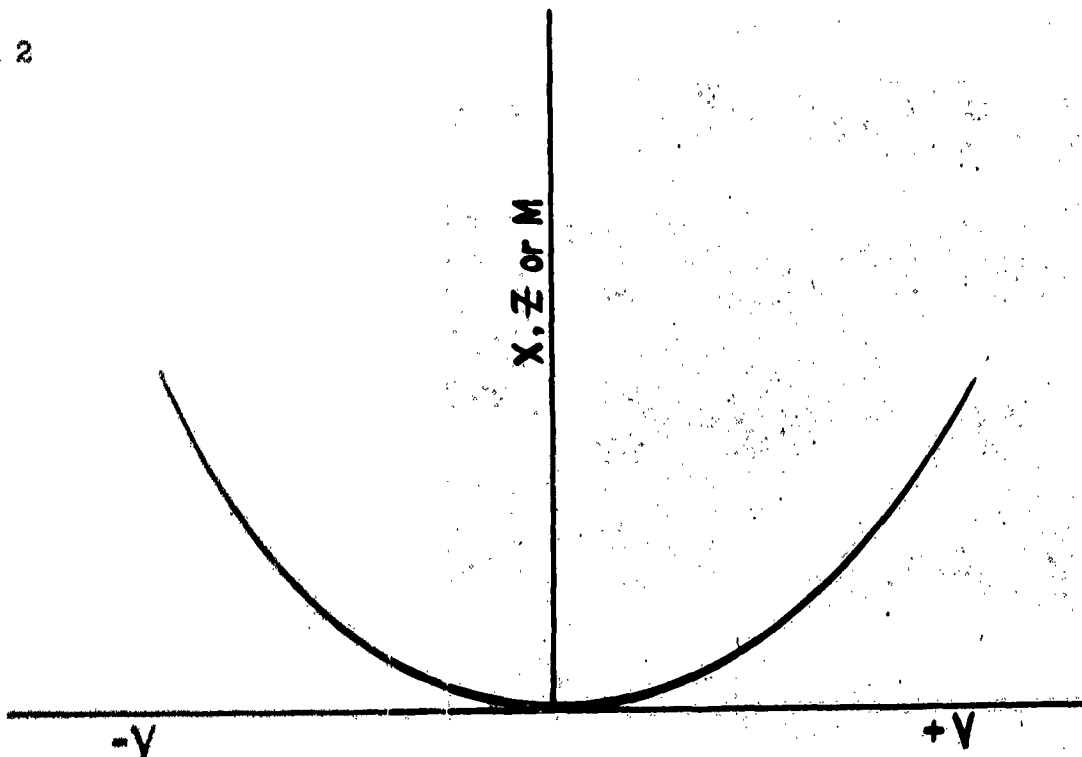


Figure II-6 Forces and Moments Caused by Side Velocity

Since it has been assumed that $V_0 = 0$, the above partial derivatives are evaluated at $V = 0$ on the curve of Figure II-6. In addition it has been assumed that u is small. It is evident that the partial derivatives of X , Z and M with respect to u are zero at $V_0 = 0$.

If, in Equations (II-19), terms of the form $\frac{1}{m} \frac{\partial X}{\partial u} u$ and $\frac{1}{I_x} \frac{\partial L}{\partial r} r$ are replaced by X_{uu} and L_{rr} , the notation is simplified. Making this simplification, in addition to setting the partial derivatives of X , Z , and M , with respect to u equal to zero, results in Equations (II-20) and (II-21).

$$\begin{aligned}
 \dot{u} &= -W_0 \dot{\theta} + X_u u + X_w w + X_\xi \dot{\xi} + X_{\delta_E} \delta_E + X_{\delta_F} \delta_F + X_{\delta_B} \delta_B \\
 &\quad + T_u u \cos \xi + T_{\delta_{rpm}} \delta_{rpm} \cos \xi - g \theta \cos \Theta_0 \\
 \dot{w} &= U_0 \dot{\theta} + Z_u u + Z_w w + Z_\xi \dot{\xi} + Z_{\delta_E} \delta_E + Z_{\delta_F} \delta_F + Z_{\delta_B} \delta_B \\
 &\quad + T_u u \sin \xi + T_{\delta_{rpm}} \delta_{rpm} \sin \xi - g \theta \sin \Theta_0 \\
 \dot{q} &= M_u u + M_w w + M_{\dot{w}} \dot{w} + M_\xi \dot{\xi} + M_{\delta_E} \delta_E + M_{\delta_F} \delta_F \\
 &\quad + M_{\delta_B} \delta_B + T_u u Z_j + T_{\delta_{rpm}} \delta_{rpm} Z_j \\
 \dot{\theta} &= \dot{\theta}
 \end{aligned}
 \tag{II-20}$$

$$\begin{aligned}
 \dot{v} &= -U_0 \dot{\theta} + W_0 \dot{\rho} + Y_v v + Y_p p + Y_r r + Y_{\delta_A} \delta_A + Y_{\delta_R} \delta_R \\
 &\quad + g \phi \cos \Theta_0 \\
 \dot{p} &= \frac{I_{xz}}{I_y} \dot{r} + L_v v + L_p p + L_r r + L_{\delta_A} \delta_A + L_{\delta_R} \delta_R \\
 \dot{r} &= \frac{I_{xz}}{I_z} \dot{p} + N_v v + N_p p + N_r r + N_{\delta_A} \delta_A + N_{\delta_R} \delta_R \\
 \dot{\phi} &= \dot{\rho} + \dot{\psi} \sin \Theta_0 \\
 \dot{\psi} &= \dot{r} / \cos \Theta_0
 \end{aligned}
 \tag{II-21}$$

Section 2

It will be noted that Equations (II-20) are functions only of the variables u , w , and θ and that Equations (II-21) are functions only of the variables p , r , v , ϕ , and ψ . Thus, as stated previously, the perturbation equations can be treated as two independent sets of equations.* Equations (II-20) are commonly referred to as the "longitudinal equations" while those of (II-21) are called the "lateral equations."

Since the longitudinal motions are independent from the lateral motions, they are treated separately in the remainder of this section.

Table II-2 summarizes the basic output and actuating quantities which can be utilized for airframe control.

The foregoing equations and Table II-2 have shown the airframe basic quantities available for control. However, before any selection of controlled variables can be made, it is necessary to consider very carefully the detailed dynamics of the airframe unalterable element. Therefore, it is necessary to discuss the lateral and longitudinal motions of the airframe and the important airplane stability derivatives (inherent or created) affecting these motions. This discussion considers the airframe as a series of transfer functions, and discusses both transient and frequency responses, arriving ultimately at several important conclusions regarding the best output variables to be used in controlling the various airframe motions.

*It should be noted that Equations (II-20) and (II-21) are independent only because of Assumption 8.

(Basic) Output Quantities <u>Longitudinal</u>	<u>Actuating Quantities</u>
<p>u forward velocity</p> <p>w vertical velocity</p> <p>q pitching velocity</p> <p>a_x forward acceleration</p> <p>a_z vertical acceleration</p> <p>α angle of attack $\approx \frac{w}{u}$</p> <p>Θ pitch angle</p>	<p>δ_E elevator deflection</p> <p>δ_B fighter brake deflection</p> <p>δ_F flap deflection</p> <p>S_{rpm} engine speed</p>
Output Quantities <u>Lateral</u>	<u>Actuating Quantities</u>
<p>v side velocity</p> <p>p rolling velocity</p> <p>r yawing velocity</p> <p>a_y side acceleration</p> <p>ψ yaw angle</p> <p>ϕ roll angle</p> <p>β sideslip angle $\approx \frac{v}{u}$</p>	<p>δ_A aileron deflection</p> <p>δ_R rudder deflection</p>

Table II-2. Basic Airframe Output and Actuating Quantities

Section 2

(c) LONGITUDINAL MOTIONS

The discussions of airframe motions in this subsection and in the remainder of the manual are based on the use of stability axes. Due to the application of Assumption 8, the selection of stability axes reduces two more terms to zero. Therefore, for stability axes,

$$(II-22) \quad \dot{H}_0 = W_0 = 0$$

Utilizing Equations (II-22), applying the Laplace transform, and rearranging Equations (II-20) so that only actuating terms appear on the right give Equations (II-23).

$$\begin{aligned}
 (II-23) \quad & (S - X_u - T_u \cos \xi) U - (X_w) w - (S X_\eta - g) \theta = \\
 & X_{\delta E} \delta E + X_{\delta F} \delta F + X_{\delta B} \delta B + T_{\delta RAM} \delta RAM \cos \xi \\
 & - (Z_u + T_u \sin \xi) U + (S - Z_w) w - (U_0 + Z_\eta) S \theta = \\
 & Z_{\delta E} \delta E + Z_{\delta F} \delta F + Z_{\delta B} \delta B + T_{\delta RAM} \delta RAM \sin \xi \\
 & - (M_u + T_u Z_\eta) U - (S M_{\dot{w}} + M_w) w + (S^2 - S M_\eta) \theta = \\
 & M_{\delta E} \delta E + M_{\delta F} \delta F + M_{\delta B} \delta B + T_{\delta RAM} \delta RAM Z_\eta
 \end{aligned}$$

The longitudinal transfer functions are obtained from the simultaneous solution of Equations (II-23) and are given for elevator deflections in Equations (II-24). Transfer functions for a_z/δ_e and \dot{a}_z/δ_e are presented in Equations (II-25) and (II-26). Note that if it is desired to obtain the equivalent equations for dive-brake or flaps inputs, merely replace δ_e by the corresponding deflection wherever it occurs, including subscripts. Transfer functions for engine rpm inputs must be obtained separately, however.

The transfer functions of Equations (II-24), (II-25), and (II-26) were obtained with the functions X_{δ_e} , X_{δ_f} , Z_{δ_f} and T_u set equal to zero. These terms are neglected, since experience has shown that they are usually quite small compared to the other terms in the equation. A more complete solution of the perturbation equations which includes the above terms is given in Reference 9.

Section 2

$$\frac{U}{\delta E} = \frac{B_u S^2 + C_u S + D_u}{\Delta}$$

$$(II-24) \quad \frac{\alpha}{\delta E} = \frac{\dot{w}}{V_0 \delta E} = \frac{A_w S^3 + B_w S^2 + C_w S + D_w}{V_0 \Delta}$$

$$\frac{\theta}{\delta E} = \frac{A_\theta S^2 + B_\theta S + C_\theta}{\Delta}$$

$$(II-25) \quad \frac{Q_z}{\delta E} = \frac{\dot{w}}{\delta E} - \frac{U_0 \dot{\theta}}{\delta E} = \frac{S(A_z S^3 + B_z S^2 + C_z S + D_z)}{\Delta}$$

$$(II-26) \quad \frac{A_x}{\delta E} = \frac{\dot{U}}{\delta E} + \frac{g\theta}{\delta E} = \frac{B_x S^3 + C_x S^2 + D_x S + E_x}{\Delta}$$

WHERE

$$B_u = Z_{\delta E} X_w$$

$$C_u = -Z_{\delta E} (g M_{\dot{w}} + M_{\dot{\theta}} X_w) + M_{\delta E} (U_0 X_w - g)$$

$$D_u = g (M_{\delta E} Z_{w\dot{\theta}} - M_{w\dot{w}} Z_{\delta E})$$

$$A_w = Z_{\delta E}$$

$$B_w = -Z_{\delta E} (M_{\dot{q}} + X_u) + M_{\delta E} V_0$$

$$C_w = X_u (Z_{\delta E} M_{\dot{q}} - M_{\delta E} V_0)$$

$$D_w = g (Z_{\delta E} M_u - M_{\delta E} Z_u)$$

$$A_\theta = Z_{\delta E} M_{\dot{w}} + M_{\delta E}$$

$$B_\theta = Z_{\delta E} (M_{w\dot{\theta}} - M_{\dot{w}} X_u) - M_{\delta E} (X_u + Z_{w\dot{\theta}})$$

$$C_\theta = Z_{\delta E} (M_{\dot{u}} X_w - M_{w\dot{u}} X_u) + M_{\delta E} (X_u Z_{w\dot{\theta}} - X_w Z_u)$$

$$A_z = A_w$$

$$B_z = B_w - U_0 A_\theta$$

$$C_z = C_w - U_0 B_\theta$$

$$D_z = D_w - U_0 C_\theta$$

$$B_x = B_u$$

$$C_x = C_u + gA_0$$

$$D_x = D_u + gB_0$$

$$E_x = gC_0$$

$$\Delta = A_0^2 + B_0^2 + C_0^2 + D_0^2 + E_0^2$$

$$A = 1$$

$$B = -M_{ir}(V_0) - M_g - Z_w - X_u$$

$$C = M_g Z_w - M_{ir}(V_0) + X_u [Z_w + M_g + M_{ir}(V_0)] - Z_u X_w$$

$$D = -X_u [M_g Z_w - M_{ir}(V_0)] - M_u X_w (V_0) + g(Z_u M_{ir} + M_u) + Z_u X_w M_g$$

$$E = g(Z_u M_w - Z_w M_u)$$

For a typical case, the factored forms of Equations (II-24) through (II-26) are given by Equations (II-27).

Section 2

$$\frac{U}{\delta E} = \frac{1}{d} [-K_{U\delta E} (-T_{U1} s + 1)(T_{U2} s + 1)]^*$$

$$\frac{\alpha}{\delta E} = \frac{1}{d} [K_{\alpha\delta E} (T_{\alpha} s + 1) \left(\frac{s^2}{\omega_{n\alpha}^2} + \frac{2\zeta_{\alpha} s}{\omega_{n\alpha}} + 1 \right)]$$

$$\frac{\theta}{\delta E} = \frac{1}{d} [K_{\theta\delta E} (T_{\theta 1} s + 1)(T_{\theta 2} s + 1)]$$

(II-27)

(II)

$$\frac{a_z}{\delta E} = \frac{1}{d} [-K_{z\delta E} s (T_{a_1} s + 1)(T_{a_2} s + 1)(-T_{a_3} s + 1)]^*$$

$$\frac{a_x}{\delta E} = \frac{1}{d} [K_{x\delta E} (T_{x_1} s + 1)(-T_{x_2} s + 1)(-T_{x_3} s + 1)]^*$$

where

$$d = \left(\frac{s^2}{\omega_{nsp}^2} + \frac{2\zeta_{sp} s}{\omega_{nsp}} + 1 \right) \left(\frac{s^2}{\omega_{nsp}^2} + \frac{2\zeta_{sp} s}{\omega_{nsp}} + 1 \right)$$

The denominator of the transfer functions gives the form of the characteristic motions of the airframe--the motions which ultimately may have to be changed for effective control. Note that the transfer functions are written in terms of quadratics, indicating two oscillatory motions with widely separated roots. An approximate factorization of the complete fourth order denominator yields:

*Note that these functions are nonminimum phase; i.e., they have either poles or zeros in the right half of the complex plane. The amplitude ratios of such functions are identical with that of the minimum phase equivalent. The phase angles are, of course, different. This difference is discussed for particular cases later.

$$\omega_{n_{sp}} = \sqrt{Z_w M_{\dot{q}} - U_0 M_{w\dot{r}}}$$

(II-28)

$$\omega_{n_p} = \frac{1}{\omega_{n_{sp}}} \sqrt{g(M_{w\dot{r}} Z_u - M_u Z_w)}$$

$$\zeta_{sp} = -\frac{(U_0 M_{w\dot{r}} + M_{\dot{q}} + Z_w)}{2\omega_{n_{sp}}}$$

$$\zeta_p = -\frac{X_u}{2\omega_{n_p}} - \frac{\zeta_{sp} \omega_{n_p}}{\omega_{n_{sp}}} - \frac{M_u (U_0 X_{w\dot{r}} - g)}{2\omega_{n_p} \omega_{n_{sp}}^2}$$

The oscillation characterized by ζ_{sp} and $\omega_{n_{sp}}$ is called the "short period" motion; it has a fast, usually well-damped, response. The oscillation characterized by ζ_p and ω_{n_p} has a long period, poorly damped response, and is known as the "phugoid." Since these are approximate factors, they cannot be universally applied. They are more accurate for those airframe configurations where the natural frequency and damping of the short period are much larger than the corresponding quantities for the phugoid, a condition which almost always exists. The factors are useful in obtaining quick estimates of airframe characteristics, and they also show the contribution of the dimensional stability derivatives to the airframe natural frequencies and damping ratios.

Frequency responses are sketched in Figures II-7 through II-11 for the longitudinal transfer functions of Equations (II-27). The curves plotted are typical of a high performance jet aircraft at a cruising flight condition.

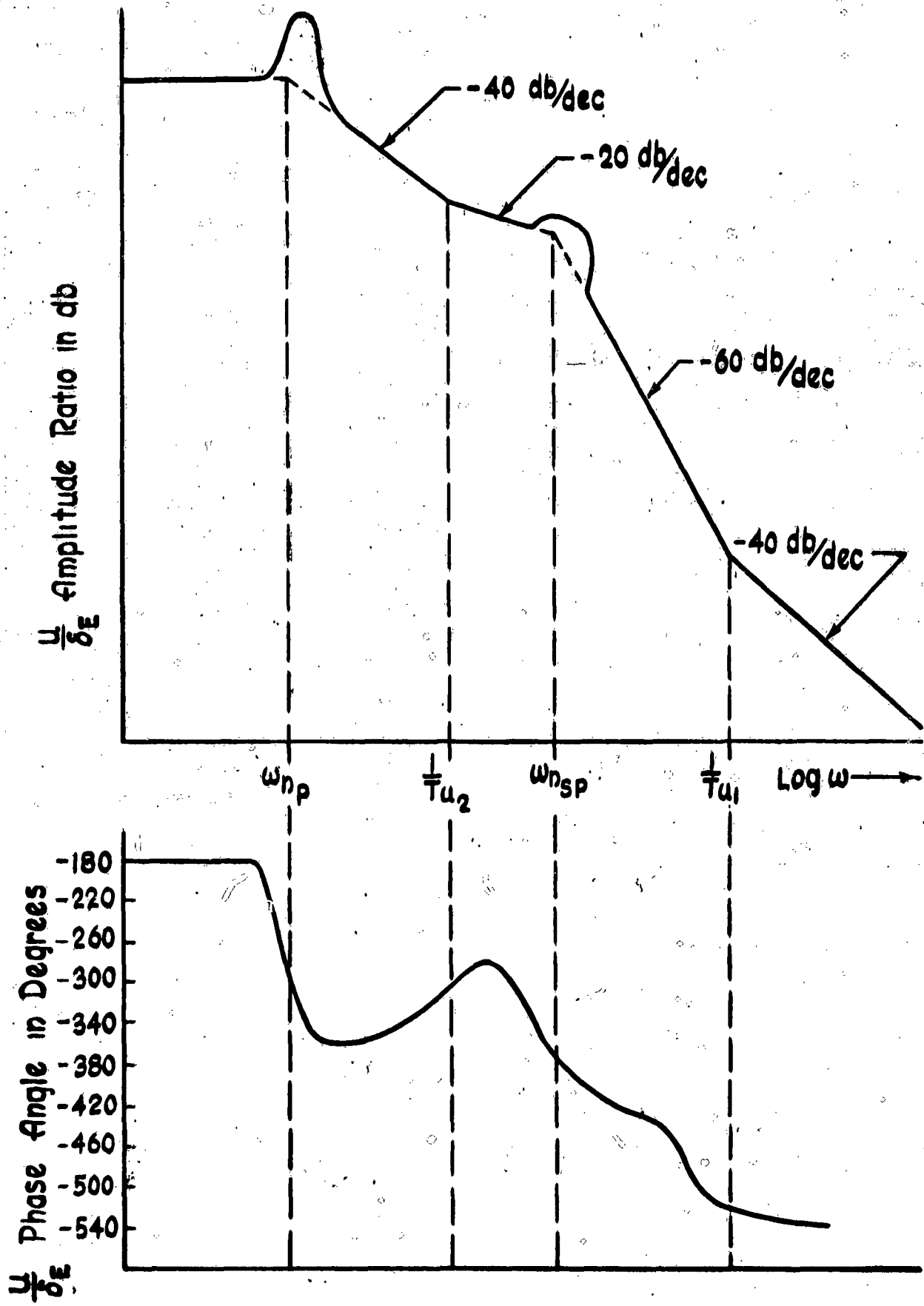


Figure II-7 Amplitude Ratio and Phase angle of $\frac{U}{\delta E}$

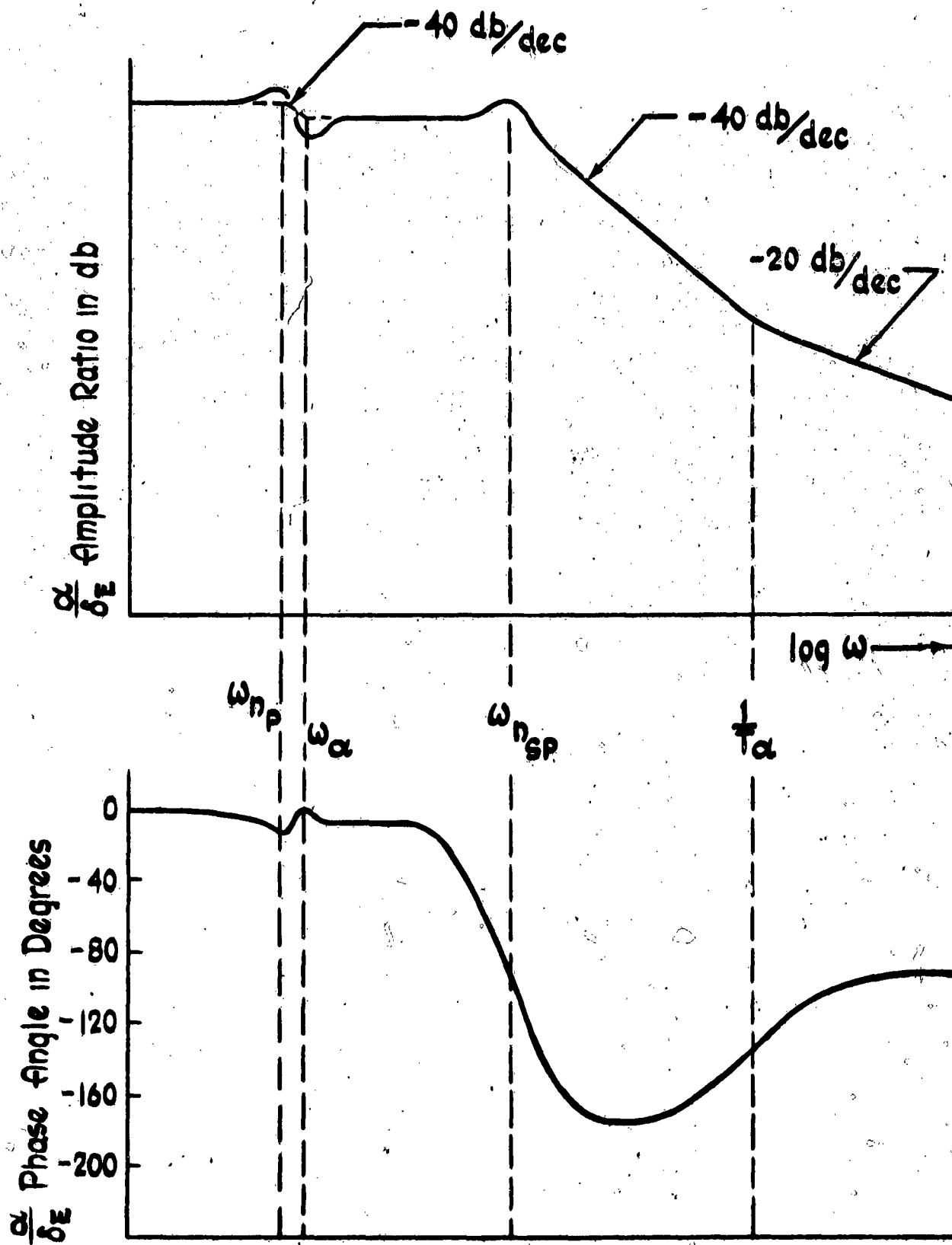


Figure II-8 Amplitude Ratio and Phase Angle of $\frac{\alpha}{\delta E}$

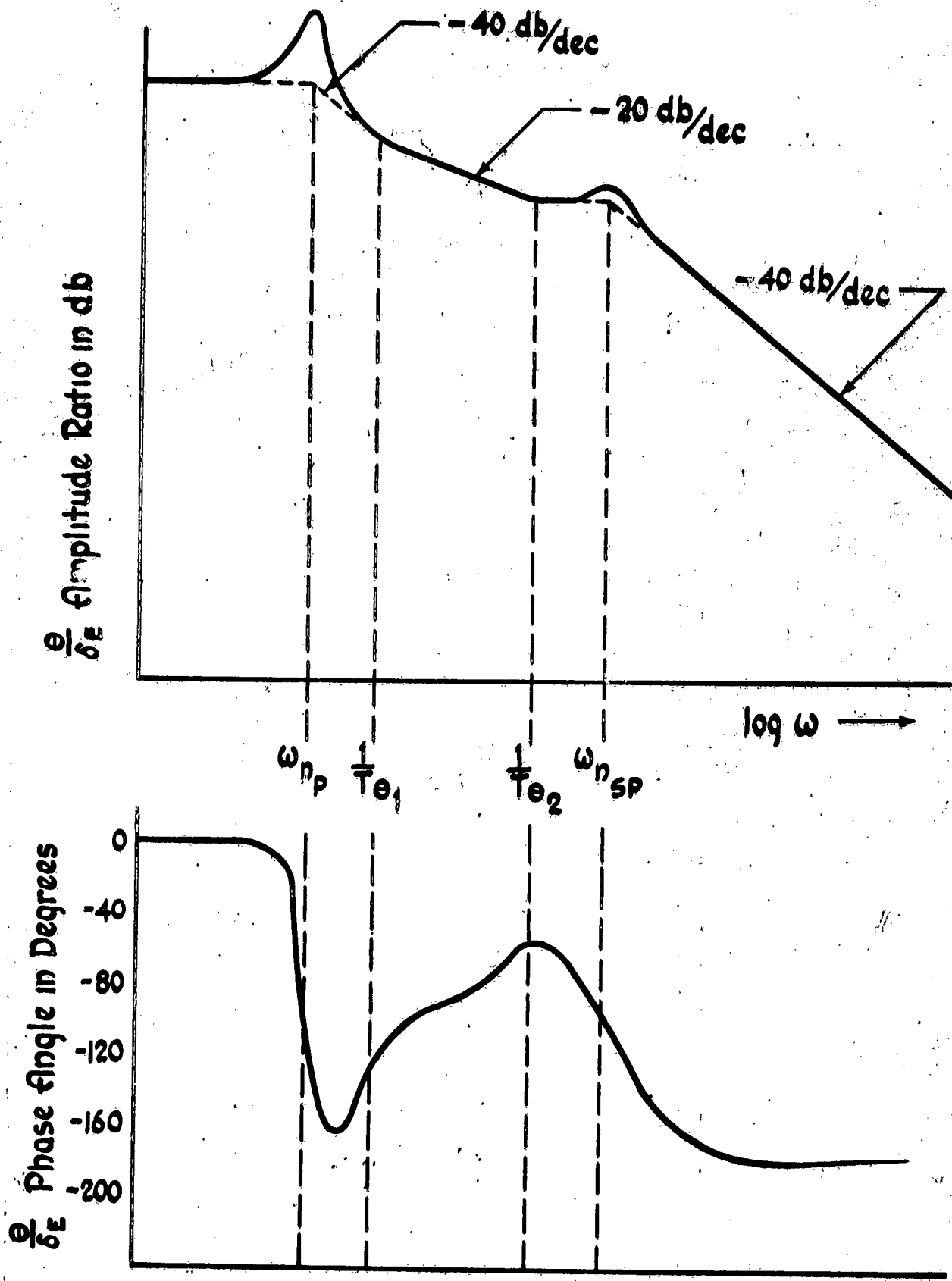


Figure II-9 Amplitude Ratio and Phase angle of $\frac{\theta}{\delta E}$

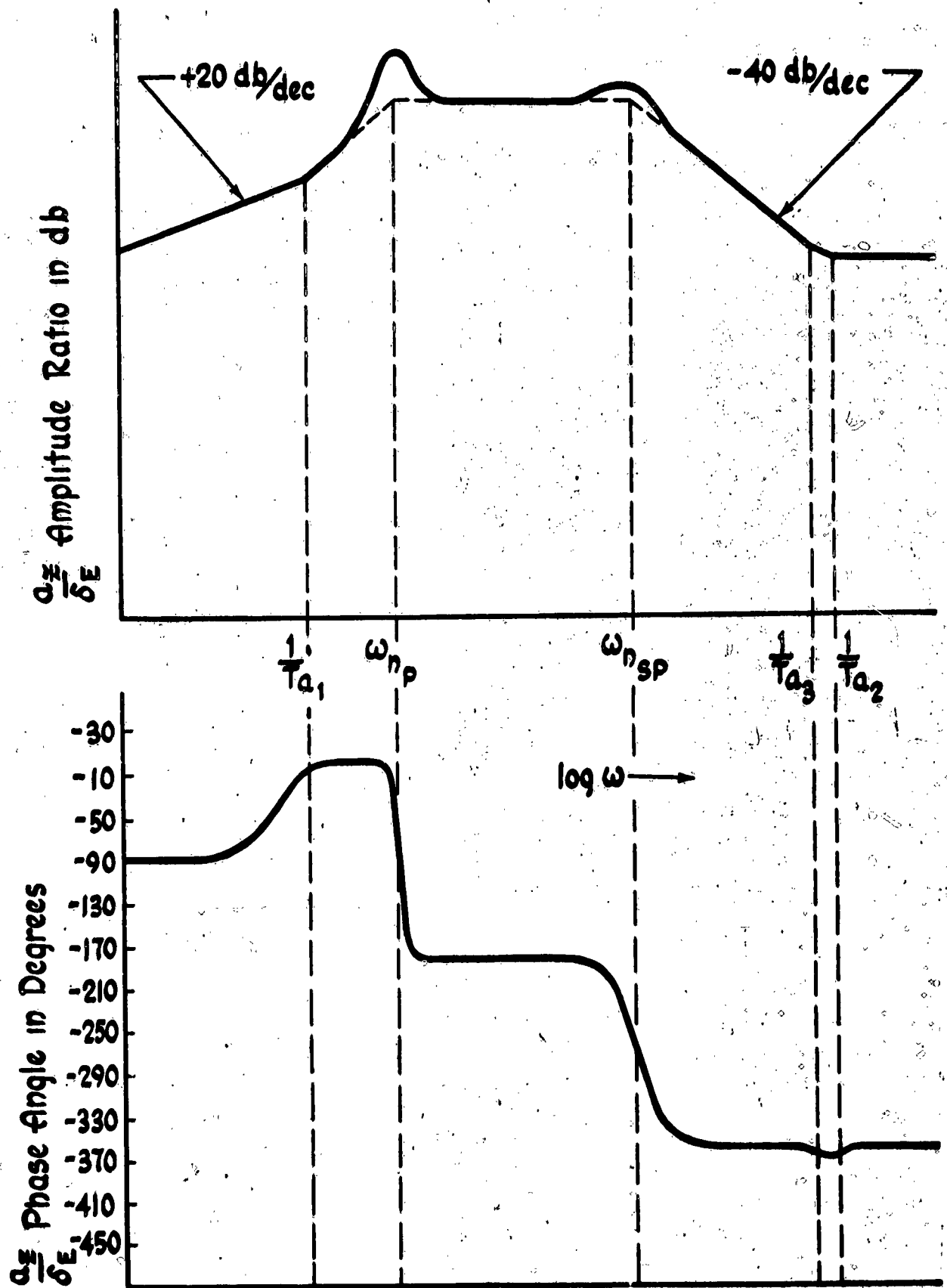


Figure II-10 Amplitude Ratio and Phase Angle of $\frac{a_E}{\delta E}$

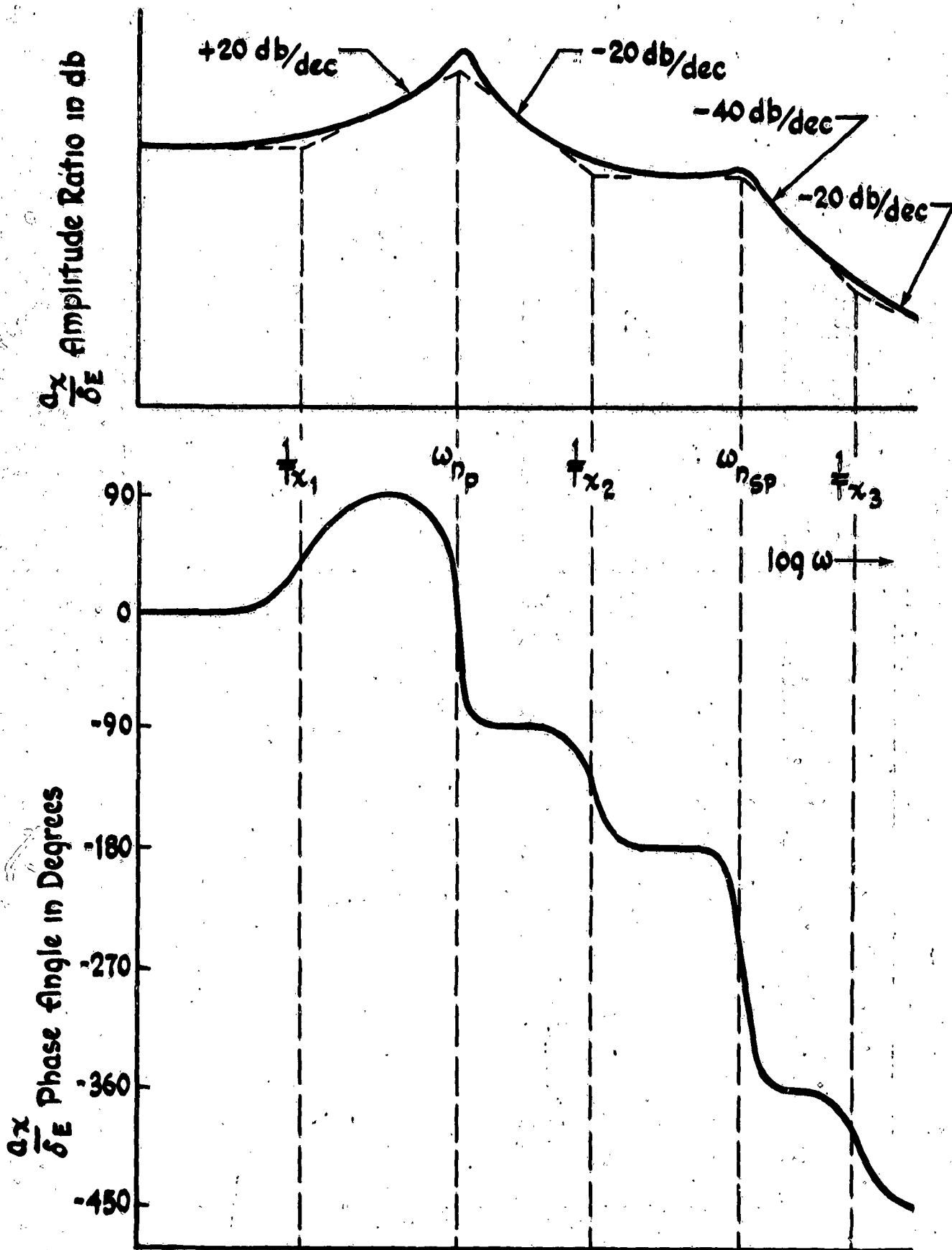


Figure II-11 Amplitude Ratio and Phase angle of $\frac{G_x}{\delta E}$

Examination of Figure II-7 indicates that larger airspeed changes occur during the phugoid than during the short period. The frequency response also indicates that an airspeed controller could control the airframe at phugoid frequencies but that control of the short period by this method would require extremely high gain.

Figure II-8 indicates that large angle of attack changes take place during the short period but that very small angle of attack variations are associated with the phugoid motion. (In fact, the numerator term containing w_{nd} almost completely cancels the phugoid portion of the denominator.) The frequency response curve shows that an angle of attack controller can stabilize the short period but that it cannot appreciably affect the phugoid. From a practical standpoint, however, angle of attack controllers are seldom used because of the difficulty in accurately measuring angle of attack.

Figure II-9 shows large pitch angle changes during the phugoid and fairly large changes during the short period. Clearly, a pitch controller could very adequately control the phugoid and the short period motions, although relatively high gain would be required for the latter purpose.

Figure II-10 indicates that large vertical accelerations of comparable magnitude exist at both phugoid and short period frequencies, and also shows the distinct possibility that no equalization would be needed in the controller.

Section 2

Figure II-11 shows that large forward accelerations exist at the phugoid frequency, and fairly large accelerations at the short period. A forward acceleration controller might be useful; however, because of the nonminimum phase terms, considerable equalization would probably be necessary for short period stabilization.

In summary, the only controlled output variables capable of being used with minimum equalization to control both the phugoid and the short period are pitch angle (or rate) and vertical acceleration. An angle of attack controller would be most useful for controlling the short period, and an airspeed controller or forward speed controller would be most useful for stabilizing the phugoid.

(d) LATERAL MOTIONS

Application of the Laplace transform to Equations (II-21) and rearranging so that only actuating terms appear on the right result in Equations (II-29).

(Again, it is assumed that $\theta_0 = w_0 = 0$.)

(II-29)

$$\begin{aligned}
 (s - Y_v)v - (Y_p s + q)\phi + [s(U_0 - Y_r)]\psi &= \\
 Y_{\dot{a}} \dot{a} + Y_{\dot{r}} \dot{r} & \\
 -(L_v)v + (s^2 - L_p s)\phi - \left(s^2 \frac{I_{xz}}{I_{xx}} + sL_r\right)\psi &= \\
 L_{\dot{a}} \dot{a} + L_{\dot{r}} \dot{r} & \\
 -(N_v)v - \left(s^2 \frac{I_{xz}}{I_{zz}} + N_p s\right)\phi + (s^2 - N_r s)\psi &= \\
 N_{\dot{a}} \dot{a} + N_{\dot{r}} \dot{r} &
 \end{aligned}$$

The lateral transfer functions can be obtained directly from Equations (II-29), and are given in Equations (II-30) through (II-33) for aileron inputs. Equivalent equations for rudder inputs may be obtained by replacing δ_A by δ_R where it occurs.

$$(II-30) \quad \frac{B}{\delta_A} = \frac{v}{U_0 \delta_A} = \frac{S(B_B S^2 + C_B S + D_B)}{\Delta_A}$$

$$(II-31) \quad \frac{\psi}{\delta_A} = \frac{A_\psi S^3 + B_\psi S^2 + C_\psi S + D_\psi}{\Delta_A}$$

$$(II-32) \quad \frac{\phi}{\delta_A} = \frac{S(A_\phi S^2 + B_\phi S + C_\phi)}{\Delta_A}$$

$$(II-33) \quad \frac{a_y}{\delta_A} = U_0 Y_v \frac{B}{\delta_A} + Y_r$$

$$\text{WHERE } B_B = -L_{\delta_A} \frac{I_{xz}}{I_{zz}} - N_{\delta_A}$$

$$C_B = L_{\delta_A} \left(\frac{g}{U_0} - N_p \right) + N_{\delta_A} \left(\frac{I_{xz}}{I_{xx}} \frac{g}{U_0} + L_p \right)$$

$$D_B = N_{\delta_A} \frac{g}{U_0} L_r - L_{\delta_A} \frac{g}{U_0} N_r$$

Section 2

$$A\psi = N_{\delta A} + \frac{I_{xz}}{I_{zz}} L_{\delta A}$$

$$B\psi = L_{\delta A} (N_p - \frac{I_{xz}}{I_{zz}} Y_v) - N_{\delta A} (Y_v + L_p)$$

$$C\psi = -L_{\delta A} Y_v N_p + N_{\delta A} L_p Y_v$$

$$D\psi = \frac{g}{U_0} (L_{\delta A} N_p - N_{\delta A} L_p)$$

$$A\phi = L_{\delta A} + N_{\delta A} \frac{I_{xz}}{I_{xx}}$$

$$B\phi = -L_{\delta A} (N_T + Y_v) + N_{\delta A} (L_T - \frac{I_{xz}}{I_{xx}} Y_v)$$

$$C\phi = L_{\delta A} (Y_v N_T + N_B) - N_{\delta A} (L_B - Y_v L_T)$$

$$\Delta\psi = S (AS^4 + BS^3 + CS^2 + DS + E)$$

$$A = 1 - \frac{I_{xz}}{I_{xx}} \cdot \frac{I_{xz}}{I_{zz}}$$

$$B = -Y_v \left(1 - \frac{I_{xz}}{I_{xx}} \cdot \frac{I_{xz}}{I_{zz}} \right) - \left(L_T \frac{I_{xz}}{I_{zz}} + N_p \frac{I_{xz}}{I_{xx}} + L_p + N_T \right)$$

$$C = (L_p N_T - L_T N_p) + Y_v \left(L_T \frac{I_{xz}}{I_{zz}} + N_p \frac{I_{xz}}{I_{xx}} + L_p + N_T \right)$$

$$+ (1 - Y_T^*) (N_B + L_B \frac{I_{xz}}{I_{zz}}) - Y_p^* (L_B + N_B \frac{I_{xz}}{I_{xx}})$$

$$D = -Y_v (L_p N_r - L_r N_p) - (1 - Y_r^*) (L_p N_B - L_B N_p) \\ - Y_p^* (N_B L_r - N_r L_B) - \frac{g}{U_0} \left(L_B + N_B \frac{I_{xz}}{I_{xx}} \right)$$

$$E = -\frac{g}{U_0} (N_B L_r - L_B N_r)$$

$$\text{WHERE } Y_r^* = \frac{Y_r}{U_0} \text{ ETC.}$$

These transfer functions have factored forms and are given for a typical case in Equations (II-34) through (II-37). Equations (II-38) through (II-41) show the factored forms for rudder inputs.

$$(II-34) \quad \frac{B}{s_A} = \frac{1}{d_A} \left[-K_{B/s_A} (T_{PA1} s + 1) (-T_{PA2} s + 1) \right]$$

$$(II-35) \quad \frac{\psi}{s_A} = \frac{1}{d_A} \left[-K_{\psi/s_A} (T_{YA1} s + 1) \left(\frac{s^2}{\omega_{n\psi}^2} + \frac{2\zeta_{YA} s + 1}{\omega_{n\psi}} \right) \right]$$

$$(II-36) \quad \frac{\phi}{s_A} = \frac{1}{d_A} \left[-K_{\phi/s_A} \left(\frac{s^2}{\omega_{n\phi}^2} + \frac{2\zeta_{\phi A} s + 1}{\omega_{n\phi}} \right) \right]$$

$$\text{WHERE } d_A = (-T_s s + 1) (T_r s + 1) \left(\frac{s^2}{\omega_{nD}^2} + \frac{2\zeta_D s + 1}{\omega_{nD}} \right)$$

$$(II-37) \quad \frac{a_y}{s_A} = U_0 Y_v \frac{B}{s_A}$$

$$(II-38) \quad \frac{B}{s_R} = \frac{1}{d_R} \left[K_{B/s_R} (T_{BR1} s + 1) (-T_{BR2} s + 1) (T_{BR3} s + 1) \right]$$

$$(II-39) \quad \frac{\psi}{s_R} = \frac{1}{d_R} \left[K_{\psi/s_R} (T_{YR} s + 1) \left(\frac{s^2}{\omega_{n\psi}^2} + \frac{2\zeta_{YR} s + 1}{\omega_{n\psi}} \right) \right] \left(\frac{1}{s} \right)$$

Section 2

$$(II-40) \quad \frac{\phi}{\delta_R} = \frac{1}{d_R} \left[K_{\phi} \frac{\delta}{\delta_R} (T_{\phi_R} s + 1)(T_{\phi_{R_2}} s + 1) \right]$$

$$\text{WHERE } d_R = (-T_S s + 1)(T_T s + 1) \left(\frac{s^2}{\omega_{ND}^2} + \frac{2\zeta_D}{\omega_{ND}} s + 1 \right)$$

$$(II-41) \quad \frac{a_y}{\delta_R} = U_0 Y_v \frac{\delta}{\delta_R} + U_0 Y_{\delta_R}^* =$$

$$\frac{U_0 Y_v K_{BDE}}{d_R} (T_{ay_{R_1}} s + 1)(-T_{ay_{R_2}} s + 1)(T_{ay_{R_3}} s + 1)(-T_{ay_{R_4}} s + 1)$$

It will be noted that the lateral transfer function denominator d_A or d_R breaks up into two real roots and one quadratic. These roots are characterized by three modes of motion.

The motion resulting from the negative real root T_S is called the "spiral mode" and is, of course, divergent when T_S is negative, as is usually the case. This root has a very long time constant indicating that the divergence occurs slowly.

The positive real root T_T describes the motion called the "roll subsidence mode" which is characterized by a short, stable rolling transient.

The quadratic mode, which is known as "dutch roll," is a yawing, rolling, and sideslipping oscillation with considerable energy in each degree of freedom. Most modern jet aircraft require artificial stabilization for the dutch

roll mode, and a detailed discussion of the design of this type of stability augmenter is presented in Chapter III.

Typical frequency responses for the lateral case are plotted in Figures II-12 through IV . The zero db lines are shown to permit discussion of relative amplitude ratio, and represent approximate gains for a straight wing fighter in the mid-altitude, mid-Mach number range.

It will be noted that the amplitude ratios at the dutch roll frequencies are approximately equal for Figures II-12, II-13, and II-14, indicating that the actual magnitudes of β , ψ , and ϕ in this mode are comparable when the airframe is excited by rudder deflection. Conversely, Figure II-17 shows that when the airframe is excited by aileron deflection, the dutch roll quadratic is nearly cancelled by a quadratic in the numerator of the ϕ/s_a transfer function, resulting in very little change in roll angle at the dutch roll frequency.

Figures II-12 and II-13 show that when the roll subsidence mode is excited by rudder motion this root is almost cancelled by a root in the numerator, which indicates that only small changes occur in ψ and β , and therefore, the motion is predominantly rolling. For aileron deflections, however, Figure II-15 shows that the roll subsidence root T_r is not cancelled in the β/s_a transfer function; therefore this mode is characterized by more sideslipping when excited by aileron deflection than when excited by rudder deflection.

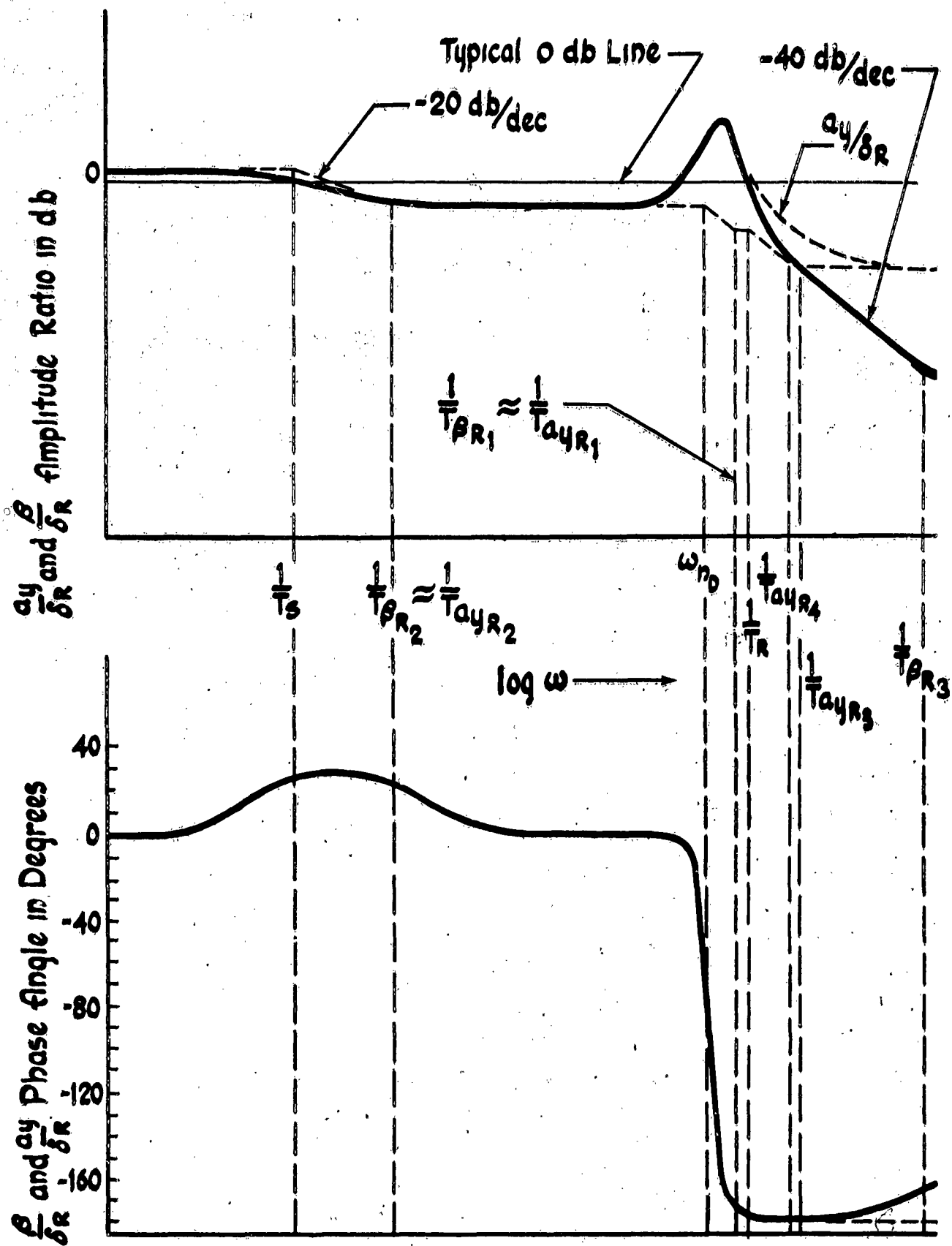


Figure II-12 Amplitude Ratio and Phase Angle of $\frac{\beta}{\delta_R}$ and $\frac{a_y}{\delta_R}$

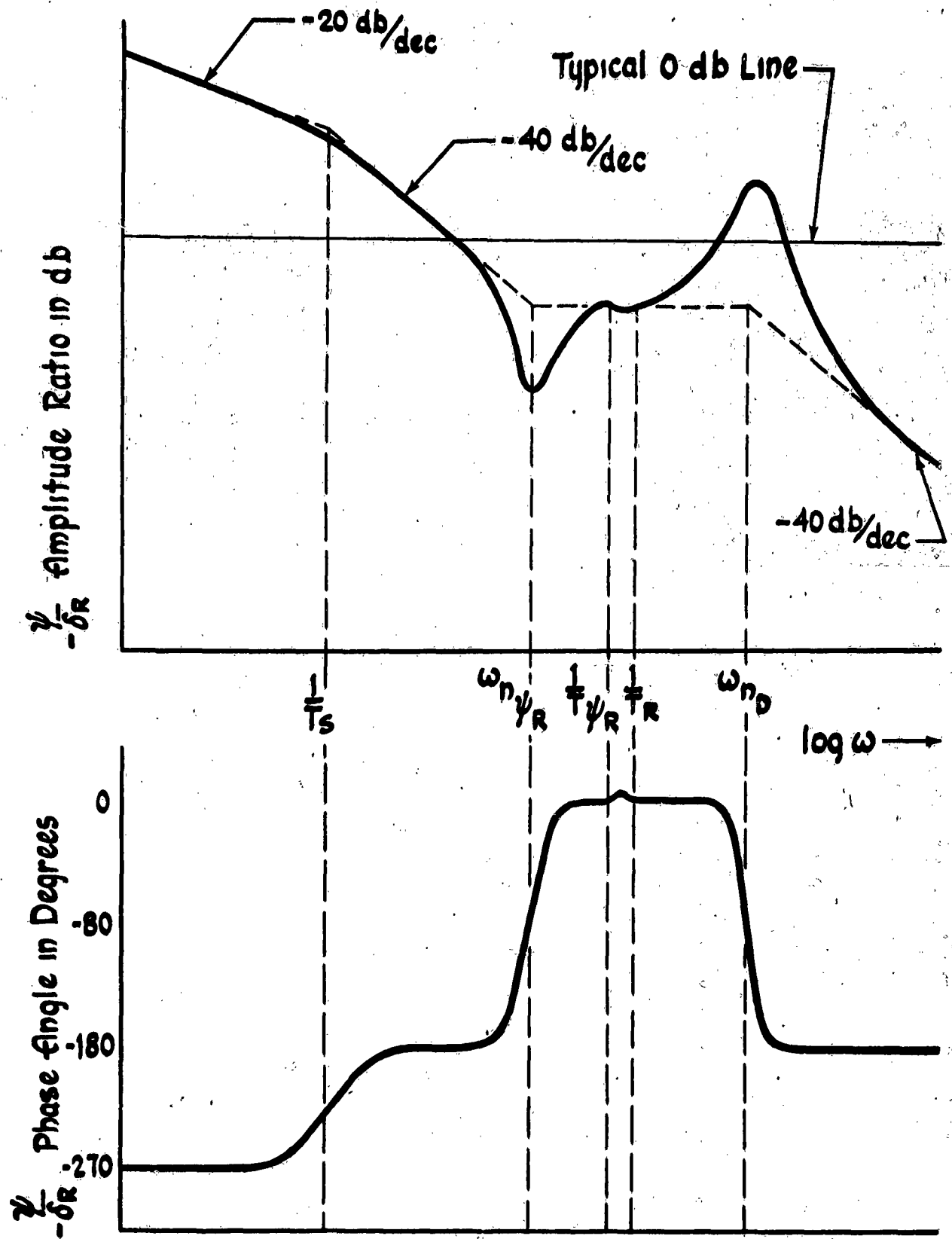


Figure II-13 Amplitude Ratio and Phase angle of $\frac{\psi}{\delta_R}$

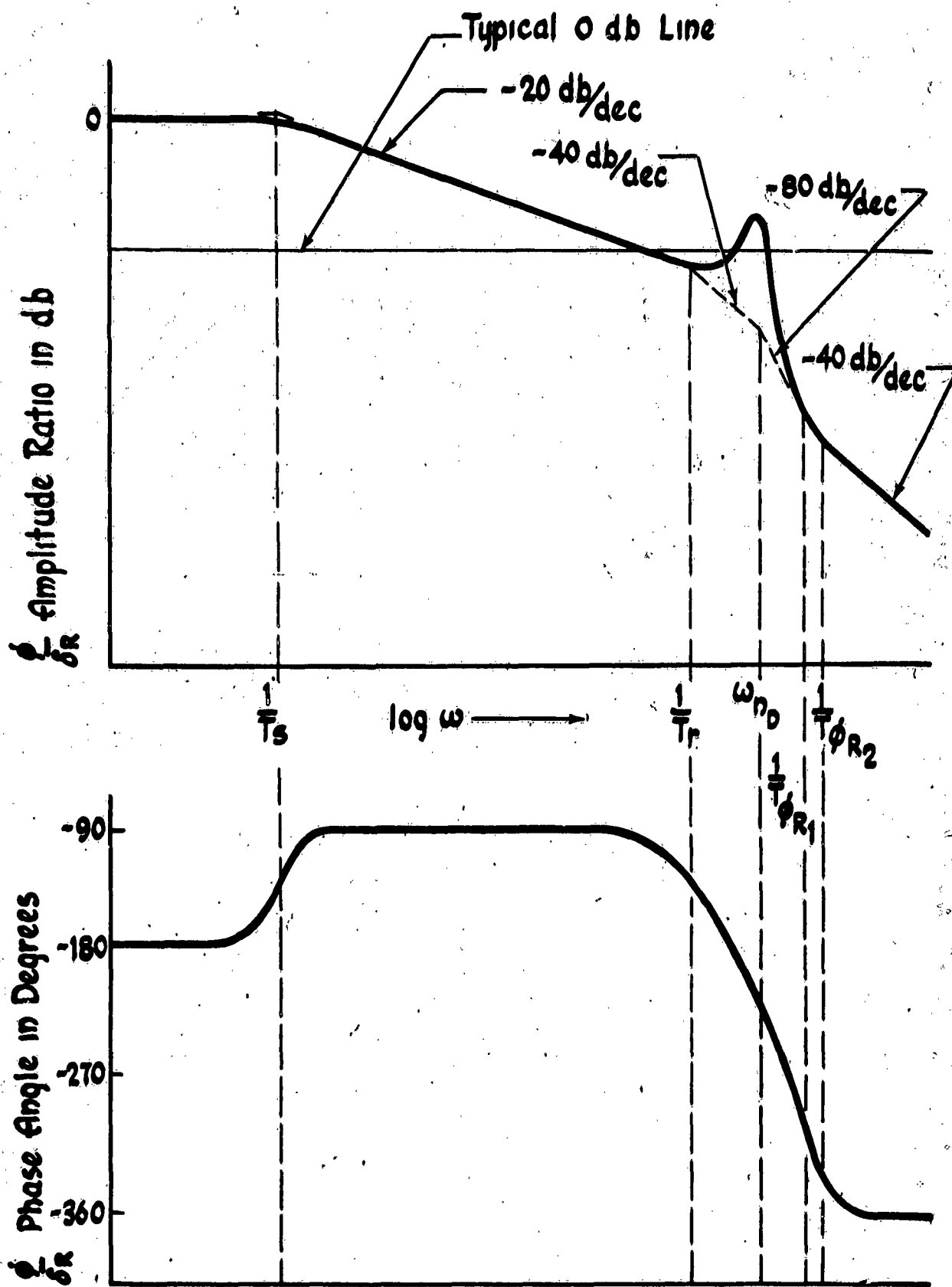


Figure II-14 Amplitude Ratio and Phase angle of $\frac{\phi}{\delta R}$

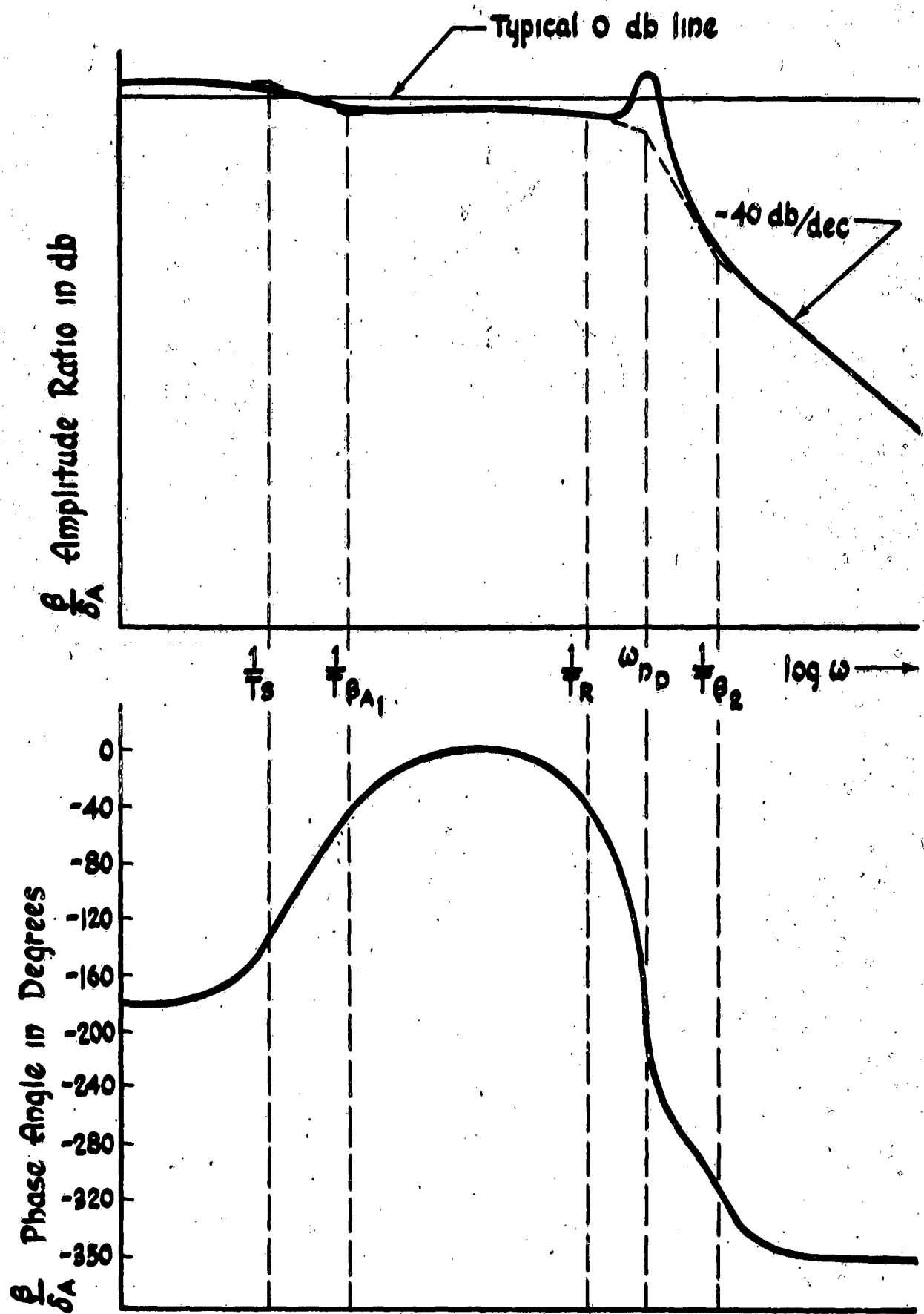


Figure II-15 Amplitude Ratio and Phase angle of $\frac{\theta}{\delta A}$

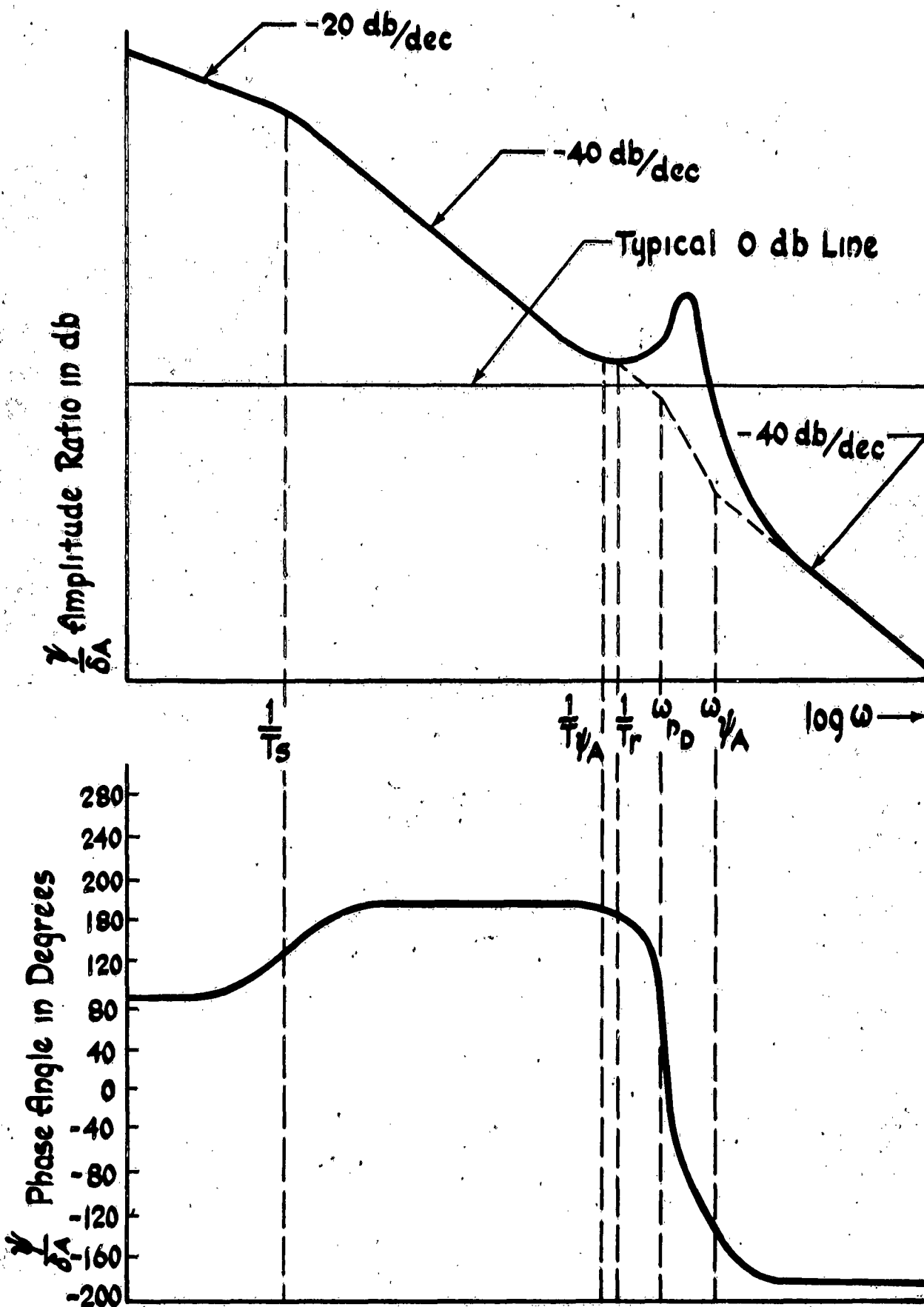


Figure II-16 Amplitude Ratio and Phase angle of $\gamma / \delta A$

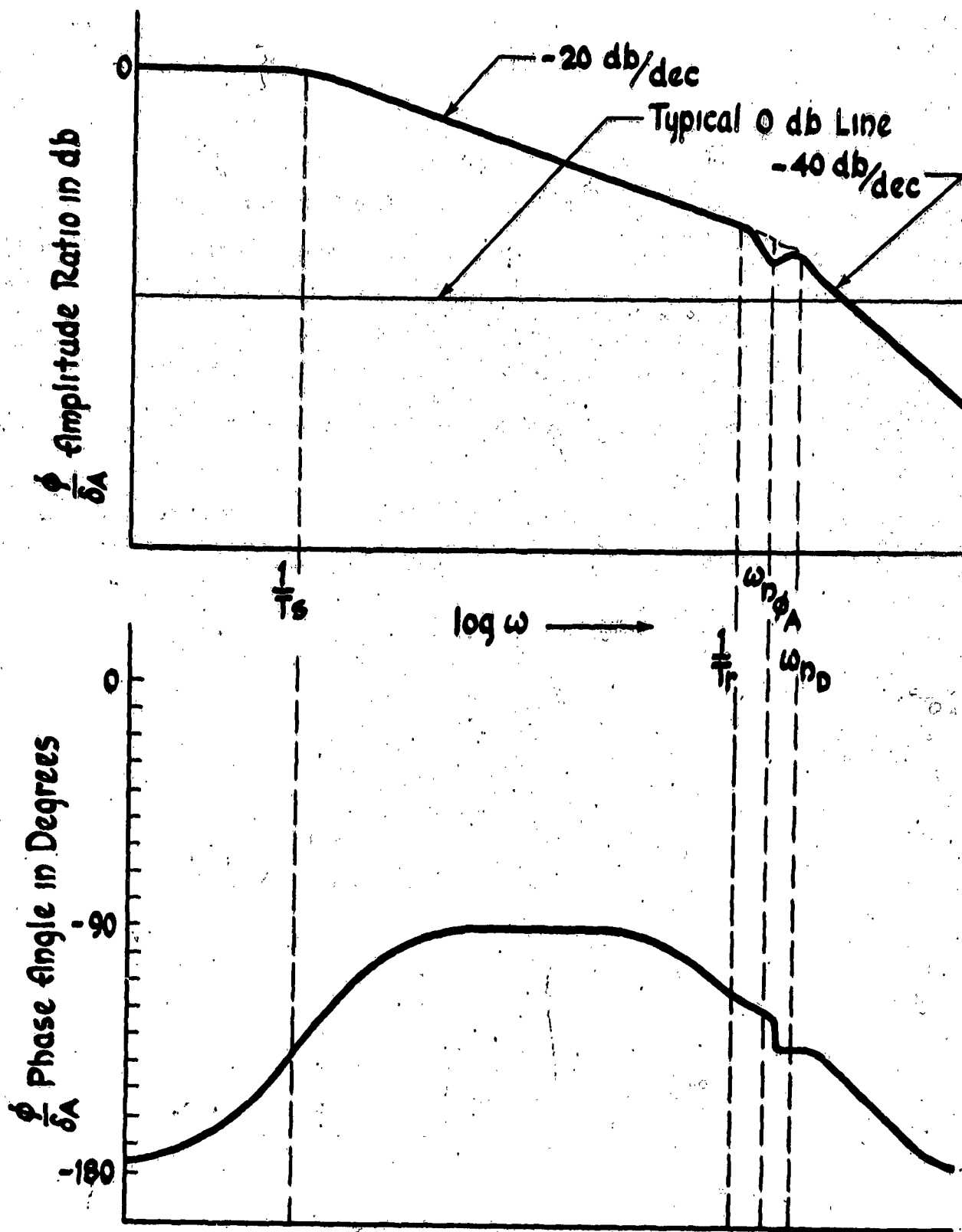


Figure II-17 Amplitude Ratio and Phase angle of $\frac{\phi}{\delta A}$

Section 2

Examination of Figures II-12 and II-15 reveals that the spiral mode is a nearly coordinated ($\beta=0$) rolling and yawing divergence since the amplitude ratios for β/s_r and β/s_a at the spiral break point are much lower than for the rolling and yawing transfer functions.

It can be concluded from the above discussion that the relative magnitudes of β , ψ , and ϕ during a lateral transient depend on whether the transient is excited by the aileron or the rudder. Some conclusions regarding methods of controlling the lateral motions will be pointed out in the discussion of the equivalent stability derivative approach.

Approximate factorizations of the complete lateral denominator yield the following approximations for the roots as functions of the aircraft stability derivatives:

$$\omega_{ND} \approx \sqrt{N_B}$$

$$s_D \approx \frac{-(Y_v + L_p + N_r) - \left(\frac{1}{T_r}\right) + \left(\frac{1}{T_s}\right)}{2\sqrt{N_B}} \quad \text{DUTCH ROLL MODE}$$

$$(II-42) \quad T_r \approx \frac{N_B}{-Y_v(L_p N_r) - L_p N_B - \frac{g}{U_0} L_B} \quad \text{ROLL SUBSIDENCE MODE}$$

$$T_s \approx \frac{Y_v(L_p N_r) + L_p N_B + \frac{g}{U_0} L_B}{\frac{g}{U_0} (L_B N_r - L_r N_B)} \quad \text{SPIRAL MODE}$$

These approximations are based on the assumption that $\frac{1}{T_S}$ and S_D are much smaller than $\frac{1}{T_R}$ or ω_{ND} , a condition which usually exists.

(e) AIRFRAME MOTIONS IN TRANSONIC FLIGHT

The preceding discussion has shown the types of airframe motion to be expected at subsonic speeds. Some of the changes in the airframe modes of motion which occur in the transonic speed range are discussed in the following paragraphs.

Consider first the phugoid mode of the airframe. At subsonic speeds, this is usually a low damped, slow oscillation. The undamped natural frequency, as given in (II-28) is proportional to $(M_w Z_u - M_u Z_w)^{1/2}$, where under normal conditions M_w, Z_u and Z_w are negative and M_u is positive. The quantity M_u is a measure of the change in pitching moment caused by a change in speed, and an increase in nose-up pitching moment usually follows an increase in speed; hence M_u is positive.

However, in the transonic region, the center of pressure moves aft to a point where increasing speed decreases the pitching moment; i.e., increasing speed pitches the nose down, tending to increase the speed further. This is known as the phugoid "tuck-under," characterized physically by static instability with airspeed and mathematically by a negative value for M_u .

Section 2

With M_u negative, the quantity $M_w Z_u - M_u Z_w$ can become negative, in which case the phugoid quadratic $\frac{s^2}{\omega_{np}^2} + 2 \frac{\zeta_p s}{\omega_{np}} + 1$ becomes:

$$(II-43) \quad - (T_1 s + 1)(-T_2 s + 1)$$

A method of controlling the "tuck-under" characteristics by means of a stability augments is discussed in Subsection f, which deals with an equivalent stability derivative approach.

A phenomenon similar to the phugoid "tuck-under" is exhibited in the dutch roll mode for certain airframe configurations. In this case, a directional divergence is caused by the nonlinear variation of the yawing moment coefficient C_n with sideslip angle β . For straight wing aircraft, the slope of C_n vs β (or $C_{n\beta}$) is normally positive, indicating static stability with sideslip angle. However, some airframe configurations exhibit negative values of $C_{n\beta}$ for large sideslip angles, in which case N_β becomes negative and ω_{nd} becomes imaginary as indicated in (II-42). The dutch roll quadratic then separates into two first order terms, one of which is divergent.

Another problem encountered at speeds near the transonic range is the increase in airframe sensitivity a_z/δ_E steady state. This ratio can be investigated most easily by examining the longitudinal equations with two degrees of freedom, i.e., with u and its derivatives equal to zero. Then Equations (II-23) become, in simplified form,

$$(II-44) \quad (S - Z_w)w - (U_0 S)\theta = Z_{fE} \delta E$$

$$(II-45) \quad -(M_w S + M_w)w + (S^2 - M_f S)\theta = M_{fE} \delta E$$

From which

$$(II-46) \quad \frac{a_z}{\delta E} = \frac{w - U_0 \theta}{\delta E} = \frac{Z_{fE} (S^2 + a_1 S + a_0)}{S^2 + 2S_{SP} \omega_{NSP} S + \omega_{NSP}^2}$$

WHERE

$$a_1 = -(M_f + U_0 M_w)$$

$$a_0 = \frac{U_0}{Z_{fE}} (M_w Z_{fE} - M_{fE} Z_w)$$

$$\omega_{NSP} = \sqrt{(Z_w M_f - U_0 M_w) \text{ AND } 2S_{SP} \omega_{NSP} = -(Z_w + U_0 M_w + M_f)}$$

In the steady state,

(II-47)

$$\frac{a_z}{\delta E|_{SS}} = \frac{Z_{fE} a_0}{\omega_{NSP}^2} = \frac{-U_0 (M_w Z_{fE} - M_{fE} Z_w)}{Z_w M_f - U_0 M_w}$$

Section 2

For some airframe configurations, this ratio varies through extremely wide limits as the speed is changed in the transonic region. The effect of the change in this ratio on an airplane whose elevator stick forces are produced primarily by a simple spring is to cause wide variations in the "stick force per g" characteristic. It is therefore necessary to augment the aerodynamic characteristics with a more elaborate artificial feel system and/or a stability augments to maintain the stick force per g within more narrow limits. The change in a_z/δ_E ratio is due primarily to a change in M_w which stems from the aft shift in the center of pressure.

The task of designing stability augments is considerably simplified if a rough attempt is first made to determine the effects of various airframe output quantity feedbacks on the system. This is accomplished by means of the equivalent stability derivative approach.

(f) THE EQUIVALENT STABILITY DERIVATIVE APPROACH

In the discussion of the longitudinal dynamics, a short summary was presented of conclusions drawn from an examination of the frequency response curves. It should be remembered, however, that only single degree of freedom control elevator was examined. In cases where there is complex coupling of control elements, the straightforward solutions to control problems are not always evident from the individual frequency response curves alone. Therefore, a considerable amount of reliance for preliminary design work in aircraft automatic control is placed upon an understanding of the effects upon the airframe motions of varying stability derivatives; that is, the controller is considered to create or augment airframe stability derivatives. In this procedure, a

perfect controller is assumed; i.e., the controller is assumed to have no time lags and no nonlinearities. Since the problems of sensing and actuation are ignored by this assumption, the procedure should be used with caution, to insure that only those controllers which are physically realizable are studied.

An example of augmenting, or artificially changing existing stability derivatives, can be examined by assuming that the airframe output quantity u , the perturbation of trimmed forward speed, is fed to the elevator through a perfect controller. Then the surface motion (in this case, elevator motion) is a direct function of u . In other words, the total elevator deflection from trim is

$$(II-48) \quad \delta E = \delta E_P + \delta E_{AUG}$$

$$\delta E = \delta E_P + K_{\delta E u} u$$

where δE_P is the elevator deflection commanded by the pilot,
 δE_{AUG} is the elevator deflection caused by the stability augmenter,
 $K_{\delta E u}$ is the ratio of elevator deflection to change in forward speed, and
 u is the change in forward speed from trim

Section 2

Substituting (II-48) into the pitching moment Equation of (II-23),

$$(II-49) \quad -M_u u - (M_{\dot{w}} s + M_{w'}) w + (s^2 - M_q s) \theta =$$

$$M_{\delta_E} (\delta_{EP} + K_{\delta_{EU}} u)$$

OR

$$(II-50) \quad -(M_u + K_{\delta_{EU}} M_{\delta_E}) u - (M_{\dot{w}} s + M_{w'}) w + (s^2 - M_q s) \theta =$$

$$M_{\delta_E} \delta_{EP}$$

Note that by this artificial means the basic airframe stability derivative

M_u has been augmented so that

$$(II-51) \quad M_{u \text{ AUG}} = M_u + K_{\delta_{EU}} M_{\delta_E}$$

By a similar procedure, using the Z force equation of (II-23), it can be shown that the basic derivative Z_u is augmented in such a way that

$$(II-52) \quad Z_{u \text{ AUG}} = Z_u + K_{\delta_{EU}} Z_{\delta_E}$$

Substituting these augmented or equivalent stability derivatives into the expression given in Equation (II-28) for the phugoid natural frequency gives

$$(II-53) \quad \omega_{np} = \frac{1}{\omega_{nsp}} \left[g (M_w Z_{u,AVG} - Z_w M_{u,AVG}) \right]^{1/2}$$

$$\omega_{np} = \frac{1}{\omega_{nsp}} \left\{ g \left[(M_w Z_u - M_u Z_w) + K_{\delta_{Ea}} (M_w Z_{\delta} - M_{\delta} Z_w) \right] \right\}^{1/2}$$

By properly choosing $K_{\delta_{Ea}}$, the quantity under the radical sign can be made positive even in the transonic speed range where the airframe by itself normally exhibits tuck-under tendencies.

Thus a cursory study of stability derivatives or, rather, equivalent stability derivatives, can give a preliminary insight into the types of feedback required to accomplish certain functions. In the above cases, it was found that δ_{Ea} feedback can eliminate the tuck-under.

An example of the creation of a new stability derivative occurs when elevator deflection is made a function of normal acceleration as shown in Equation (II-54).

$$(II-54) \quad \delta_E = \delta_{EP} + K_{\delta_{Ea}} a_z$$

Section 2

where

δ_{EP} is the elevator deflection commanded by the pilot

$$K_{\delta_{a_2}} = \frac{\delta_{E_{AUG}}}{a_2}$$

$\delta_{E_{AUG}}$ is elevator deflection caused by augments.

Substituting (II-54) into (II-23) will show that three new derivatives can be created. These are

$$(II-55) \quad X_{a_2} = K_{\delta_{a_2}} X_{\delta_E}$$

$$Z_{a_2} = K_{\delta_{a_2}} Z_{\delta_E}$$

$$M_{a_2} = K_{\delta_{a_2}} M_{\delta_E}$$

With these additional derivatives, the two degree of freedom equations, (II-44) and (II-45), become

$$(II-56) \quad (S - Z_{ww})w - (U_0 S)\theta - Z_{a_2} a_2 = Z_{\delta_E} \delta_{EP}$$

$$(II-57) \quad -(SM_{ww} + M_{ww})w + (S^2 - M_{\theta} S)\theta - M_{a_2} a_2 = M_{\delta_E} \delta_{EP}$$

$$(II-58) \quad (S)w - (U_0 S)\theta - a_2 = 0$$

Simultaneous solution of the above three equations for a_z/δ_E results in

$$(II-59) \quad \frac{a_z}{\delta_E} = \frac{Z_{\delta_E} (s^2 + a_1 s + a_0)}{-(1 - Z_{a_z}) (s^2 + 2\zeta_{SP}' \omega_{n_{SP}}' s + \omega_{h_{SP}}'^2)}$$

where a_1 and a_0 are the same as in (II-46) and

$$\omega_{n_{SP}}' = \frac{[Z_{w'} M_g - U_0 M_w - U_0 M_w + U_0 (M_w Z_{a_z} - M_{a_z} Z_w)]}{1 - Z_{a_z}}$$

$$2\zeta_{SP}' \omega_{n_{SP}}' = - \frac{(Z_{w'} + M_g + U_0 M_w) + Z_{a_z} (U_0 M_w + M_g)}{1 - Z_{a_z}}$$

Two important features of normal acceleration feedback can be noted from (II-59). First, the short period natural frequency and damping ratio are altered, and second, the steady state load factor sensitivity can be increased or decreased depending on the sign of Z_{a_z} and M_{a_z} as shown in (II-60).

$$(II-60) \quad \frac{a_z}{\delta_E / s} = \frac{U_0 (M_w Z_{\delta_E} - M_{\delta_E} Z_w)}{(Z_{w'} M_g - U_0 M_w) + U_0 (M_w Z_{a_z} - M_{a_z} Z_w)}$$

Section 2

The above discussion has illustrated how stability derivatives can be created by making control surface deflections functions of airframe output quantities. A similar discussion would show that the stability derivative L_{ψ} , which is plotted in Figure II-24, would be created by making aileron deflection a function of the yaw angle ψ .

From the particular example used here, it can be concluded that the use of normal acceleration feedback in a longitudinal stability augments materially affects the handling qualities of the basic airframe, not only from the stability standpoint, but also from the control standpoint. By providing some means for varying K_{Sa_z} as a function of flight condition, the stick force per g characteristics of the airframe can be optimized over a wide range of flight conditions.

The effects of varying certain of the lateral stability derivatives are illustrated by Figures II-18 through II-24. Many of the effects shown on the curves are those expected on the basis of the approximate factorizations. Other effects, however, are more subtle and require mention. A complete set of these curves, for both the lateral and longitudinal derivatives, is contained in Reference 9.

For larger values of N_r (Figure II-18), dutch roll damping improves and the spiral root becomes stable. For very large values of N_r , the dutch roll mode splits into two real roots, one of which has a rather long time constant. It is interesting to note that with very large values of N_r , a new mode of oscillation is introduced which has an extremely

low frequency. The derivative N_x has little effect on the roll subsidence root.

The curves for the derivative N_p (Figure II-19) show that a slight negative increase causes the dutch roll to go unstable. A large positive increase increases the damping and frequency of the dutch roll but causes the roll subsidence root to drop off very rapidly until it becomes unstable.

Figure II-20 indicates that increasing N_B has little effect on either the spiral or roll subsidence mode. It does, however, increase the frequency of the dutch roll. Decreasing N_B beyond a certain point causes the dutch roll roots to become real, one of which becomes negative.

Decreasing L_x , as shown in Figure II-21, has little effect on any roots except the spiral root which tends to become stable.

As is expected, the rolling moment L_p , Figure II-22, due to rolling velocity has little effect on the dutch roll but sharply influences the roll subsidence mode. A negative increase of L_p decreases the roll subsidence time constant and tends to make the spiral mode stable.

The effects of varying L_B (Figure II-23), are similar qualitatively to the other roll coupling derivative L_x . There is very little influence on any of the roots, except that a positive increase tends to make the spiral mode stable.

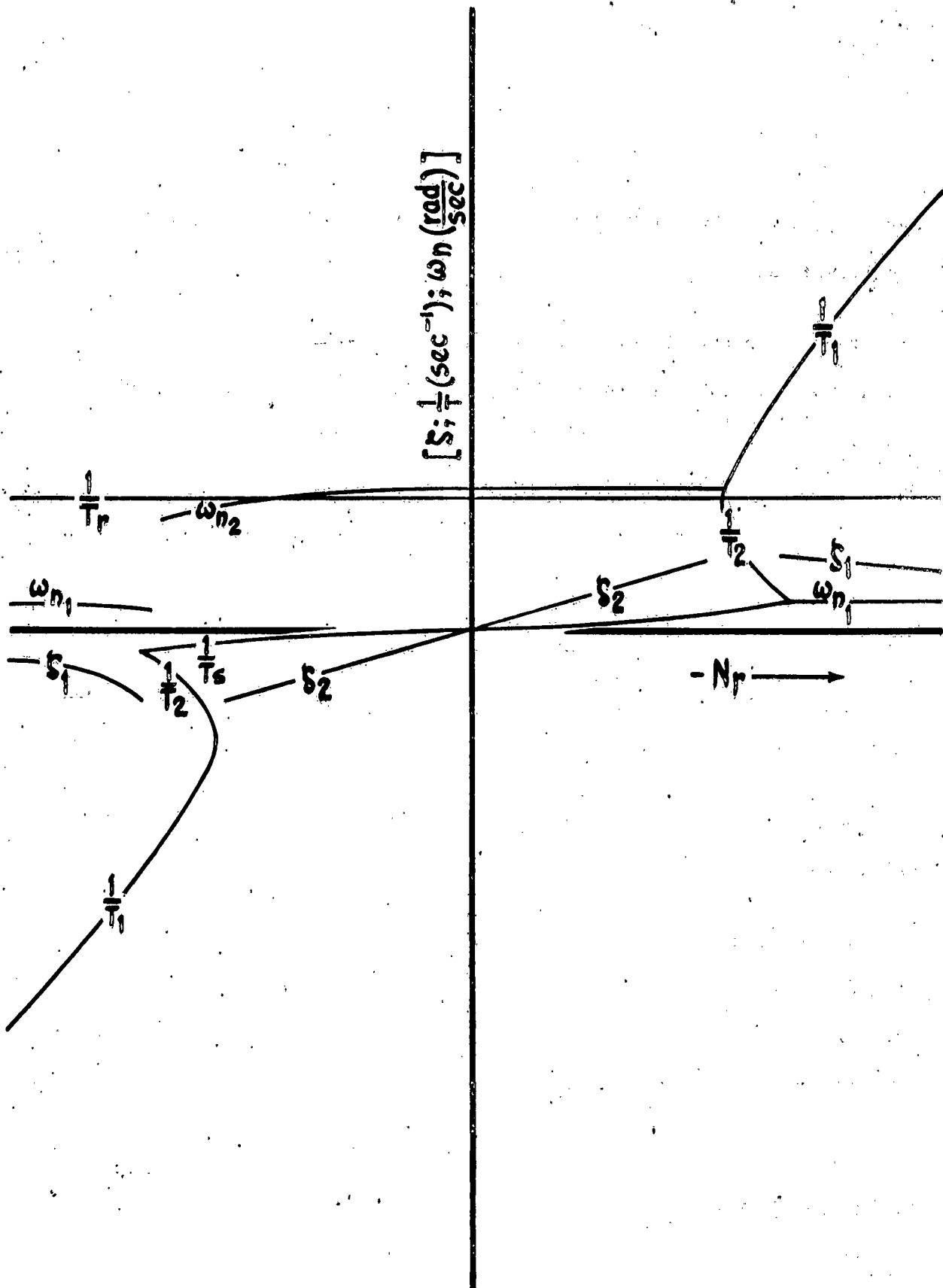


Figure II-18 Effect of N_r on Parameters of the Lateral Characteristic Equation

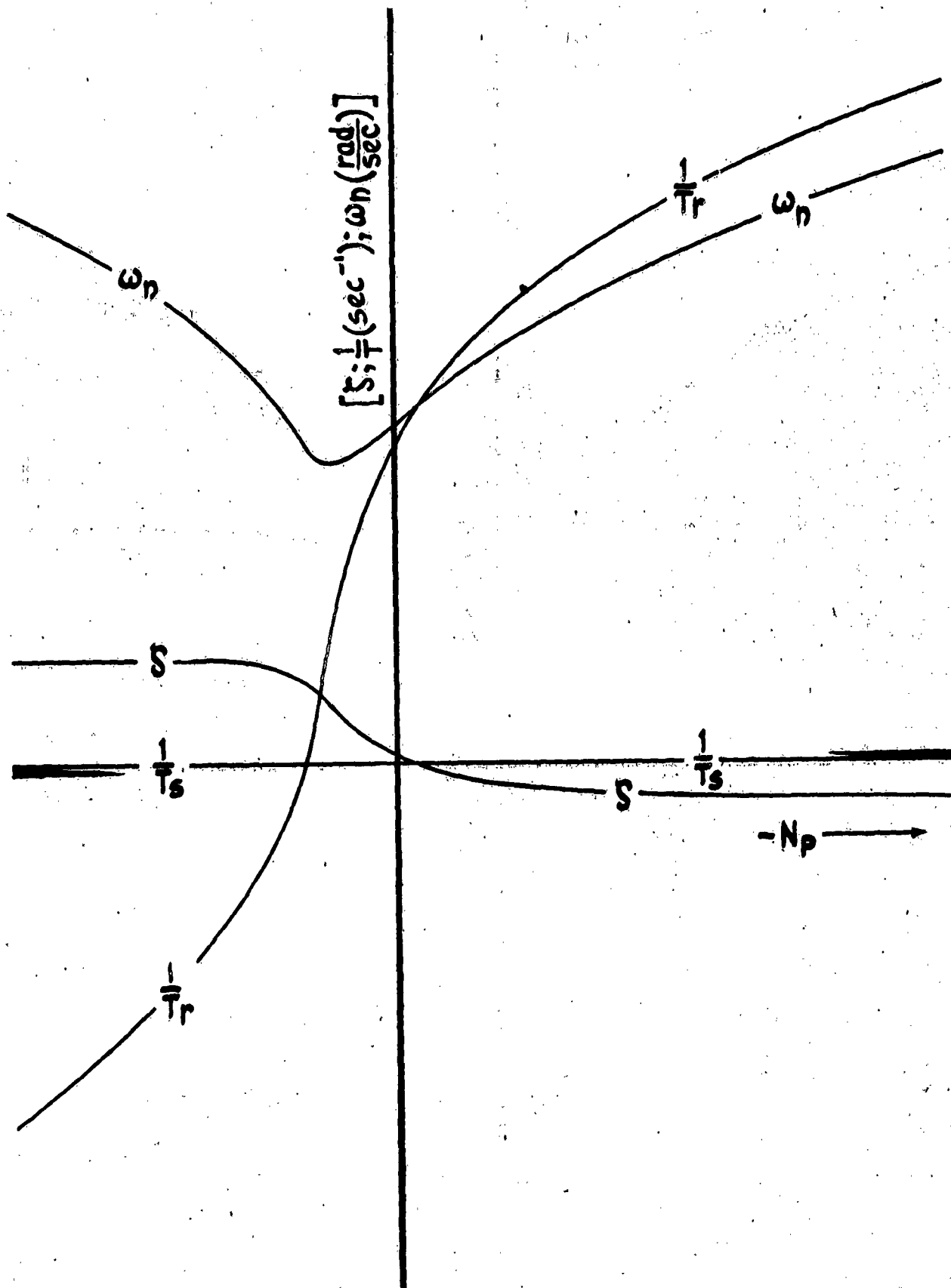


Figure II-19 Effect of N_p on Parameters of the Lateral Characteristic Equation

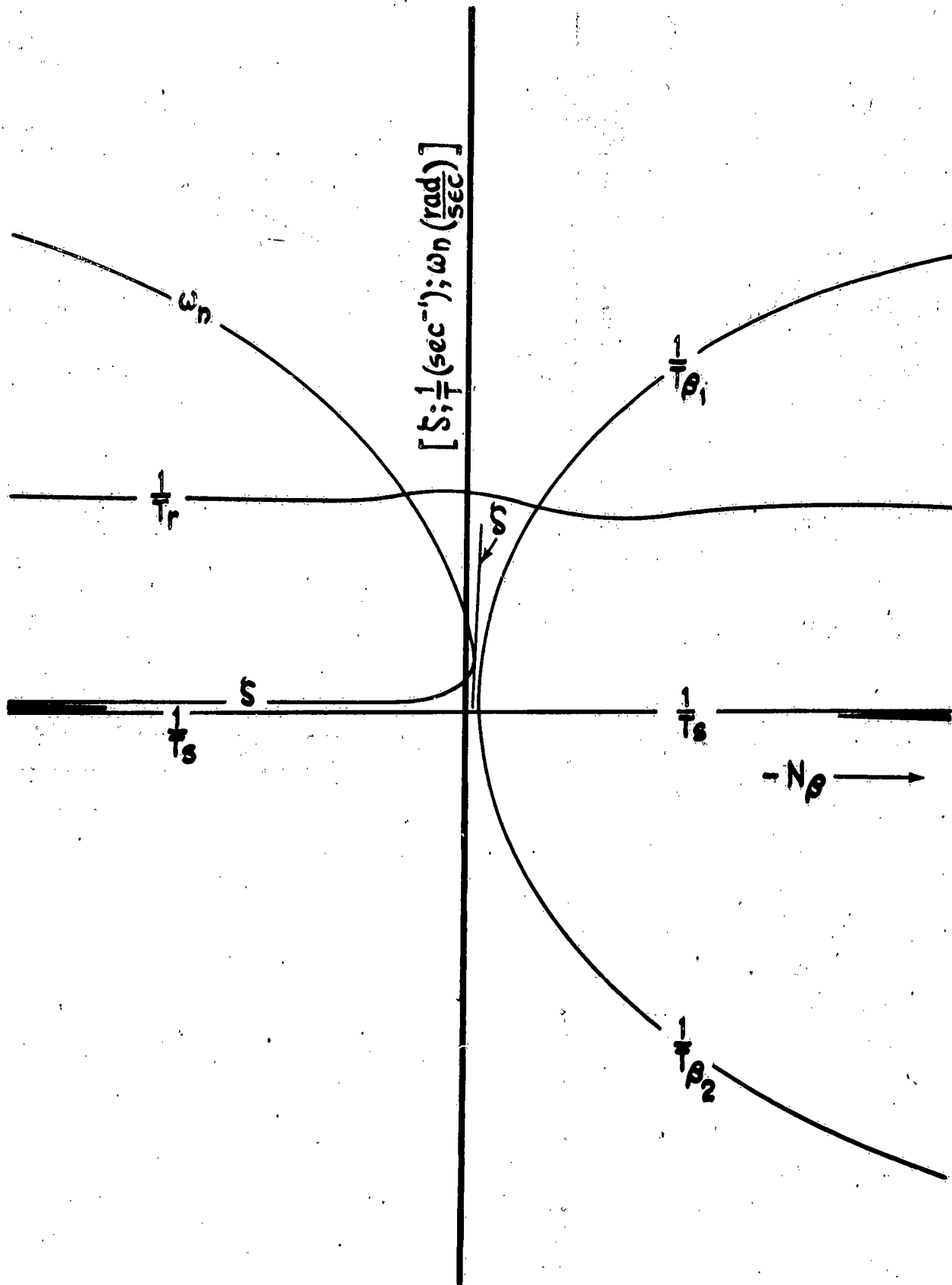


Figure II-20 Effect of N_p on Parameters of the Lateral Characteristic Equation

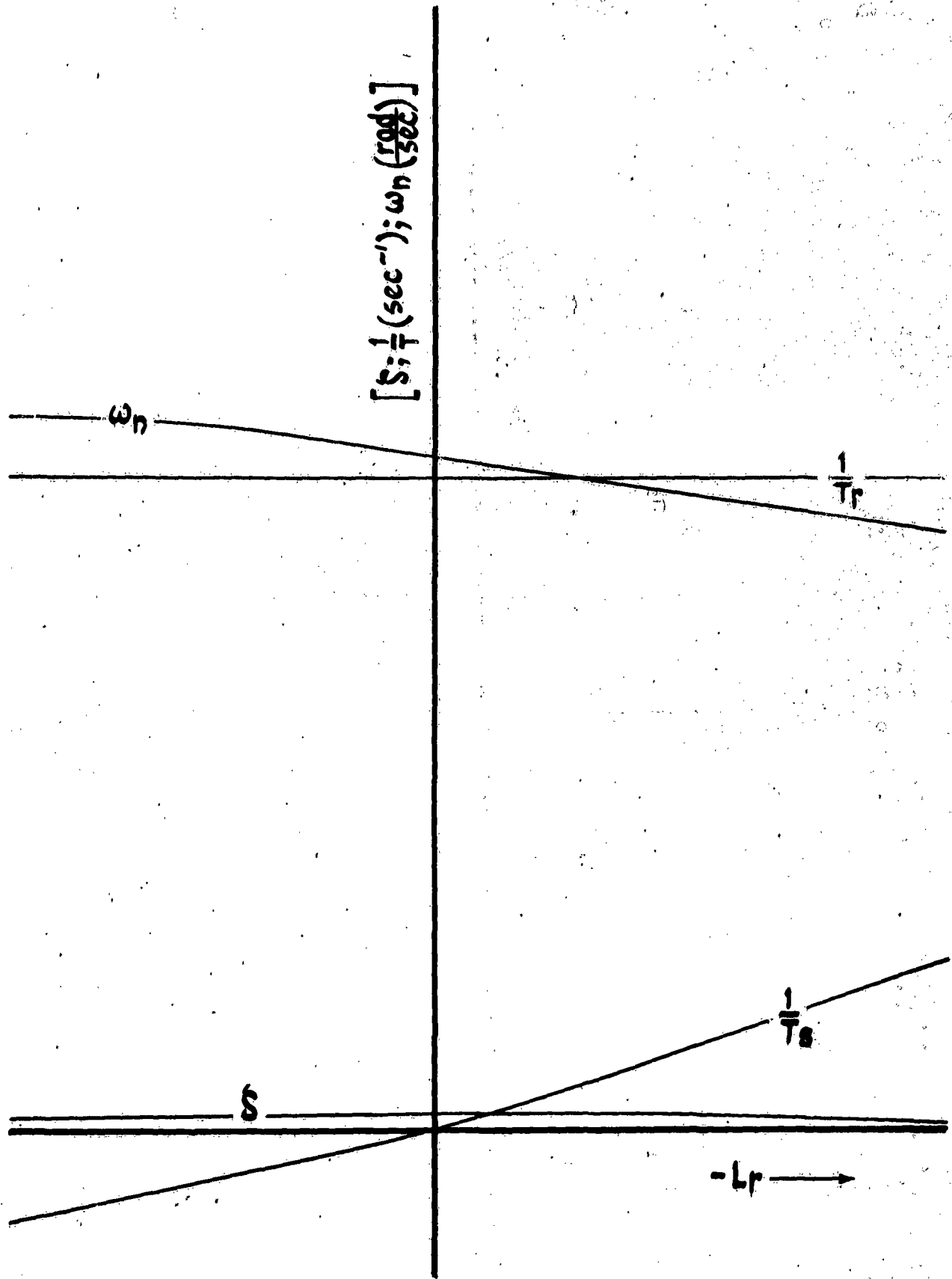
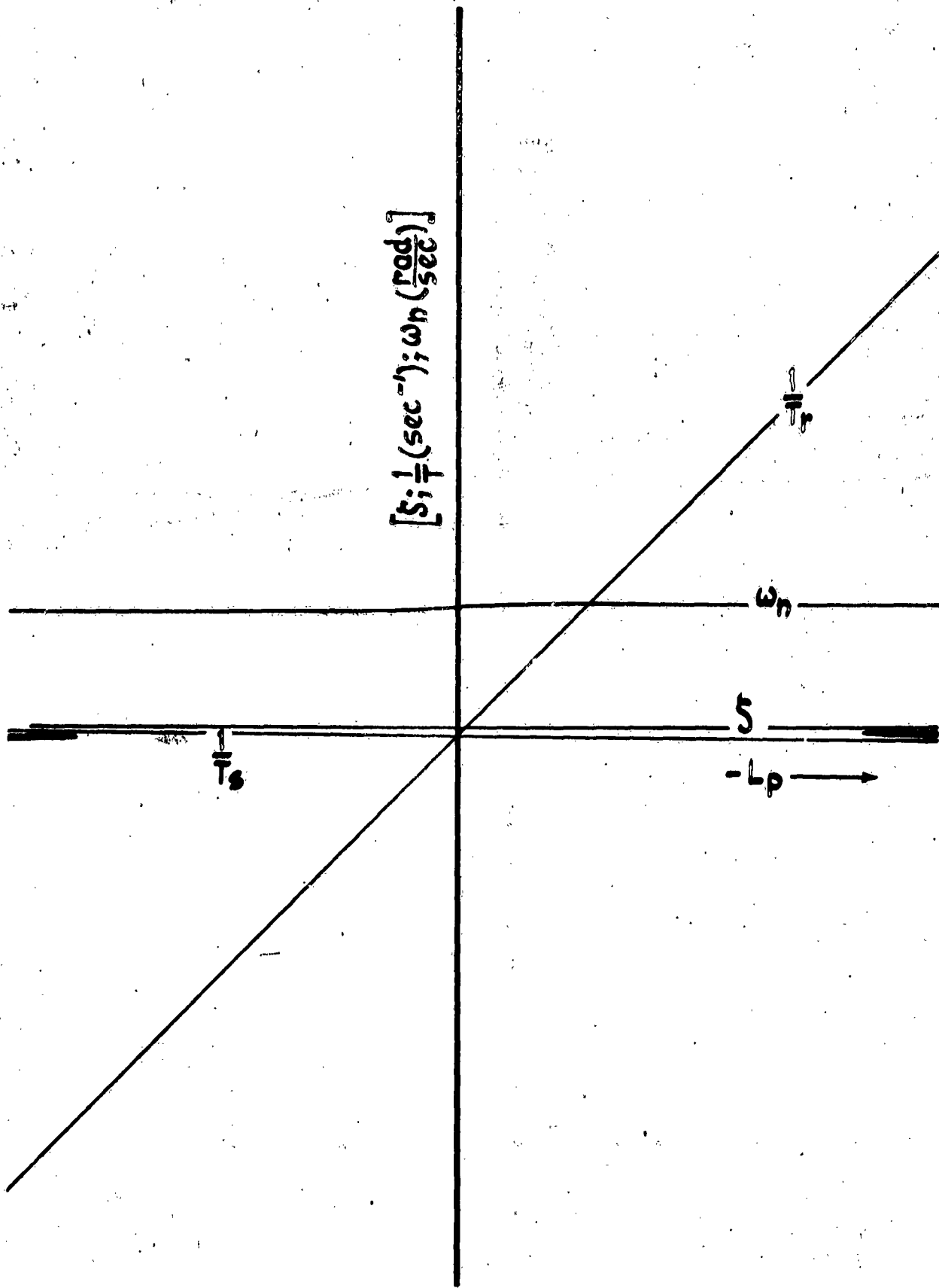


Figure II-21 Effect of L_r on Parameters of the Lateral Characteristic Equation



$$\left[\frac{2\zeta\omega_n}{\omega_n^2} \pm i \sqrt{1 - \zeta^2} \right]$$

Figure II-22 Effect of L_p on Parameters of the Lateral Characteristic Equation

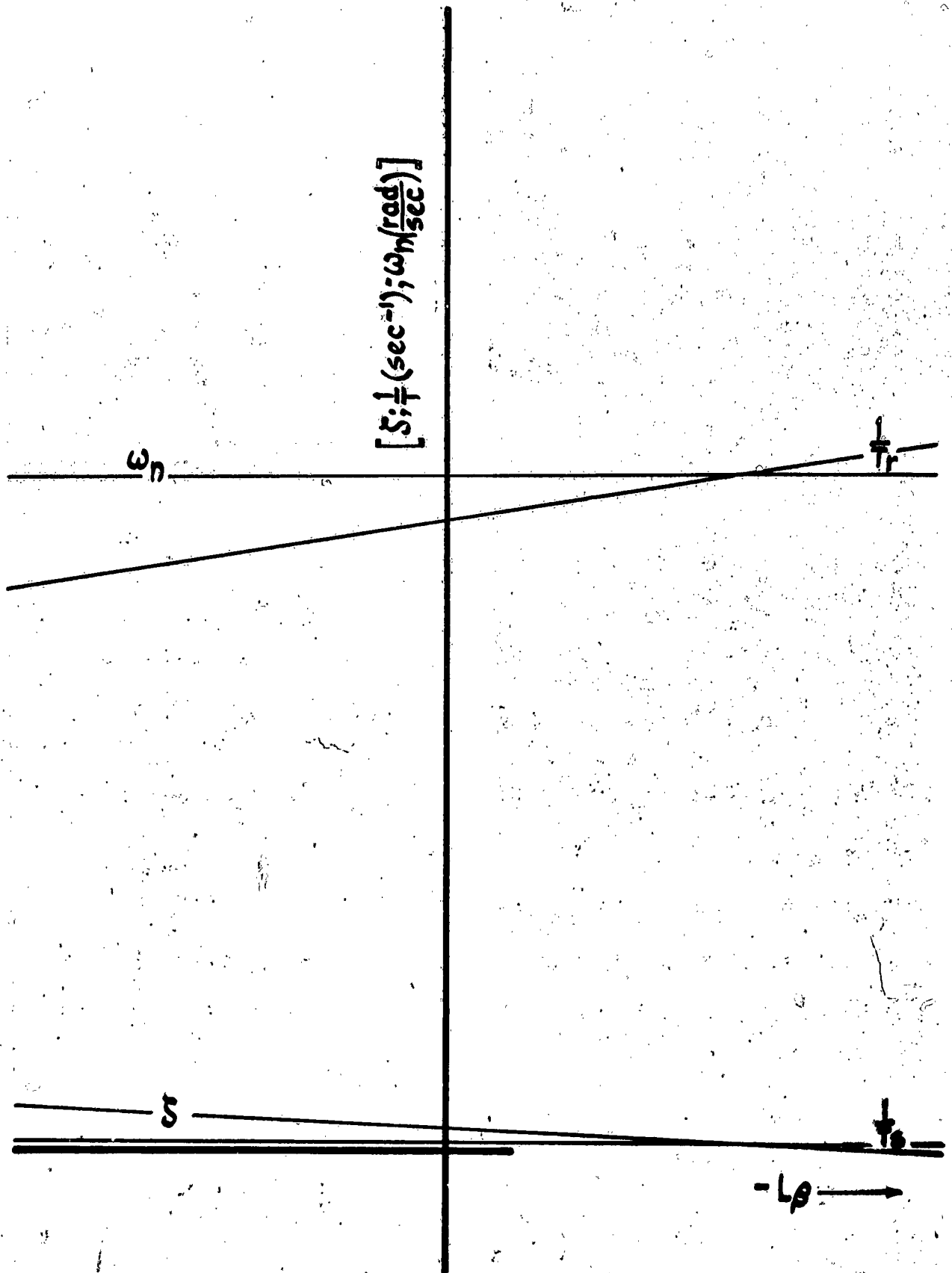


Figure II-23 Effect of L_p on Parameters of the Lateral Characteristic Equation

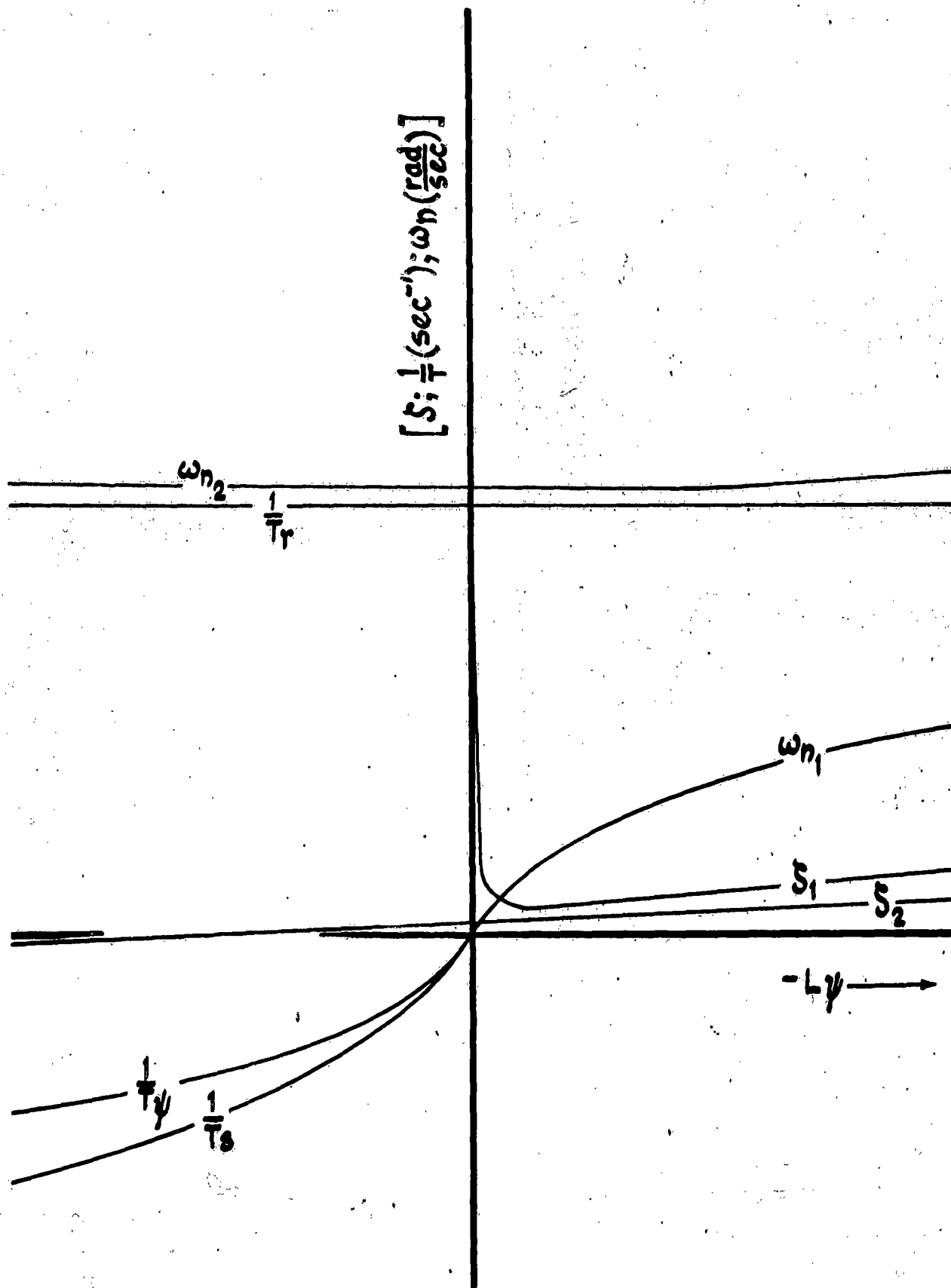


Figure II-24 Effect of $L\psi$ on Parameters of the Lateral Characteristic Equation

The derivative $\dot{\psi}$ does not usually exist physically. However if such a derivative were manufactured by an augmenting device, its effects might be something like those shown in Figure II-24. Notice that the dutch roll mode is not affected by the introduction of $\dot{\psi}$, but that new and undesirable roots are created.

SECTION 3 - THE HUMAN PILOT

In the design of automatic flight control systems, the designer is dealing with a closed loop system comprised of the airframe, the human pilot, and the flight control system. The human pilot's primary function in the closed loop is to sense errors from the desired flight conditions and to actuate the control system to eliminate these errors. The design of the flight control system must enable him to perform his stability and control functions as efficiently as possible. This requires a closed loop analysis of the responses of the whole system to transient disturbances and to inputs from the control surfaces or throttle. Omitting any component of the system from the analysis leads to inaccuracy, and therefore it would be desirable to have a transfer function to represent the pilot response in stabilizing and controlling the airplane.

The purpose of such a transfer function is, of course, to determine analytically the response of a human pilot in the performance of his task. If the stimulus from the environment (or at least an idealized version of it) could be specified as a function of time, then a transfer function for the human pilot would enable the subject's response to be specified as a function of time. Such transfer functions of course cannot

Section 3

describe higher-level, decision-making functions of the human pilot, but they may describe those responses he has learned to make to stimuli he expects to encounter in performing the task for which he is trained. For example, it may be possible to obtain a transfer function specifying the elevator deflection that a trained pilot will produce in response to a sharp wind-gust of the type encountered in flying, but there is no hope that a transfer function could predict the pilot's response when some emergency necessitates a reasoned decision about the proper course to follow, especially if the decision has emotional connotations for the pilot.

Even if the attempt to obtain transfer functions is limited to situations which have become routine for the pilot through training, certain major difficulties make it impossible to determine a unique transfer function. In the first place, the wide variability in reaction time and thresholds for sensory perception among different individuals means that a proposed transfer function must include several parameters which can be varied to account for these individual differences. This in itself is not too serious a drawback. A flight control systems designer could use mean values for these parameters and then vary them to cover the expected range of values; however, experimental results show that, given the same stimulus, three different pilots may respond in three different ways.

The second difficulty is that a normal individual's response to the same stimulus varies considerably from time to time. For instance, as the pilot's attention varies, he may ignore stimuli which ordinarily would cause a response. Thus, the pilot's threshold is not constant for a given stimulus. Furthermore,

numerous studies have shown that a pilot varies his gain, increasing it when necessary, or decreasing it when he is not certain about what to do or when he is simply indifferent. Another source of variation in an individual pilot's response is his ability to predict in various ways: He may use a simple, linear extrapolation, or he may, after being exposed to a varying stimulus for a time, be able to predict completely its future course.

The third difficulty, and the most severe one, is that a transfer function which adequately determines the pilot's response to one type of input, say to a step function, will not be valid for a different type of input, say a sine wave. For any linear system, the transfer function, by definition, is independent of input.

Moreover, there are other nonlinearities in human responses; as a result, the total response to an input stimulus cannot be determined by a linear transfer function. Among these nonlinearities are the following characteristics: the reaction-time delay, during which no response at all is made; the threshold for perceiving the stimulus; the tendency for pilots to underexert when trying to produce large forces or displacements and to overexert when producing smaller forces or displacement; sensory illusions; the upperbounds to forces or rates of motion which pilots can produce; the phenomenon of total prediction; the range effect, in which a subject, after responding to a number of stimuli of roughly the same intensity, will respond in the same way to a new stimulus of a much

Section 3

different intensity; and finally a random jerkiness which is found superimposed on human responses. The conclusion is that it is impossible to represent a human pilot by a single linear transfer function, even subject to the restriction of dealing only with routine, learned responses.

All the known experiments that have been conducted to investigate pilot response have been made subject to the restriction that the pilot was engaged in controlling only a single degree of freedom. There is still hope that a set of transfer functions with variable parameters can be developed which will approximate within satisfactory limits the pilot's response in certain specific tasks. However, since the experiments to determine such approximations have all been conducted in situations during which the pilot was engaged in controlling a single degree of freedom, he was consequently called upon to make only one type of response; therefore these approximate transfer functions cannot be assumed applicable to situations where the pilot is controlling several variables at once. This means that these transfer functions are not necessarily valid for predicting the pilot's response in complicated maneuvers, such as landing or making coordinated turns. However, it is felt that they may be valid for stability investigations, for example in stabilizing the pitch of an airplane in gusty weather, or in controlling a yawing or rolling oscillation. They may also be valid for use in simple one degree of freedom control problems, such as that resulting when a pilot pulls out of a dive or enters a climb. The intelligent use of these transfer functions, however, requires that the designer have a thorough understanding of their limitations.

Since it is not practical to present this background material here, the reader is referred to Reference 10, which includes a comprehensive summary of the information collected on the subject to mid 1954, as well as a selected bibliography. In addition, Reference 10 contains a detailed discussion of such pilot characteristics as accuracy, threshold, force limitations, and time lags.

SECTION 4 - THE SURFACE CONTROL SYSTEM

One of the components of the over-all airplane system which has in the past been considered relatively unalterable to the automatic flight controls designer is the surface control system. For the purpose of this discussion, the surface control system is assumed to include the cockpit controls, the surface actuating package, all the associated equipment which is necessary to interconnect them, and the force producer which is used to provide artificial feel.

A typical elevator control system is shown in Figure II-25. The bobweight shown provides the pilot with forces proportional to airframe normal acceleration, and the artificial feel spring provides forces proportional to stick deflection. The trim motor is included to allow the forces to be trimmed to zero at any desired surface trim angle.

Previous manuals in this series have been devoted exclusively to the hydraulic surface actuating system (Reference 11) and to the artificial feel system (Reference 12), and the reader who is interested in the design of these systems is referred to these manuals. A brief discussion is

Section 4

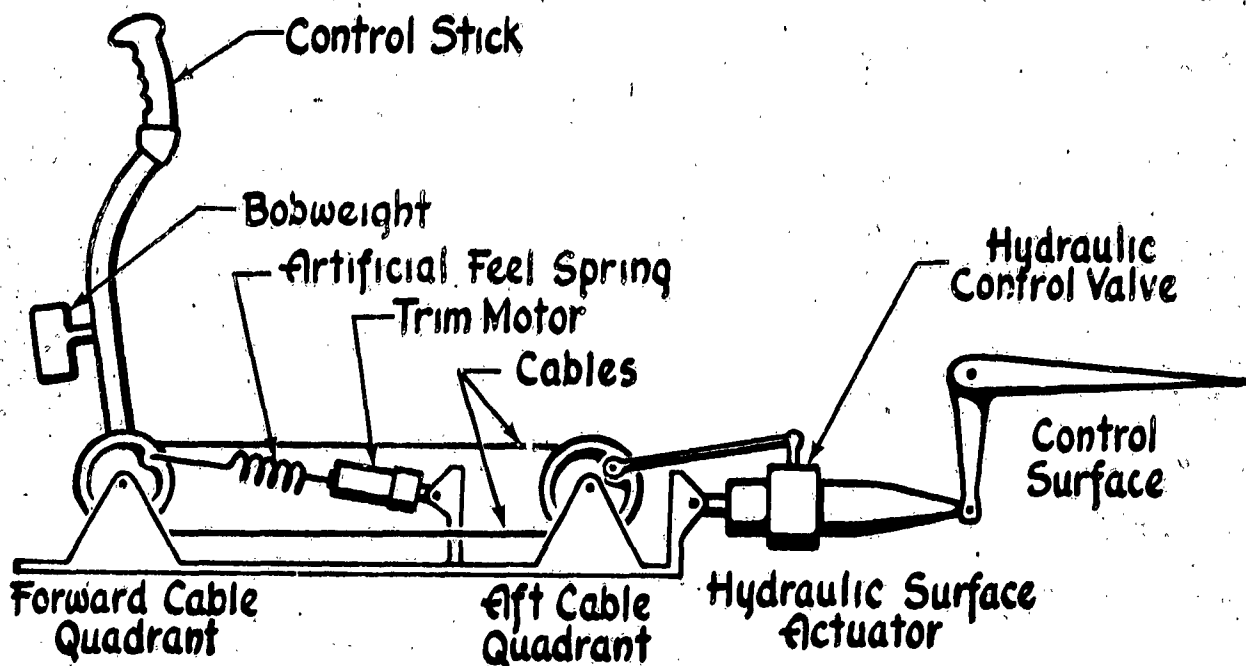


Figure II-25 Surface Control System

given below of those characteristics of the surface control system which are most important to the automatic flight control systems designer.

Controller actuators can be physically connected into the surface control system by means of either parallel or series connection. The parallel connection is identical to that of Figure II-25 except for the addition of the controller actuator cable and cable drums shown in Figure II-26. For this type of connection the controller actuator and the pilot work into essentially the same loads, and motion of the controller actuator is reflected by corresponding motion of the cockpit controls.

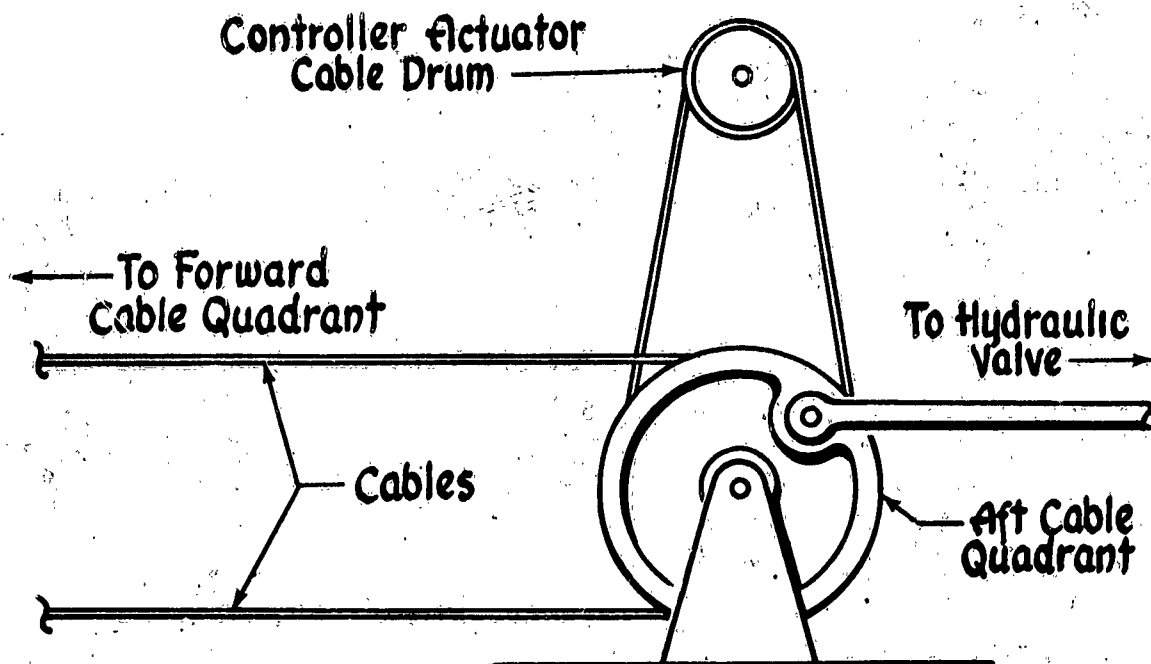


Figure II-26 Surface Control System Showing Parallel Controller Actuator Installation

The series installation (Figure II-27), however, supplies signals to the surface actuator without moving the cockpit controls, and therefore the loads imposed on the controller actuator differ greatly from those of the parallel connection. These differences will be discussed in more detail later.

Because of the high loads involved, most present day surface actuators are designed to provide 100% of the required surface hinge moment. This requirement is met through the use of an irreversible hydraulic servomechanism operating from an essentially constant pressure source.

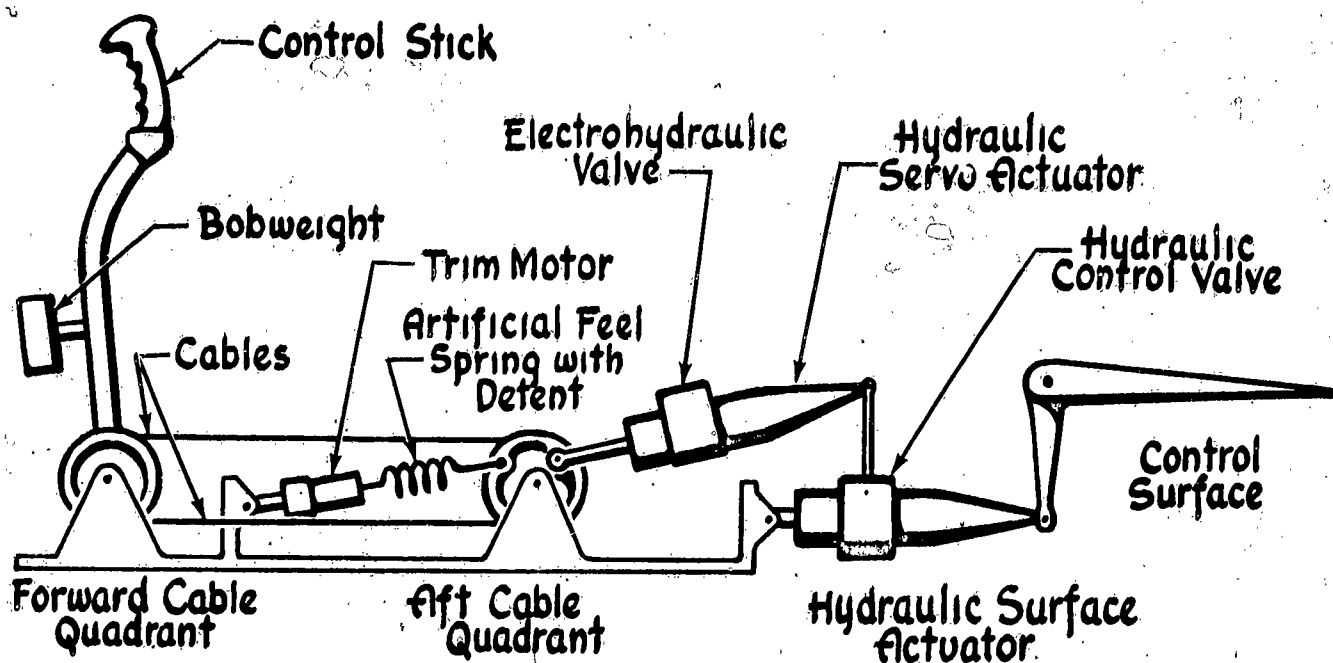


Figure II-27 Surface Control System Showing Series Controller Actuator Installation

Among the characteristics of the surface actuator which are important to the automatic controls designer are the time constant and threshold. The time constant is not of primary importance on a manually controlled airplane since the pilot is capable of rate judgment and can make necessary corrections, within limits, for a large phase lag of the hydraulic system airframe combination. This means that he can introduce a relatively large amount of phase lead since the frequencies involved are usually low. However, the amount of lead which can be introduced through the automatic flight control equipment is limited; therefore, it becomes important that the combined phase curve of the automatic flight control system, hydraulic system, and airframe allow the gain

to be adjusted to give satisfactory control of the airplane. Since the airframe frequency response is dictated by its designed configuration, it is unalterable, and since the phase lead which can be introduced by the automatic flight control equipment is limited, the hydraulic actuator must be capable of making the combined system function satisfactorily. Therefore, it is essential that the surface control system designer coordinate closely with the automatic flight control system designer, to ensure that the two systems are compatible.

When the natural frequency of the surface actuator is substantially higher than that of the automatic flight control system or the rigid airframe, the surface actuator can often be represented by the following transfer function:

$$(II-61) \quad \frac{\delta}{\sigma_v} = \frac{K_h}{T_h s + 1}$$

In Equation (II-61), δ is surface deflection, σ_v is valve deflection relative to the airframe, K_h is the gearing between the actuator and the surface, and T_h is the time constant discussed above. The validity of Equation (II-61) should be checked for each individual system because the construction of the hydraulic valve may cause the actuator to have higher time constants for small inputs. A complete discussion of this phenomenon is given in Reference 11.

Section 4

Another hydraulic system parameter which is important to the automatic controls designer is velocity limiting which occurs when the hydraulic control valve has been completely opened. This can occur when the controller actuator maximum velocity is higher than that of the surface actuator. Tolerable minimums for this characteristic should be determined during the analysis and synthesis phase of the automatic flight control system.

Another important nonlinearity of the hydraulic system is a very small flatspot which occurs when the control valve is near neutral. This flatspot consists of both a threshold, because the valve must be moved through the valve overlap before any flow occurs, and a deadband because the cylinder pressure must build up to overcome the cylinder surface friction. The second effect is usually the more important.

This flatspot manifests itself as a backlash effect as shown in Figure II-28. Backlash of this sort must be kept very small to maintain accuracy of control and to minimize flutter. It seldom exceeds a value of $1/10$ degree of surface deflection.

Aerodynamic loads acting against the hydraulic actuator may reduce the area inside the hysteresis loop so that the curve of Figure II-28 changes to one showing less hysteresis plus a threshold, since the effect of valve overlap is eliminated. In the case of the rudder, where the surface is aligned with the slipstream, the flatspot occurs at neutral (trim), as shown in Figure II-29.

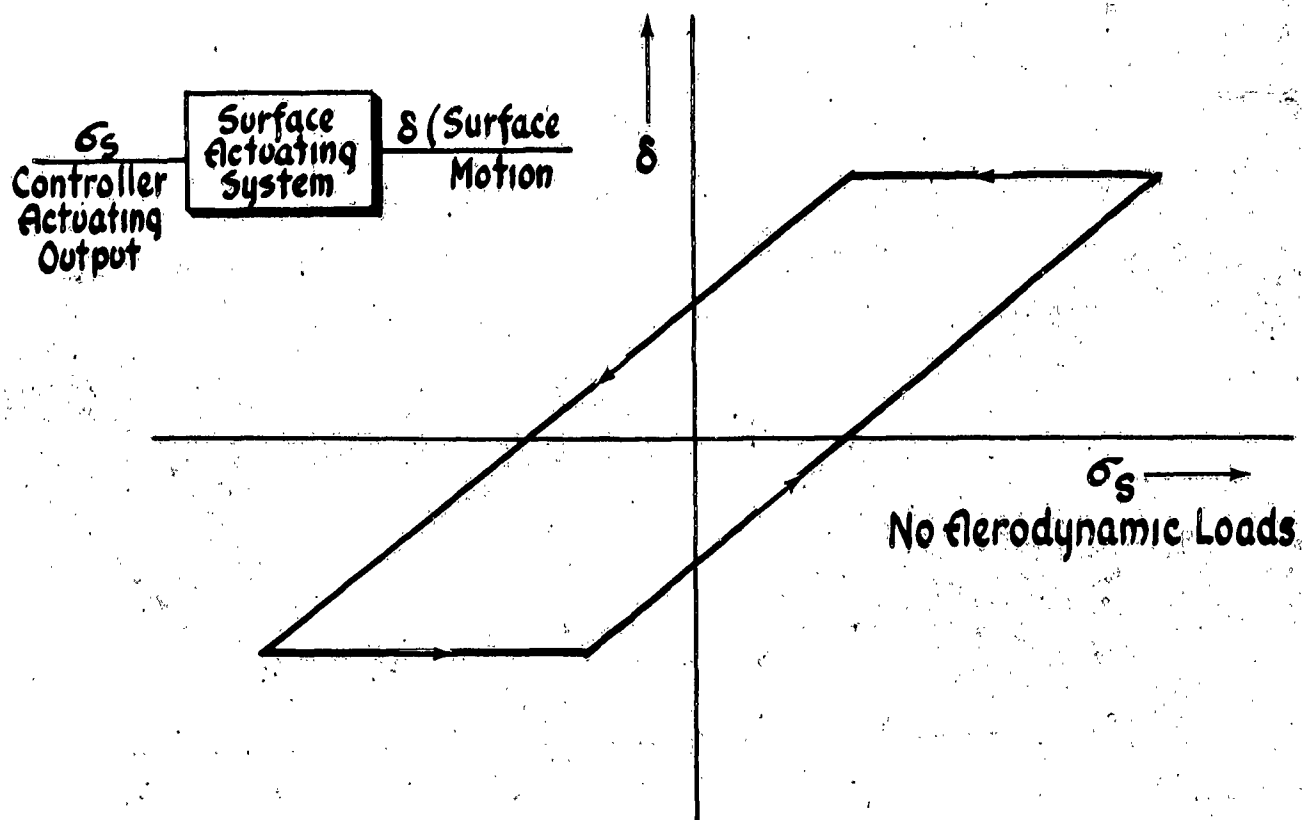


Figure II-28 Hydraulic System Static Characteristic

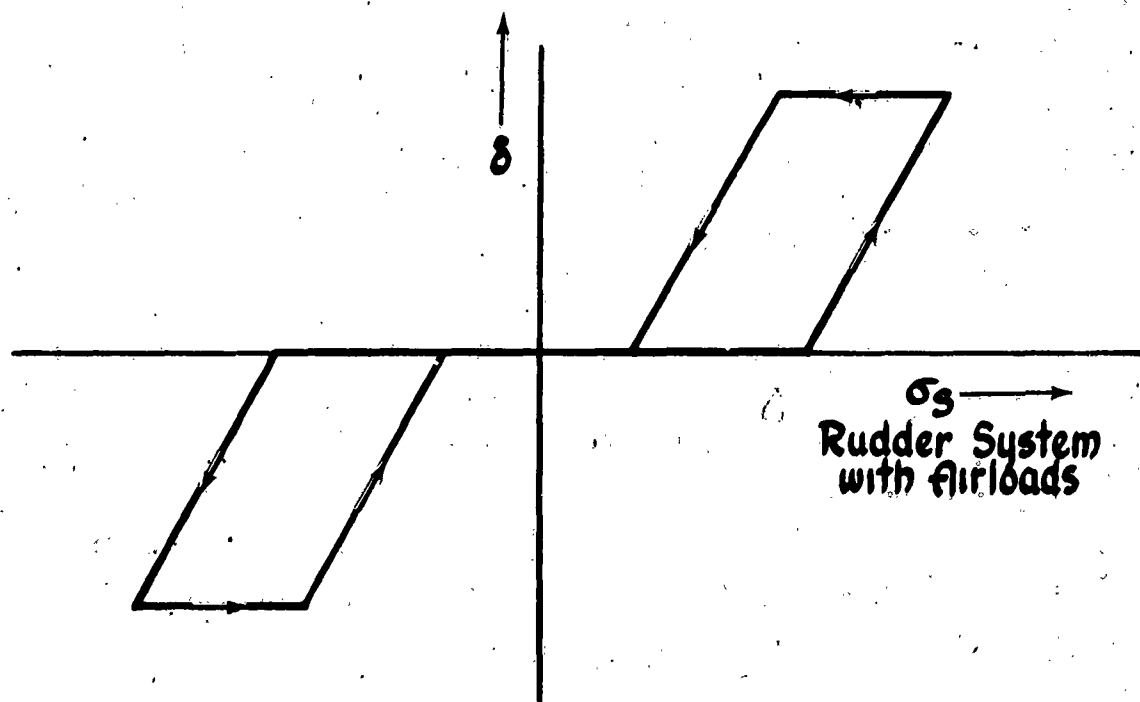


Figure II-29 Hydraulic System Static Characteristic

Section 4

Surfaces like the ailerons and elevators generally have a hinge moment acting upon them at trim so that the flatspot occurs away from neutral. Figure II-30 illustrates this type of curve.

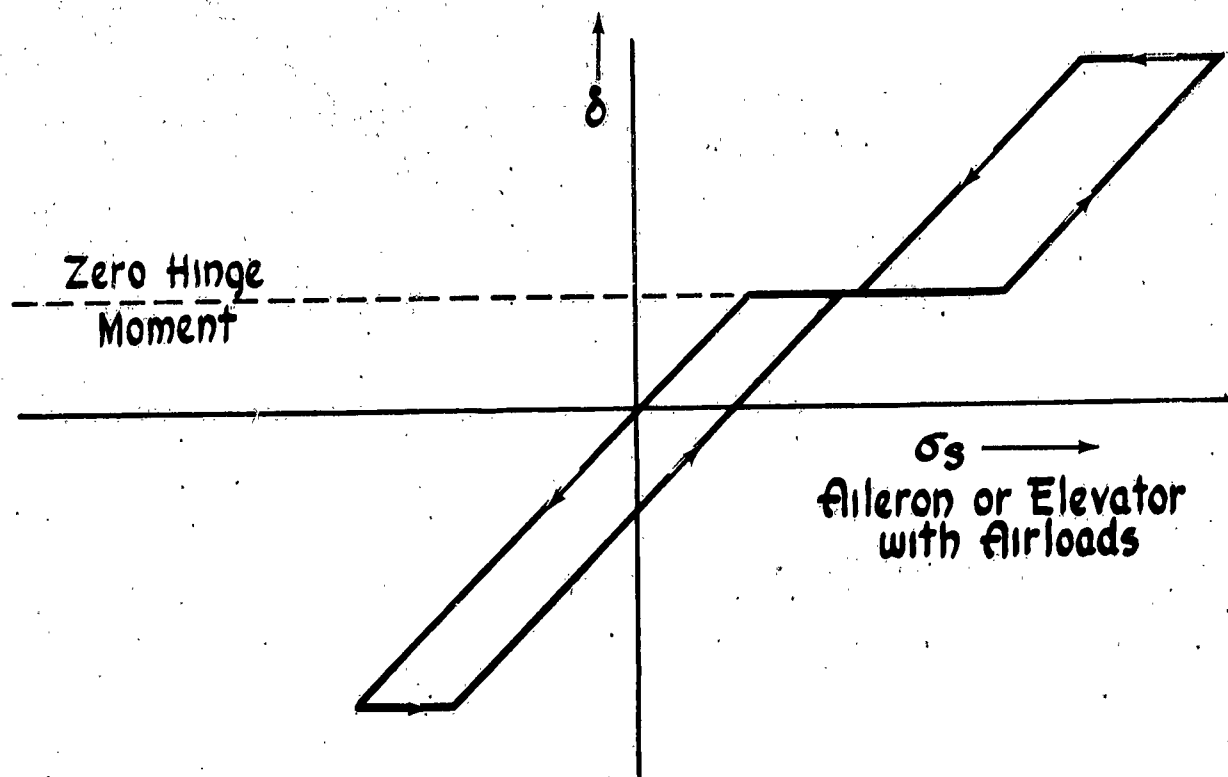


Figure II-30 Hydraulic System Static Characteristic

In the transonic regime, separation may occur at the control surface, and the aerodynamic load may be reduced to zero within the backlash range. This transonic effect aggravates the control surface backlash. Furthermore, it may introduce effective backlash into the airframe block.

Backlash itself between the surface tie point and the valve is effectively preloaded out on some installations by using two hydraulic cylinders, one of which is loaded against the other.

Another surface control system characteristic which must be given consideration by the automatic flight controls designer is the load imposed on the controller actuator. For the parallel installation shown in Figure II-26, the torque loads imposed upon the controller actuator can be considered to be made up of spring, frictional, and inertial elements. For the elevator control system, the effect of the bobweight must also be taken into account.

The spring load normally consists of a spring gradient, which is not necessarily linear, and a preload as shown in Figure II-31. These loads, assuming a linear spring, can be expressed as

$$(II-62) \quad T_s = T_{SP} \cdot (\text{sgn } \sigma_s) + K_s \sigma_s$$

where σ_s is servo rotation, K_s is the spring gradient, and where "sgn" denotes "algebraic sign of." In certain applications, the spring gradient is made the sum of a constant value and a value proportional to

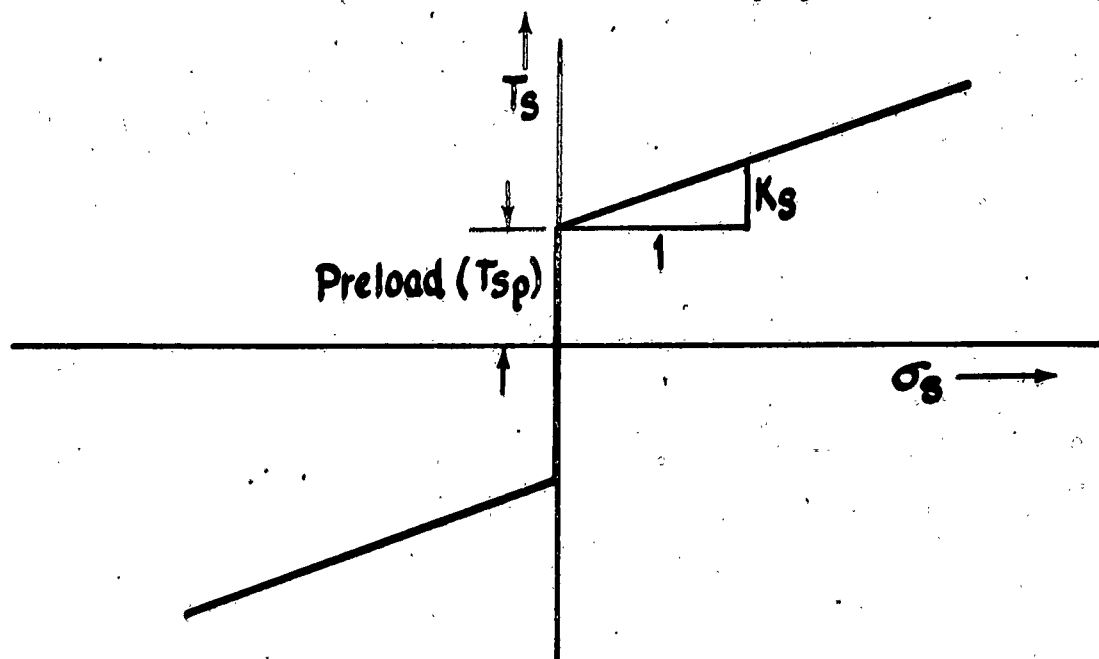


Figure II-31 Typical Spring Loads II-87

Section 2

some function of airspeed to obtain proper feel characteristics. The preload is imposed upon the system to attain reasonable centering of control even though there is control system friction present.

Coulomb friction, which accounts for practically all the frictional loads, is made up of contributions from several sources: (1) cables and pulleys, which give rise to friction concentrated at the pulleys but usually considered distributed, (2) concentrated loads due to the hydraulic valve, and (3) concentrated loads due to bearing surfaces throughout the installation. In addition to Coulomb friction, there are the high stiction forces due to the valves, particularly after long period of control system inactivity. These effects are shown in Figure II-32.

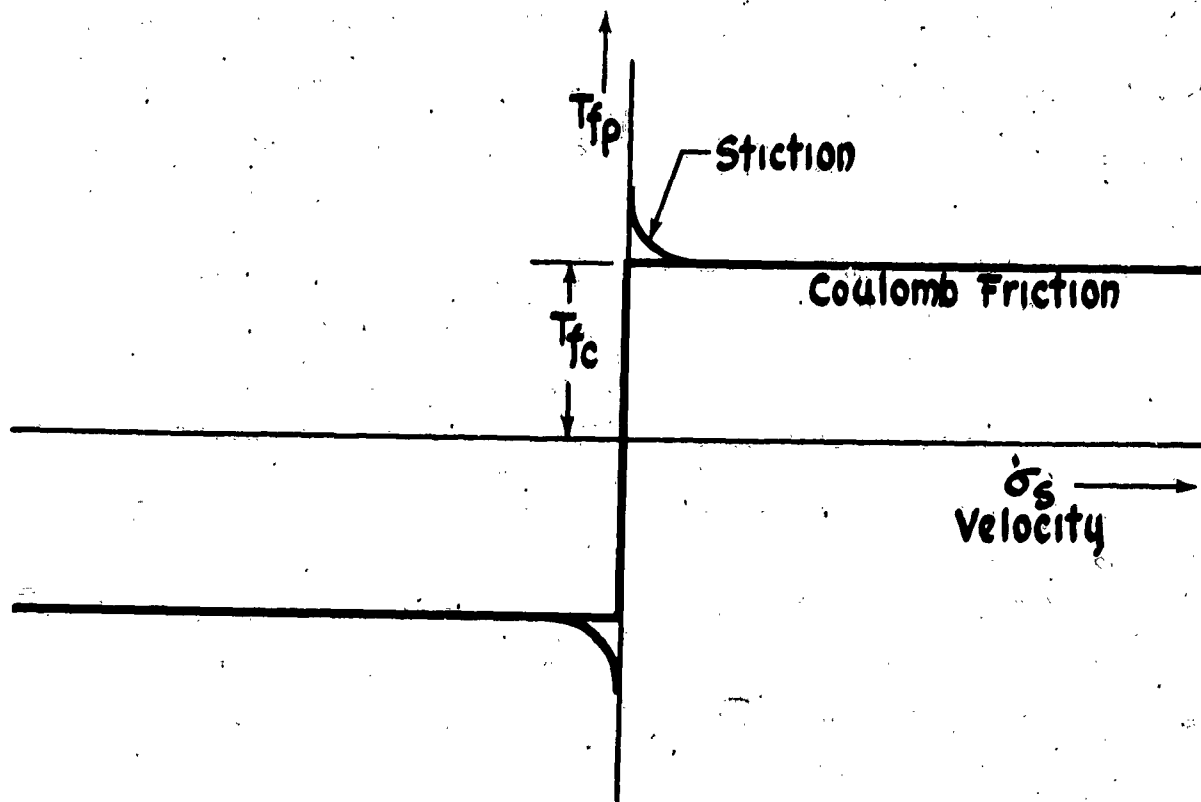


Figure II-32 Typical Friction Loads

The frictional loads, neglecting stiction, can be expressed as

$$(II-63) \quad T_f = T_{fc} \operatorname{sgn} \dot{\sigma}_s$$

The final type of load to be considered is inertial and is due to the masses of all the moving parts of the control system. If a bobweight is a part of the system, a large portion of the effective inertia may be sensitive to the load factor. The inertial torque is then given by

$$(II-64) \quad T_I = K_n (\eta - 1) + I \ddot{\sigma}_s$$

where K_n is the bobweight constant in unit torque at the actuator drum per g, and η is the normal acceleration in g's. Equation (II-64) is plotted in Figure II-33.

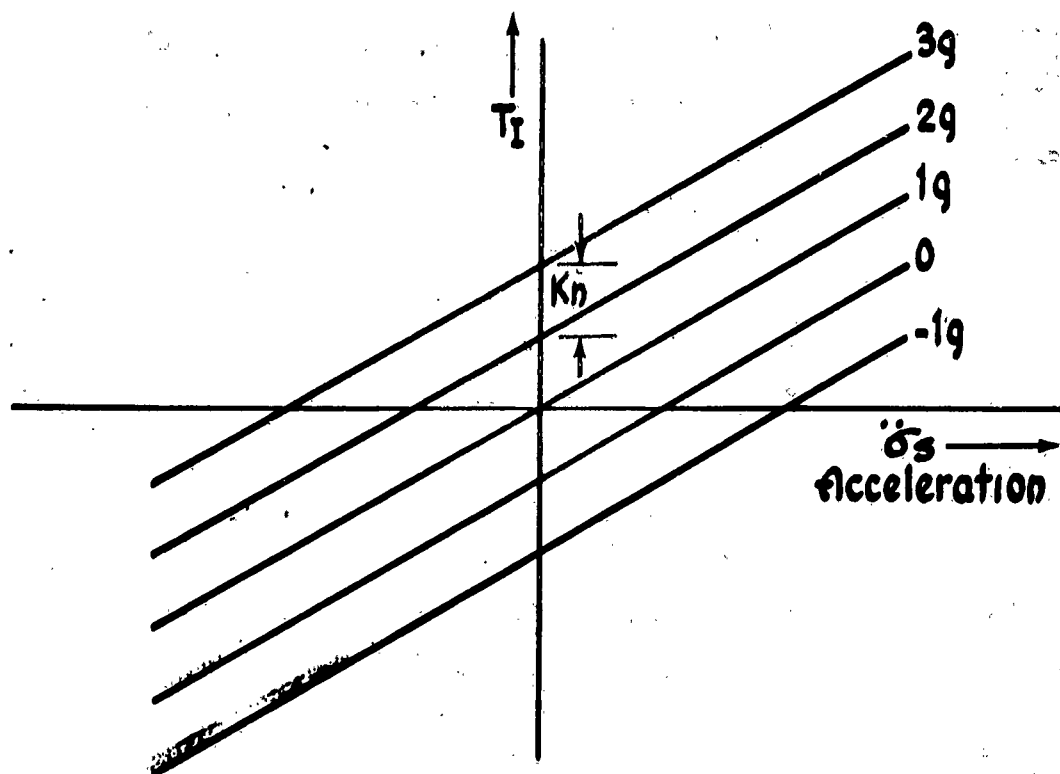


Figure II-33 Typical Inertial Loads

Section 4

The discussion above applies to both push rod and cable systems where the push rods or cables can be considered to act like rigid elements. The total torque on the actuator shaft is then

$$(II-65) \quad T = T_S + T_f + T_I$$

$$T = K_n \dot{\theta} + I \ddot{\theta} + T_c \operatorname{sgn} \dot{\theta} + K_s \theta + T_{sp} \operatorname{sgn} \dot{\theta}$$

This total load must be considered very carefully to make certain that the proper controller actuator is used. Note that the load seen by an actuator which directly moves the surface (without full-power surface actuators) is of the same general form as that discussed for the parallel installation.

The total load curve of (II-65) with the exception of the inertial loads, can be visualized as a hysteresis loop for any given surface amplitude, as shown in Figure II-34.

It should also be noted that although backlash may be present somewhere in the system, the effective backlash from the valve to the controller actuator or stick can be kept very small or often completely preloaded out of well-designed systems.

The series installation, one example of which is shown in Figure II-27, is frequently used when stability augmentation during pilot controlled flight is to be incorporated in the aircraft. It is important to note that because

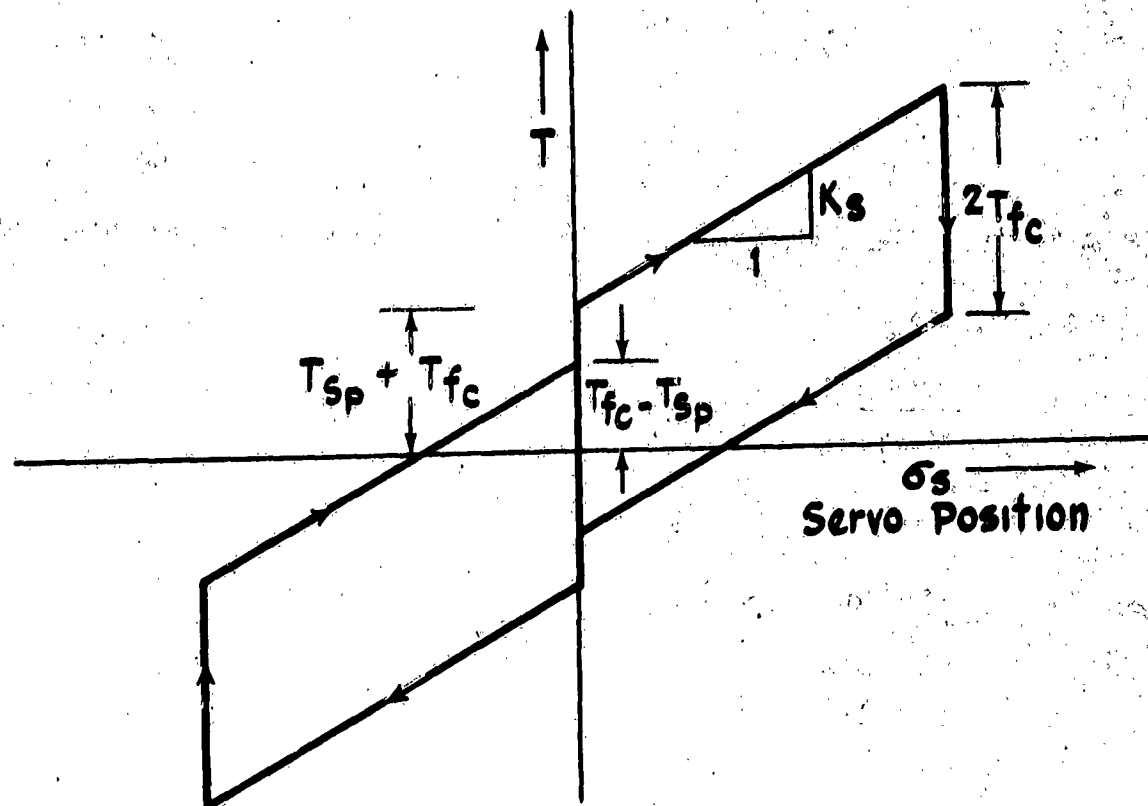


Figure II-34 Hysteresis Loop for a Typical Control System

stability augmentation modifies the required feed characteristics, the artificial feel system can be considerably simplified. A discussion of this concept is given in Reference 12.

In the series installation, the actuator is essentially an adjustable extendor within the cable or push rod system. For satisfactory feel characteristics, it is important that the pilot be unaware of any system movement originating from the operation of the controller actuator; i.e., movement of this sort must not be transmitted to the cockpit controls. For motion to get to the valve, but not to the cockpit controls requires an irreversible anchor for the extendor to operate from; i.e., the

Section 5

mechanical impedance looking from the actuator toward the valve must be much less than the impedance looking toward the cockpit controls. This is usually accomplished by installing the actuator as near the valve as possible, and by providing an irreversible anchor by a mechanism such as a detent.

The controller actuator load for the series installation is then made up of the coulomb friction and the inertia of the moving masses between the actuator and the valve. It is occasionally desirable to place a portion of the feel springs and preload in this circuit. The total load is then

$$(II-66) \quad T = I \ddot{\sigma}_s + T_c \text{SGN} \dot{\sigma} + K_s \sigma_s + T_{sp} \text{SGN} \sigma$$

Normally, however, the load is made up of inertia and coulomb friction only, with almost all the friction load being due to the valve. The load seen by a series installed actuator is therefore very nonlinear, and careful design is required to achieve practical results.

SECTION 5 - SENSORS

To utilize the airframe output quantities listed in Table II-2 for automatic control, they must be sensed, or "picked up," by some means, and this section presents a discussion of some of the devices which are used for this purpose. A qualitative discussion of the gyroscope is presented in Subsection (a). Since gyroscopes are probably used more than any other sensor, it is

important for the automatic flight control system designer to have a thorough understanding of their performance. For this reason, the complete equations describing the behavior of the commonly used forms of the gyroscope are derived in the Appendix. Subsections (b) through (e) discuss the application to automatic flight control systems of accelerometers, local flow direction detectors, local flow magnitude detectors, and altitude sensors. The section is summarized in subsection (f) which includes a table relating the airframe output quantities to the sensors used in measuring them.

(a) GYROSCOPES

Among the airframe output quantities listed in Table II-2 as available for use in automatic control are the airframe angular displacements (ϕ, θ, ψ) and angular rates ($\dot{\phi}, \dot{\theta}, \dot{\psi}$). The device which has been universally utilized for sensing these quantities is the gyroscope.

The gyroscope consists of a rotor (gyro) spinning at high speed and mounted in a set of rings (gimbals) so as to have one or two degrees of angular freedom (see Figure II-35).

Both "free" and restrained gyros are used for aircraft automatic control; however, in practice there are almost always some torques acting to restrict the rotational freedom of the rotor axis in some way, so that there is no clear-cut distinction between free and restrained gyros.

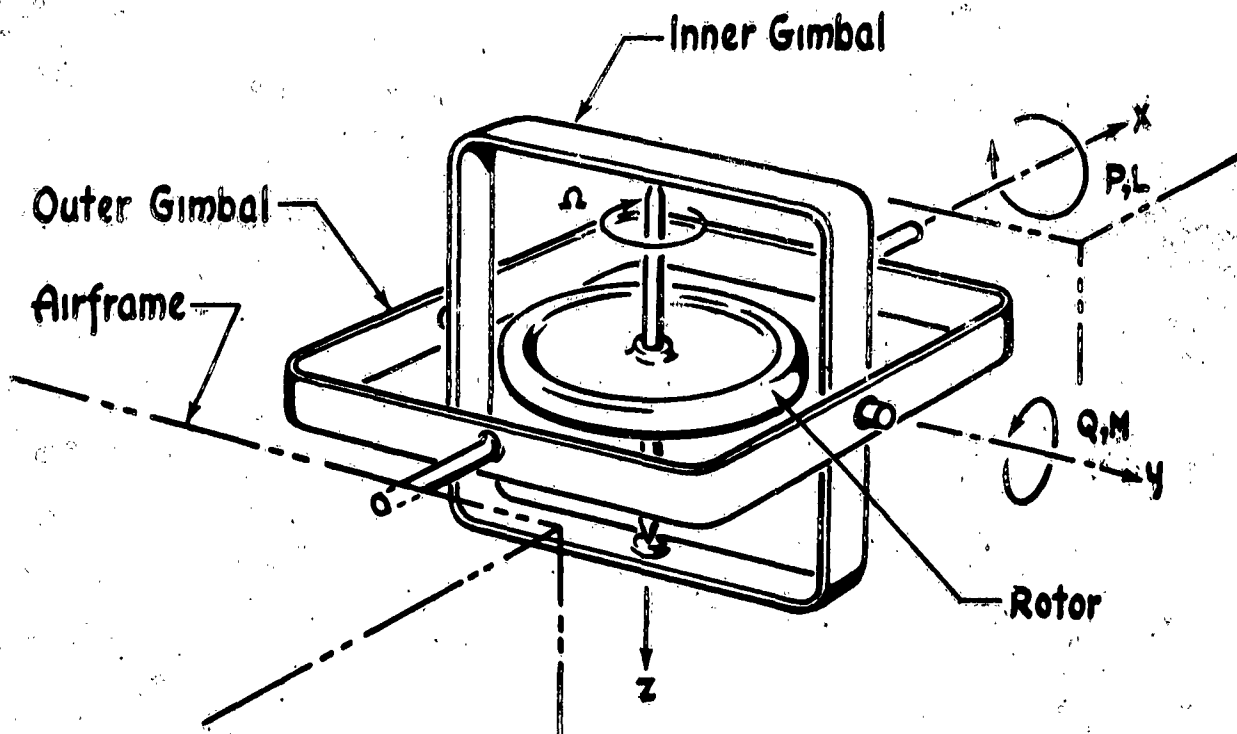


Figure II-35 Two Degree of Freedom Gyroscope

Furthermore, the same laws, the classic laws of Newton, govern the behavior of both types, the free gyroscope being only a special case wherein the restraining torques are zero. The vector equations describing the behavior of the gyroscope are derived in the Appendix, using the laws of Newton. For purposes of discussion these vector equations can be reduced to the scalar equation

$$(II-67) \quad \omega_p = \frac{I}{\omega_s I}$$

plus the rule that the spin vector precesses toward the torque vector. In Equation (II-67), ω_p is the angular velocity called "precession" of the spin axis, T is the torque applied to the spin axis, ω_s is the angular velocity of the rotor about the spin axis, and I is the moment of inertia of the rotor. Equation (II-67) states that if a torque is applied tending to change the angular orientation of the spin axis, the spin axis will rotate (precess) about an axis at right angles to both itself and the axis about which the torque is applied, and at a rate proportional to the applied torque and inversely proportional to the product of the spin velocity and the rotor moment of inertia. The latter product is called the "angular momentum" and is designated by

$$(II-68) \quad H = \omega_s I$$

Then Equation (II-67) can be written as

$$(II-69) \quad \omega_p = \frac{T}{H}$$

which is identical to Equation A-21 of the Appendix.

The law governing the behavior of the gyroscope is reversible, that is, an angular velocity input results in a torque output against whatever restraints are provided, and a torque input results in an angular velocity output. In either case, Equation (II-69) applies.

Section 5

If no torques are applied to the spin axis, the gyro angular orientation remains fixed with respect to inertial (celestial) space, and in this configuration it can be used to measure angular displacement of its case, when suitable pickoff devices are used to measure the angles between the case and the spin axis. Gyroscopes of this type are commonly used in automatic flight control systems to measure the angular orientation of the airframe, the so-called "vertical" gyro being used to measure pitch and roll angle (θ and ϕ) and the "directional" gyro being used to measure airframe heading (ψ).

VERTICAL GYROS

The vertical gyro is orientated as shown in Figure II-35, which shows the gyro spin axis aligned with the airframe z axis. The gimbal orientations correspond to level flight. Vertical gyros are always supplied with an erection mechanism whose purpose is to keep the spin axis aligned with the local vertical. The erection mechanism is required for several reasons. First, since the spin axis tends to remain fixed with respect to inertial space, the gyro would sense the rotation of the earth and the curvature of the earth as the airplane is flown at constant altitude. One purpose of the erection mechanism then, is to change the gyro reference from celestial to terrestrial. Another reason for requiring an erection mechanism is that it is impossible to fabricate gyros with frictionless gimbals. Thus, as the airplane rotates about either the x or y axis, torque is applied to the spin axis through the friction in the gimbal bearings, causing the gyro to precess about the other gimbal axis. This would cause an unpredictable wander of the gyro spin axis. Other undesirable torques are

caused by such factors as unbalances in the gimbals or in the gyro, shifts of the center of gravity with respect to the gimbal axes due to play in the bearings or differential thermal expansions or convection air currents striking the gyro rotor.

The erection mechanism for a vertical gyro consists of two devices (usually mercury switches), one attached to each gimbal and used to determine the direction of the net airframe acceleration vector. Each of these switches operates a separate torque motor to apply torque about the proper gimbal axis to align the spin axis with the airframe net acceleration vector. Erection is normally cut out during a coordinated turn to prevent the gyro from erecting to an acceleration vector not representing gravity.

To minimize the coupling effects between the dynamics of the erection system and those of the automatically controlled airframe, and to minimize the effects of transient accelerations along the x and y airframe axes, the erection mechanism is designed to operate slowly, rates of two to six degrees per minute being typical. Many vertical gyros have two erection rates, the faster of which is used to provide quick erection to minimize the time required for the gyro to become operable after the system is first turned on.

Section 5

For those cases where the erection system natural frequency is much lower than that of the airframe phugoid, the gyro can be represented as a pure gain and its transfer function becomes

$$(II-70) \quad \frac{V_G}{\theta \text{ OR } \phi} = K_g$$

where V_G is the voltage from the gyro pickoff. This transfer function tends to be more accurate at low speeds, since the phugoid period in seconds is roughly equal to one fifth the airspeed in miles per hour. At higher speeds where the phugoid and erection system frequencies are closer together, it may be necessary to use Equation (II-71) for the gyro output voltage in the longitudinal mode.

$$(II-71) \quad V_G \approx K_g \theta + \frac{K_g' \ddot{u}}{\omega_{ng}^2 + \frac{2\zeta}{\omega_{ng}} s + 1}$$

In Equation (II-71), ω_{ng} is the erection system natural frequency, \ddot{u} is the airframe acceleration along the x axis, and ζ is its damping ratio. Since the erection system is quite nonlinear, the approximation of Equation (II-71) should be used only when small deviations from the vertical are being considered.

A photograph of a vertical gyro is shown in Figure II-36.

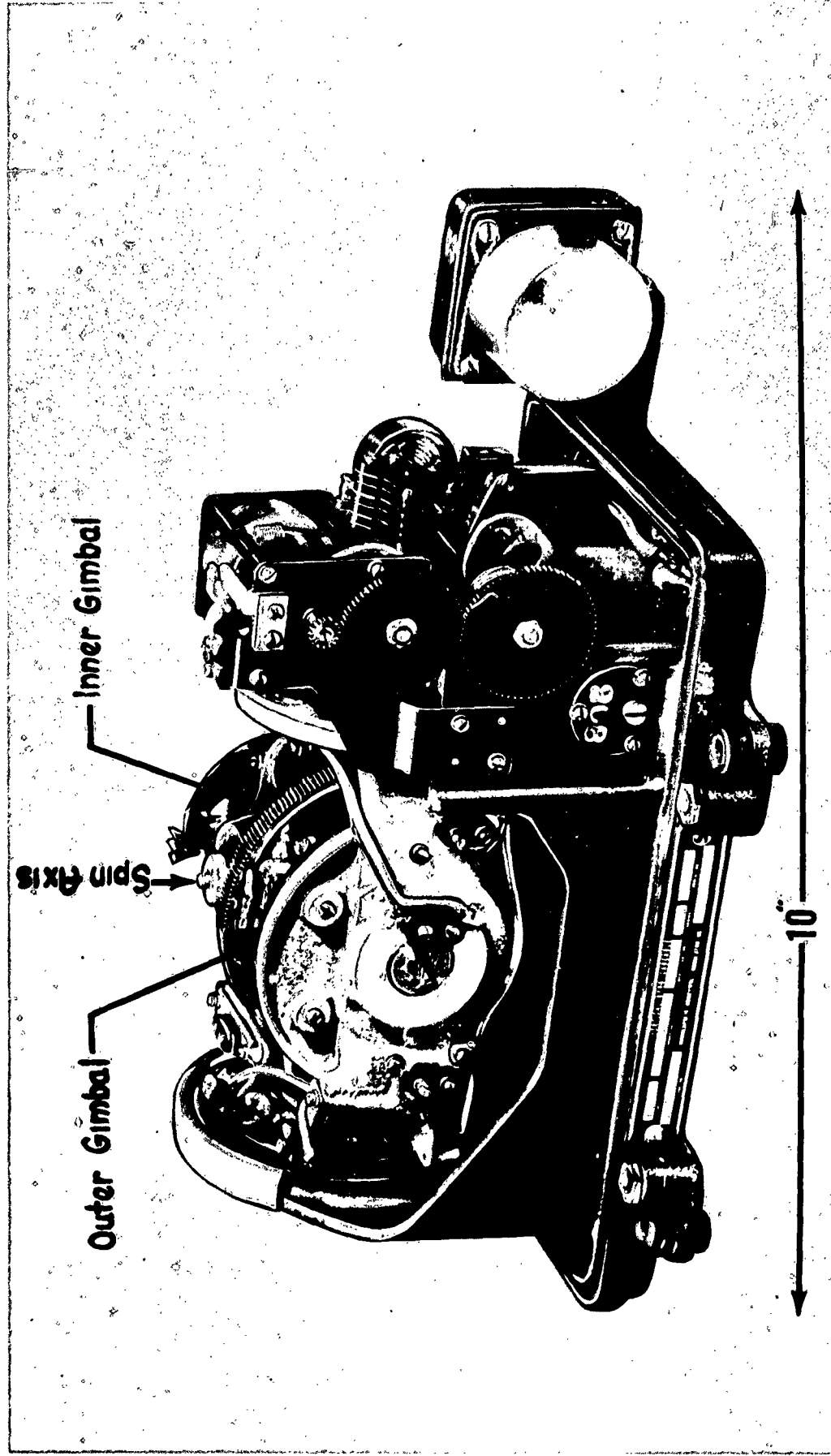


Figure II-36 Vertical Gyro

Section 5

DIRECTIONAL GYROS

Two degrees of angular freedom are also used for the directional gyro; however, in this case the gyro spin axis is maintained in a horizontal plane by one of the torquing motors and aligned with some specific compass direction (usually north and south) by the other torquing motor. The latter torque motor is usually energized by the error voltage originating in a synchro transmitter whose rotor is attached to the gyro outer gimbal and whose stator is attached to the gyro case. The stator windings are excited by a remote compass transmitter. (See Reference 13 for a more thorough discussion of the gyro compass.)

In actual practice both the vertical and directional gyros give accurate indications only when the gimbal axes are orthogonal. For example, reference to Figure II-35 shows that for a pitch angle of 90° , the condition known as "gimbal lock" occurs wherein the outer gimbal axis is aligned with the gyro spin axis. For this condition the gyro is not sensitive to roll angle. In the case of the directional gyro, errors are introduced whenever yawing occurs in the presence of a roll angle, such as during a coordinated turn. The equations describing these conditions are derived in the Appendix.

RATE GYROS

The rate gyro makes use of Equation (II-69) by measuring the torque which is generated by the gyro due to an angular velocity input. A single degree of freedom gyro is used for this purpose, and the generated torque is normally absorbed by means of a spring which restricts the motion of the gimbal (see

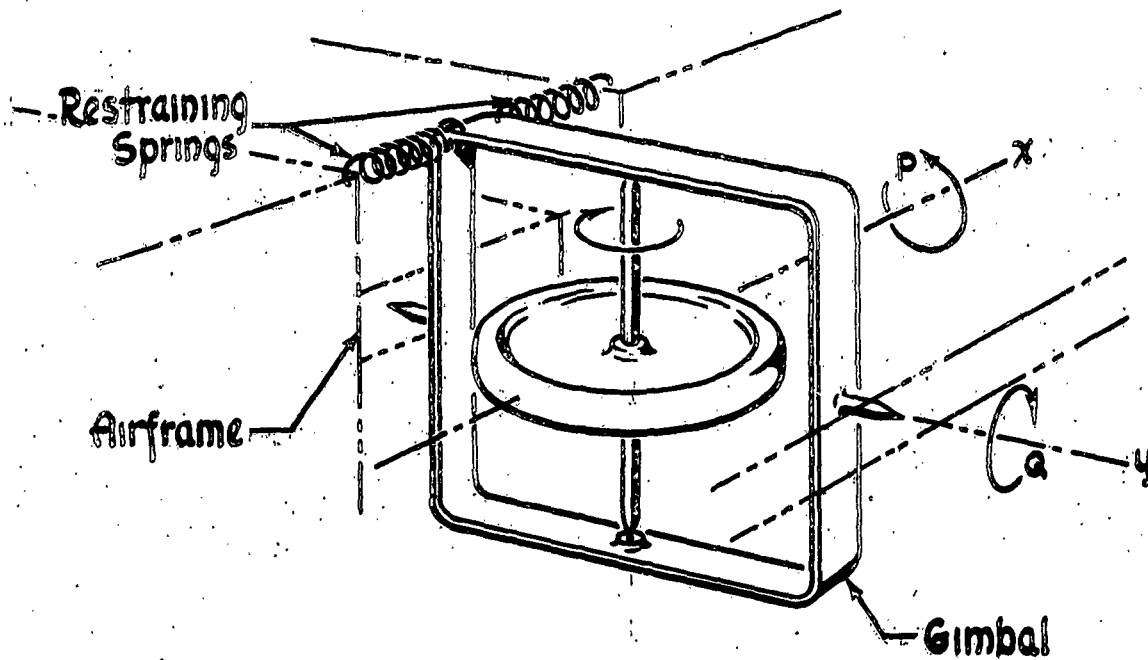


**Figure II-37 Single Degree of Freedom Restrained Gyroscope
(oriented to sense rate of roll)**

Figure II-37). Rewriting Equation (II-69) to solve for the torque applied to the spring gives

$$(II-72) \quad T = \omega H$$

Section 5

where ω is the airplane angular velocity. For a rate gyro mounted as shown in Figure II-37, the equation becomes

$$(II-73) \quad T = PH$$

where p is the airframe roll rate. If the gyro of Figure II-37 is restrained about the y axis by a spring constant K_S , viscous friction B , and coulomb friction F , and if the moment of inertia of the gimbal and spinning rotor about the y axis is I_Y , then the system equation becomes

$$(II-74) \quad T = PH = I_Y \ddot{A}_Y + B \dot{A}_Y + F(\text{SGN } \dot{A}_Y) + A_Y K_S$$

where A_Y is the angular rotation of the gimbal about its axis, referenced to the gyro case. If the friction is neglected, the transfer function is

$$(II-75) \quad \frac{A_Y}{P} = \frac{H/K_S}{\frac{s^2}{\omega_n^2} + \frac{2S}{\omega_n} s + 1}$$

where

$$(II-76) \quad \omega_n = \sqrt{\frac{K_S}{I_Y}} \quad \text{AND} \quad S = \frac{B}{2I_Y \omega_n} = \frac{B}{2\sqrt{K_S I_Y}}$$

If an electrical pickoff is attached to the gyro to measure the gimbal rotation, the equation becomes

$$(II-76) \quad \frac{V_G}{P} = \frac{K_V A_Y}{P} = \frac{H \left(\frac{K_V}{K_S} \right)}{\frac{s^2}{\omega_n^2} + \frac{2\zeta}{\omega_n} s + 1}$$

It will be noted that the gyro threshold due to friction can be expressed as

$$(II-77) \quad P = \frac{F}{H}$$

Resolution of potentiometers or thresholds of other types of pick-offs must be added to this minimum signal to obtain the total minimum detectable signal.

Two forms of geometrical cross-coupling occur in rate gyros, one caused by gimbal rotation when the gyro is indicating an angular rate and the other caused by the effects of the airframe angle of attack upon the axis about which the airplane rotates. Both effects introduce error in the measurement of the desired rate and introduce gyro outputs in response to rotation of the airframe about other axes. The equations describing these effects are derived in the Appendix.

A photograph of a rate gyro is shown in Figure II-38.

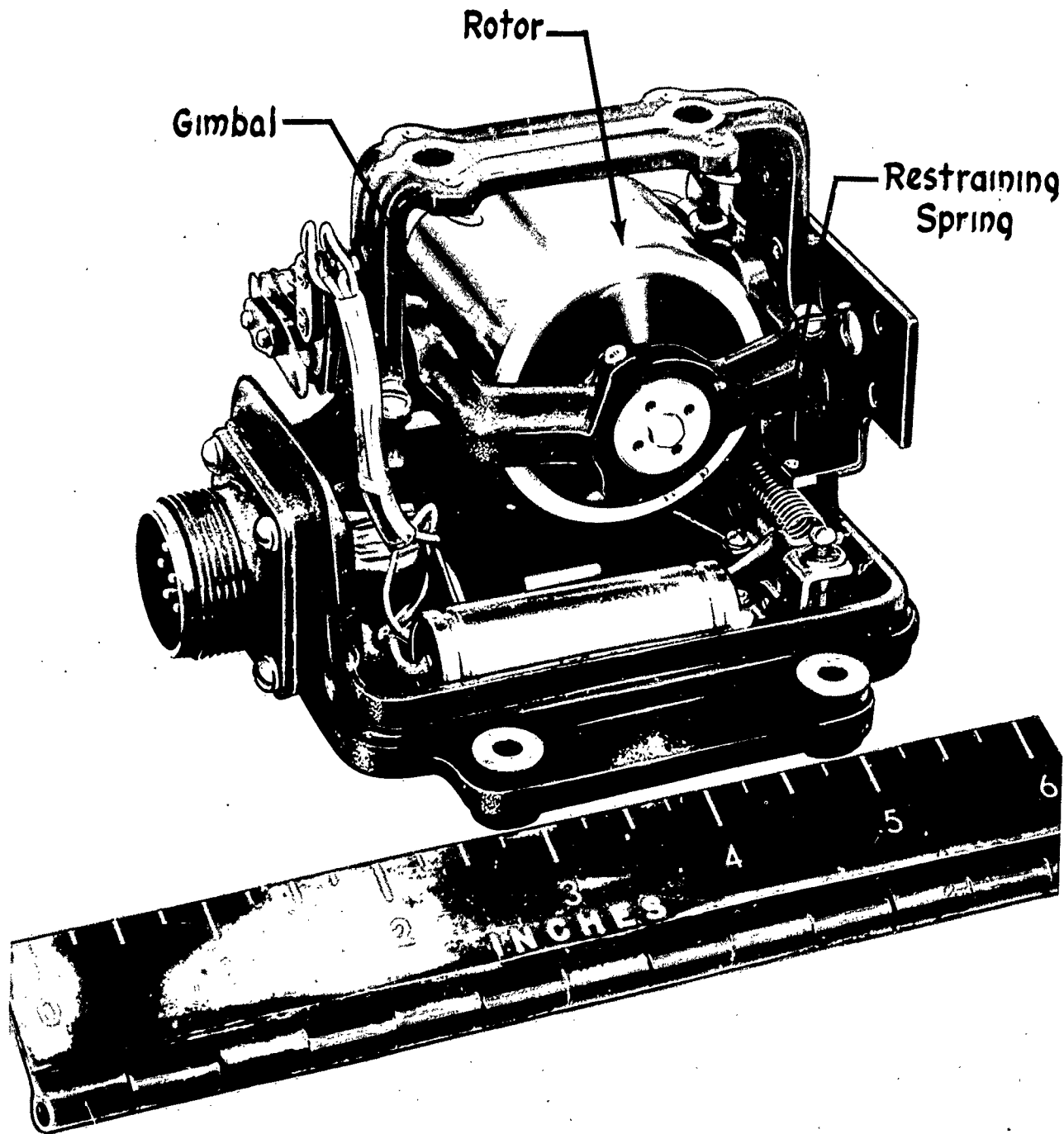


Figure II-38 Rate Gyro

(b) ACCELEROMETERS

Accelerometers are used to sense the linear and angular accelerations of the airframe. They consist almost universally of a mass of relatively high density which is constrained to translate or rotate against a restraining force or torque (usually a spring) as a result of applied acceleration. The mass is usually a solid, although it may be a liquid as in the case of the bubble linear accelerometer or the liquid rotor angular accelerometer. Although these accelerometers differ somewhat in construction details, the behavior of most of them can be adequately described by a second order equation. To illustrate the method, the equation describing the behavior of a linear spring restrained mass accelerometer will be derived.

The schematic diagram of the accelerometer to be considered is shown in Figure II-39. Assume that the case of the accelerometer shown in the diagram has an acceleration in a direction parallel to the accelerometer sensitive axis and that the sensitive axis is inclined to the horizontal by an angle θ . The forces acting on the sensitive mass are given by the following relation:

$$(II-78) \quad B\dot{Y}_{mc} + KY_{mc} + F_{SN} \dot{Y}_{mc} + M_c \sin \theta = M(\ddot{Y}_c - \ddot{Y}_{mc})$$

where Y_{mc} is the motion of the sensitive mass relative to the accelerometer case, B is the damping coefficient, K is the spring rate of the restrain-

Section 5

ing spring, and F is the coulomb friction. Rearranging Equation (II-78) gives

$$(II-79) \quad \ddot{Y}_{mc} + \frac{B}{m} \dot{Y}_{mc} + \frac{K}{m} Y_{mc} + \frac{F}{m} \text{sgn} \dot{Y}_{mc} = \ddot{Y}_c - g \sin \theta$$

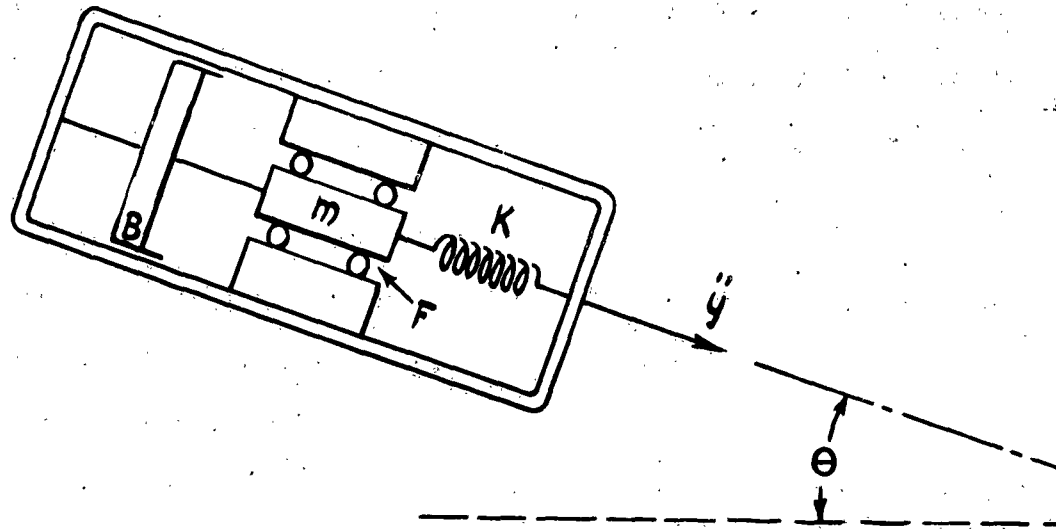


Figure II-39 Schematic Diagram of Linear Accelerometer

It will be noted that the motion or displacement of the sensitive mass is not proportional to the acceleration of the case whenever a component of the gravity vector lies along the accelerometer sensitive axis. If the quantity on the

right side of Equation (II-79) is expressed by

$$(II-80) \quad a = \ddot{Y} - g \sin \theta$$

then Equation (II-79) can be written as

$$(II-81) \quad \ddot{Y}_{mc} + \frac{B}{m} \dot{Y}_{mc} + \frac{K}{m} Y_{mc} + \frac{F}{m} \operatorname{sgn} \dot{Y}_{mc} = a$$

If the friction is neglected, the transfer function is given by

$$(II-82) \quad \frac{Y_{mc}(s)}{a} = \frac{1}{s^2 + \frac{B}{m}s + \frac{K}{m}} = \frac{\frac{m}{K}}{\frac{s^2}{\omega_n^2} + \frac{2\zeta}{\omega_n}s + 1}$$

WHERE

$$\omega_n^2 = \frac{K}{m} \quad \text{AND} \quad \zeta = \frac{B}{2m\omega_n}$$

Then, if a suitable pickoff device is attached to the sensitive mass so that its motion can be measured, the transfer function becomes

$$(II-83) \quad \frac{e_a(s)}{a} = \frac{\frac{m}{K} K_v}{\frac{s^2}{\omega_n^2} + \frac{2\zeta}{\omega_n}s + 1}$$

where K_v is the sensitivity of the pickoff in volts per unit distance.

Section 5

The motion threshold of the sensitive mass can be expressed as

$$(II-84) \quad a_T = \frac{F}{m}$$

To obtain the total threshold, the threshold of the pickoff device must be added to that given by Equation (II-84).

It is of some interest to note the behavior of the accelerometer for various forcing frequencies. When the frequency of the applied acceleration is much less than ω_n , the phase lag of the unit is small and the output is proportional to acceleration. When the frequency of the applied acceleration is approximately equal to ω_n , the phase lag of the unit is approximately 90° and the output is proportional to the velocity of the accelerometer case. Similarly, when the frequency of the case motion is much higher than ω_n , the phase lag is approximately 180° and the output is therefore proportional to the input displacement.

Typical accelerometers which are currently being used as sensors in automatic flight control systems are shown in Figures II-40 and II-41. Figure II-40a shows the sensing unit of a bubble accelerometer. It consists of a plastic block containing a cavity which is almost filled with a semiconducting liquid. Motion of the bubble due to acceleration, changes the resistance between the plate at the bottom of the cavity and the electrodes at the top. Figure II-40b shows two of these sensing units mounted in a case. In this application, the sensing units are interconnected to form a resistance bridge. This type of

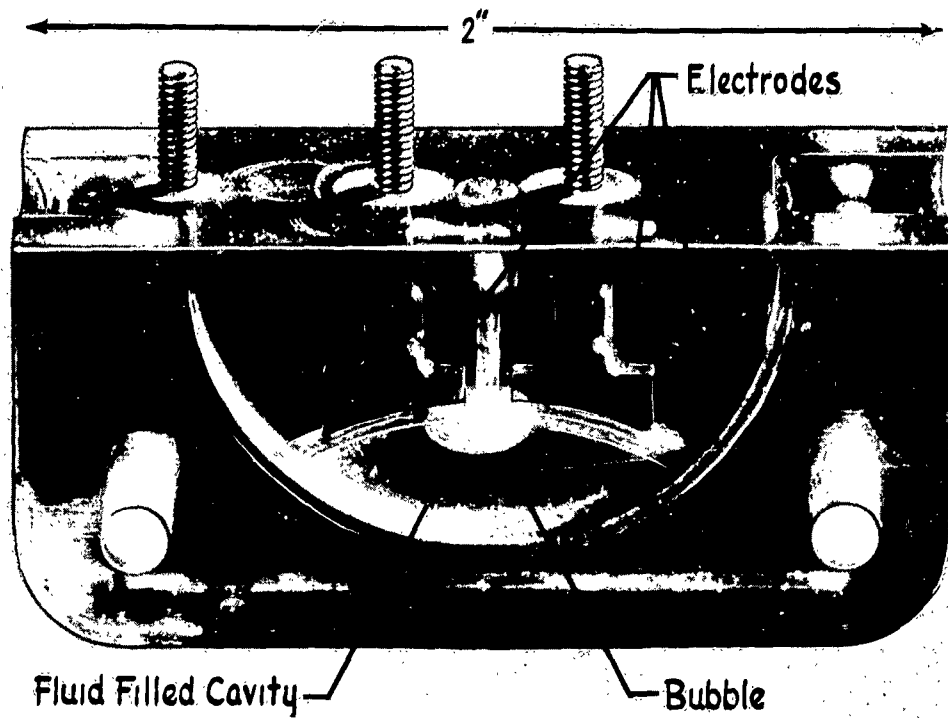


Figure II-40_a Bubble Accelerometer Sensing Unit

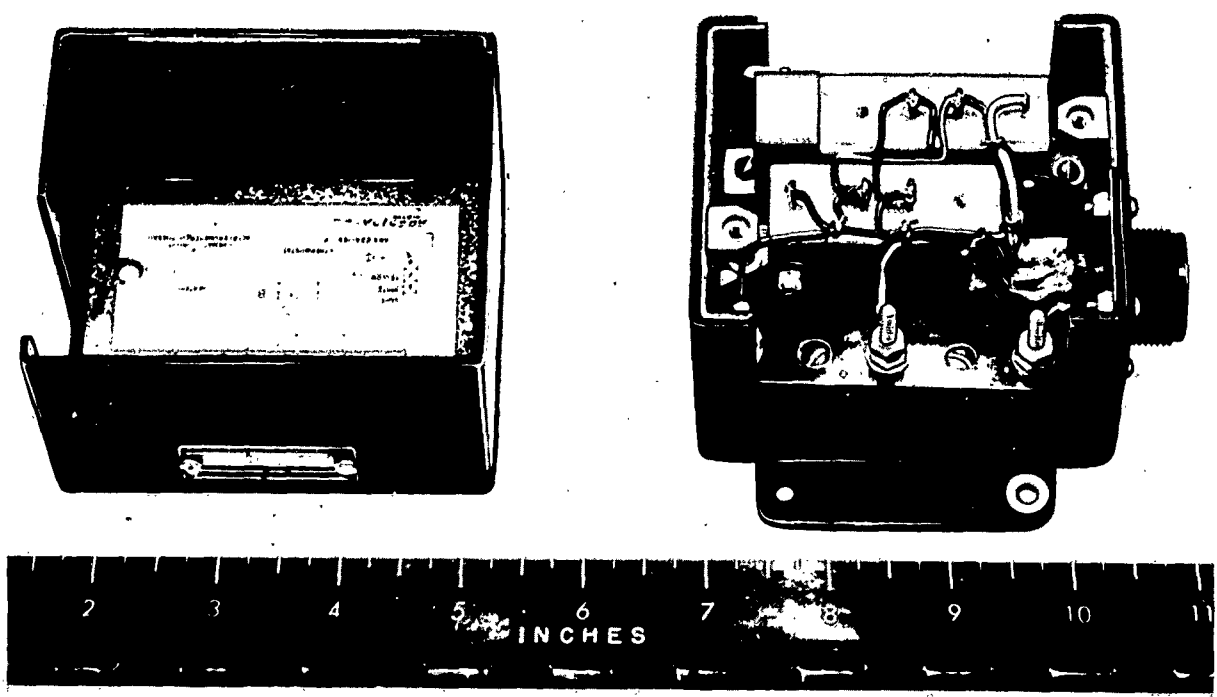


Figure II-40_b Bubble Accelerometer (top removed)

Section 5

accelerometer can only be used to measure longitudinal and lateral accelerations because it derives its spring effect from the acceleration which is applied vertically through the sensing unit. This fact makes the accelerometer sensitivity a function of the airplane normal acceleration.

The accelerometer shown in Figure II-41 is of the spring mass damper type. The seismic mass is mounted on the armature of an "E" coil pickoff, and the armature is attached to the accelerometer case through a cantilever spring. Damping is provided by filling the chamber containing the mass with fluid.

When properly oriented and located at the airframe center of gravity, accelerometers can be used to measure a_x the forward acceleration, a_y the side acceleration, and a_z the vertical acceleration.

An accelerometer can be used to give a reasonably accurate indication of sideslip angle. Equation (II-85) gives the transfer function for a_y/s_r as

$$(II-85) \quad a_y/s_r = U_0 Y_v \frac{\beta}{s_r} + U_0 Y_{\beta}^*$$

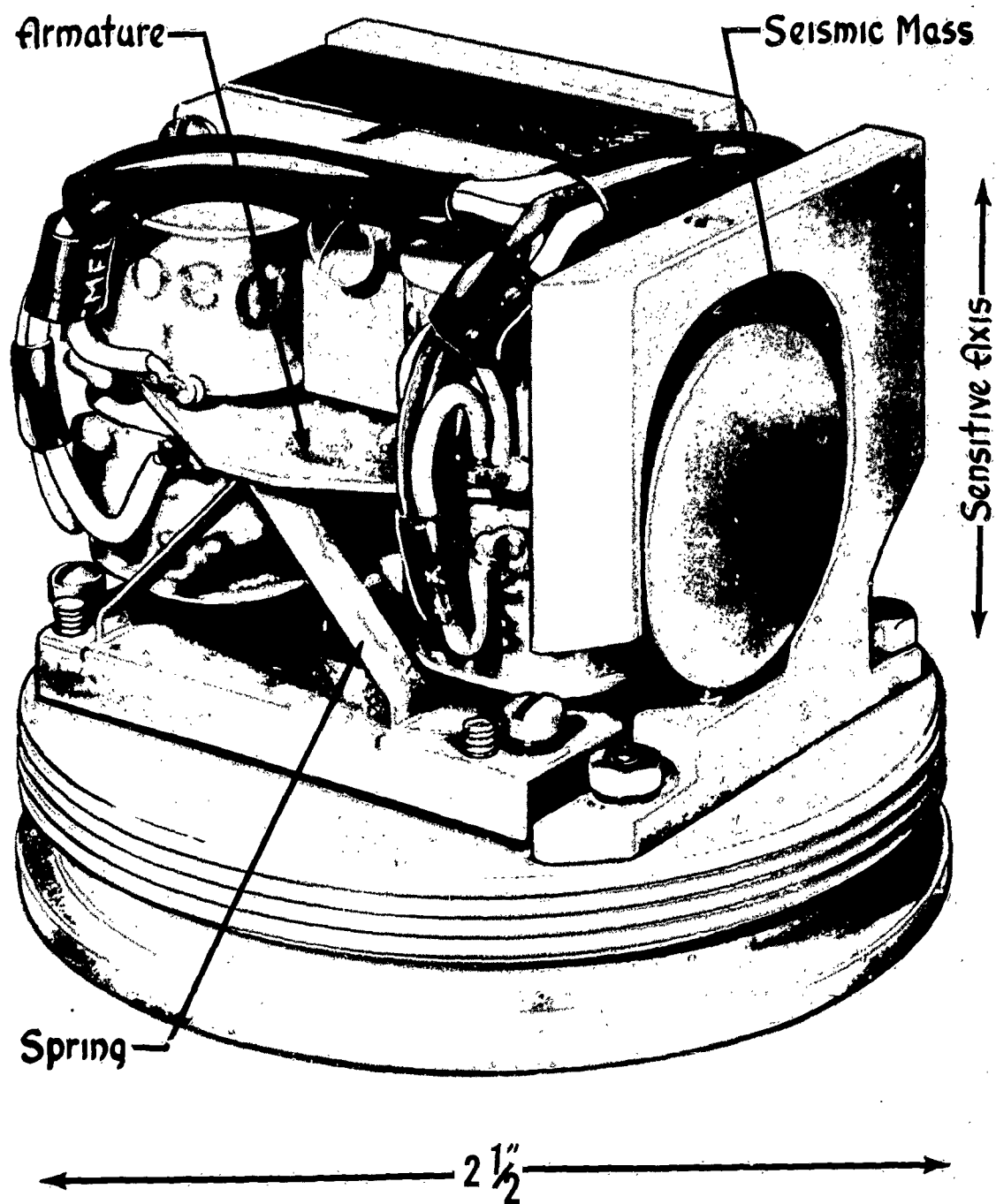


PHOTO coutesy of
WIANCKO ENGINEERING
PASADENA, CALIF.

Figure II-41 Spring-mass-damper accelerometer

Section 5

Equation (II-85) can be rewritten as

$$(II-86) \quad a_y = Y_\beta \beta + Y_{\dot{\beta}} \dot{\beta}$$

since $Y_{\dot{\beta}}^* = Y_{\dot{\beta}} / U_0$, and since $Y_\beta = Y_\beta U_0$. If a signal proportional to $\dot{\beta}$ is subtracted from a_y , the resulting signal is proportional to sideslip angle. Since sideslip angle and side velocity are related by the expression

$$(II-87) \quad v = U_0 \beta$$

side velocity can also be obtained by this method.

In a similar manner, the airframe angle of attack can be obtained by means of a normal accelerometer. The airframe lift coefficient is given by

$$(II-88) \quad C_L = \frac{a_z W}{q S}$$

where a_z is the normal acceleration, W is the airframe weight, q is dynamic pressure ($\frac{1}{2} \rho U_0^2$), and S is the area of the wing. In terms of angle of attack α , the lift coefficient can be expressed as

$$(II-89) \quad C_L = C_{L_\alpha} \alpha + C_{L_0}$$

where C_{L_α} is the lift curve slope and C_{L_0} is the lift coefficient when

$\alpha = 0$. Equating (II-88) and (II-89) gives

$$(II-90) \quad C_{L\alpha} \alpha + C_{L_0} = \frac{a_z W}{g_s}$$

Solving for α ,

$$(II-91) \quad \alpha = \frac{a_z W}{g_s C_{L\alpha}} - \frac{C_{L_0}}{C_{L\alpha}}$$

This relationship is sometimes used to compute angle of attack for fire control purposes.

(c) LOCAL FLOW DIRECTION DETECTORS

It would be desirable in many cases to sense directly the airframe sideslip angle β and angle of attack α so that these airframe output quantities could be used for automatic control. Since these angles are defined in terms of the relative wind, their direct measurement involves measurement of the relative wind direction, or the direction of relative motion of the air as it passes over the airframe. This is usually accomplished by means of a vane, a probe, dual pressure pickups, or some similar device.

Section 5

Direct measurement of these quantities, however, suffers from the rather serious disadvantage that the direction of the local flow is not a direct indication of the desired airframe output quantities because of the disturbances which exist near the airframe. At subsonic speeds, these disturbances extend for some distance ahead of the airframe. Consequently, the true angle of attack or sideslip must be computed from the indicated angle. Additional data, such as indicated airspeed and Mach number, are usually required to perform this computation. Moreover, the characteristics of the sensors themselves are difficult to predict by analysis, and it is often necessary to determine them by experiment. These two disadvantages require that a flight test program be conducted to determine a suitable location for the sensor, to determine the sensor characteristics, and to determine the equation relating true angles to indicated angles. Because of the above disadvantages, these devices are normally used only for special applications, such as the measurement of rocket jump angle for fire control systems. Since their use is quite specialized, no further discussion will be presented here.

(d) LOCAL FLOW MAGNITUDE DETECTORS

Local flow magnitude detectors are actually pressure sensors and are used to give an indication of the velocity at which the airframe is moving through the air. Depending on the equations to which these sensors are mechanized, their outputs are proportional in the steady state to indicated airspeed, true airspeed, Mach number, or differential pressure. These devices are used as primary sensing units when airspeed or Mach number is being controlled directly,

or as a means of changing controller characteristics as a function of airspeed to compensate for changes in airframe characteristics.

Since the dynamic characteristics of local flow magnitude detectors depend to a large extent upon the characteristics of the pitot-static system into which they are connected, it is not considered practical to present a detailed discussion here. However, it can be said that these sensors can often be approximated by the following transfer function

$$(II-92) \quad \frac{V}{P} = \frac{K}{\left(\frac{s^2}{\omega_n^2} + \frac{2\zeta s}{\omega_n} + 1\right)(T_S + 1)}$$

where V is the sensor output, P is the pressure presented to the sensor by the pitot static system, ζ and ω_n are constants describing the sensor mechanical system, and T_S is the time constant describing the sensor pressure system. Usually, the dynamics associated with ζ and ω_n are unimportant, but the time lag T_S may become large enough to require consideration. In addition, the characteristics of the pitot-static system should be carefully analyzed because this system is often characterized by a larger time lag than T_S .

Section 5

(e) PRESSURE ALTITUDE SENSORS

Pressure altitude sensors indicate altitude by measuring the static air pressure. When used as primary sensors for automatic control, they must have an extremely low threshold if the altitude control loop is to be easily stabilized. Like most pressure sensors, the sensing element usually consists of an aneroid bellows; the requirement for low threshold is often met by repositioning the bellows by servo action after a change in altitude. Care should be taken in mounting these units in the airframe, for they are sometimes sensitive to linear and angular accelerations. In addition, the static air line connected to the unit should be carefully selected to minimize the time lag in the pressure changes presented to the sensor. The static pressure system should also be studied to determine the effect of airframe angle of attack on the pressure in the system.

(f) SUMMARY

To summarize the discussion of sensing elements, the basic quantities of Table II-2 are repeated with other quantities added; possible sensors for measuring these quantities are also listed.

Section 5

Basic Output Quantity
Longitudinal

u forward velocity
 w vertical velocity
 q pitching velocity
 a_x forward acceleration
 a_z vertical acceleration
 α angle of attack
 θ pitch angle
 $\ddot{\theta}$ pitching acceleration
 A altitude

Sensor
(Sometimes limited to special conditions)

Accelerometer; Local flow magnitude detector
 Accelerometer; Local flow direction detector
 Rate gyro
 Accelerometer
 Accelerometer
 Accelerometer; Local flow direction detector
 Stabilized gyro
 Angular accelerometer; two linear accelerometers
 Altitude sensor

Basic Output Quantity
Lateral

v side velocity
 p rolling velocity
 r yawing velocity
 a_y side acceleration
 ψ yaw angle
 $\ddot{\psi}$ yaw acceleration
 ϕ roll angle
 $\ddot{\phi}$ roll acceleration
 β sideslip angle

Sensor

Accelerometer; Local flow direction detector
 Rate gyro
 Rate gyro
 Accelerometer
 Stabilized gyro
 Angular accelerometer; two linear accelerometers
 Stabilized gyro; Rate gyro
 Angular accelerometer; two linear accelerometers
 Accelerometer; Local flow direction detector

Table II-3. Sensor Application

Section 6

SECTION 6 - THE SYSTEM CONTROLLER

The system controller is the nerve center of the automatic flight control system. Its functions are:

1. To accept signals from the sensors or command sources
2. To modify these signals as required by different component characteristics (e.g., converting ac to dc electrical signals)
3. To effect signal phase lead or lag as required for desired system response.
4. To amplify the signals to a power level sufficient for operation of the servo actuators

Since most present day automatic flight control systems convey information by electrical means, the control unit normally consists of such devices as electrical modulators, demodulators, amplifiers, phase-shifting networks, summers, limiters, and switches to provide the functions listed above. Basic elements are normally the vacuum tube, the transistor, or the magnetic amplifier. Each has its limitations. Compared to the transistor, the vacuum tube is heavier, larger, less efficient and less rugged. It is more linear than the transistor, however, and higher amplification is possible. Since the transistor is relatively new, it has not been used until recently for aircraft applications. The basic limitations of currently available transistors are their gain change due to ambient temperature variations and their failure under high temperature conditions. When the temperature problem has been solved, transistors will probably largely replace most vacuum tubes for flight controllers, since their light weight, small size, and low power requirements, as well as their resulting low heat rejection are unmatched by other amplifying elements.

The magnetic amplifier is the heaviest and the bulkiest of the three, and its frequency response is inferior to the transistor or the vacuum tube. It also suffers from high temperature problems due to the characteristics of currently available rectifiers.

The transfer function for the system control unit cannot be presented here since it is determined completely by the over-all system requirements and by the characteristics of the other components. The system control unit transfer function is one of the outputs of the system synthesis procedure discussed in the next chapter. It is the one completely alterable element in the system.

SECTION 7 - CONTROLLER ACTUATORS

The basic purpose of a controller actuator is to change the output signals from the system control unit to a form suitable for application to the surface actuator so that the surface motion can be made some specified function of the controller output. Since the controller output is usually electrical, and the required input to the surface actuator is usually mechanical, the controller actuator must be a device which transduces a voltage into a mechanical displacement. As discussed in Section 4 of this chapter, the mechanical load which the actuator must displace is quite nonlinear, and for this reason the controller actuator is normally made to function as a position servomechanism. The following brief development derives the equations for a position servo working into a load consisting of a typical surface actuating system.

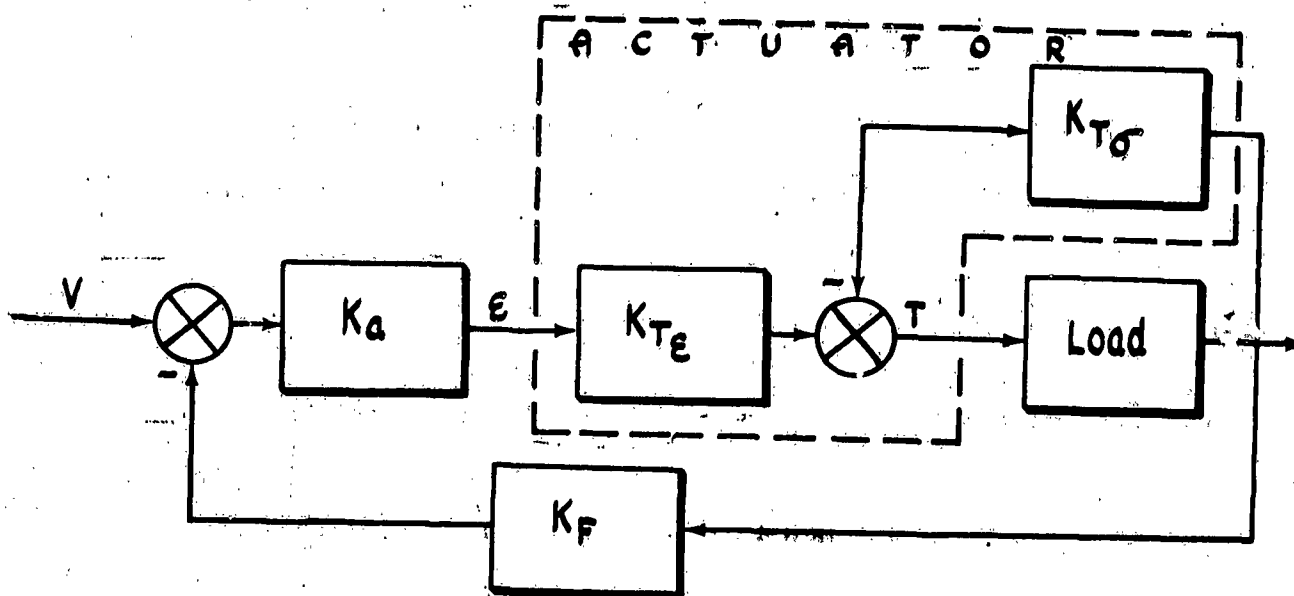


Figure II-42 Block Diagram of Loaded Positional Servo System

Figure II-42 shows a generic block diagram of a position servo. No specific type of actuator should be inferred from the diagram. The diagram and the following development are valid for any actuator which can be adequately represented by the two blocks shown. Both the two phase ac motor and the electrohydraulic actuator which are discussed later in this section fall into this classification.

In Figure II-42, the actuator inertia is assumed to be part of the load, and the time lag between the application of the voltage \mathcal{E} and the resultant output torque or force is assumed to be negligible. The constant K_{T_E} represents the slope of the actuator torque-voltage curve at zero output velocity, K_{T_O} represents the slope of the actuator torque-speed curve, V

is the control unit output voltage, and σ is the load displacement.

The torque or force applied to the load is given by

$$(II-93) \quad T = K_a K_{T_E} E - K_{T_\sigma} \dot{\sigma}$$

The load equation of motion for series actuation was given by

Equation (II-66) as

$$(II-66) \quad T = I \ddot{\sigma}_s + T_{f_c} \text{SGN} \dot{\sigma}_s + T_{sp} \text{SGN} \sigma_s + K_s \sigma_s$$

Equating (II-66) and (II-93) and rearranging gives

$$(II-94) \quad -\sigma_s = \frac{I \ddot{\sigma}_s + T_{f_c} \text{SGN} \dot{\sigma}_s + T_{sp} \text{SGN} \sigma_s - K_a K_{T_E} E + K_{T_\sigma} \dot{\sigma}}{K_s}$$

From Figure II-41,

$$(II-95) \quad E = V - K_F \sigma_s$$

Section 7

Substituting (II-95) into (II-94) results in

$$(II-96) \quad -\sigma_s = \frac{I\ddot{\sigma}_s + T_{fc} \text{sgn}\dot{\sigma}_s + T_{sp} \text{sgn}\sigma_s - K_a K_{TE} V + K_F K_{TE} \sigma_s + K_{Tf} \dot{\sigma}}{K_s}$$

Solving for σ_s gives

$$(II-97) \quad \sigma_s = \frac{K_a K_{TE} V}{K_s + K_F K_a K_{TE}} - \frac{I\ddot{\sigma}_s + T_{fc} \text{sgn}\dot{\sigma}_s + T_{sp} \text{sgn}\sigma_s + K_{Tf} \dot{\sigma}}{K_s + K_F K_a K_{TE}}$$

If K_a is very large, (II-97) reduces to

$$(II-98) \quad \sigma_s \approx \frac{K_a K_{TE} V}{K_s + K_F K_a K_{TE}} \approx \frac{V}{K_F}$$

This result is in agreement with the intuitive conclusion that if the output torque can be made large enough for small voltage inputs, the actuator is essentially irreversible and therefore actuator position is independent of the load. In practice, of course, this condition cannot be achieved exactly; however, it is approached by using a positional servo with very high open loop gain.

Many types of actuators have been used in automatic flight control systems. Among these are:

1. Continuously running electric motor with power output controlled by voltage applied to a magnetic clutch.
2. Armature controlled dc electric motor
3. The two phase ac electric motor
4. Hydraulic actuator controlled by electrohydraulic valve
5. Relay-controlled dc electric motor

Of these, the most popular have been the two phase ac motor and the electrohydraulic actuator.

The two phase ac motor is normally used only when the load is relatively small, since it is difficult to cool this type of motor for sizes above 1/7 horsepower. This motor requires two phase

excitation, one phase being excited by a fixed voltage and the other phase by the servo amplifier. The output torque is roughly proportional to the product of these two voltages when they are 90° apart in phase, and the direction of the torque is determined by the polarity of the control voltage.

The open loop transfer function of the unloaded two phase motor is given by

$$(II-99) \quad \frac{\sigma}{E} = \frac{K_{T\theta}/B}{s(J/Bs+1)} \times \frac{1}{T_s+1}$$

where J is the motor inertia and B is the slope of the motor torque-speed curve. The time constant T is caused by the winding reactances, and is usually less than $1/4 \frac{J}{B}$. If the load is composed only of inertia and damping, the transfer function of (II-99) still applies if J represents the inertia of the motor plus the load and B represents the damping of the motor plus the load.

In addition to displacement feedback, it is usually found necessary in practice to use rate feedback to obtain satisfactory damping. The closed loop transfer function in this configuration is

$$(II-100) \quad \frac{\sigma}{V} = \frac{K_0}{s^2 + 2\zeta\omega_n s + \omega_n^2}$$

WHERE

$$\omega_n = \frac{\sqrt{K_T K_1}}{J}$$

$$\zeta = \frac{B + K_T K_2}{2\sqrt{K_T K_1} J}$$

$$K_0 = K_T / J$$

K_2 IS THE RATE FEEDBACK GAIN AND

K_1 IS THE DISPLACEMENT FEEDBACK GAIN

The winding inductance lag, T , has been neglected in (II-100). As in the case of Equation (II-99), Equation (II-100) also applies for the loaded condition if the values of J and B used in Equation (II-100) include the load inertia and damping. Typical values for ω_n are .5 to 20 radians per second, with ζ adjusted as desired between 0.3 and 0.7.

Section 7

A photograph of a two phase ac servomotor with a built in rate generator is shown in Figure II-43.

The electrohydraulic servo actuator is becoming more and more popular for flight control application. This popularity arises from the following advantages:

1. High natural frequencies easily obtained
2. Low electrical power requirements
3. High power to weight ratio
4. High force to inertia ratio
5. No practical size limitation; available in sizes varying from fractional horsepower to many horsepower

Physically, the electrohydraulic actuator consists of a hydraulic ram which is controlled by an electrohydraulic valve. Although several manufacturers produce electrohydraulic valves, most of them are similar in operation. A typical valve which is used for flight control application is shown schematically in Figure II-44.

The operating principle is quite simple. The electrical signal moves the flapper between the two nozzles, unbalancing pressures P_1 and P_2 thus causing displacement of the valve spool. Since the valve spool is spring loaded, the displacement of the spool will be proportional to the unbalance in pressure.

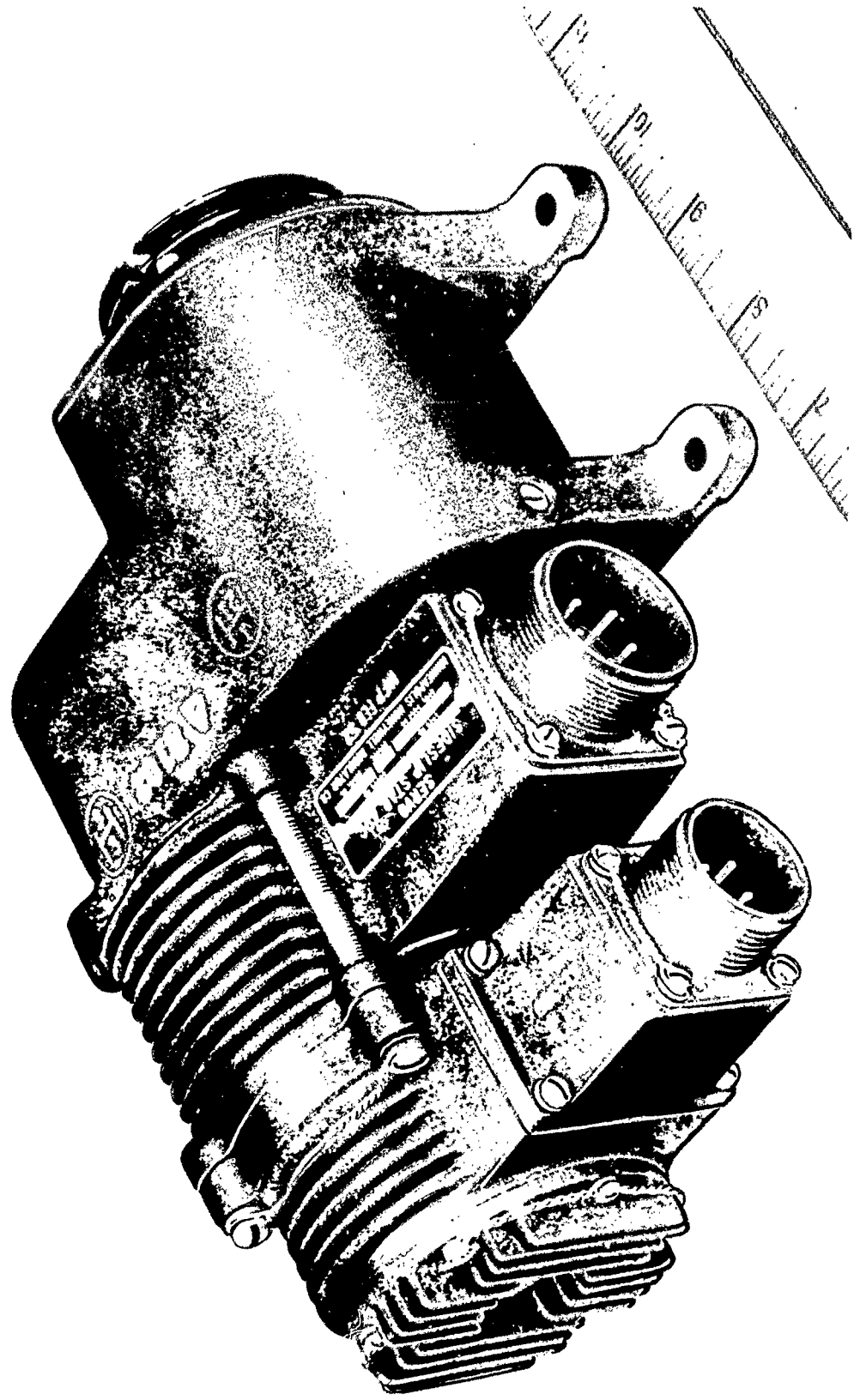
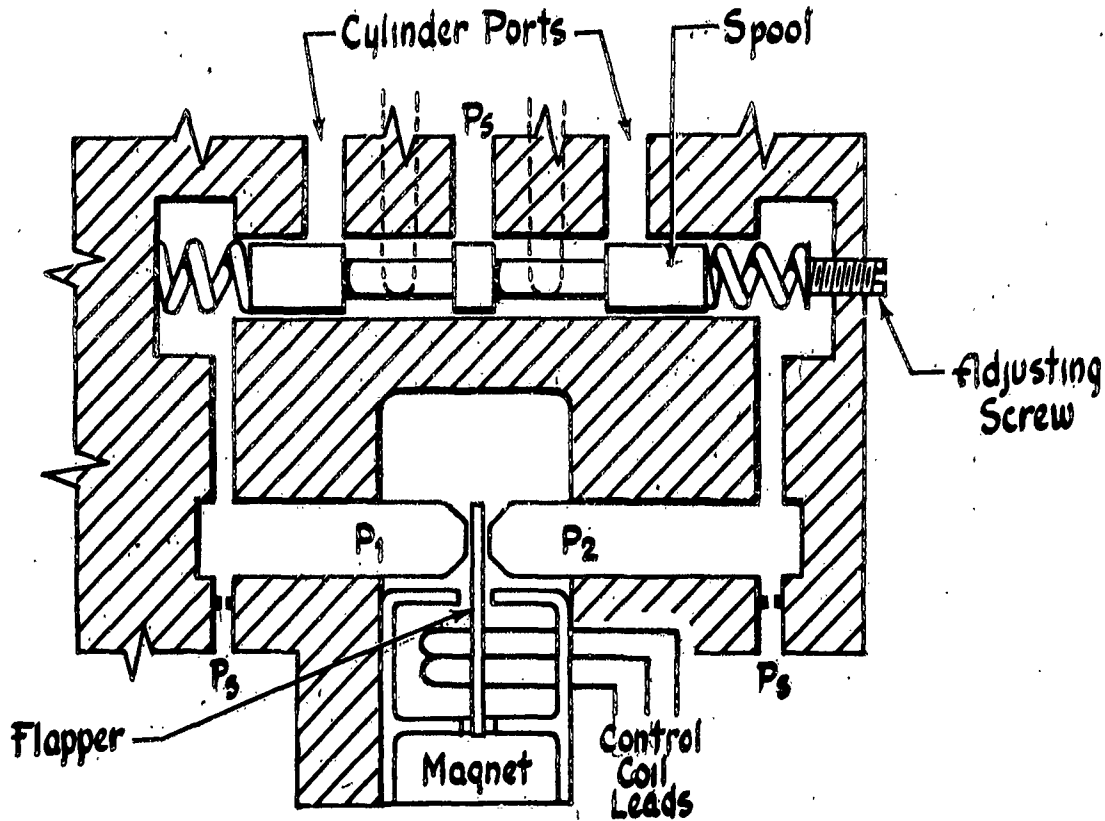


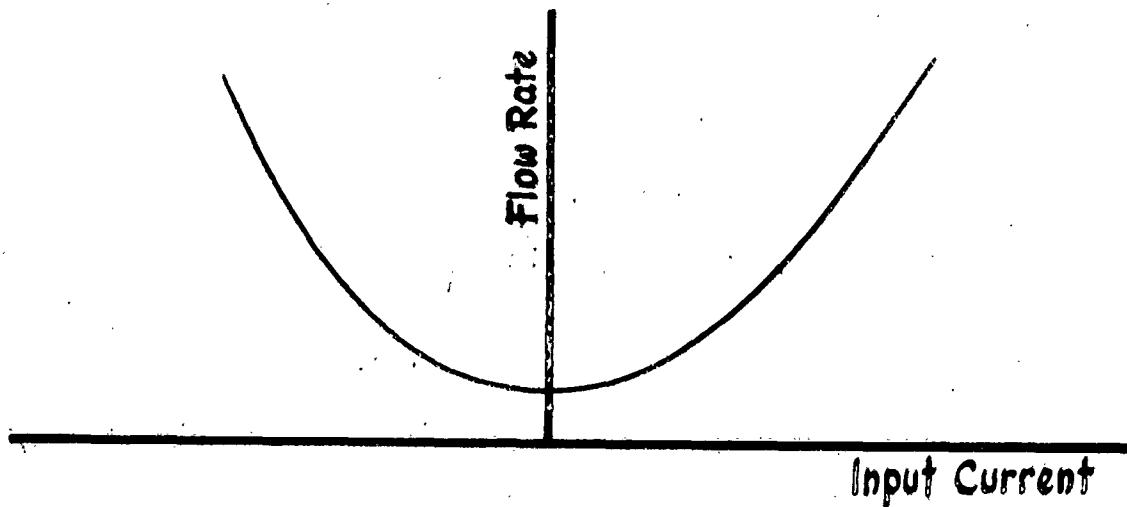
Figure II-43 Two Phase Servo Actuator



P_s = System Pressure.

Figure II-44 Schematic Diagram of Electrohydraulic Valve

A typical flow curve for a valve of this type is sketched in Figure II-45.



II-128 Figure II-45 Coil Differential Current Electrohydraulic Valve Flow Curve

In practice, the electrohydraulic actuator is used as a position servo as shown in the block diagram of Figure II-46.

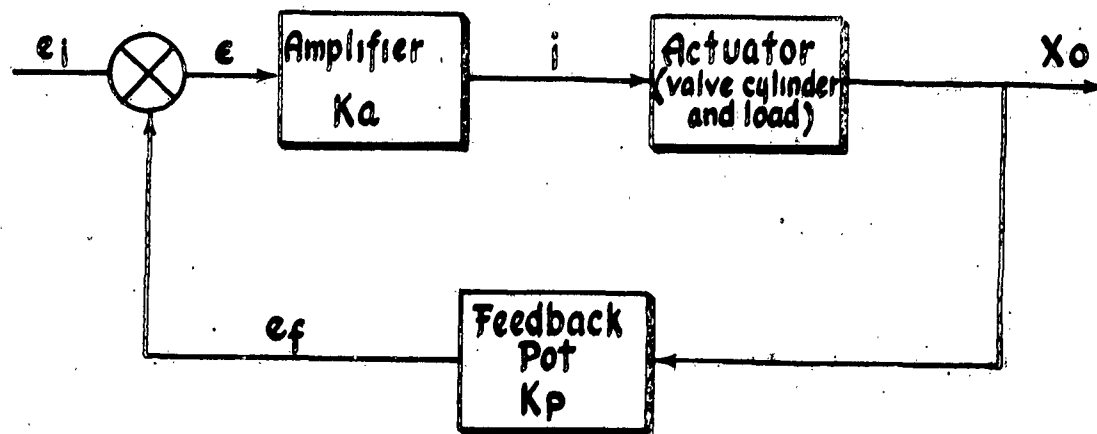


Figure II-46 Block Diagram of Position Servo Using an Electrohydraulic Actuator

The amplifier transfer function is assumed to be the constant K_a . The time constant for the valve coil RL circuit can be neglected because it is usually of the order of one-half millisecond or less.

Using the methods developed in Reference 11, the actuator-load network diagram is constructed as shown in Figure II-47.

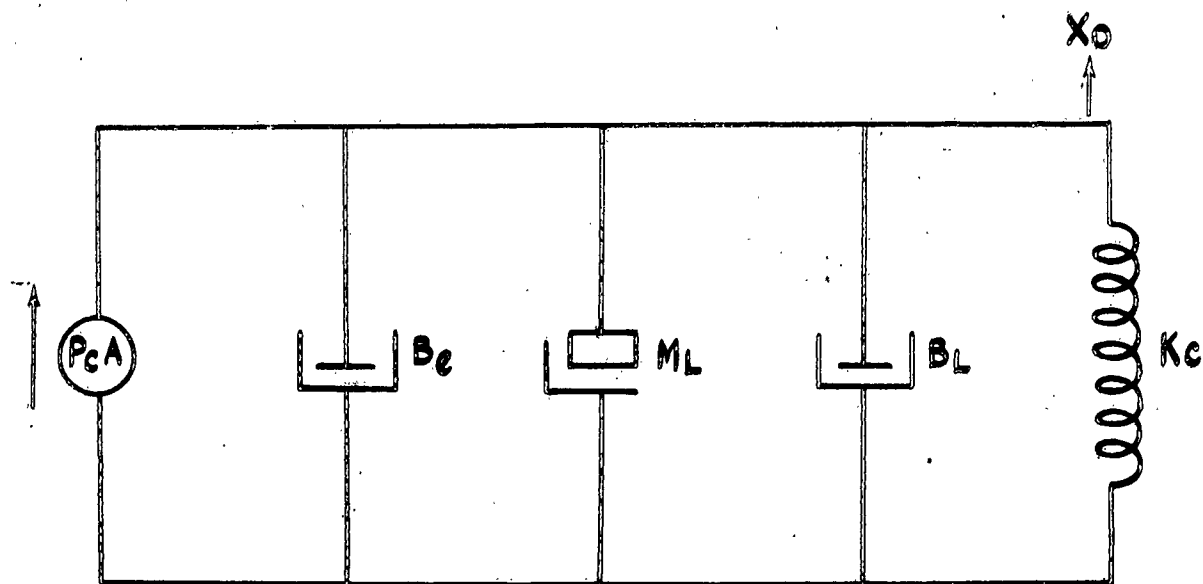


Figure II-47 Actuator-Load Network Diagram

The equation of motion of the above system is

$$(II-101) \quad [M_L S^2 + (B_L + B_c)S + k_L] X_o = P_c A$$

- where
- X_o = output motion of the piston relative to cylinder (in.)
 - P_c = differential pressure across the piston (lb/in.)
 - A = area of cylinder
 - B_c = damping between cylinder and piston (lb sec/in.)
 - B_L = damping of load (lb-sec/in.)
 - M_L = mass of load (lb sec²/in.)
 - k_L = spring rate of load (lb/in.)

Two additional equations may be developed for the cylinder flow relationships:

$$(II-102) \quad q = C_i i - C_p P_c$$

where q = cylinder flow
 i = valve differential current (proportional to valve displacement)

$$C_i \equiv \frac{\partial q}{\partial i} \quad (\text{slope of the valve flow curve})$$

$$C_p \equiv \frac{\partial q}{\partial P_c}$$

and

$$(II-103) \quad q = A S X_o + \frac{A^2}{k_o} S P_c$$

The term C_p is analogous to the slope of the torque-speed curve for an electric motor and gives rise to similar damping effects.

In Equation (II-103), k_o = spring constant of oil within cylinder.

Equations (II-102) and (II-103) may be combined to form the equation,

$$(II-104) \quad P_c A = \frac{C_i i - A S X_o}{\frac{A S}{k_o} + \frac{C_p}{A}}$$

Section 7

It is convenient to introduce still another relationship describing the force source ($P_c A$). A virtual servo output displacement X^* (which is fictitious physically) may be visualized as acting through the oil spring k_o to produce displacement of the piston (or actual servo output). Thus the resulting force is

$$(II-105) P_c A = k_o (X^* - X_o)$$

Equating (II-104) and (II-105) results in

$$X^* \left(\frac{A^2}{C_p} + k_o \right) - k_o X_o = \frac{A c_i}{C_p} i$$

or

$$(II-106) X^* (B_{Cp} s + k_o) - k_o X_o = k_f i$$

where $B_{Cp} \equiv \frac{A^2}{C_p}$

is the effective damping due to flow

and $k_f \equiv \frac{A c_i}{C_p}$

is the effective static servo flexibility,
also due to flow

Equations (II-101), (II-105), and (II-106) may be combined to form the open loop expression

$$(II-107) \quad \frac{X_o}{L} = \frac{k_o k_f}{M_L B_{cp} s^3 + [B_{cp}(B_c + B_L) + k_o M_L] s^2 + [B_{cp}(k_o + k_L) + k_o(B_c + B_L)] s + k_o k_L}$$

Equation (II-107) may be simplified by comparing the values of certain parameters of the physical system. Since $B_{cp} \gg B_c + B_L$

and $k_o \gg k_L$, this equation may be approximately factored,

yielding

$$(II-108) \quad \frac{X_o}{L} = \frac{k_o k_f}{(B_{cp} s + k) \left[M_L s^2 + \left(B_c + B_L + \frac{k_o M_L}{B_{cp}} \right) s + k_o \right]}$$

or

$$(II-109) \quad \frac{X_o}{L} = \frac{K_c}{(\tau_1 s + 1) \left(\frac{s^2}{\omega_n^2} + \frac{2\zeta}{\omega_n} s + 1 \right)}$$

Section 7

where

$$K_c = k_4/k_L$$

$$\tau_1 = B_{cp}/k_L$$

$$\omega_n^2 = k_o/M_L$$

$$\frac{2\zeta}{\omega_n} = \frac{B_c + B_L}{k_o} + \frac{M_L}{B_{cp}}$$

The effective damping term B_{cp} is usually very high, yielding an extremely low first order "break frequency," $\omega_{\tau_1} = \frac{1}{\tau_1} \ll 1$

rad/sec. Conversely, the undamped natural frequency $\omega_n = \sqrt{k_o/M_L}$

may be very high since the oil spring constant is relatively large and the load mass is often small.

With the information now available, the block diagram of Figure II-46 may be redrawn as shown in Figure II-48.

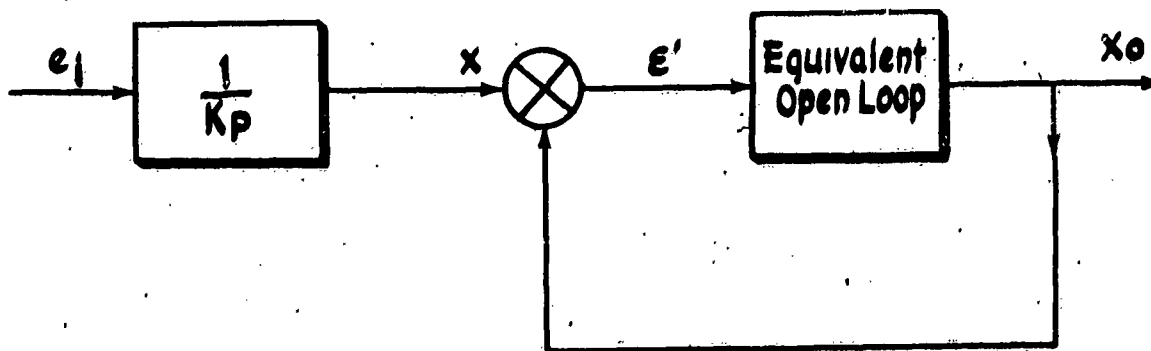


Figure II-48 Equivalent Block Diagram of an Electrohydraulic actuator

The equivalent open loop of Figure II-48 is

$$(II-110) \frac{X_o}{E_i} = \frac{K_c K_p K_a}{(T_s + 1) \left(\frac{s^2}{\omega_n^2} + \frac{2\zeta s}{\omega_n} + 1 \right)}$$

The Bode plot corresponding to Equation (II-110) is shown in Figure II-49.

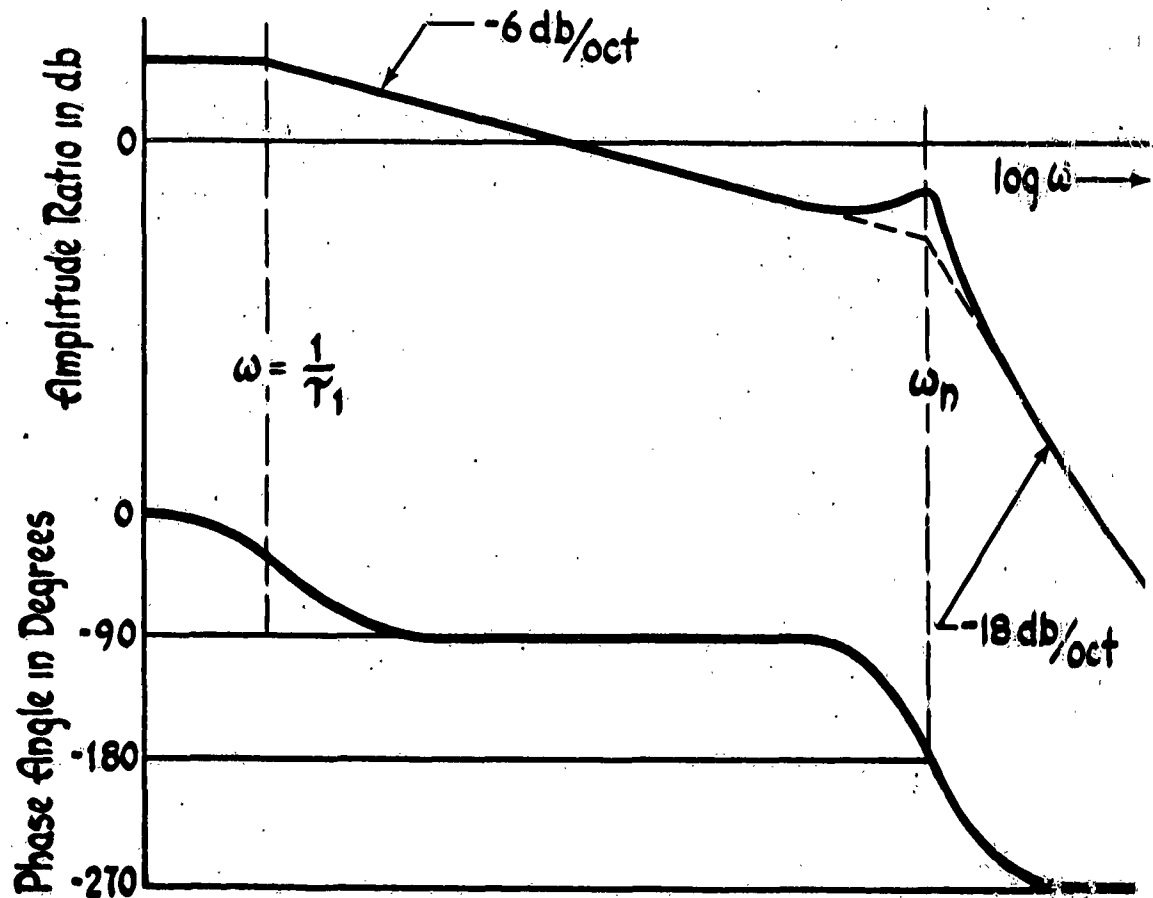


Figure II-49 Bode Plot of an Electrohydraulic Actuator

Section 7

Figure II-49 shows that the loop may be closed so that the closed loop approximates a first order system, up to a relatively high frequency, and possesses low position error coefficients.

Since $\frac{1}{\tau_1}$, is normally much less than ω , the open loop transfer

$$(II-111) \frac{X_o}{E'} \approx \frac{k_a k_p k_c}{\tau_1 s + 1}$$

From Figure II-48, the closed loop transfer function then becomes

$$(II-112) \frac{X_o}{V} \approx \frac{1/k_p}{\frac{\tau_1}{k_a k_p k_c} s + 1}$$

The approximation of (II-112) tends to be more accurate for a series installation, since the mass of the load is then smaller.

A photograph of an electrohydraulic actuator is shown in Figure II-50.

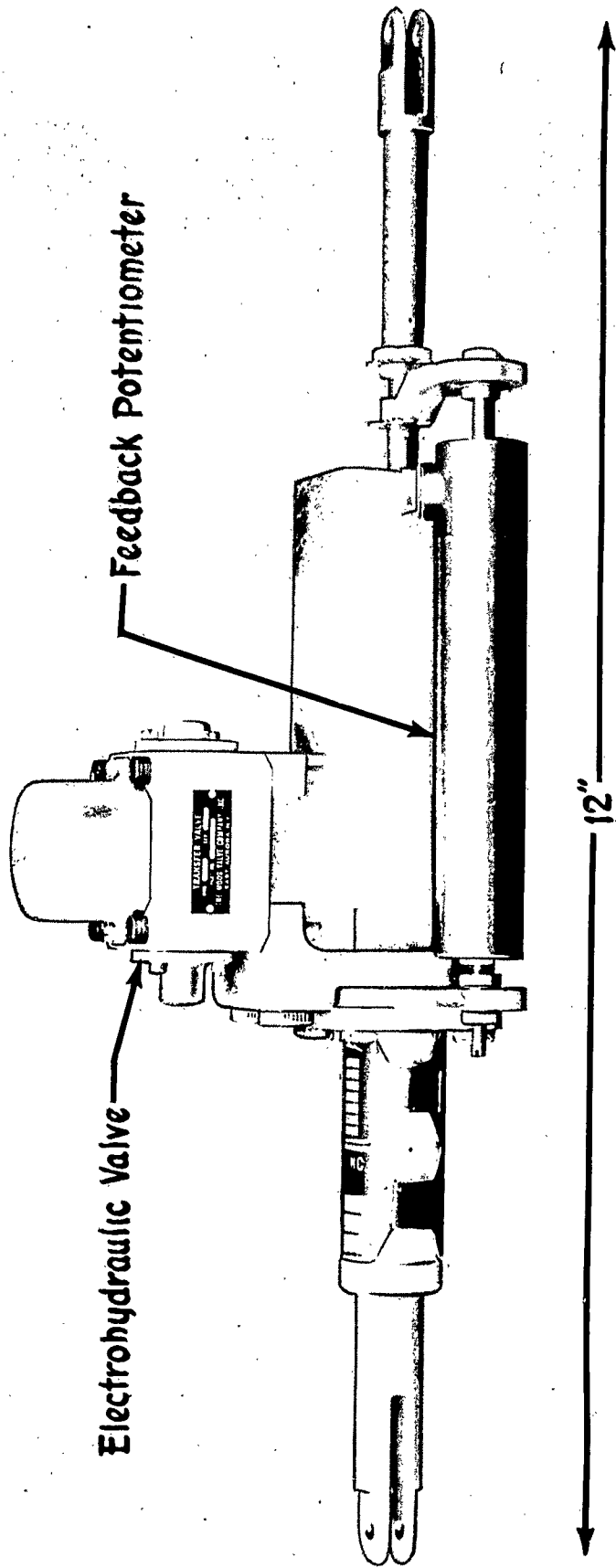


Figure II-50 Electrohydraulic Actuator

CHAPTER III
DESIGN METHODS

SECTION 1 - INTRODUCTION

This chapter discusses a procedure for designing automatic flight control systems. It is, of course, not the only method by which a successful design can be accomplished, but it is a method which experience has shown to be quite satisfactory. A qualitative discussion of the procedure is presented in Section 2 of this chapter, and Section 3 illustrates its use by tracing the actual design of a stability augmentor which is currently in operational use.

SECTION 2 - SYSTEM DESIGN PROCEDURE

(a) PRELIMINARY ANALYSIS

The preliminary steps in the design of any system are, of course, concerned with the determination of the system requirements. In the case of an automatic flight control system, this must usually be accomplished by first determining the over-all requirements of the airframe-automatic flight control system combination.

The requirements for the complete airplane system originate from two major sources: Military Specifications and Government Operating Requirements. Present military specifications for flying qualities of piloted aircraft are based to a large extent on a series of flight test investigations and the resulting opinions of the pilots.

Section 2

Desirable stability and control characteristics based on these studies are contained in the military specification of Reference 15. Along with other considerations dealing with pilot comfort and safety, this specification states minimum requirements for the following:

1. Dynamic stability of the airframe longitudinal short period and lateral dutch roll modes
2. Static directional and longitudinal stability
3. Spiral divergence
4. Control forces
5. Maneuverability

The specification referred to above is intended to apply primarily for the conditions under which the airplane is being controlled directly by the pilot through the manual controls. This specification is of interest to the automatic controls designer, however, because of its effect on the surface controls systems and because it is often necessary to provide stability augmenters to ensure that the specification is met.

Although a general specification for aircraft automatic pilots has been used in the past to establish requirements for the performance of an airplane

under automatic control,* differences in tactical requirements, differences in the function performed by automatic flight control systems, and differences in airframe and surface control systems characteristics have created a trend toward the preparation of a detail specification for each system. This detail specification is usually prepared jointly by the customer and the contractor after giving consideration to the Government Operating Requirements and the airframe and surface control systems characteristics.

A set of Government Operating Requirements (often abbreviated GOR) is issued by the government for each type of airplane purchased and usually forms a part of the contract. The GOR contains those airframe requirements which originate from tactical considerations of the aircraft mission. Some examples of these requirements are listed below:

1. Stability in excess of the flying qualities specifications
2. Minimization of steady state sideslip
3. Pilot relief during cruise
4. Automatic steering during firing, bombing runs, or landing approach
5. Cruise control for maximum range or maximum endurance
6. Climb or descent control
7. Mach control

*A proposed general specification for automatic flight control systems has been circulated for comment, but as of this writing, this specification has not been released. A new specification, MIL-C-5900, bearing the title "General Specification for Automatic Flight Control Systems," (Reference 18) was released 25 March 1955. However this specification consists merely of the old Air Force Specification No. 27500D with a new cover sheet.

Section 2

7. Altitude control
8. Automatic terrain clearance control

The requirements for the complete airplane system, as obtained from the military specifications and considerations of the airplane mission, are used to derive the requirements for the automatic flight control equipment after the characteristics of the controlled element have been determined.

DETERMINATION OF THE CONTROLLED ELEMENT CHARACTERISTICS

A detailed study of the airframe characteristics will show the modes of automatic control that will be required to ensure that the complete airplane system requirements are met. This study can be made in the preliminary design stage of the airplane, since the airframe characteristics are established at this time and preliminary stability derivatives will be available. This study can conveniently be made by means of the airframe perturbation equations. Approximate airframe damping and natural frequencies can be obtained by means of the approximate factors for the airframe equations of motion. It is often helpful to plot these quantities as a function of Mach number and altitude to aid in establishing critical areas. Bode plots are then constructed for as many flight conditions as necessary to verify those flight conditions which appear to be most critical. Preliminary information regarding which airframe output quantities should be controlled can be determined from the Bode plots, as discussed in Section 2 of Chapter II. Airframe damping can be obtained on the analog computer by examination of the airframe transient response to impulse type surface deflections. The study of the effects of controlling

various airframe output quantities is usually made by considering the controller and feedback elements as simple gains. This procedure is directly analogous to the one used in Chapter II, Section 2e in the discussion of the equivalent stability derivative approach.

The results of the computer study will establish the requirements for the automatic flight control system, for they will show whether stability augmentation is required, and will indicate those airframe output quantities which should be controlled.

(b) ANALYSIS AND SYNTHESIS

At this point in the design procedure it is helpful to construct a preliminary functional block diagram of the automatic flight control system. Information used to construct this diagram comes from many sources. The study conducted in the preceding phase will provide information regarding those airframe output quantities which best lend themselves to control as well as those airframe input quantities which show the most promise of providing satisfactory control. A knowledge of the state of the art of sensing devices is valuable here to establish which of the possible airplane variables suitable for control can be satisfactorily measured. In general, an intimate knowledge of system requirements and the characteristics of the various elements, coupled with a detailed understanding of the possible means of achieving the ends required, is the main basis for selecting the proper elements for composing a functional block diagram.

Section 2

The configuration of the functional block diagram will indicate the types of sensing devices required, since the diagram will show which airframe output quantities must be controlled. This will indicate whether accelerometers, rate or displacement gyros, local flow magnitude and direction sensors are required, or whether some combination of these or other sensors may be used. Even though the specific units to be used are not chosen at this point, good judgment is required because it is not always wise to measure directly the quantity being controlled. For example, it is shown in Section 3b of this chapter that sideslip angle can be measured better with a lateral accelerometer than with a local flow direction detector. It is decisions of this sort that must be made at this time. Final selection of sensing elements is usually made in the latter part of the analysis and synthesis phase, after the effect of varying sensor dynamics has been determined, and after the required physical nature of the sensor output has been decided (i.e., electrical, ac or dc, mechanical, etc.)

A detailed functional block diagram can now be drawn which shows all signal paths and the types of sensing and actuating elements to be used. The next step in the design is to determine the desired characteristics for the controller and for each of the other alterable blocks. A brief summary follows of the degree of alteration which may be available to the flight controls designer for the various blocks in the system.

1. Airframe. In the preliminary design phase, certain airframe parameters can be modified to some extent for the purpose of simplifying the automatic flight control system requirements. Many of the airframe parameters however, must be established by other considerations, such as maximum altitude, maximum speed, and landing speeds. When the airframe design has progressed beyond the preliminary stages, it must usually be considered unalterable by the automatic flight control system designer, unless some completely unacceptable characteristic is revealed.

2. Surface Actuating System. If time scheduling permits, it is extremely advantageous not to finalize the design of the surface actuating system until after the functional block diagram has been constructed. At this time, decisions have been made concerning the type of automatic control required, and it is often possible to achieve great simplification by integrating the manual and automatic actuating systems. In addition, it is sometimes found to be impossible to achieve satisfactory automatic control when actuating devices are required to operate through manual control systems that were designed without giving consideration to the stability augments or autopilot. To insure optimum performance for the system combination, it is desirable if the same steps as those outlined here for the design of the automatic control system can be followed simultaneously for the manual surface actuating system. This procedure permits the integration of the pilot's force producing mechanism and surface actuating mechanism with the stability augments and autopilot.

Section 2

3. Controller Actuator. The alterability of the controller actuator is somewhat limited by the characteristics of the surface actuating system since this system makes up a part of the load of the controller actuator. This restriction establishes the range of acceptable maximum output torque or force, and establishes the method by which the force or torque is transmitted to the surface actuator. Aside from this restriction, the controller actuator, as in the case of the sensing device, is alterable within the limits of available off-the-shelf items or of units which can be developed in time for use.
4. Sensing Devices. Sensing devices are limited as to type by the block diagram. They are alterable within the limits of available off-the-shelf items or units capable of being designed in time for use. It is sometimes economically desirable to use a device already in the airplane if no serious compromise in performance is caused by this choice.
5. System Controller. This unit is completely alterable. It is this block which is used to compensate for the characteristics of the other blocks by providing equalization and amplification for optimum system performance.

The exact procedure used to determine the desirable characteristics for each of the alterable blocks depends to a great extent upon the amount of preliminary information available before the study begins, the degree of alteration available, and on the individual preferences of the designer with regard to such techniques as root locus, Bode plots, Nyquist criteria, and analog

computation. In addition, it is always necessary to make some basic assumptions, since it is never possible to take everything into consideration. These assumptions should be carefully listed in great detail for later verification by actual test. These considerations may modify the procedure outlined below; however, the procedure is sufficiently general to cover most cases.

If no initial conditions have been established for the sensors and actuators (they are alterable within the limits of available off-the-shelf items or of units which can be designed in time for use), it is frequently advantageous to consider these components as simple gains in the initial stages. Using the airframe perturbation equations, Bode plot and/or root locus studies are then made for inner loops or, for those parts of the system block diagram capable of being analyzed separately. The purpose of these studies is to determine the equalization and gain necessary for satisfactory system performance. If the part of the system under analysis is complex, the results of the paper study should be verified by means of the analog computer.

The next step should be to incorporate what are considered to be realistic dynamics for the sensors and actuators and to repeat the Bode plot and/or root locus studies. Any necessary changes in system equalization or gain can be determined as well as the effects of varying the characteristics of the sensors and actuators. The results of this study should also be verified on the analog computer.

Section 2

As a result of the above study, the tolerable ranges for the characteristics of the sensing and actuating elements can be established, and a catalog search can be made for the purpose of choosing specific components. If components with the desired characteristics are not available, it will be necessary to initiate the design of such components, or to evaluate the deterioration in system performance due to shortcomings of components that are available, or to rearrange the functional block diagram to permit optimum use of available components.

After selecting actuators and sensors, the linear static and dynamic characteristics of these components should be incorporated into the mathematical model representing the system under study. If these characteristics are different from those considered above, the equalization and system gains previously chosen should be checked. This can be accomplished either by Bode plot and/or root locus studies, or by the use of the analog computer.

The analog computer should also be used to study the effects of the component nonlinearities. These studies frequently suggest redesign or shifting of physical equipment or modification of equalization so that the undesirable effects of the nonlinearities can be minimized.

After the above procedure has been carried out for every part of the system which can be separately analyzed, the various parts should be combined, adding one part or loop at a time, until the entire system is represented.

After completing the perturbation studies, it is sometimes advisable to extend the analysis and synthesis phase of the design procedure to include a study of system performance when subjected to large scale maneuvers. The complete, six degree of freedom airframe equations of motion should be used for this investigation. The decision as to whether such an extension of the analysis and synthesis phase should be made depends largely on the configuration of the automatic flight control system and on the characteristics of the airframe. If the automatic flight control system consists of both lateral and longitudinal channels, the study utilizing the complete airframe equations of motion should almost certainly be made, since experience has shown that systems whose parameters have been adjusted for optimum performance for small disturbances from level flight are not necessarily properly adjusted for large disturbances; in fact, such systems may be completely unstable under these conditions (see Reference 16). Even when the system under design consists merely of a single channel stability augments, the performance of the system during large scale maneuvers should be determined if the airframe exhibits strong inertial coupling (as most supersonic airplanes do). The results of these studies may reveal that no set of parameters provides satisfactory performance for both small and large disturbances, in which case it may be necessary to rearrange the functional block diagram to utilize other airframe output quantities which will provide satisfactory performance.

Section 2

The desired result of the above study is the detailed system block diagram, with the characteristics of each block completely specified.

As mentioned earlier, individual preferences may place more emphasis on the use of the analog computer or some technique other than that indicated here. In addition, if intentional nonlinearities are included, some of the more recent developments in the analysis of these mechanisms should, of course, be utilized (see Reference 17).

(c) PROTOTYPE SYSTEMS

The prototype systems are the physical manifestations of the mathematical models for the equalizers and other components, which were derived in the preceding phase. At least two versions of the prototype systems are usually fabricated, the first of which is a developmental model. A developmental model (sometimes called a "breadboard" model) is normally constructed from layout sketches and wiring schematics, rather than from formal drawings. It is usually constructed in such a way that it has the desired functional characteristics; however, its physical layout may be different from that anticipated for the production system. For example, the developmental model for the electronic portion of the system might be constructed on any convenient chassis, utilizing any convenient physical arrangement of components but would consist of the circuit configuration planned for the production version.

The developmental model is utilized for initial component and system tests to determine how accurately the physical equipment represents the mathematical models. These tests include the determination of components and system frequency response, loading effects, linearity, saturation levels, switching transients, noise characteristics, etc. The developmental model is also used to conduct closed loop flight simulation tests as discussed in the following subsection. The equipment is modified when necessary, as the testing progresses.

The preproduction model is the second version of the prototype equipment which is normally constructed. It is designed and fabricated during the test program of the developmental model. This preproduction model therefore reflects the results of the developmental model test program and, in addition, is designed and packaged for simplicity, reliability, and producibility. The tests discussed above are repeated for the preproduction system, and in addition, the preproduction system is utilized for test stand and airplane ground and flight tests as discussed in the following subsection.

(d) TESTING PROTOTYPE SYSTEMS

Many special devices have been developed during the last few years which facilitate automatic flight control system testing. Some examples are ultra low frequency oscillators, mechanical sine wave generators, force and displacement transducers, force producers, direct writing oscillographs, and automatic curve plotting machines. In addition, at least one manufacturer has developed a device which gives a direct

Section 2

indication of amplitude ratio and phase lag for conducting frequency response tests. In lieu of this device, frequency responses can be determined by recording input and output sine waves simultaneously on a direct writing oscillograph. Amplitude ratios and phase angles can then be computed from these traces.

Initial tests for a prototype system are made on the individual components. As discussed previously, these tests are made to determine how accurately the physical equipment represents the mathematical models that were derived during the synthesis phase. These test results are usually in the form of input-output relationships and show such characteristics as frequency response, static gain, and linearity. Frequency responses should be obtained for several representative amplitudes at frequencies throughout the frequency range of interest for comparison with those assumed during the synthesis phase. When the component tests have been completed, and the components have been modified as dictated by the test results, the developmental model is subjected to system tests, in which the components are interconnected in the same manner as for operational use in the aircraft. The characteristics of the sensors, the surface actuating system, and the airframe are simulated by means of an analog computer, and representative loads are applied to the controller actuators. Modulators, demodulators, and scale changing devices are used as necessary to make the analog computer signals compatible with those of the controller. The system can then be operated under conditions which resemble those encountered in flight. Complete system open and closed loop frequency responses

can be obtained, as well as system transient response to representative inputs. These data can then be compared to the results obtained during the analysis and synthesis phase when the entire system was analoged. The results of this comparison will reveal any differences between predicted and actual performance of the prototype system when operating with the airframe and surface control system. Of course, the accuracy of the results is limited by the accuracy of the simulation of the airframe and surface control system.

A more accurate representation of operational conditions is obtained through the use of a control systems test stand. Since this involves the use of the physical components of the surface actuating system, errors which might be introduced by its simulation are eliminated. Additional and more realistic tests are permitted because the human pilot control loop can be closed, thus simulating actual flight.

A typical test stand consists of a steel framework upon which are mounted all the essential elements of the actual control system of the airplane. These include the complete surface actuating system, pilot's seat, cockpit controls, and artificial feel devices. Pilot control forces which originate from effects such as the force applied to a bobweight due to airplane acceleration are produced artificially by force-producing devices which respond to signals from the analog computer. The automatic control equipment to be tested is installed on the test stand in a manner representing as closely as possible the actual airplane installation. Simulated aerodynamic loads are applied to the control surface by means of mechanical or hydraulic springs and dampers.

Section 2

A pilot's display is often included to simulate as many as possible of the visual stimuli to which the pilot responds in flight. Cockpit instruments which are commonly simulated are the g-meter, airspeed indicator, altimeter, artificial horizon, turn and bank indicator, and flight path indicators. For certain applications an oscilloscope may be employed to simulate computing gun sight indicators and pilot's automatic fire control displays.

Figure III-1 is a view of a simulator from above and aft, and shows the rudder, the elevator, and one aileron. The control cables and hydraulic system are located beneath the catwalk and cannot be seen in the photograph. A view of the cockpit area showing the pilot's seat, the control stick and rudder pedals, the actuator of a force producing device, and part of the pilot's display is shown in Figure III-2.

As in the case of the bench simulation, the airframe dynamics are simulated by means of an analog computer. The computer inputs are voltages proportional to control surface deflections, and its outputs can be voltages proportional to any or all of the airframe output quantities. These voltages are then used to operate the pilot's display equipment, the simulated force producers, the controlled platforms (when these are used), as simulated sensor inputs to the controller and for recording airframe response on the oscillograph.

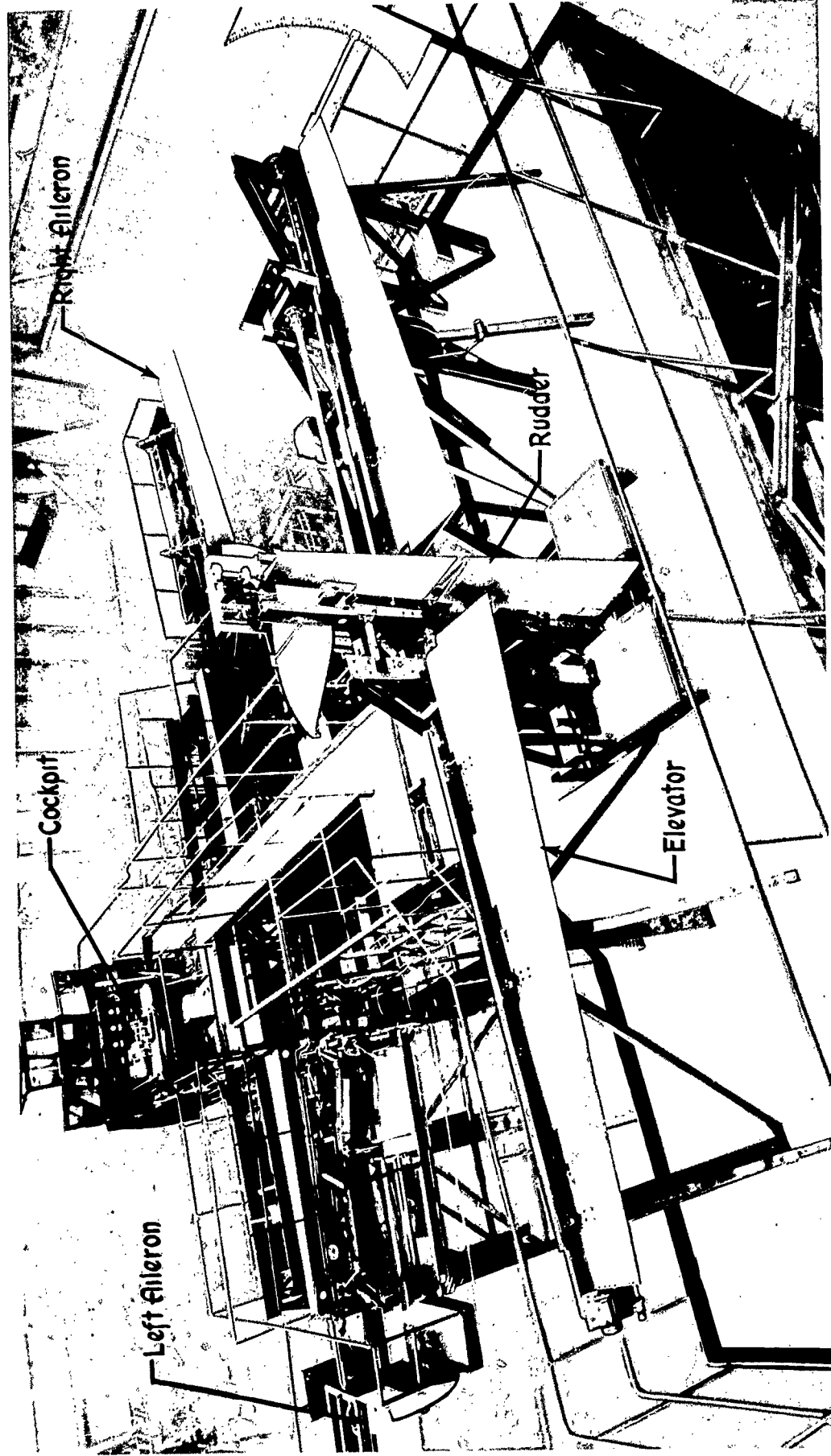


Figure III-1 Control System Test Stand

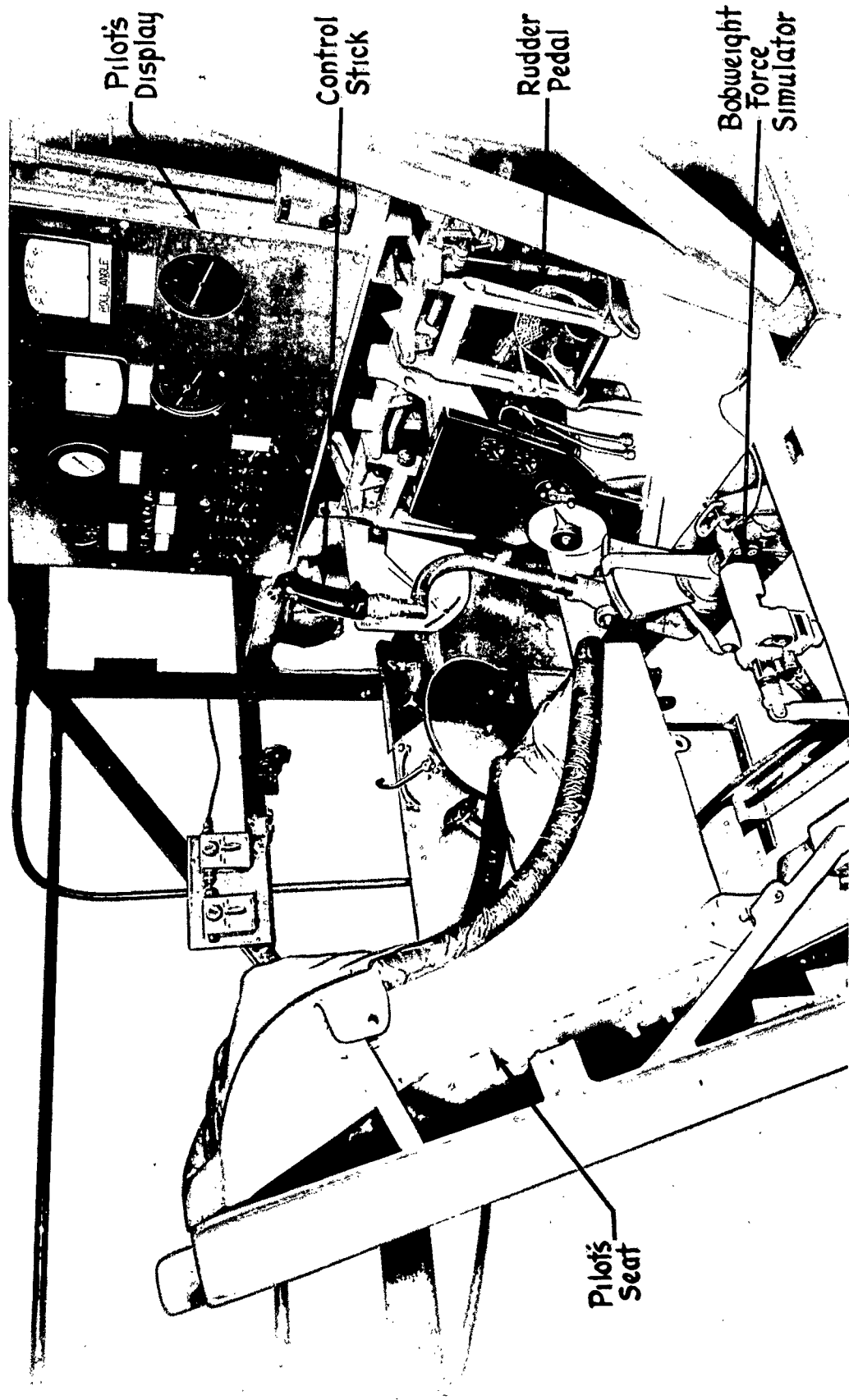


Figure III-2 Cockpit Control System Test Stand

The controlled platforms mentioned above (occasionally called "tilt tables" or "roll tables") are sometimes used to produce physical inputs to the motion sensors. This equipment usually takes the form of a platform whose angular attitude is controlled, in one or more degrees of freedom, by signals from the analog computer. By this means, physical inputs can be produced for rate and displacement gyros and for low range lateral and longitudinal accelerometers when the sensors are mounted on the platform. Technical difficulties associated with obtaining adequate speed of response for large platforms have in the past restricted the use of such devices to applications requiring small displacement of sensors of relatively low inertia, except for special research installations. When a controlled platform is not used, the sensors are simulated by means of an analog computer.

Additional equipment is required to make the form of the signals in the simulated equipment compatible with those in the real equipment. For example, the angular rotation of the control surface must be changed to a voltage before it can be used by the analog computer as an input to the airframe equations. This is usually accomplished by a potentiometer type pickoff which is attached to the control surface. Modulators, demodulators, and scale changing devices are used to change the form and level of electric signals.

Section 2

A block diagram showing a setup for testing a stability augments or one channel of an autopilot on a control system test stand is shown in Figure III-3.

Without using a human pilot, open and closed loop frequency responses can be obtained on the test stand and compared to those of the complete system analog which was developed during the synthesis phase. Since most surface control systems are somewhat nonlinear, the effect of input amplitude on the frequency response should be determined. If the nonlinear effects are greater than anticipated, design changes can be made so that the undesirable effects of the nonlinearities can be minimized. If a sinusoidal force is required for use in conducting the frequency response tests, this can be conveniently obtained by means of the bobweight force simulator, if one is available, by applying an electrical sine wave input to the simulator. Stick-free transient tests can be conducted by deflecting and then releasing the proper cockpit control manually. A method of obtaining system response to arbitrary force inputs consists of applying the desired electrical function to the bobweight force simulator.

As mentioned previously, the use of the test stand permits additional and more realistic tests to be conducted for those operating modes in which the human pilot is included in the control loop. For these configurations, tests can be conducted with a pilot sitting in the cockpit and "flying" the simulator by observing the instruments mounted on the pilot's instrument panel. Such tests permit pilot evaluation of a system much earlier in the design

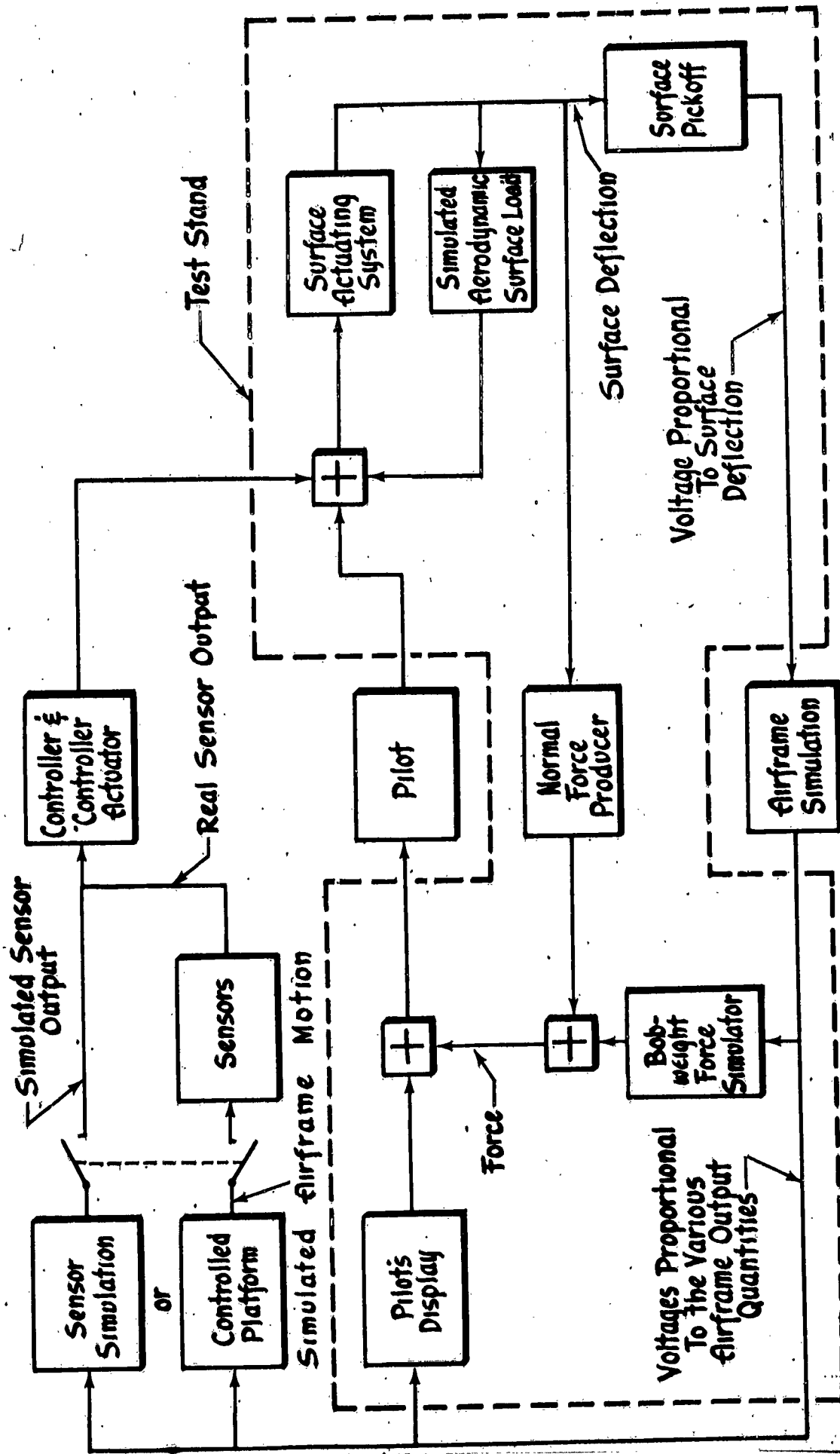


Figure III-3 Block Diagram of Test Setup Using a Control System Test Stand

Section 2

program than by any other method. Since actual operating conditions are much more closely simulated than was the case when the entire system was analoged, the test stand provides information that would otherwise be obtained only in flight. This reduces the magnitude of the flight test program. Quite realistic tests can be arranged for certain conditions which arise due to the tactical mission of the aircraft. For example, if the system under test is a stability augments whose purpose is to aid the pilot in aiming his weapons, a simulated tracking condition could be mechanized, including the dynamics of the gunsight. For this condition the gun sight pipper might be represented as one trace on the face of a dual beam oscilloscope, the other beam being used as a target indication. In this manner, the effect on tracking proficiency of varying system parameters can be rapidly determined at a sufficiently early date to permit any indicated design changes to be conveniently made.

Another important application of the controls test stand is found in investigating the results of possible component failures which might cause sudden, large amplitude, surface deflection. In this application, a systematic program is conducted to effect various failures such as tube failures, and open and short circuits. It is usually wise to obtain results for these tests both with and without the pilot in the loop, since experience has shown that the pilot sometimes causes a more severe maneuver than if he had not reacted at all. In those cases where there is any question regarding the structural safety of the airplane because of component failures, tests of this nature are almost mandatory

because of the danger involved in determining these effects in flight.

The greatest limitation in ground tests involving the use of the human pilot lies in the difficulty of adequately simulating the cues to which he responds in flight. Although a pilot's display can be constructed which will adequately supply the pilot with visual stimuli to simulate instrument flight, for non-instrument flight the pilot responds in some unknown way to such cues as the apparent motion of clouds or the earth and the position of the horizon and other airplanes. Completely ignored are the effects of such factors as his physical orientation, and the accelerations to which he would be subjected in actual flight. For these reasons, test stand tests should be restricted to those conditions in which the effects of the above limitations are considered unimportant.

At the completion of the test stand program, the prototype equipment should be installed in an airplane for ground tests. These will provide verification of the results obtained on the test stand. If a flight simulation program was not conducted on the test stand, the procedures as outlined above should be carried out with the airplane substituted for the test stand. In addition, tests should be conducted to establish suitable inspection test procedures to be used for the production system.

Section 2

Flight simulation tests on the airplane are conducted in the same manner as outlined for the test stand. All the comments made above with respect to test procedures and test equipment for the control system test stand apply to the ground airplane tests, including the use of the analog computer to simulate flight. If an extensive program has been conducted on the test stand, this portion of the airplane ground tests will probably be limited to verifying that the performance of the system on the airplane does not differ significantly from the performance observed on the test stand. This can often be accomplished without the use of a human pilot, but with the aerodynamic loop closed, by obtaining frequency and transient responses for comparison with previous test stand results. Conversely, if the test stand was not utilized, it will be useful to carry out airplane ground tests similar in nature and scope to those mentioned in the discussion of the test stand. As mentioned previously, such tests have the dual advantage of saving flight time (and therefore cost) and of determining the effects of varying system parameters much more rapidly than could be accomplished in flight.

Inspection test procedures are required to ensure that malfunctioning components are not installed in airplanes when the system reaches the production stage. In addition, most automatic flight control systems require individual adjustments after installation in the airplane to compensate for component and airplane tolerances. Procedures for accomplishing this must be developed and written in such a way that the tests can be conducted by

mechanics or technicians not familiar with automatic control system theory. Since these test procedures are often quite complicated, even for a single channel stability augments, it is almost mandatory that experiment be relied upon to some extent if a realistic test procedure is to be developed. A method which experience has shown to be satisfactory consists of first writing a preliminary but detailed test procedure and then carrying out this procedure on an airplane at the earliest possible date and modifying as necessary. The first system available for this test will normally be the prototype system installed in the airplane used for ground tests.

The final evaluation of the operating characteristics of an automatic flight control system is, of course, made by means of flight test. The magnitude of the flight test program depends to a large extent on the type of system being tested and on the amount of ground test that preceded. If a thorough flight simulation program has been conducted by means of either the controls test stand or airplane ground test for a system in which the airframe dynamics are adequately simulated by the linearized perturbation equations, the flight test may consist of no more than verification of the results previously obtained on the ground. For more complex systems, however, such as a multi-channel maneuverable autopilot, some development work and optimization of system parameters must be accomplished during the flight test phase.

Section 2

This condition arises primarily from the effects of those airframe and pilot characteristics which were neglected during the previous tests.

The same airframe output and input quantities which were recorded during ground tests should be recorded in flight. A sufficient number of additional quantities should be recorded to facilitate analysis of system operation in the event that unexpected modes of operation occur. In addition, those quantities which define flight condition and airframe configuration should be recorded. The recording devices for flight test normally consist of a photographic type recording oscillograph and a motion picture camera. The oscillograph accepts voltages from the sensors and transducers, and the camera is used to photograph an instrument panel (usually called a "photopanel") upon which are mounted duplicates of applicable pilot's flight instruments. Sensors for flight test instrumentation can be any of those discussed previously for use with automatic flight control systems.

The initial stages of the flight test program should consist of a repetition of those tests which were conducted in the flight simulation ground tests to verify the results obtained there. Depending on the type of system being tested, it may then be desirable to extend the program to those conditions which were not simulated during ground tests. These may consist of simulated tactical situations or large scale turning maneuvers involving considerable coupling between longitudinal and lateral airframe modes which are difficult to simulate on the analog computer. Since these represent new

test conditions, the results of this phase may call for some redesign or readjustment of system parameters.

(e) DESIGN OF PRODUCTION COMPONENTS

The design of the production components cannot be said to occur chronologically at this point, but it should be completed at approximately the same time as the flight test program for the prototype equipment. It can be said to begin at the time the sensors and actuators are chosen. Design work then continues throughout the synthesis and analysis phase, utilizing the design requirements which are derived there, until the system controller has been designed. This normally completes the preliminary design work, and the preproduction system is fabricated to these drawings. As the preproduction system testing progresses, design changes are made and the equipment modified as the test results dictate. In this manner, production design work is completed at the conclusion of the flight testing of the preproduction system.

The results of the design procedure to this point consist of the system and component detail specifications and a complete set of drawings. These are used by the production facility or by an outside vendor to manufacture production components.

(f) TESTING OF PRODUCTION SYSTEM

Three tasks remain to be accomplished at this point:

1. To establish test procedures to be used for routine inspection of production components and systems

Section 2

2. To verify that operation of the production system does not differ significantly from that of the prototype
3. To conduct qualification tests.

One method of conducting inspection tests for the individual components is by means of a bench standard system. To construct the bench standard, detailed tests are conducted on each component of the automatic flight control system until a complete set of components is found whose characteristics fall approximately in the center of their individual tolerance bands. This set of components is then interconnected in a normal manner to form a complete operating bench standard system. Additional equipment, such as controlled platforms, junction boxes, signal sources, simulated actuator loads, and measuring and recording devices, are required to operate the bench standard system. Routine inspection tests are conducted by substituting the component to be tested for its equivalent in the bench standard. Its operation is then checked with the standard components. The inspection tests should, of course, be as brief and as straightforward as possible since they will be conducted by nontechnical personnel, but they must be of sufficient detail to ensure that components not meeting the requirements of the drawings and specifications will not be accepted for use.

In the first production airplane installation, the inspection test procedure previously derived with the aid of the prototype system should be verified. As mentioned earlier, this test provides a check of system operation for the airplane installation and a means of making any necessary adjustments.

This inspection test procedure is used for each airplane installation throughout the production run.

To verify that the operation of the production airplane installation does not differ significantly from that of the prototype system, it will usually be necessary to conduct more extensive tests than those of the routine inspection for the first production installation. Despite good intentions, some differences will always exist between prototype and production systems because, in general, they will not be fabricated by the same people or to the same drawings. The prototype system is made to the preliminary drawings and then modified during prototype testing as dictated by the test results. Due to the pressures of a tight schedule, these modifications are often made in haste and may therefore not adhere to good design practice. Such deficiencies would, of course, be corrected in the production version, but these changes sometimes have unexpected effects on system operation. For example, a change in the design for an actuator mounting bracket between prototype and production has been known to cause instability in the production system due to time lag introduced by a reduction in structural rigidity. To determine the magnitude of such effects, open loop frequency response tests should be conducted as well as tests to determine the system threshold and backlash. If these tests reveal significant differences from the prototype system, the aerodynamic loop should be closed by means of the analog computers to determine the effects on closed loop operation.

Section 2

To provide final evaluation of the production system, a brief flight test program should be conducted. This may consist of repeating a few of the tests that were conducted for the preproduction system. If a thorough ground test program has been conducted, flight test for the production system should be quite brief and may be accomplished in one or two flights.

In addition to the quality control maintained by the inspection tests, the military services demand assurances that flight equipment will have an adequate service life and will operate satisfactorily in any environment likely to be encountered. These assurances must take the form of the results of tests performed in accordance with certain military specifications. The military specification of Reference 19 establishes uniform procedures for testing aeronautical and associated equipment under simulated and accelerated climatic and environmental conditions. In the past, actual tests to be conducted have been determined jointly by the customer and the contractor. Applicable paragraphs of Reference 19 were then called out in the detail specification for the system. A recently proposed specification* calls out explicit environmental tests for each type of automatic flight control system. These tests must be conducted on production components, and it is desirable to perform the tests as early as possible so that any indicated design changes can be incorporated before an appreciable portion of the production contract has been completed.

*See footnote, bottom of page III-3.

SECTION 3 - AN EXAMPLE DESIGN PROBLEM

This section describes the step by step procedure which was used in the actual design of a stability augments. Although the system discussed is relatively simple compared to a complete automatic flight control system, the problems encountered in its design are sufficiently typical to illustrate the design procedure discussed in Section 2.

(a) PRELIMINARY ANALYSIS

As indicated in the previous section, the first step in the design of an automatic flight control system is the determination of the requirements, and these in turn are derived from the requirements for the complete aircraft system. To simplify this analysis, only the lateral directional requirements are considered here. The airplane under consideration is a rocket firing jet fighter and its mission is to intercept and destroy bomber type aircraft through the use of an automatic fire control computer. The mechanization of the fire control computer used is based on the assumption that the airframe sideslip angle is zero. On this basis, hit probability considerations require that the sideslip angle be less than .005 radians at the time the rockets are fired. On the basis of the mission described above, the following airplane system requirements can be listed:

Section 3

1. Spurious lateral directional displacements must be minimized to permit a smooth tracking run to be made.
2. Transient sideslip angle must be minimized and steady state sideslip kept less than .005 radians to provide satisfactory hit probability.
3. The flying qualities specification for the damping of the lateral directional oscillation must be met.

Requirement No. 3 imposes a minimum damping ratio no larger than $\zeta = 0.15$ *. Since a damping ratio this low would permit a considerable amount of spurious lateral directional motion, Requirements 1 and 2 are more severe. Therefore, a system meeting Requirements 1 and 2 will easily meet the dutch roll damping requirements of the handling qualities specifications. Assume that it has been determined (by analog computer studies or by some other means) that the basic airframe will not meet the dutch roll damping requirements of the specifications, and therefore that some form of stability augmentation will be required. The immediate problem consists of determining the type of automatic control which shows the most promise of ensuring that the above requirements are met.

(b) ANALYSIS AND SYNTHESIS

One commonly used method for augmenting dutch roll stability is to make the rudder deflection a function of yaw velocity (r). This tends to augment the stability derivative N_r , and as shown in Figure II-18, will increase the damping of the dutch roll mode. Although the yaw rate damper tends to reduce dynamic sideslip, it in no way minimizes steady state sideslip angle, and since this is one of our requirements, another device would be required to accomplish this.

*At the time this system was designed, the specification of (Reference 20 and 21) were applicable.

SECTION 3 - AN EXAMPLE DESIGN PROBLEM

This section describes the step by step procedure which was used in the actual design of a stability augments. Although the system discussed is relatively simple compared to a complete automatic flight control system, the problems encountered in its design are sufficiently typical to illustrate the design procedure discussed in Section 2.

(a) PRELIMINARY ANALYSIS

As indicated in the previous section, the first step in the design of an automatic flight control system is the determination of the requirements, and these in turn are derived from the requirements for the complete aircraft system. To simplify this analysis, only the lateral directional requirements are considered here. The airplane under consideration is a rocket firing jet fighter and its mission is to intercept and destroy bomber type aircraft through the use of an automatic fire control computer. The mechanization of the fire control computer used is based on the assumption that the airframe sideslip angle is zero. On this basis, hit probability considerations require that the sideslip angle be less than .005 radians at the time the rockets are fired. On the basis of the mission described above, the following airplane system requirements can be listed:

A more satisfactory method of providing augmentation is to control sideslip angle, since this permits minimization of transient and steady state sideslip as well as improvement in dutch roll damping. The most direct way of achieving this sort of control is to measure sideslip angle and to use this signal, after subjecting it to proper equalization, to control the rudder as shown in the block diagram of Figure III-4.

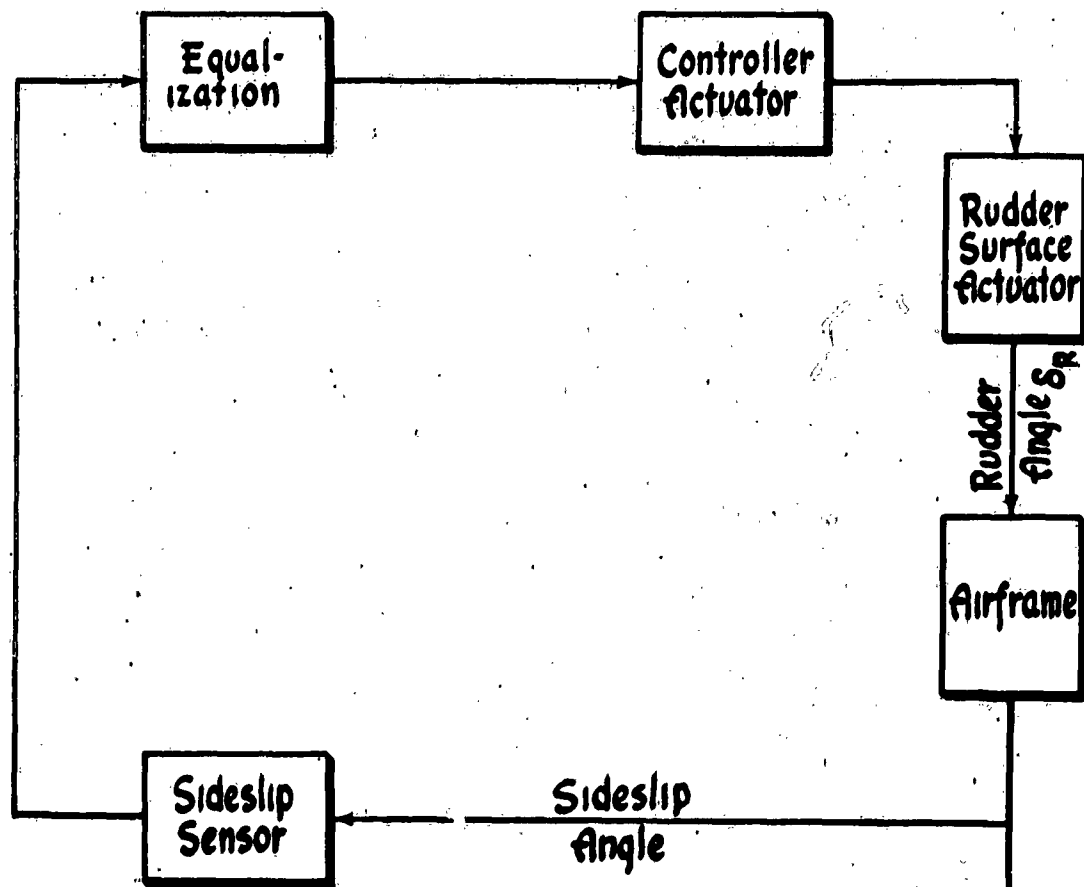


Figure III-4 Preliminary Functional Block Diagram for Sideslip Stability Augmentor

Section 3

It will be noted that the system as proposed requires the use of a device to measure sideslip angle. Direct measurement of sideslip by local flow direction detectors is difficult because these detectors have certain basic faults* in addition to being subject to adverse angle of attack effects and local flow disturbances. For these reasons, direct measurement of sideslip angle was not used.

It was shown in Equation (II-86) that an accelerometer provides a reasonably satisfactory measure of sideslip angle. In particular, it was shown that for an accelerometer located at the c.g. of an airframe,

$$(III-1) \quad a_y = Y_{\delta_R} \delta_R + Y_{\beta} \beta$$

where

a_y = lateral acceleration sensed by the accelerometer at the c.g.

$Y_{\delta_R} \delta_R$ = the rudder deflection contribution to a_y

$Y_{\beta} \beta$ = the sideslip angle contribution to a_y

Equation (III-1) shows that the lateral acceleration at the airframe c.g. is proportional to sideslip β whenever $\delta_R = 0$.

*See Chapter II, Section 5.

The effect of δ_R could be removed by subtracting an electrical signal proportional to $Y_{\delta_R} \delta_R$ from the accelerometer signal; however, this requires additional equipment.

The effect of the rudder motion on the accelerometer signal can be reduced by the method illustrated in Figure III-5. This figure shows the accelerometer located forward of the airframe c.g. The position which gives minimum rudder effect is the center of percussion, which is defined as the point along a body about which the body starts to rotate without translation for a force impulse at a specific point. For a force impulse at the rudder, the position of the center of percussion for an airframe is given by

$$(III-2)^* \quad l_x = \frac{K_z^2}{l_x}$$

where K_z is the airframe radius of gyration about the z axis and l_x and l_x are shown in Figure III-5.

The acceleration at the center of percussion will be denoted by a_y' and is given by

$$(III-3) \quad a_y' = a_y + l_x \ddot{r} = Y_{\delta_R} \delta_R + Y_{\beta} \beta + l_x \ddot{r} \approx Y_{\beta} \beta$$

*See for example, Leigh Page, Introduction to Theoretical Physics, D. Van Nostrand & Co., New York, 1935, pp 132.

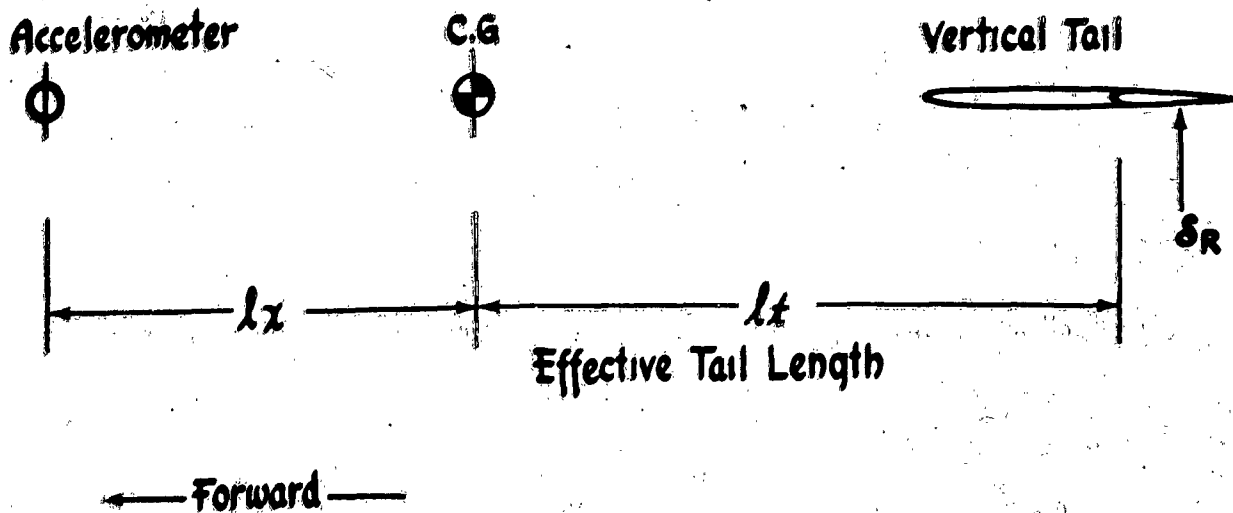


Figure III-5 Center of Percussion Relationships

To determine how this accelerometer position will affect the characteristics of the controlled element, a composite Bode diagram was constructed as shown in Figure III-6. This figure shows a_y/s_r , a_y'/s_r , and β/s_r plotted on the same diagram. Inspection of this diagram reveals the following interesting points.

- (1) At frequencies below the dutch roll natural frequency, either accelerometer position gives a satisfactory indication of sideslip angle.
- (2) At frequencies above the dutch roll natural frequency, neither accelerometer position provides signals exactly proportional to sideslip angle, although the center of percussion gives a more accurate indication than does the c.c.
- (3) Satisfactory performance can be obtained more easily with an accelerometer located at the center of percussion because of the lower amplitude ratio at the higher frequencies.

On the basis of these considerations it was concluded that good system performance could be obtained if a suitable accelerometer could be found.

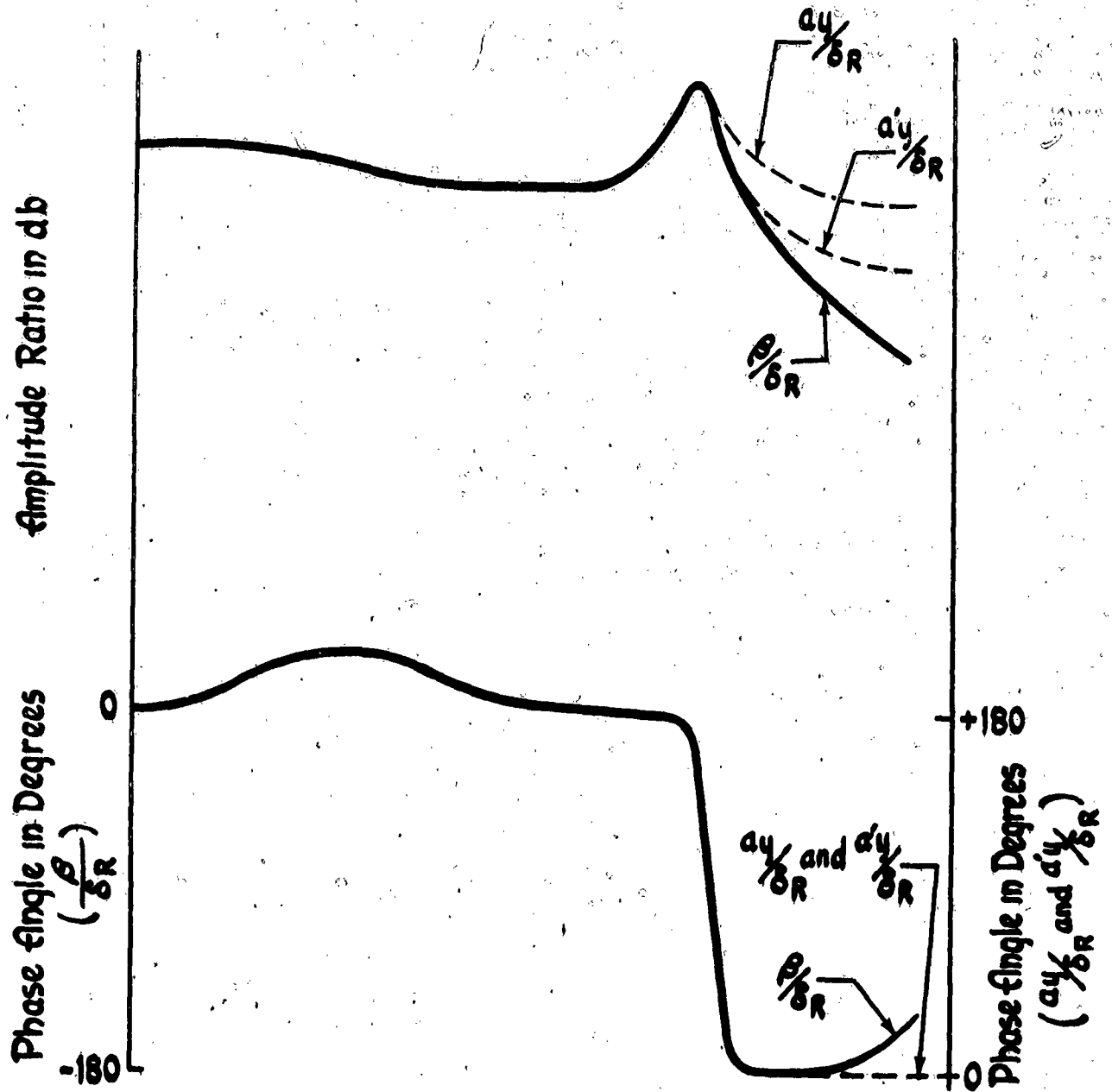


Figure III-6 Comparison of Sideslip Angle, Acceleration at Center of Gravity and Acceleration Forward of Center of Gravity

The block diagram for the system using lateral acceleration as the controlled airframe output quantity is shown in Figure III-7.

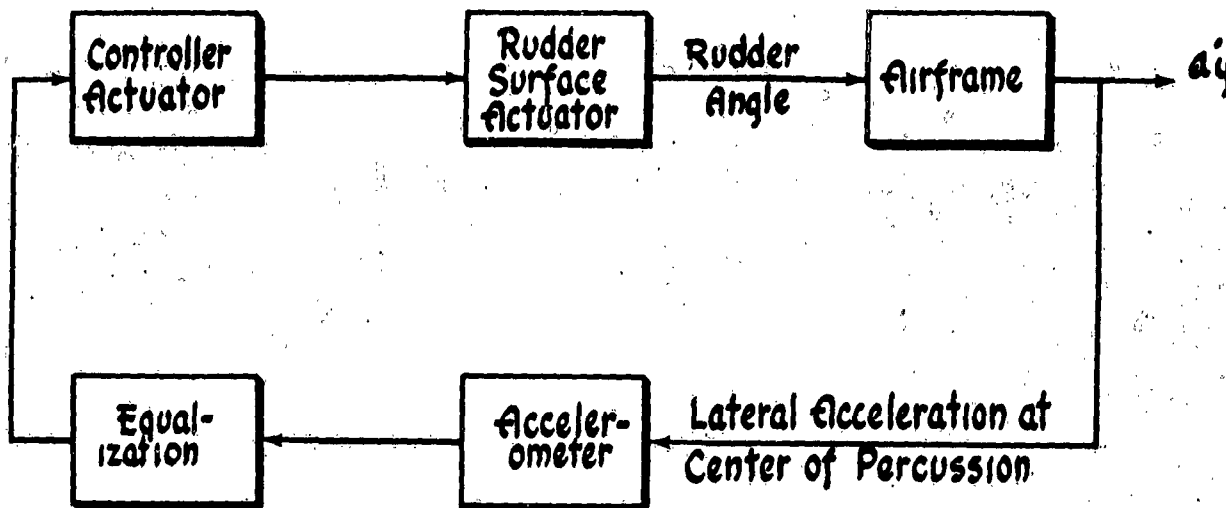


Figure III-7 Preliminary Block Diagram for Sideslip Stability Augmentor with Lateral Acceleration

Locating the accelerometer forward of the c.g. has one serious drawback: it would adversely affect the coordination in aileron turns. This is illustrated in Figure III-8 which shows that a yawing acceleration occurs when a turn is entered. The $l_x \dot{\psi}$ contribution to the accelerometer signal (see Equation (III-3)) would cause a rudder deflection which would oppose the yawing acceleration, thus causing the airframe to sideslip as it enters the turn. After a steady state turn is established, however, there would be no effect due to $l_x \dot{\psi}$, since $\dot{\psi}$ is zero.

R = Radius of Turn
 r = Rate of Turn

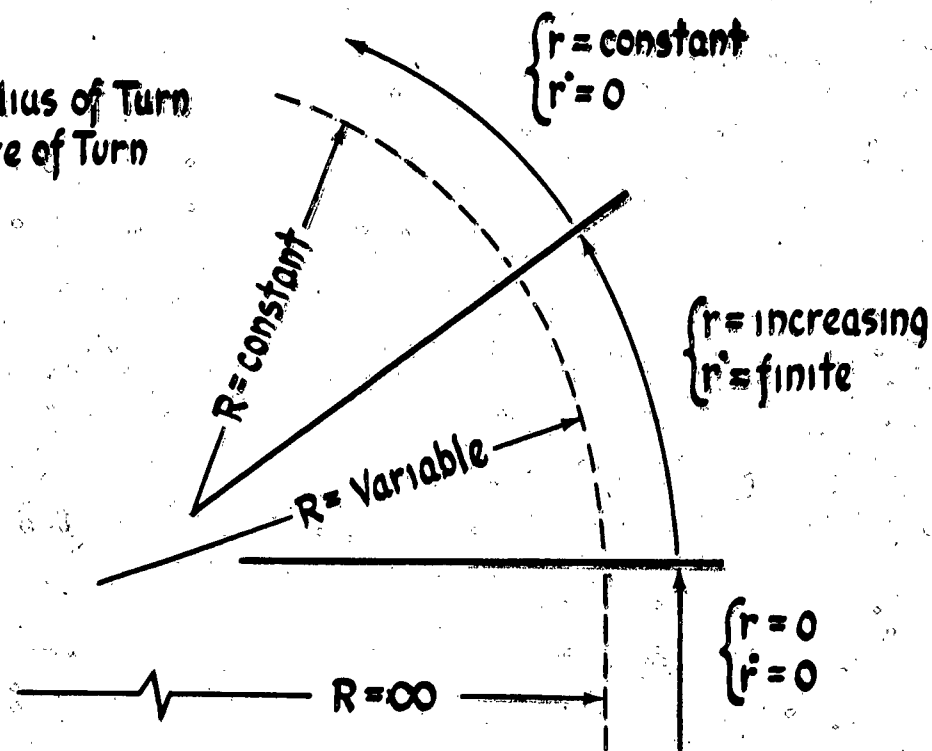


Figure III-8 Geometry of Turn

One simple method for counteracting this tendency is to provide to the rudder a lagging signal proportional to the aileron deflection. Thus, when right aileron is applied, this lagging aileron signal will deflect the rudder to the right to counteract the $L_x \dot{\delta}$ portion of the accelerometer signal. This method was used in this example and the determination of the magnitude of the time lag will be demonstrated in the section dealing with the analog computer study.

Section 3

Since sideslip stabilization is to be used in manual flight, it is advantageous to use a series linkage to tie the actuator into the rudder surface actuator. This will allow the pilot to add rudder motion to the stability aug-
menter when he desires to sideslip the airplane. In addition, the rudder motions due to the augments are not fed back to the pilot through pedal motion, and thus, confusing feel characteristics are avoided. The restrictions which this requirement places on the controller actuator would depend, of course, on the surface actuating system configuration. In this example, the surface actuating package had been previously designed as a fully powered hydraulic system, but the design of the artificial feel mechanism had been delayed pending determination of the requirements for the controller actuator.

It is advantageous to include manual rudder trim in the system to minimize problems arising from the series installation of the actuator. This is easily done by feeding a signal proportional to the desired trim angle into the rudder actuator, as shown in Figure III-9.

Little can be said about the system control unit at this point, except that it must accept signals from the accelerometer, aileron position sensor and pilots trim sensor, provide equalization in accordance with requirements yet to be determined, and provide driving signals to the actuating device which are proportional to the modified sensor signals. The signals to the controller will almost certainly be electrical and may be either ac or dc depending on the types of sensors available.

This concludes the derivation of the basic system configuration. The system block diagram showing all signal paths and the general types of sensing and actuating elements to be used is presented in Figure III-9. The stability augments as shown should provide good two control operation, since it will tend to minimize sideslip, even for aileron inputs. This should permit the pilot to fly the airplane without using the rudder pedals.

A list of the sensing and actuating elements along with their desirable characteristics, as thus far determined is presented below.

1. Accelerometer - Must be capable of providing an electrical output proportional to lateral acceleration.
2. Aileron position sensor - Must produce an electrical signal proportional to aileron deflection. A cable driven potentiometer would provide this signal.
3. Pilot's trim device - Must provide an electrical signal which indicates the pilot's desired rudder trim angle. A knob driven potentiometer located in the cockpit would accomplish this function.
4. Actuator - Must be capable of providing an output motion proportional to an electrical input from the control unit. Series installation is required, and an extensible link type actuator is a natural for this.

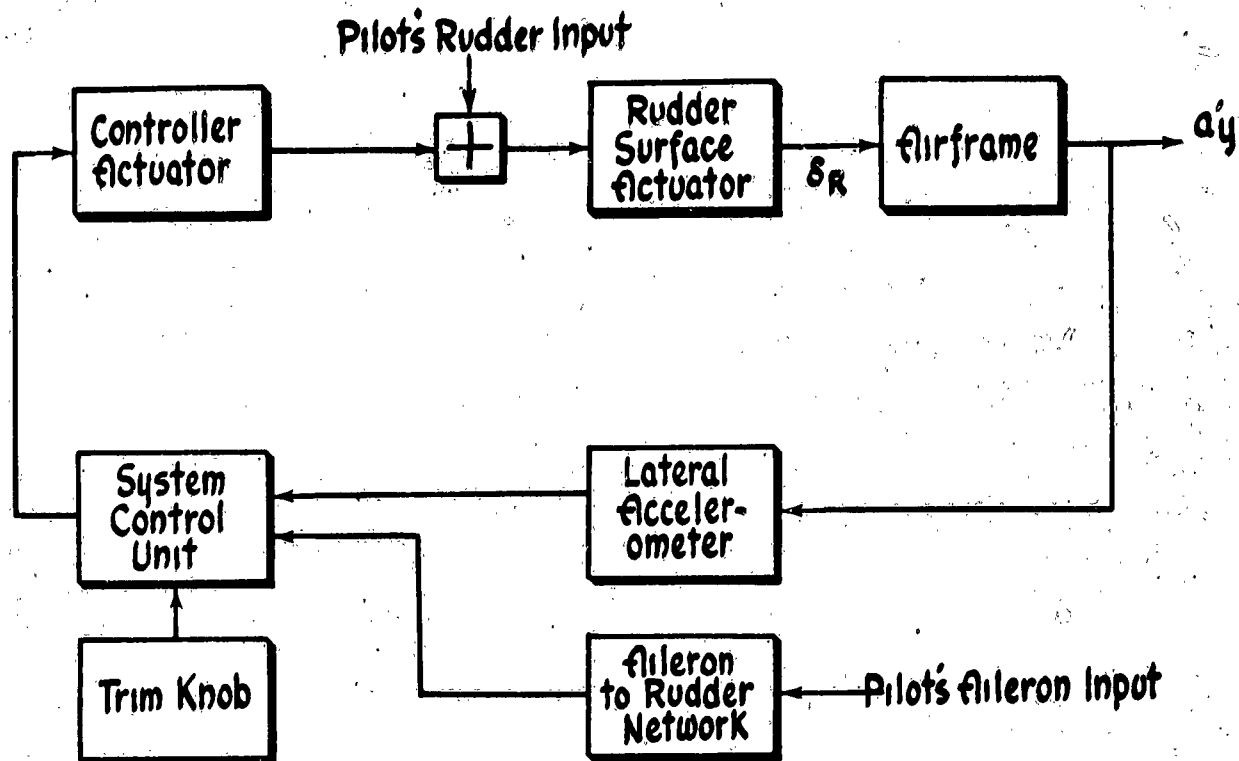


Figure III-9 Final Block Diagram for Sideslip Stability Augmentor

It was felt that a factor which might make the choice of the accelerometer very critical was the threshold requirement. Aside from stability considerations the accelerometer threshold for this application must be sufficiently low that the requirement for maintaining steady state sideslip below 0.005 radians could be met. Since the system configuration depended on the possibility of obtaining a suitable accelerometer, a catalog search was made at this time rather than waiting until after the detail analysis as is usually done.

The required accelerometer threshold can be obtained through the use of Equation (II-33) which is repeated here for reference.

$$(III-4) \frac{a_y}{g_r} = U_0 Y_r \frac{B}{\delta_r}$$

Equation (III-4) gives the relationship between a_y and B , and since, in the steady state $a_y = a'_y$, Equation (III-4) can be written as:

$$(III-5) \frac{a'_y}{g_{ss}} = U_0 Y_r B$$

This relationship is plotted as a function of g_c (impact pressure) for several values of B in Figure III-10.

It was decided that the accelerometer should have a threshold corresponding to a sideslip angle no larger than one tenth the system requirement of .005 radians. Although this ratio is somewhat arbitrary, the accelerometer threshold is made much less than the system requirement to make allowances for the thresholds and deadbands in the other components. From Figure III-10, it will be noted that the accelerations equivalent to $B = .0005$ radians decreases with g_c . The accelerometer threshold should therefore be established at the lowest value of g_c which is considered representative of a tactical flight condition. This value is approximately 140 psf which corresponds to .75 Mach number at an altitude

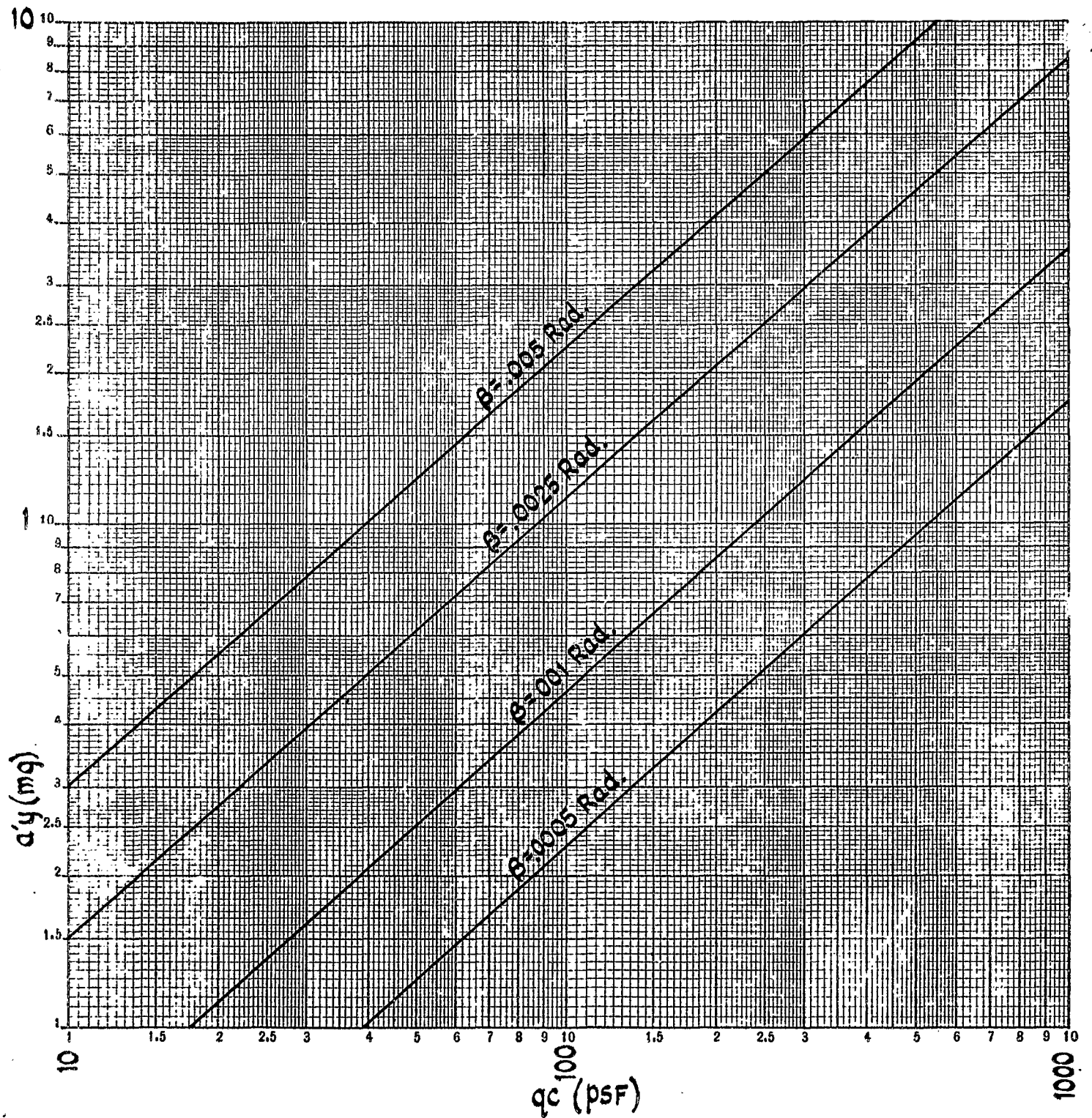


Figure III-10 Steady State Lateral Acceleration ($a'y$) vs. q_c (psf)
For the Indicated Steady Sideslip Angles

of 45,000 feet. For this condition, the value of $a'_{y/SS}$ corresponding to $\beta_{SS} = .0005$ radians is approximately 0.3 milli-G's.

To insure that the phase lag of the accelerometer would be small in the frequency range of interest, the minimum accelerometer natural frequency was established at ten times the airframe maximum natural frequency. Reference to Table III-1 shows ω_{nd} to be approximately 2.2 radians per second or .35 cps. On this basis, the minimum natural frequency for the accelerometer was chosen as 3.5 cps.

A catalog search revealed a qualified accelerometer with the following characteristics.

1. Threshold less than 0.1 milli-G's.
2. Linearity $\pm 5\%$
3. Range $\pm 0.3G$
4. Natural frequency 3 cps
5. Damping Ratio 0.3
6. Sensitivity, 8v/G when excited by 115V, 400 cps

Although the natural frequency of this accelerometer is slightly below 3.5 cps, it was found to be the only qualified accelerometer available which met the threshold requirement. It was therefore decided to utilize the characteristics of this accelerometer in the analysis and synthesis phase to determine whether satisfactory performance could be achieved. It is a spring-mass-damper accelerometer

Section 3

and its transfer function was derived in Chapter II and given by Equation (II-83). It is repeated here in slightly different form.

$$(III-6) \frac{e_a(s)}{a_y} = \frac{K_a}{\left(\frac{s}{\omega_{na}}\right)^2 + \frac{2\zeta_a s}{\omega_{na}} + 1}$$

where

$$\omega_{na} = 20 \text{ RAD/SEC}, \zeta_a = 0.3 \text{ AND } K_a = 8 \text{ VOLTS PER G'S}$$

Since a satisfactory electrohydraulic series servo actuator had been developed for a previous system, it was decided that this actuator should be used for the sideslip stability augments. The open loop transfer function for this actuator when driving a spring restrained load was given in Equation (II-111) as

$$(III-7) \frac{\sigma}{I} = \frac{K_c}{\tau s + 1}$$

where $K_c = k_f / k_L$ and $\tau = B_{cp} / k_c$. The symbols k_f and B_{cp} are defined in Chapter II Section 7, and k_L is the load spring rate. Since for this particular series installation, the load spring rate will be small enough to be neglected, Equation (III-7) is written as

$$(III-8) \frac{\sigma}{i} = \frac{k_F/k_L}{B_{cp}/k_L s + 1} = \frac{k_F}{B_{cp} s + k_L}$$

Setting $k_L = 0$ results in

$$(III-9) \frac{\sigma}{i} = \frac{k_F}{B_{cp} s}$$

The electrohydraulic actuator is used as a position servo as shown in Figure III-11, where K_a is the amplifier gain, K_p is the feedback potentiometer gain and σ is the actuator displacement.

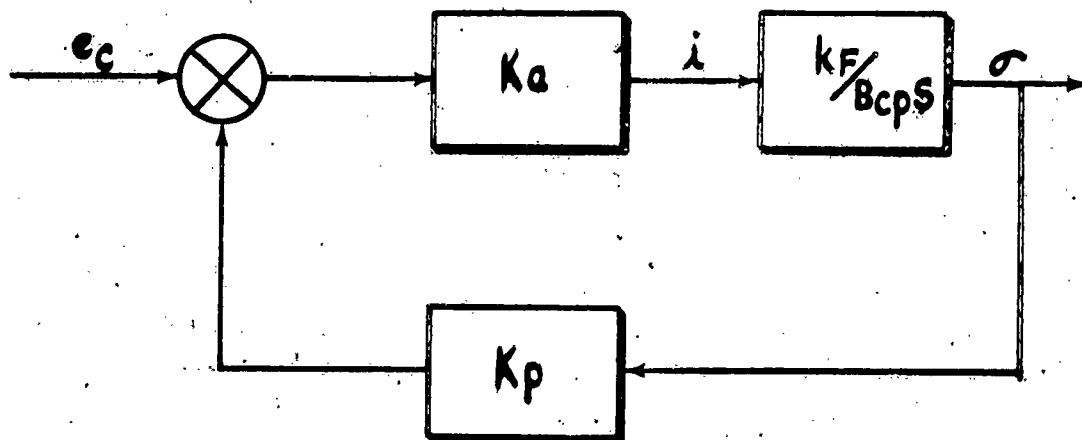


Figure III-11 Controller-Actuator Control Loop

Section 3

The closed loop transfer function for Figure III-11 is given by

$$(III-9) \frac{\sigma}{e_c} = \frac{K_a k_F}{B_{cp} s + K_a K_p k_F} = \frac{\frac{1}{K_p}}{\frac{B_{cp} s + 1}{K_a K_p k_F}}$$

or

$$(III-10) \frac{\sigma}{e_c} = \frac{K_M}{\tau_M s + 1}$$

where $K_M = \frac{1}{K_p}$ and $\tau_M = \frac{B_{cp}}{K_a K_p k_F}$

Due to the difficulty in accurately determining B_{cp} and k_F , the loop was adjusted for optimum performance experimentally. After this adjustment it was found that $\tau_M = .03$ seconds. The gain control K_M is left to be determined as an alterable design element of the system during the detail design procedures subsequent to the system analysis and synthesis.

The surface actuator for the aircraft under consideration consisted of a full-powered hydraulic system. It was found experimentally that this system could be represented by

$$(III-11) \frac{\delta_R}{\sigma} = \frac{K_H}{\tau_H s + 1}$$

where $\tau_H = 0.03$ seconds, and $K_H = 10.6$ deg/inch.

The airframe transfer function is given by

$$(III-12) \quad \frac{a'_y}{sR} =$$

$$= \pm K_{ay} \frac{(-T_{ayR1} s+1)(T_{ayR2} s+1)(T_{ayR3} s+1)(-T_{ayR4} s+1)}{(T_s s+1)(T_R s+1)\left(\frac{s^2}{\omega_{nd}^2} + \frac{2\zeta s}{\omega_{nd}} + 1\right)} \frac{\text{"g"}}{\text{DEG}}$$

Numerical values for Equation (III-12) are given in Table III-1 for seven flight conditions.

The basic sideslip stability augments is shown with these transfer functions in Figure III-12. The remaining problem is to determine the equalization required in the system control unit.

*Note that T_{ayR3} and T_{ayR4} differ from T_{ayR3} and T_{ayR4} as given in Equation (II-41) because of the relocation of the accelerometer.

Section 3

CONDI- TION	MACH NO.	ALT. FT.	WEIGHT	C.G. POSI- TION	K_{a4} g ^{1/2} /deg	$\frac{1}{\text{Tay} R_1}$	$\frac{1}{\text{Tay} R_2}$	$\frac{1}{\text{Tay} R_3}$	$\frac{1}{\text{Tay} R_4}$	$\frac{1}{T_5}$	$\frac{1}{T_R}$	ω_{nd}	L_D
I	.26	5,000	33,000	22%	.102	-.0177	1.02	2.39	-2.34	.001	.789	.669	.129
II	.75	45,000	33,000	22%	-.0068	-.008	.657	2.41	-2.42	-.005	.706	1.09	.0035
III	.35	5,000	33,000	22%	-.014	-.0199	1.17	3.54	-3.55	-.01	1.25	1.20	.023
IV	.77	35,000	37,000	23%	-.0145	-.007	.69	3.04	-3.05	-.004	.75	1.23	.01
V	.85	35,000	37,000	23.3%	-.027	-.005	.81	3.47	-3.47	-.0025	.86	1.34	.013
VI	.70	20,000	37,000	23.3%	-.0355	-.005	1.11	3.97	-3.97	-.002	1.16	1.49	.025
VII	.85	10,000	37,000	*2.3%	.0904	-.0014	2.24	5.90	-5.93	.00048	2.28	2.19	.04

Table III-1 Numerical Values for Equation IV-9

It will be noted from the preceding discussion and from Figure III-12 that the only alterable block remaining in the system is the system control unit. The remaining steps in the analysis and synthesis

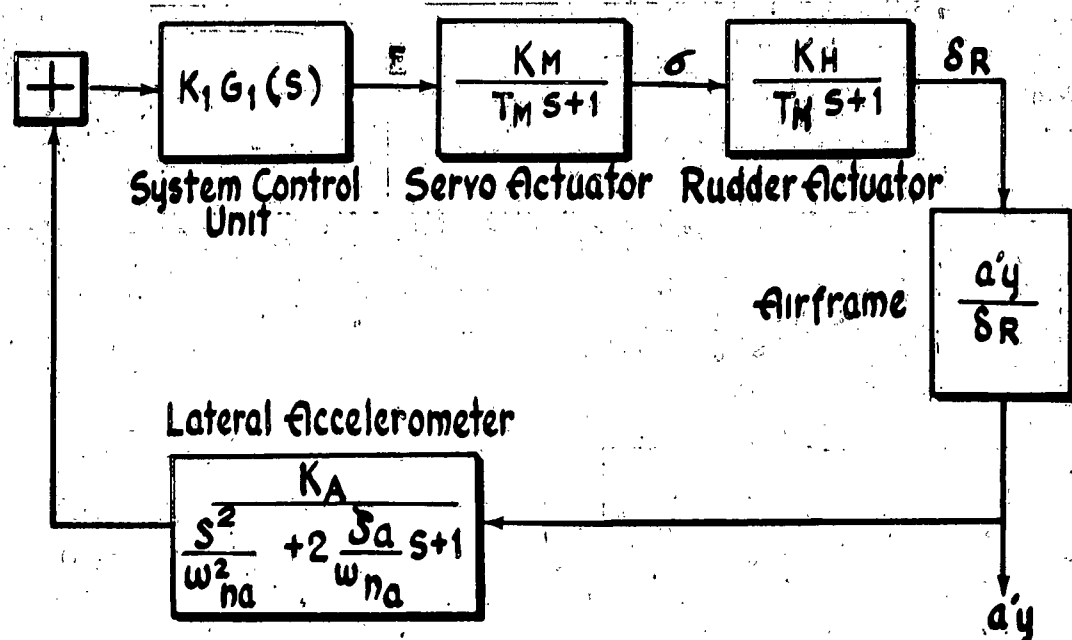


Figure III-12 Basic Loop of Sideslip Stability Augmentor

phase are concerned with determining those characteristics of the system control unit which will provide performance meeting the system requirements. This is accomplished by Bode plots and root locus and the results are verified on the analog computer.

Section 3

Figure III-13 is a generic Bode plot of the $\frac{d_i}{\delta_n}$ transfer function (for the spirally divergent conditions) and of the complete open loop transfer function indicated in Figure III-12, in which the system control unit is represented by a pure gain, K_i . It is apparent that with a pure gain term for the system control unit, there is no value of system gain ($K_{OL} = K_A K_i K_M K_H K_{d_i}$) which can be used satisfactorily. This fact is even more evident in the root locus sketch corresponding to the Bode plot of Figure III-13. The root locus sketch is shown in Figure III-14.*

From the root locus, it can be seen that there is only a very slight increase in dutch roll damping, as the system gain is increased. As the system gain is increased further, the dutch roll damping begins to decrease. Note also that when the gain is high enough, the dutch roll becomes unstable.

To increase the dutch roll damping, a lead term of the form $\frac{T_A s + 1}{T_A s + 1}$ must be used in the system control unit to increase the phase margin near dutch roll frequencies. The lead circuit will arbitrarily be chosen so that the phase angle is increased by about 60° for the lowest dutch roll natural frequency to be expected which is approximately 0.6 radian per second. Choosing $\frac{1}{T_A}$ to be 0.3 radian per second should satisfy this condition. The generic Bode plot now appears as in Figure III-15.

To attenuate high frequency noise inputs and also to provide for a larger operating gain margin, a lag must be used in conjunction with the lead so that the system control unit transfer function becomes

*For simplicity, the assumption has been made that $T_{AYR_2} = T_R$ in the root locus diagram of Figure III-14. In addition, all the root locus diagrams used in this example are based on a phase angle of 0 degrees rather than 180 degrees, due to the sign change which occurs in the controller. (See reference 8, page III-21.)

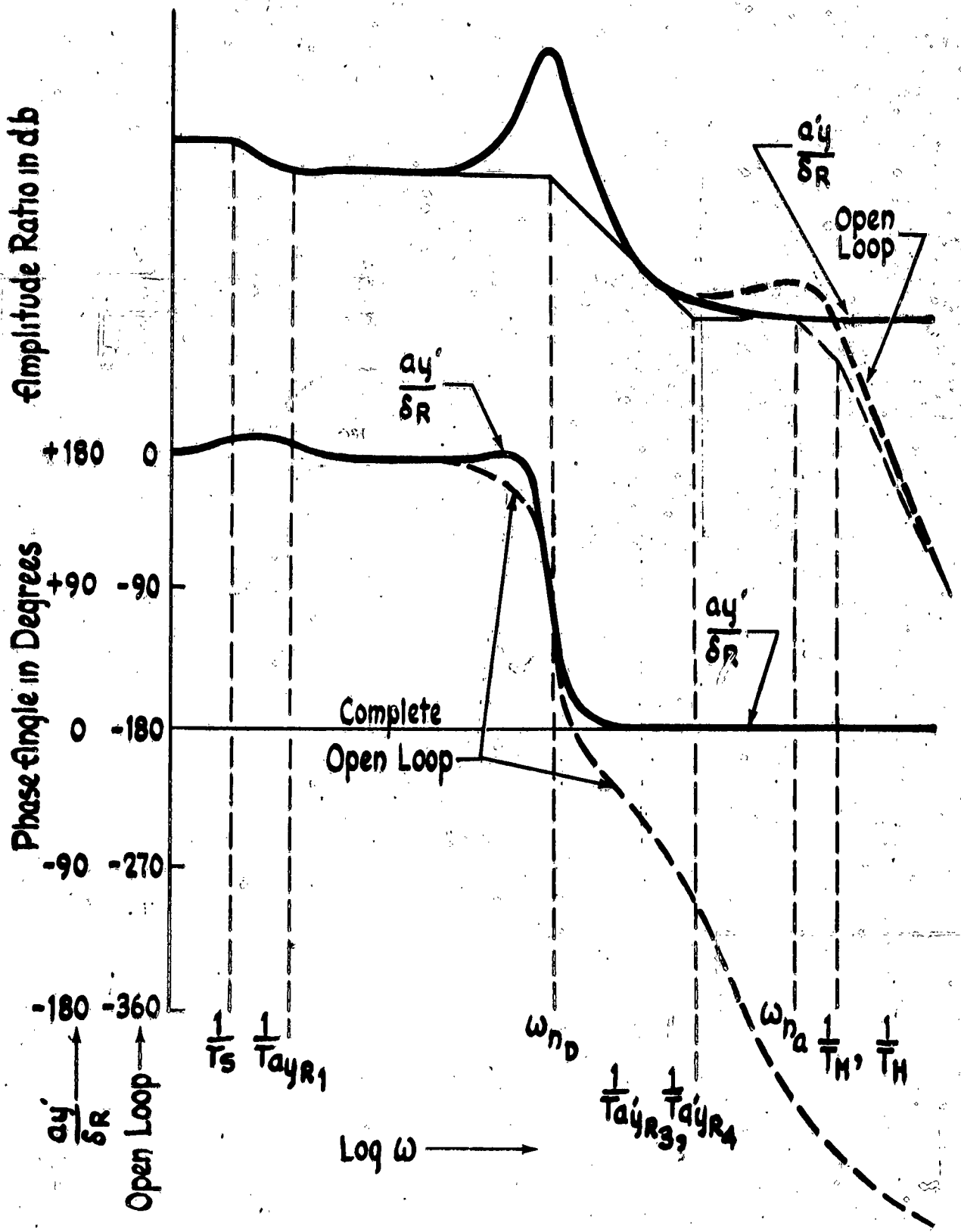


Figure III-13 Generic Bode Plot for $\frac{aY'}{\delta R}$ and for $\frac{aY'}{\delta R} \cdot \frac{\delta R}{\sigma} \cdot \frac{\sigma}{E} \cdot \frac{E}{V_a} \cdot \frac{V_a}{aY'}$ with Pure Gain in the System Control Unit

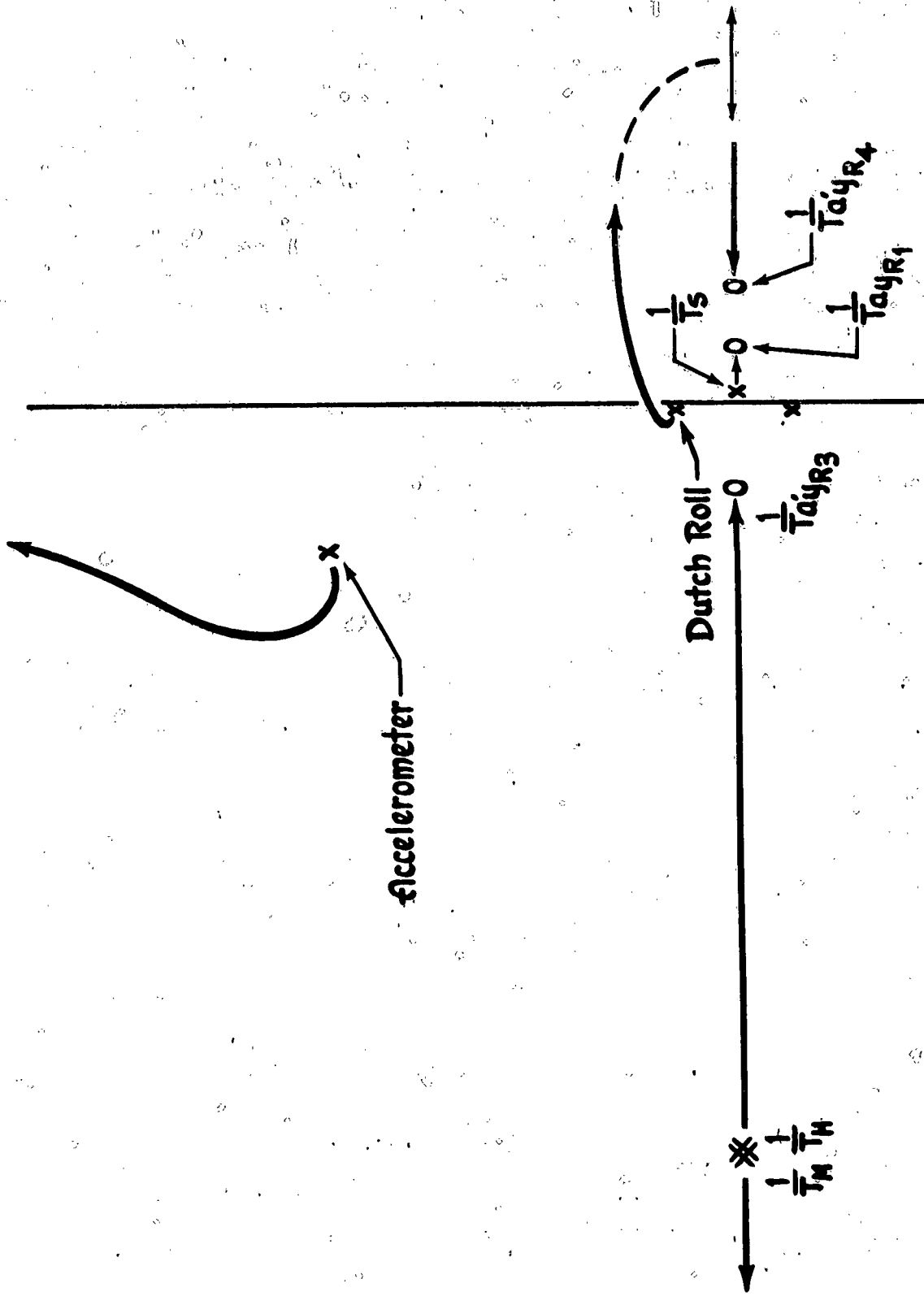


Figure III-14 Root Locus Plot of Sideslip Stability Element with Pure Gain in System Control Unit

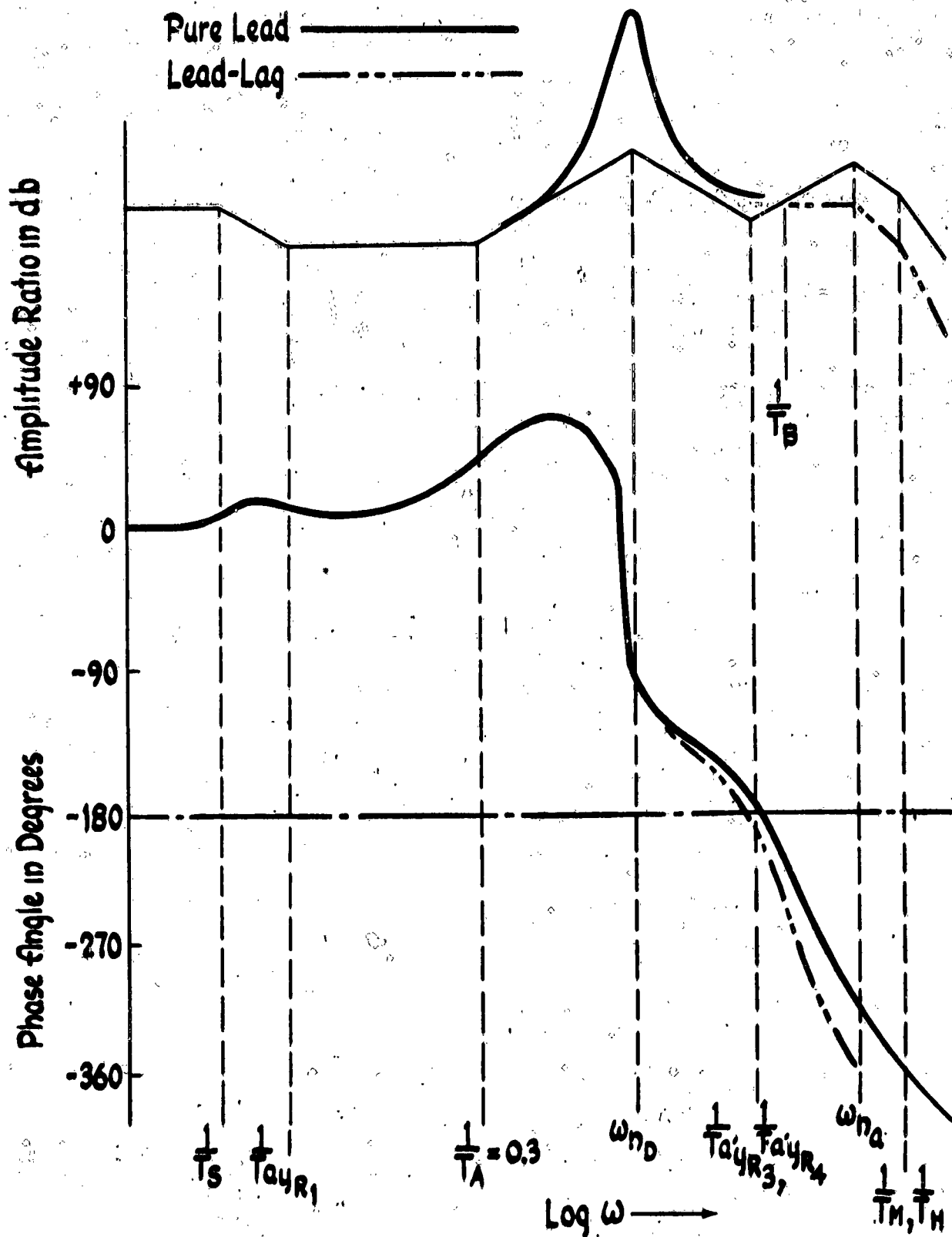


Figure III-15 Generic Bode Plot of Sideslip Stability Augmenter with Pure Lead and Lead-Lag in System Control Unit

Section 3

$$(III-13) \quad K_1 G_1(s) = K_1 \frac{T_A s + 1}{T_B s + 1}$$

The effect of the lag term on the equalized airframe controller combination is shown in Figure III-15.

To simplify the nomenclature, the term K_{CONT_1} , is introduced where

$$(III-14) \quad K_{CONT_1} = \frac{K_{OL}}{K_{a'y}} = [K_1 K_M] K_H K_A$$

The term in brackets $[K_1 K_M]$ represents the alterable gain elements in the physical system.

Note that with the lead-lag network, a rather large value of controller gain K_{CONT_1} , can be used before system instability sets in. This is indicated in the root locus plot in Figure III-16. It should also be noted that the magnitude of the lag time constant T_B is critical. The effect of T_B is shown in the root locus plots in Figure III-17.

In Figure III-17a, the $\frac{T_A}{T_B}$ ratio is relatively small, and as a result, the effective phase lead from the $(T_A s + 1)$ term is reduced. Consequently, the advantage gained by using the lead term is lessened and the root locus plot resembles that for the pure gain system shown in Figure III-14. As T_B is decreased, the Dutch roll damping can be increased more and more, as indicated in Figure III-17b.

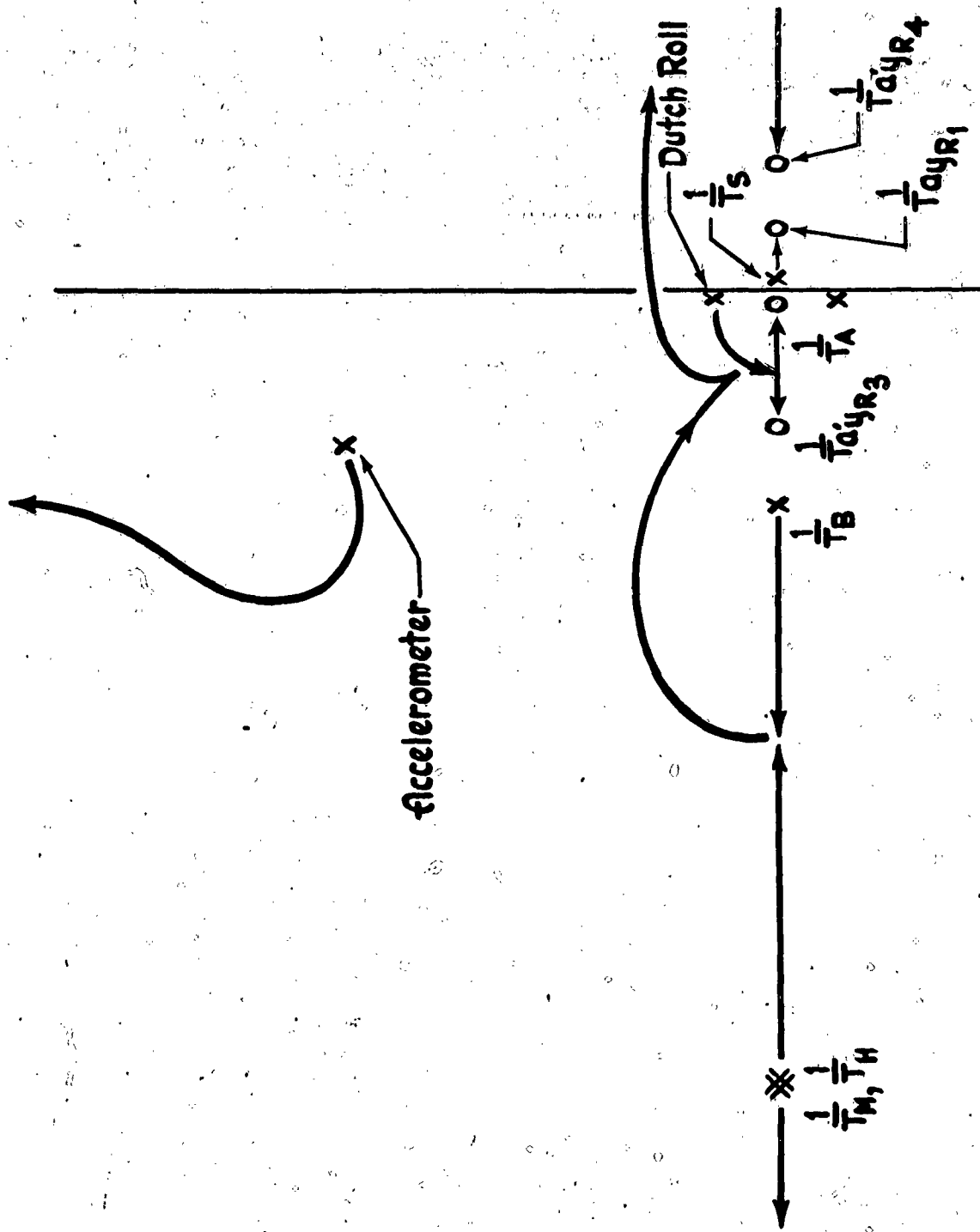


Figure III-16 Root Locus Plot of Sideslip Stability Augmentor with Lead-Lag System Control Unit

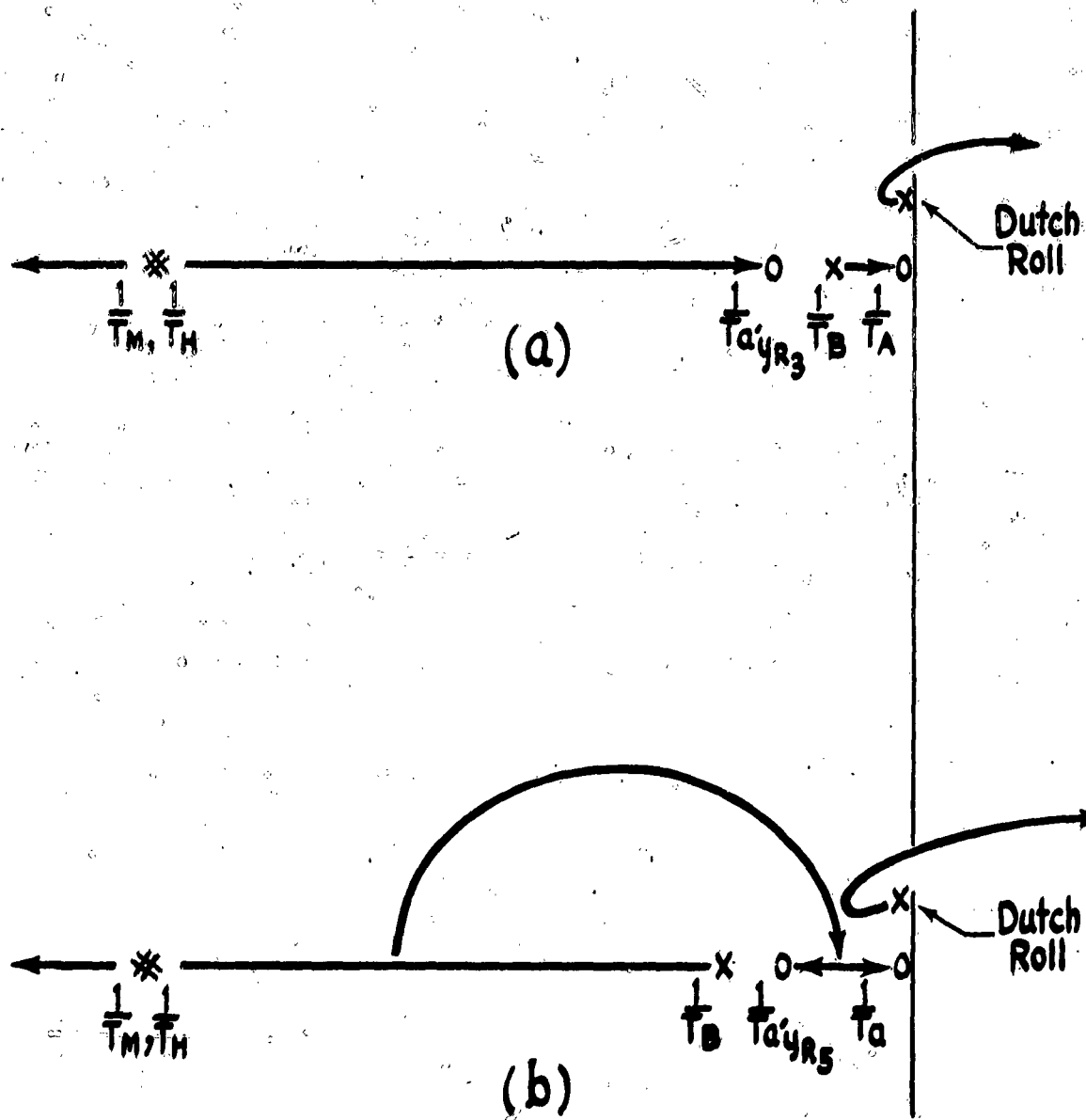


Figure III-17 Effect of T_B Variation on Sideslip Stability Augmenter Response

Since the dutch roll natural frequency varies with flight condition, it will be necessary to vary the characteristics of the controller lead lag network with some flight parameter, to provide proper equalization throughout the flight regime of the airplane. As demonstrated above, this can be conveniently done by varying the controller lag time constant T_B . Since the airframe steady state gain also varies through wide limits it will also be necessary to vary the controller steady state gain K_{CONT} , with some flight parameter.

The determination of the two controller parameters K_{CONT} and T_B was accomplished by means of Bode plots, as shown in Figure III-18. The controller steady state gain K_{CONT} was chosen first by selecting a system zero db line, or "closure line" in such a way that a 40 degree phase margin is obtained near the dutch roll natural frequency. The value for K_{OL} was then measured directly from the Bode plot and K_{CONT} determined by means of Equation (III-14). Application of this procedure to the seven flight conditions listed in Table III-1 provided the values shown for K_{CONT} in Table III-2 and Figure III-19.

COND	f_c (PSF)	$K_{a'y}$ (g/deg)	$K_{CONT}, K_{a'y}$ (db)	$\frac{V}{V}$	K_{CONT} (deg/g)
I	85	0.102	+17	6.69	65.5
II	140	0.00683	- 8	.398	56.9
III	155	0.0142	- 6	.5	35.2
IV	245	0.0145	-8.5	.376	25.9
V	310	0.027	-8	.398	14.75
VI	375	0.0355	-7	.446	12.55
VII	880	0.0904	-9	.355	3.93

Table III-2 Preliminary Estimates for K_{CONT}

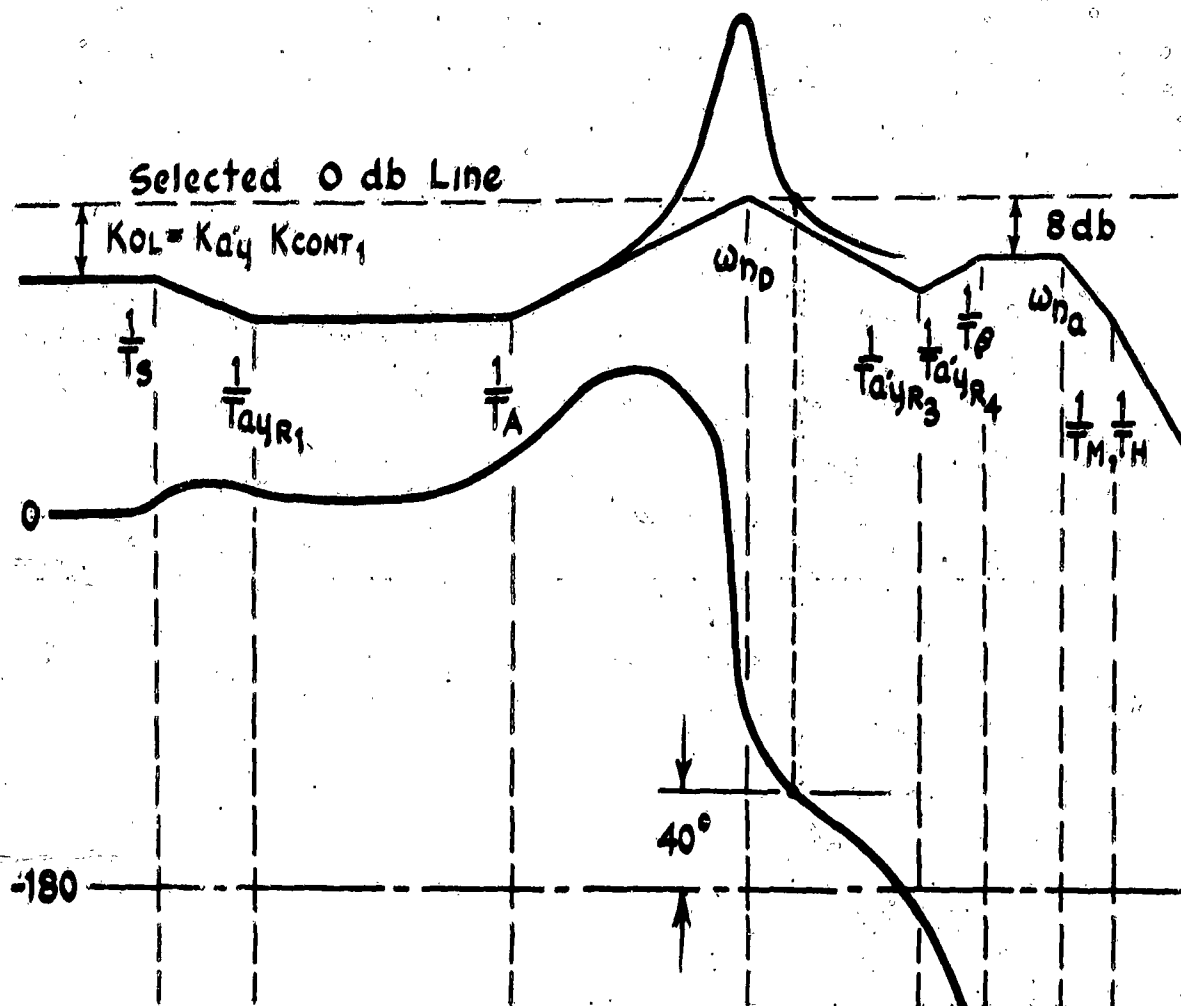


Figure III-18 Generic Amplitude Plot of Sideslip Stability Augmenter System Illustrating First Estimation of K_{CONT1} and T_B

The selection of T_B was based on the assumption that an 8 db difference between the gain line and the asymptote break at $\frac{1}{T_B}$ is adequate to give a satisfactory gain margin (see Figure III-18). Again T_B can be measured easily from the Bode plot and the results for the seven flight conditions are given in Table III-3 and are plotted as a function of f_c in Figure III-20.

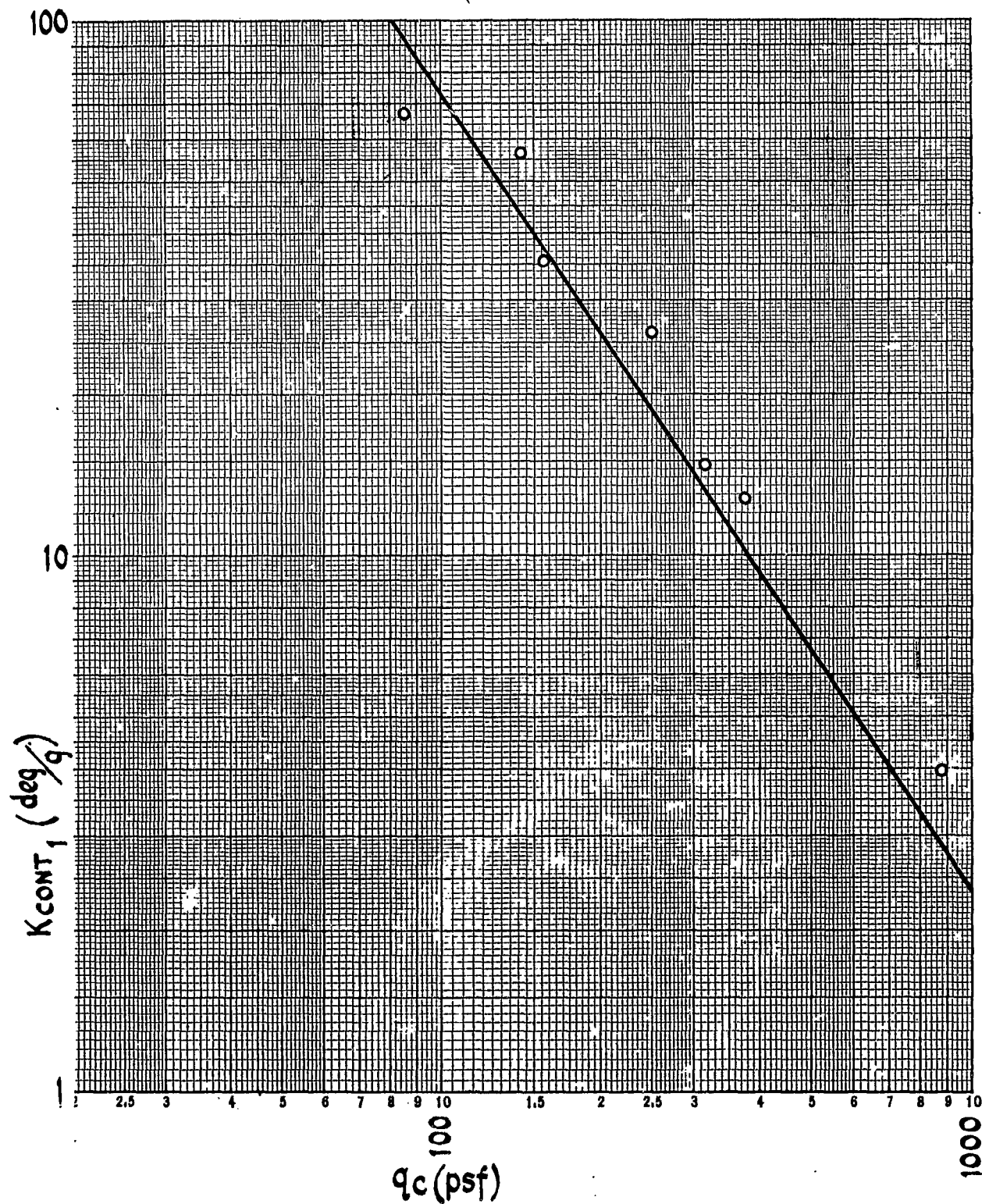


Figure III-19 Preliminary Estimate for K_{CONT_1}

Section 3

COND.	$\frac{1}{T_B}$	T_B
I	5.6	.179
II	2.7	.37
III	5.3	.189
IV	3.8	.263
V	4.5	.222
VI	5.3	.189
VII	8.3	.121

Table III-3 Preliminary Estimates for T_B

A straight line approximation to the plotted points is drawn in Figure III-20. This curve can be obtained physically by a linear potentiometer positioned by f_c . The two lower points correspond to Condition I and III, and are ignored because they do not represent combat flight conditions.

Assuming that the values of K_{cont} , and T_B given in Figures III-19 and III-20 are correct, the sideslip stability augments system would give adequate damping ratio (ζ in the order of 0.6 or 0.7) for the dutch roll oscillation. However, there is one basic fault with the system as it now stands.

Consider Figure III-18 and the K_{ac} column in Table III-2. For all but one condition, the system open loop gain K_{oc} is a relatively small value. It is a well-known fact that for any servo system, the steady state

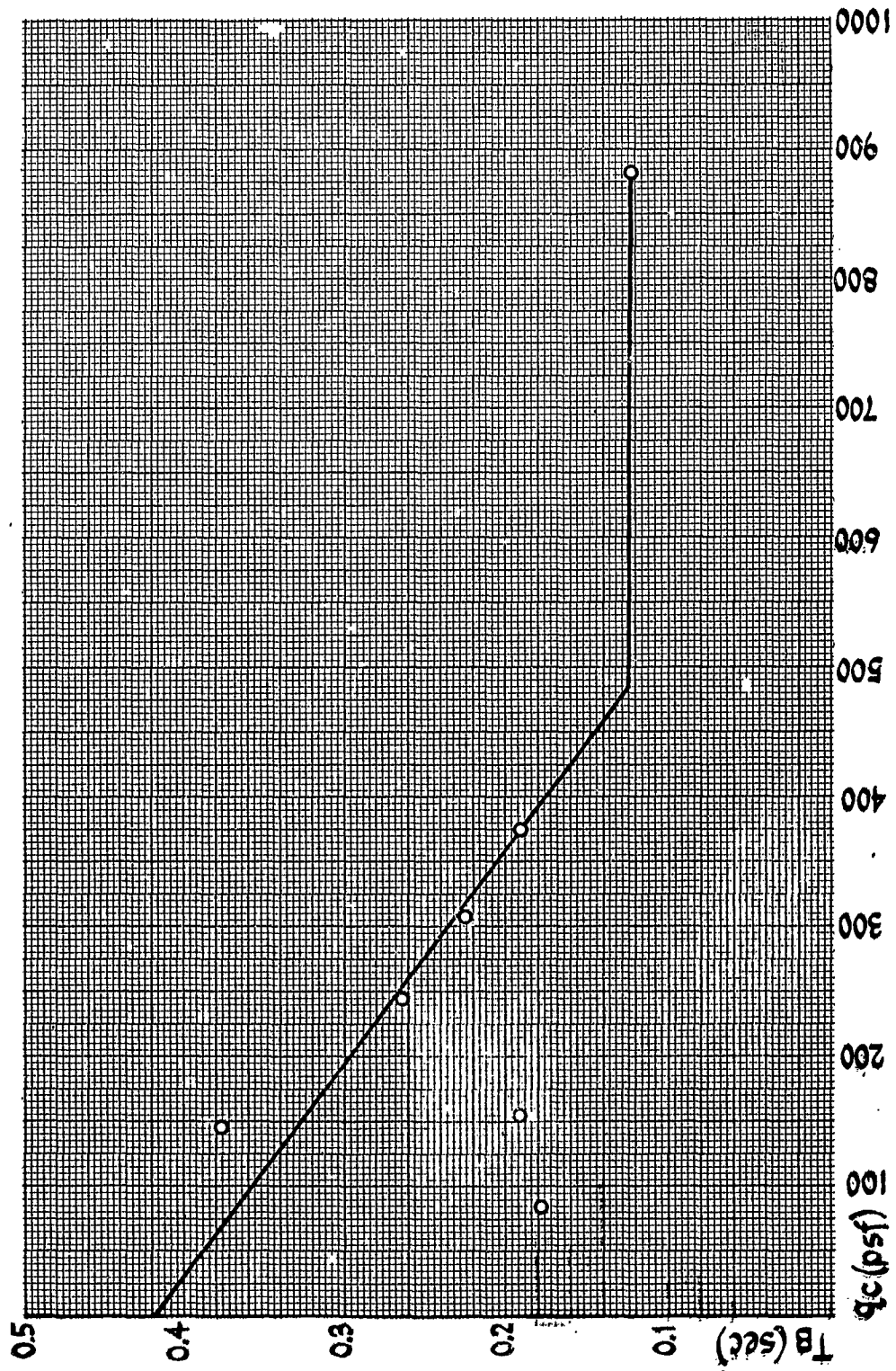


Figure III-20 Preliminary Estimates for T_b

Section 3

errors increase as the system gain decreases. For the sideslip stability augments system, the low system gains lead to poor trimming characteristics which are manifested by steady state sideslip angles or side accelerations. The poor trimming characteristics of the system can be remedied by raising the controller gain. However, raising the gain indiscriminately would make the system unstable as indicated by the Bode and root locus plots. What is actually required is the raising of the dc or low frequency system gain to improve the trimming qualities without altering the dutch roll equalization previously determined.

One method of improving the trimming qualities is to add a pure integrator in parallel with the lead-lag rate circuit. Then the complete system control unit transfer function becomes

$$(III-15) \quad K_1 \frac{T_A s + 1}{T_B s + 1} + \frac{K_2}{s}$$

which can be rewritten as

$$(III-16) \quad K_2 \frac{\frac{s^2}{\omega_{ne}^2} + 2 \frac{s}{\omega_{ne}} + 1}{s(T_B s + 1)}$$

where

$$\omega_{ne} = \sqrt{\frac{K_2}{K_1 T_A}} = \sqrt{\frac{K_{CONT_2}}{K_{CONT_1} T_A}}$$

$$s = \frac{\omega_{ne}}{2} \left(\frac{K_1}{K_2} + T_B \right) = \frac{\omega_{ne}}{2} \left(\frac{K_{CONT_1}}{K_{CONT_2}} + T_B \right)$$

$$K_{CONT_2} = K_2 K_M K_H K_A$$

It will be noted that the equalization lead break frequency ω_{ne} is related to K_{CONT_2} , the controller gain through the integrator. This relationship is such that the complete open loop Bode diagram near and above the dutch roll frequency is changed very little by the addition of the integrator. This is apparent in Figure III-21, which is the generic Bode plot for the complete system for two values of K_{CONT_2} (after K_{CONT_1} and T_B have been adjusted to give good dutch roll characteristics).

Note that at frequencies above ω_{nd} , the Bode plots of Figures III-18 and III-21 are similar. Note also that although both gains will give zero steady state positional error, the system with the higher K_{CONT_2} gain (curve #2) will reach the steady state sooner than the lower gain system. This is evident from the fact that the subsidence mode introduced by closing the loop has a time constant T_c , which is approximately equal to the reciprocal of the frequency at which the system zero db line intersects the low frequency portion of the open loop system amplitude curve.* It is evident therefore, that the trimming time constant, T_c can be selected by proper choice of the controller gain through the integrator K_{CONT_2} .

The desired value of T_c was based on the required value for trimming rate during the last few seconds prior to firing the rockets. The only

*See Reference 8 for a discussion of the relationships between open and closed loop systems.

Section 3

requirement for rapid trim changes during this time arises when a significant change in airspeed is made. Since one of the requirements of the fire control system used in this airplane specifies that essentially constant airspeed should be maintained during the last 10 seconds prior to firing, it was decided that it would be desirable if any steady state sideslip were reduced to a negligible value in 10 seconds. Since a first order lag reaches 95 per cent of its final value in three time constants, the requirement can be stated mathematically as

$$(III-17) \quad 3 \tau_c = 10 \quad \text{or} \quad \frac{1}{\tau_c} = 0.3$$

It should be noted that the selection of the controller gain based on the desired value of τ_c does not necessarily result in a system with satisfactory stability. Since the requirement for stability was of prime importance, while the desired value of τ_c was considered to be of secondary importance, K_{CONT_2} was selected by the following method. The controller gain K_{CONT_2} was selected to give the desired value of τ_c when this selection did not result in a system phase margin of less than 40 degrees. For those cases where K_{CONT_2} as selected above resulted in phase margins of less than 40 degrees, K_{CONT_2} was reduced to obtain the desired phase margin, which of course resulted in larger values for τ_c . Actual values of $K_{OL} = K_{CONT_2} K_{A/y}$ were determined graphically by the method shown in Figure III-22.

Application of the procedure to the seven flight conditions of Table III-1 resulted in values for K_{CONT_2} as given in Table III-4 and Figure III-23.

$$K_{OL} G_{OL}(s) = \left[K_{CON} T_2 \left(\frac{s^2 + 2\frac{\delta}{\omega_{n1}} s + 1}{s(T_B s + 1)} \right) \left(\frac{1}{T_H s + 1} \right) \left(\frac{1}{T_H s + 1} \right) \left(\frac{1}{\frac{s^2}{\omega_{na}^2} + 2\frac{\delta_{asH}}{\omega_{na}}} \right) \left(\frac{a_y}{\delta_R} \right) \right]$$

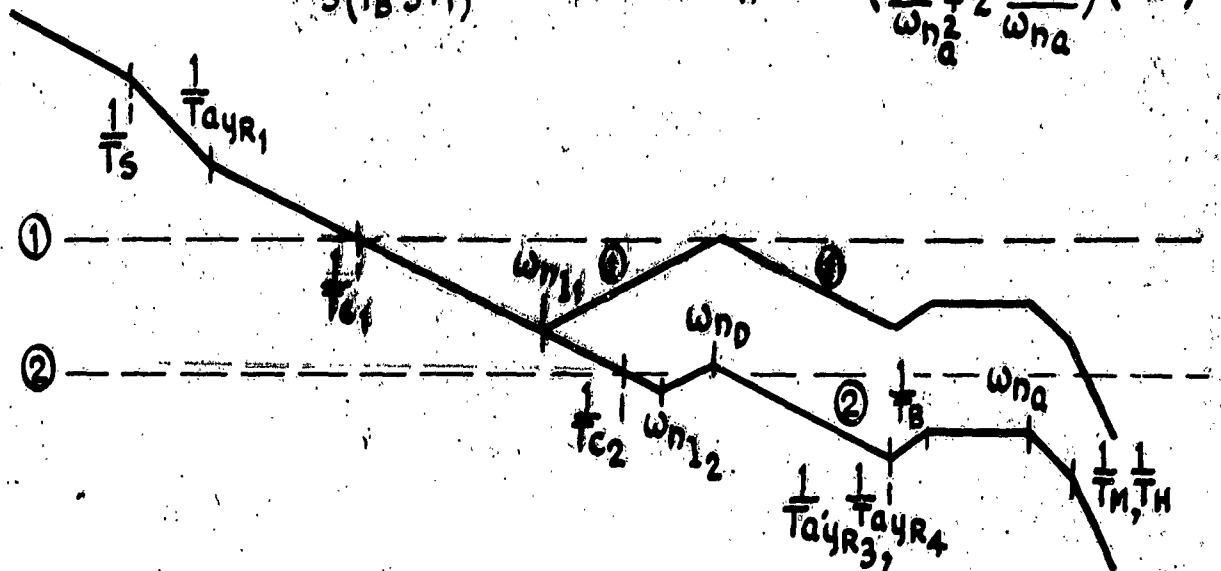


Figure III-21 Generic Amplitude Plot of Sideslip Stability Augments System with Integration added to Dutch Roll Rate Circuit Showing Effect of Integration Gain K_2

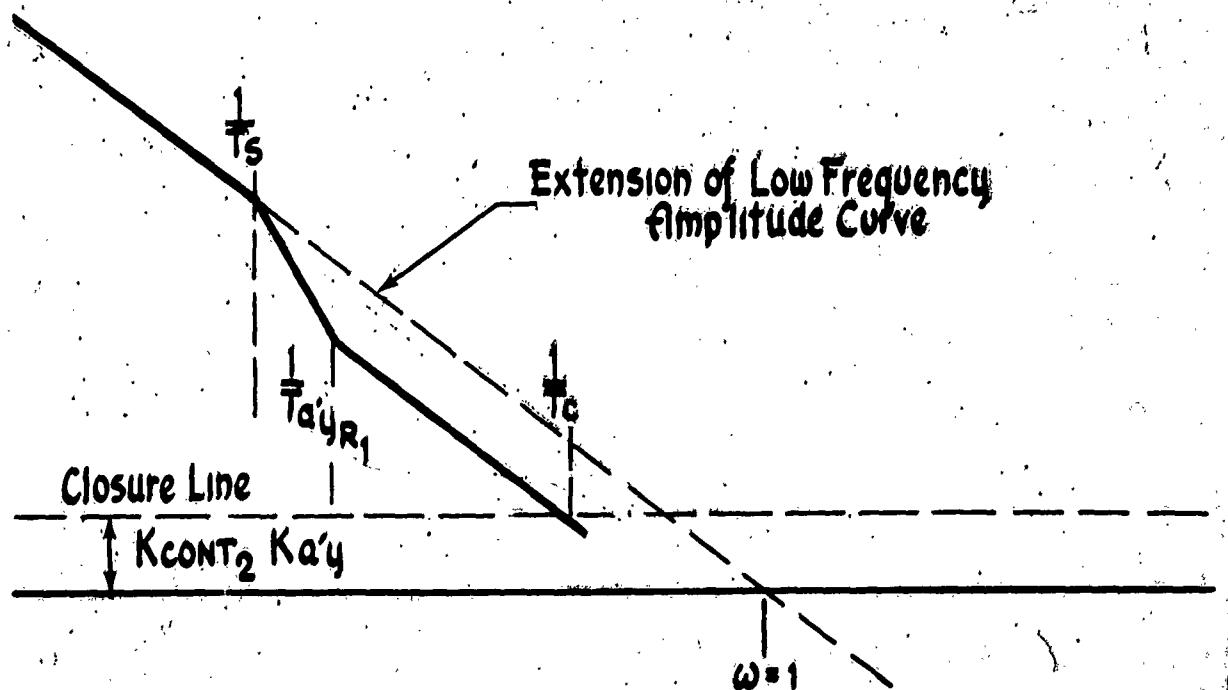


Figure III-22 Generic Amplitude Plot of the Sideslip Stability Augments System Illustrating the First Estimation of $K_{CON} T_2$

Section 3

COND.	q_c (PSF)	$K_{a'y}$ (g/DEG)	dB	$K_{CONT_2} K_{a'y}$	K_{CONT_2} ($\frac{DEG/SEC}{g}$)
I	85	0.102	+14.5	5.31	52
II	140	0.00683	-6.5	.473	69.2
III	155	0.0142	-4.5	.59	41.6
IV	245	0.0145	-5.5	.53	36.5
V	310	0.027	-4.5	.59	21.9
VI	375	0.0355	-2.5	.75	21.1
VII	880	0.0904	-1.5	.84	9.3

Table III-4 Preliminary Estimates for K_{CONT_2}

Here again, the calculated points can be approximated by a function of impact pressure. In this case, $K_{CONT_2} \propto q_c^{-1}$

Using the preliminary estimates for K_{CONT_1} , T_B , and K_{CONT_2} as given by the straight line approximations in Figure III-19, III-20, and III-23, the Bode plots corresponding to the seven flight conditions are given in Figure III-24 through III-30. From the figures, it can be seen that for each of the conditions,

$$(III-18) \quad 3 T_c \leq 12 \text{ SECONDS}$$

$$\text{gain margin} \geq 6 \text{ db}$$

$$\text{phase margin} \geq 40 \text{ degrees}$$

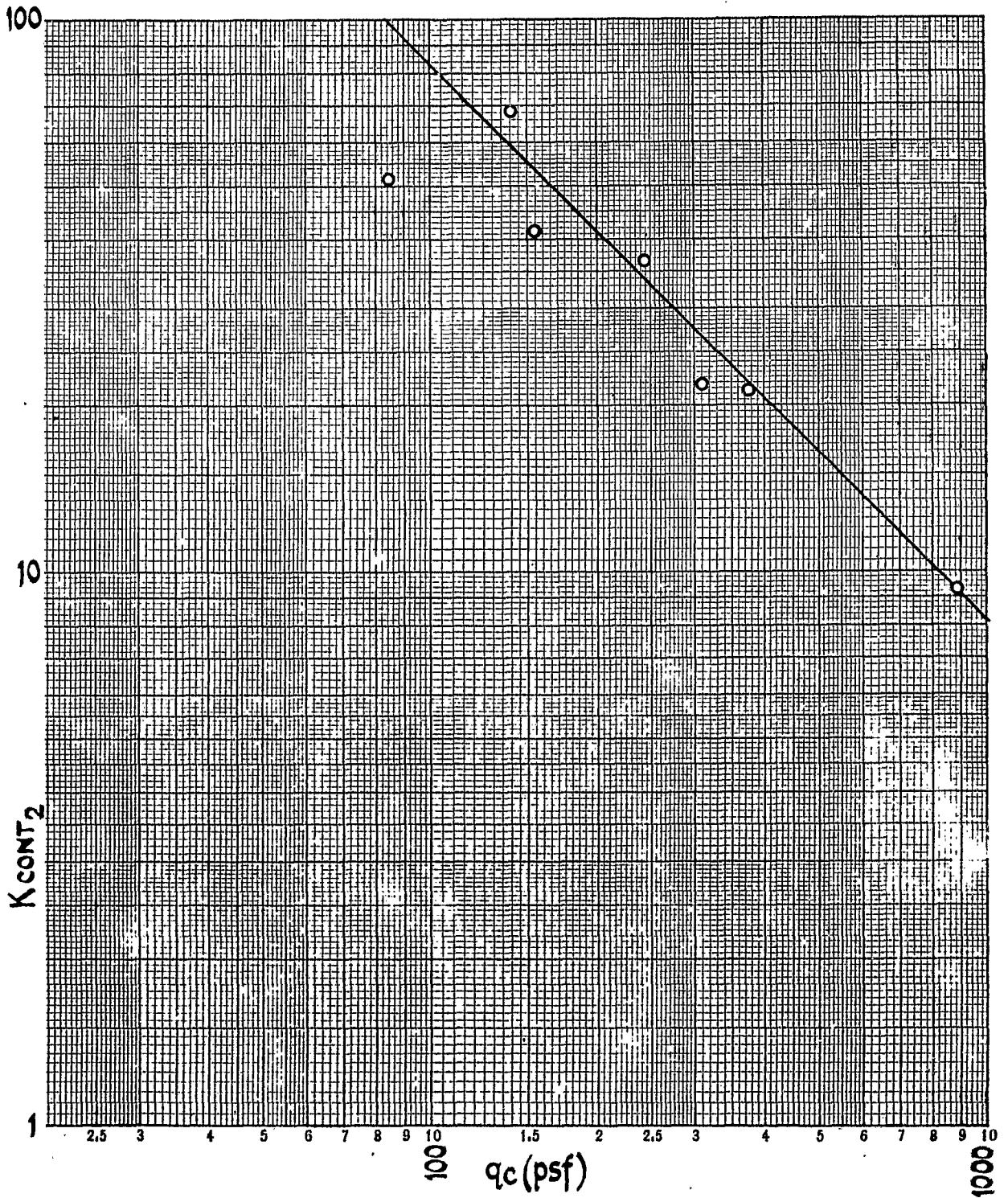


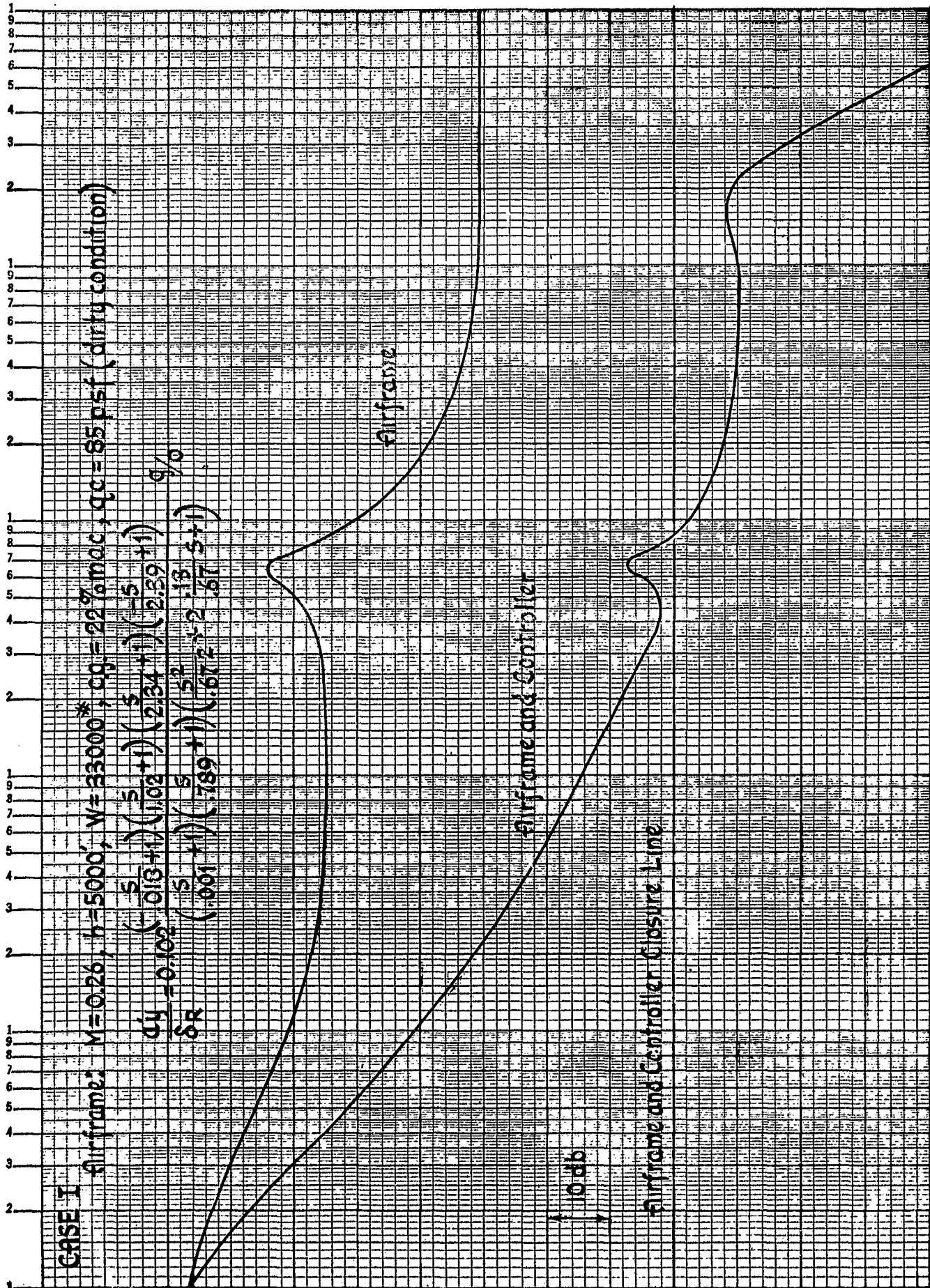
Figure III-23 Preliminary Estimate for K_{CONT2}

CASE I

Airframe: $M=0.26$, $h=5000'$, $W=33000'$, $cg=22\%$ mac, $qc=85$ psf (dirty condition)

$$\Delta Y = 0.102 \left(\frac{5}{0.13+1} \right) \left(\frac{5}{1.02+1} \right) \left(\frac{5}{2.34+1} \right) \left(\frac{5}{2.39+1} \right)$$

$$\Delta R = \left(\frac{5}{.001+1} \right) \left(\frac{5}{.789+1} \right) \left(\frac{5^2}{.672+2.13.5+1} \right) \%$$



Amplitude Ratio in db

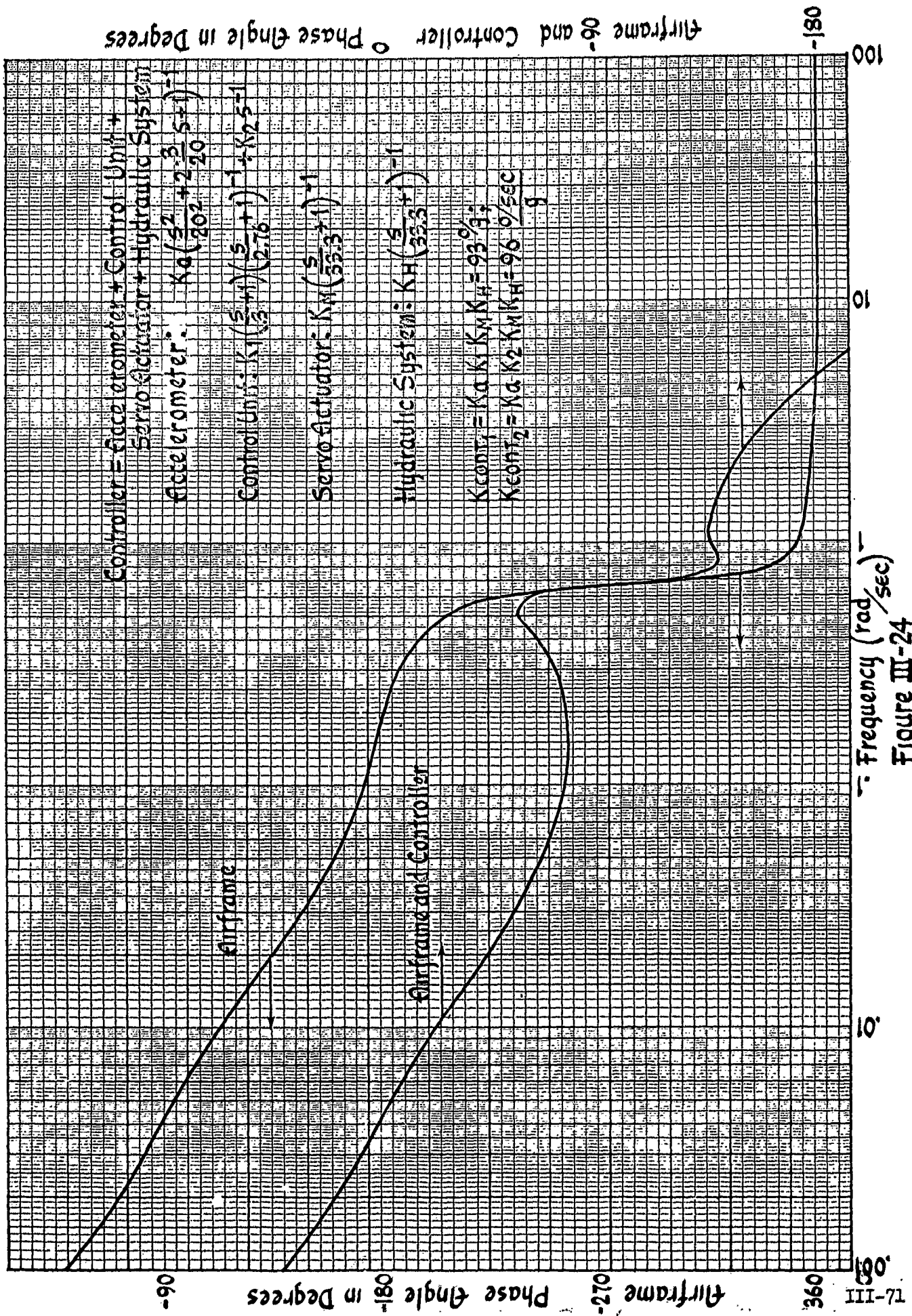
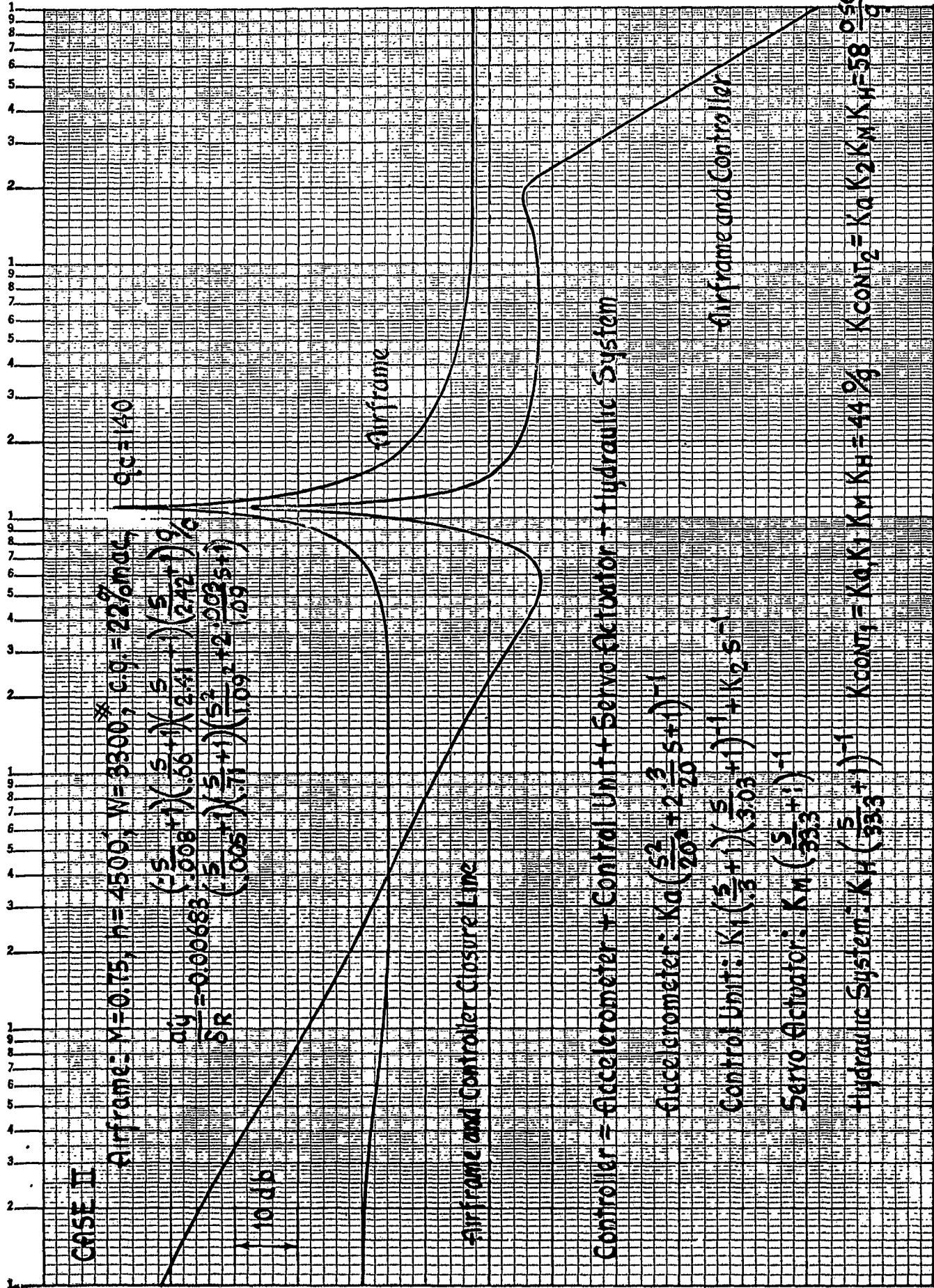


Figure III-24



CASE II

Airframe: $M=0.75, n=4500, W=3300, C.G.=22\%MAC, g_c=140$

$$\frac{dy}{\delta R} = -0.00683 \left(\frac{s}{0.08} + 1 \right) \left(\frac{s}{2.41} + 1 \right) \left(\frac{s}{2.42} + 1 \right) \frac{g}{c}$$

$$\frac{\delta R}{dy} = \left(\frac{0.05}{s} + 1 \right) \left(\frac{s}{1.09} + 2.008s + 1 \right) \left(\frac{s}{1.09} + 2.008s + 1 \right)$$

10 db

Airframe and Controller Closure Line

Airframe

Airframe and Controller

Controller = accelerometer + Control Unit + Servo Actuator + Hydraulic System

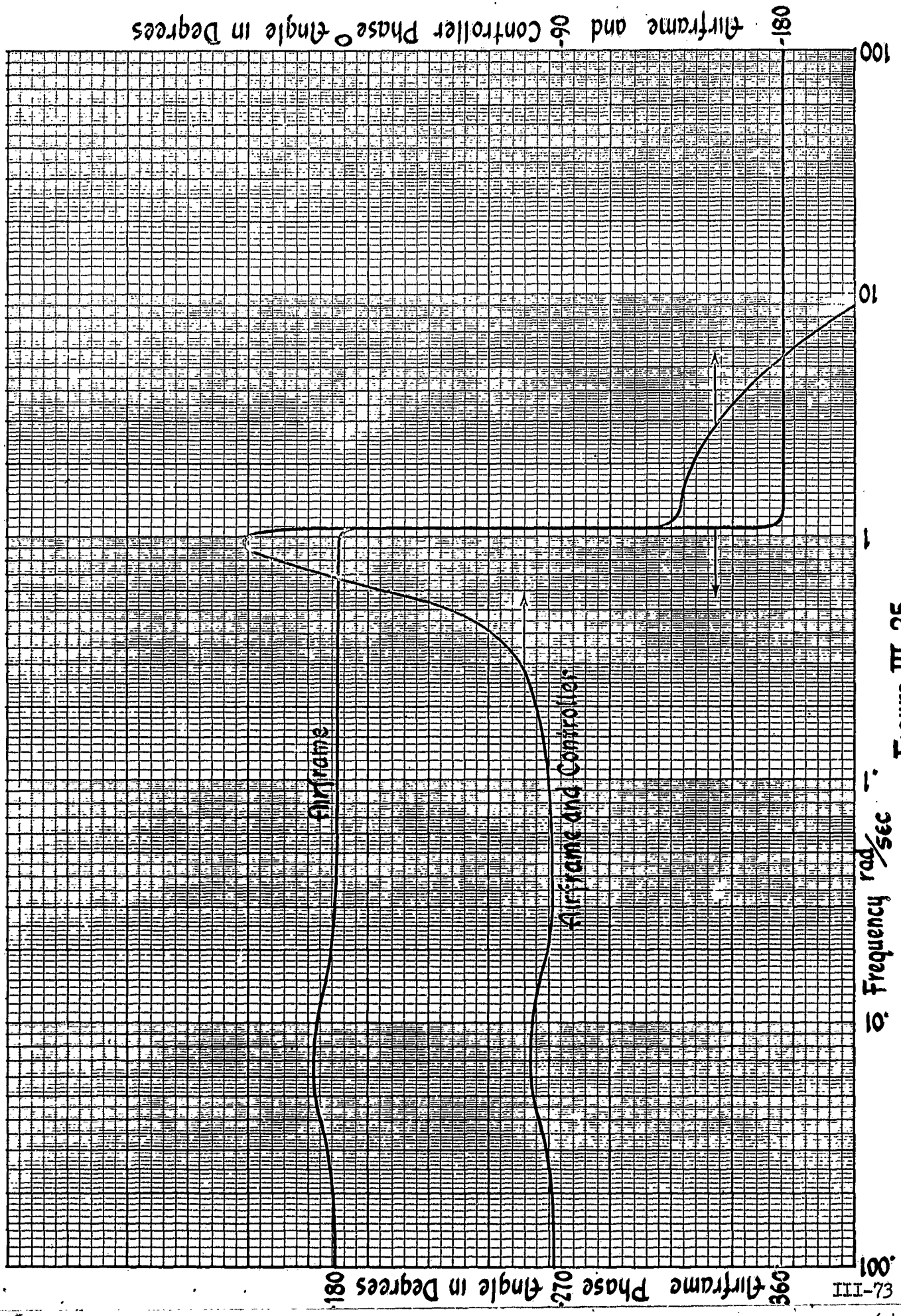
accelerometer: $K_a \left(\frac{s^2}{20} + 2 \frac{3}{20} s + 1 \right)^{-1}$

Control Unit: $K_1 \left(\frac{s}{3} + 1 \right) \left(\frac{s}{3.03} + 1 \right)^{-1} + K_2 s^{-1}$

Servo Actuator: $K_M \left(\frac{s}{33.3} + 1 \right)^{-1}$

Hydraulic System: $K_H \left(\frac{s}{33.3} + 1 \right)^{-1}$

$K_{CONT1} = K_a K_1 K_M K_H = 44\%$ $K_{CONT2} = K_a K_2 K_M K_H = 58 \frac{0.5 \text{ sec}}{g}$



081 Airframe and Controller Phase Angle in Degrees

Airframe

Airframe and Controller

Frequency rad/sec

081 Airframe Phase Angle in Degrees

Figure III-25

CASE III

Airframe: $M = 0.35$, $h = 5000$, $W = 33000$, $q_0 = 22\% mac$, $q_c = 15\% psf$

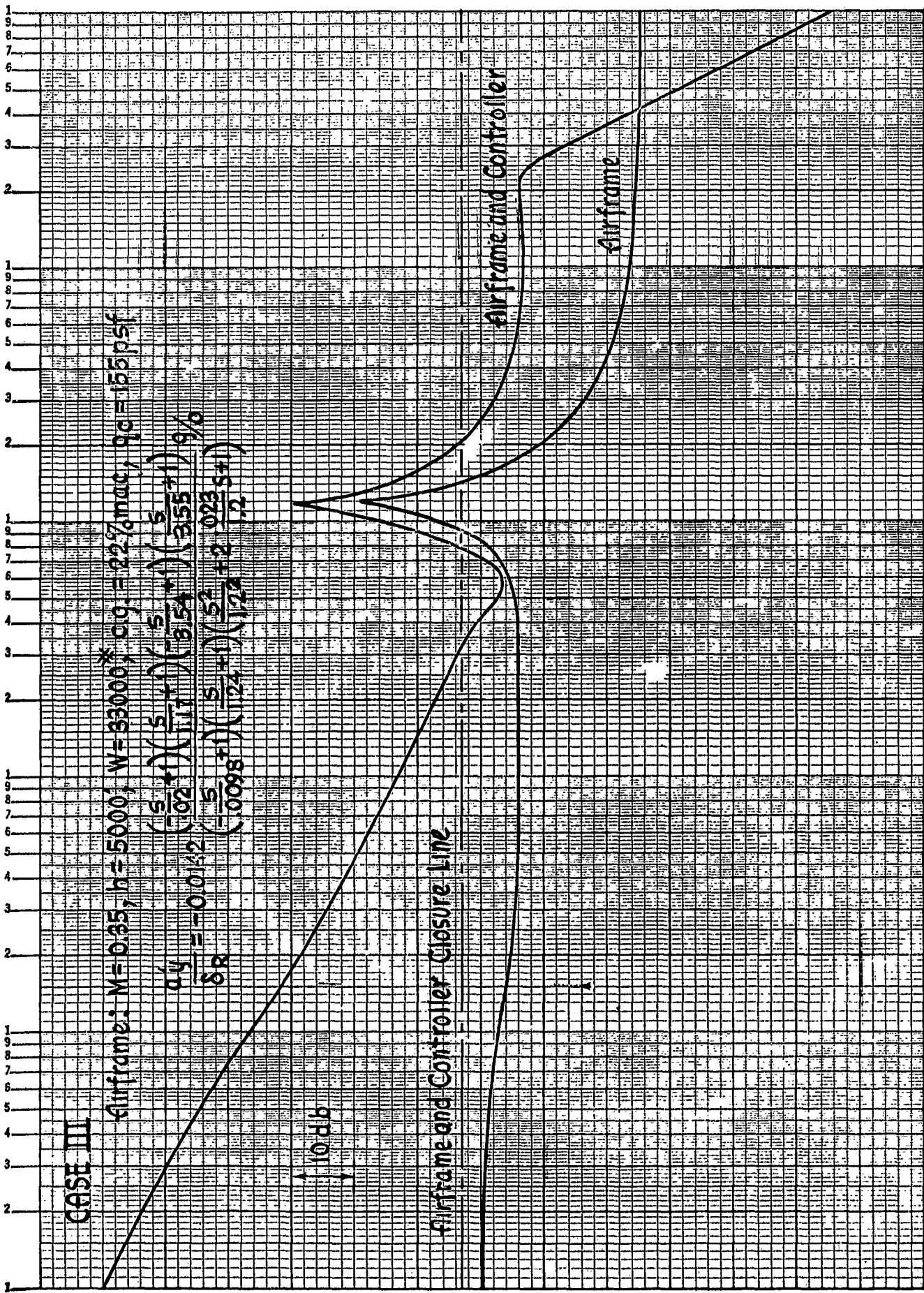
$$\frac{a_4}{\delta R} = 0.0142 \frac{\left(\frac{5}{1.17}\right) \left(\frac{5}{8.54}\right) \left(\frac{5}{3.55}\right) \left(\frac{5}{9}\right)}{\left(\frac{5}{0.098}\right) \left(\frac{5}{1.24}\right) \left(\frac{5.2}{1.22}\right) \left(\frac{2.023}{1.2}\right) \left(\frac{5}{1.2}\right)}$$

9R011

Airframe and Controller Closure Line

Airframe and Controller

Airframe



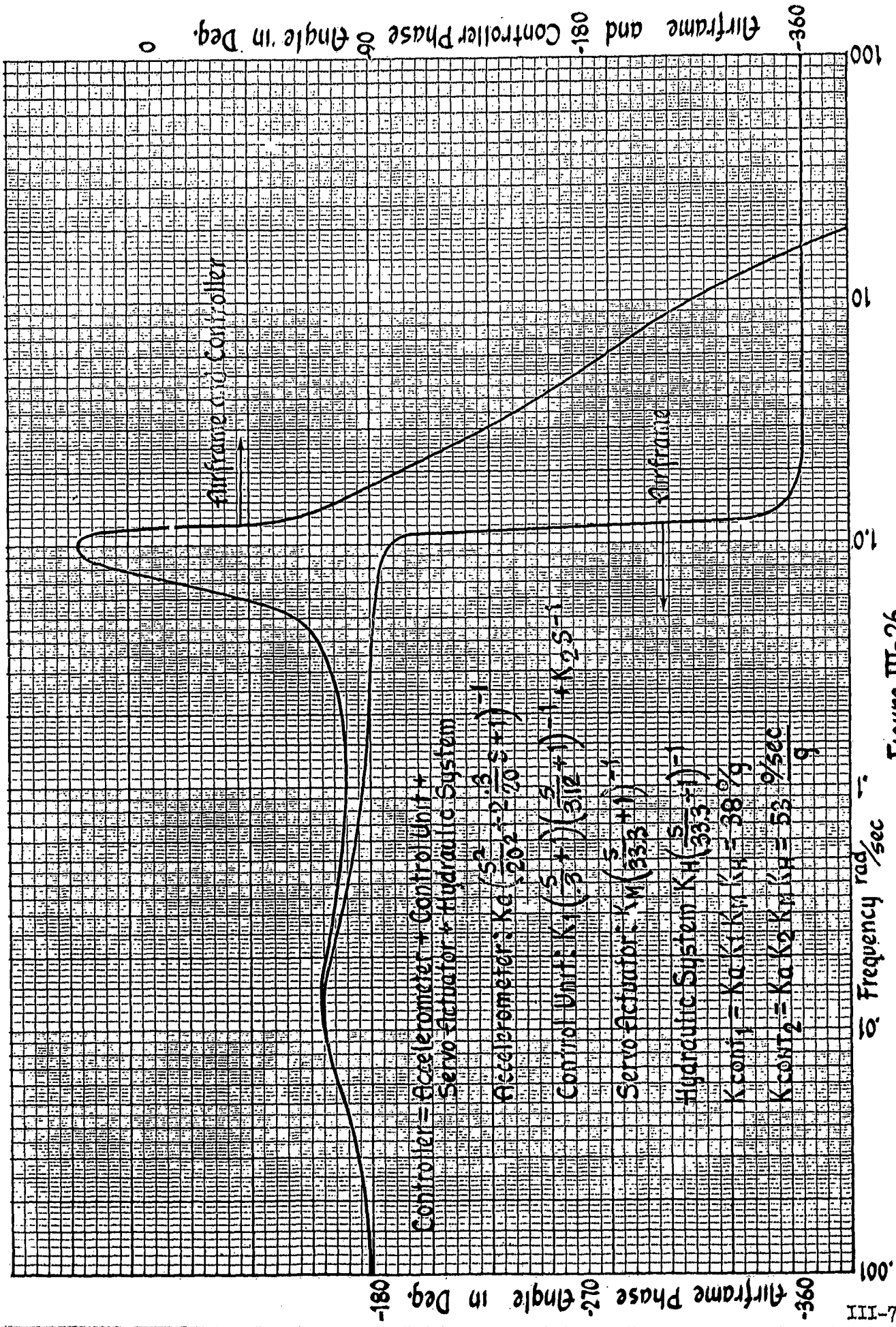


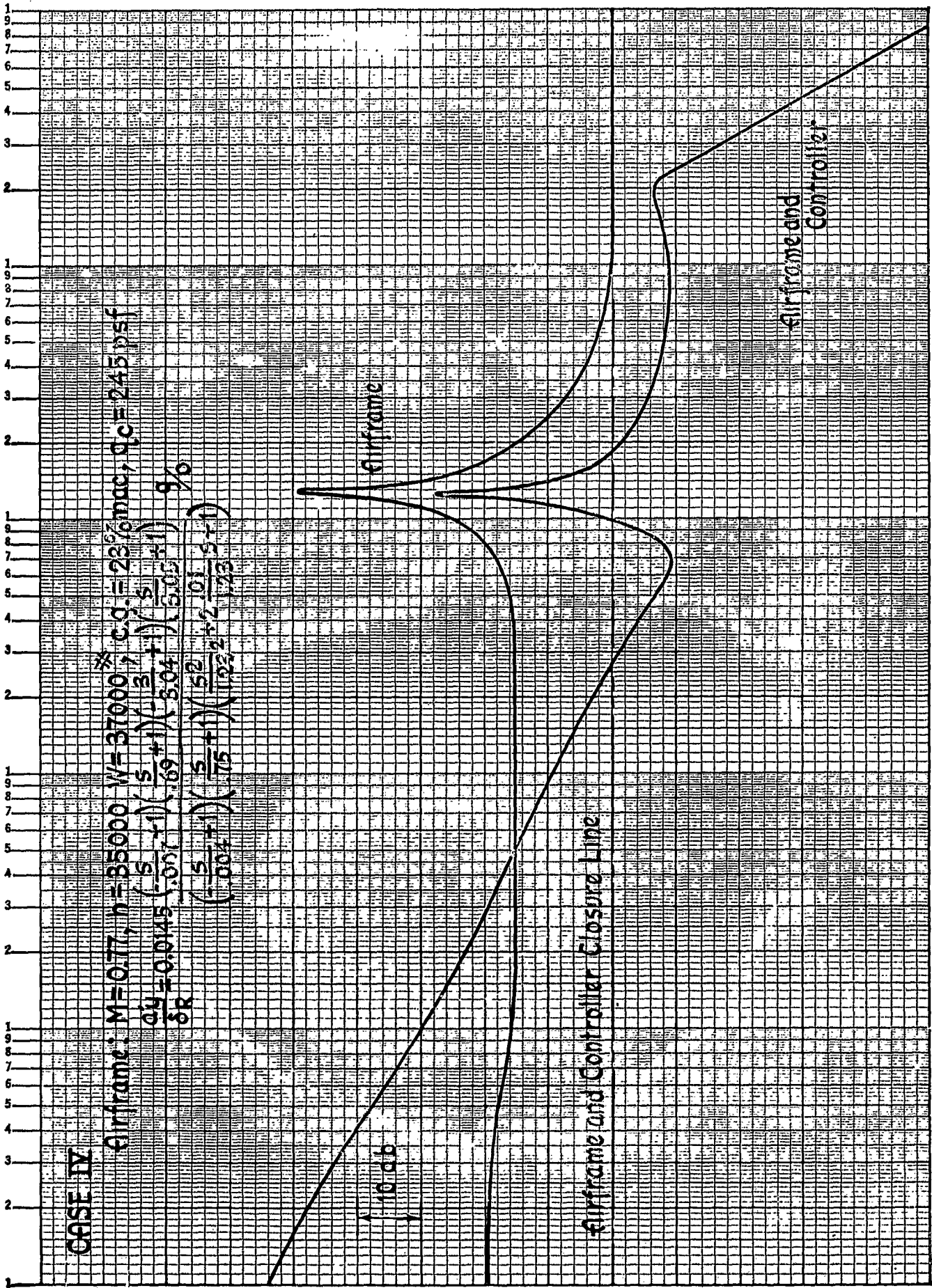
Figure III-26

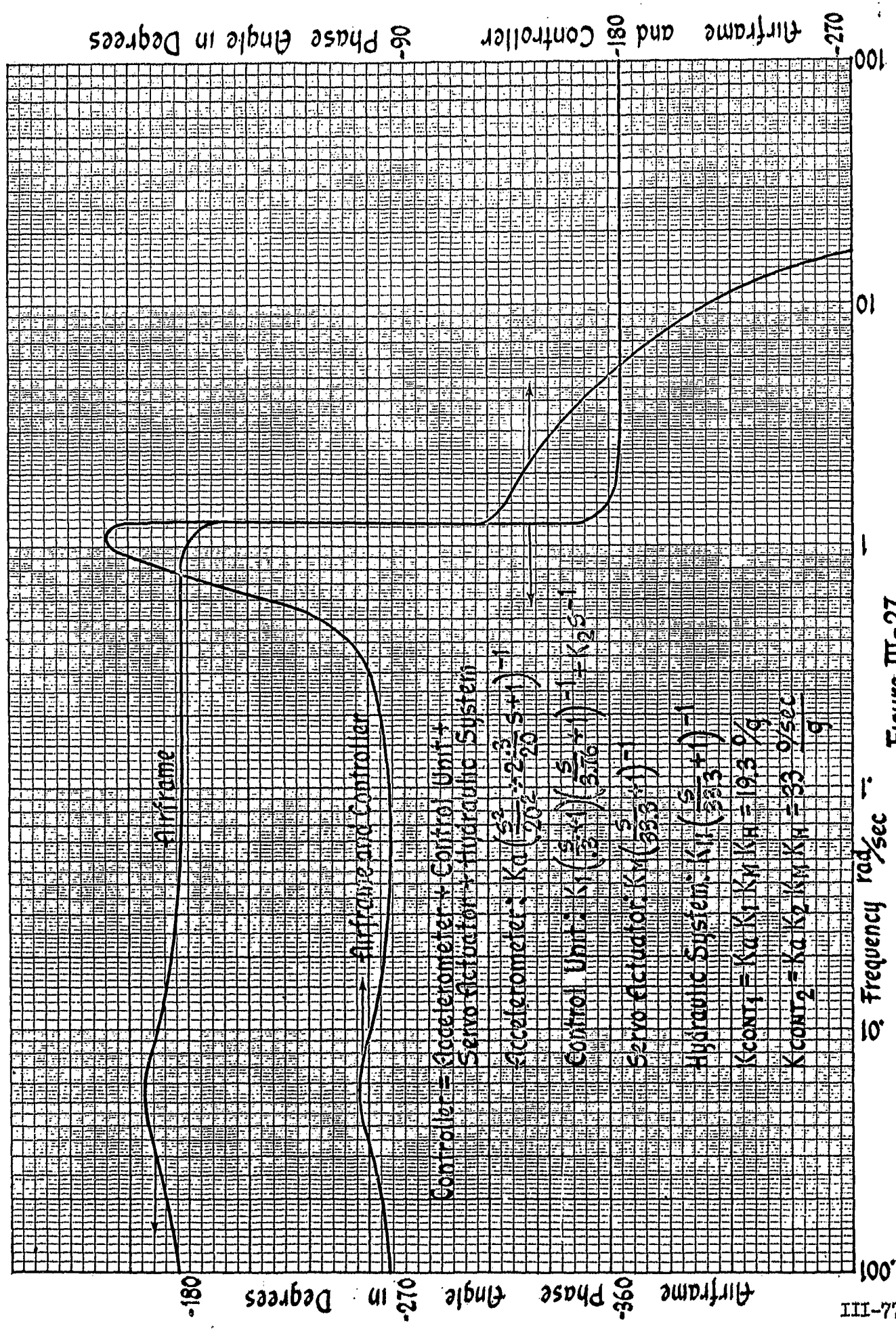
CASE IV

Airframe: $M=0.77$, $n=35000$, $W=37000$, $C.D.=23\%$, mac , $q_c=245$ psf

$$\frac{Q_4}{\delta R} = 0.0145 \left(\frac{s}{.057} + 1 \right) \left(\frac{s}{.69} + 1 \right) \left(\frac{s}{3.04} + 1 \right) \left(\frac{s}{5.05} + 1 \right) \%$$

$$\left(\frac{s}{.004} + 1 \right) \left(\frac{s}{.175} + 1 \right) \left(\frac{52}{1022} + 1 \right) \left(\frac{101}{173} + 1 \right)$$





Airframe and Controller Phase Angle in Degrees

Airframe

Airframe and Controller

Controller = Accelerometer + Control Unit + Servo-actuator + Hydraulic System

Accelerometer: $K_a \left(\frac{s^2}{20} + 2.3s + 1 \right) - 1$

Control Unit: $K_1 \left(\frac{s}{3} + 1 \right) \left(\frac{s}{3.76} + 1 \right) - 1 = K_2 s^{-1}$

Servo-actuator: $K_M \left(\frac{s}{33.3} + 1 \right)^{-1}$

Hydraulic System: $K_1 \left(\frac{s}{533} + 1 \right) - 1$

$K_{CONT_1} = K_a K_1 K_M K_H = 19.3 \%$

$K_{CONT_2} = K_a K_2 K_M K_H = 33 \frac{0/sec}{g}$

Frequency rad/sec

Figure III-27

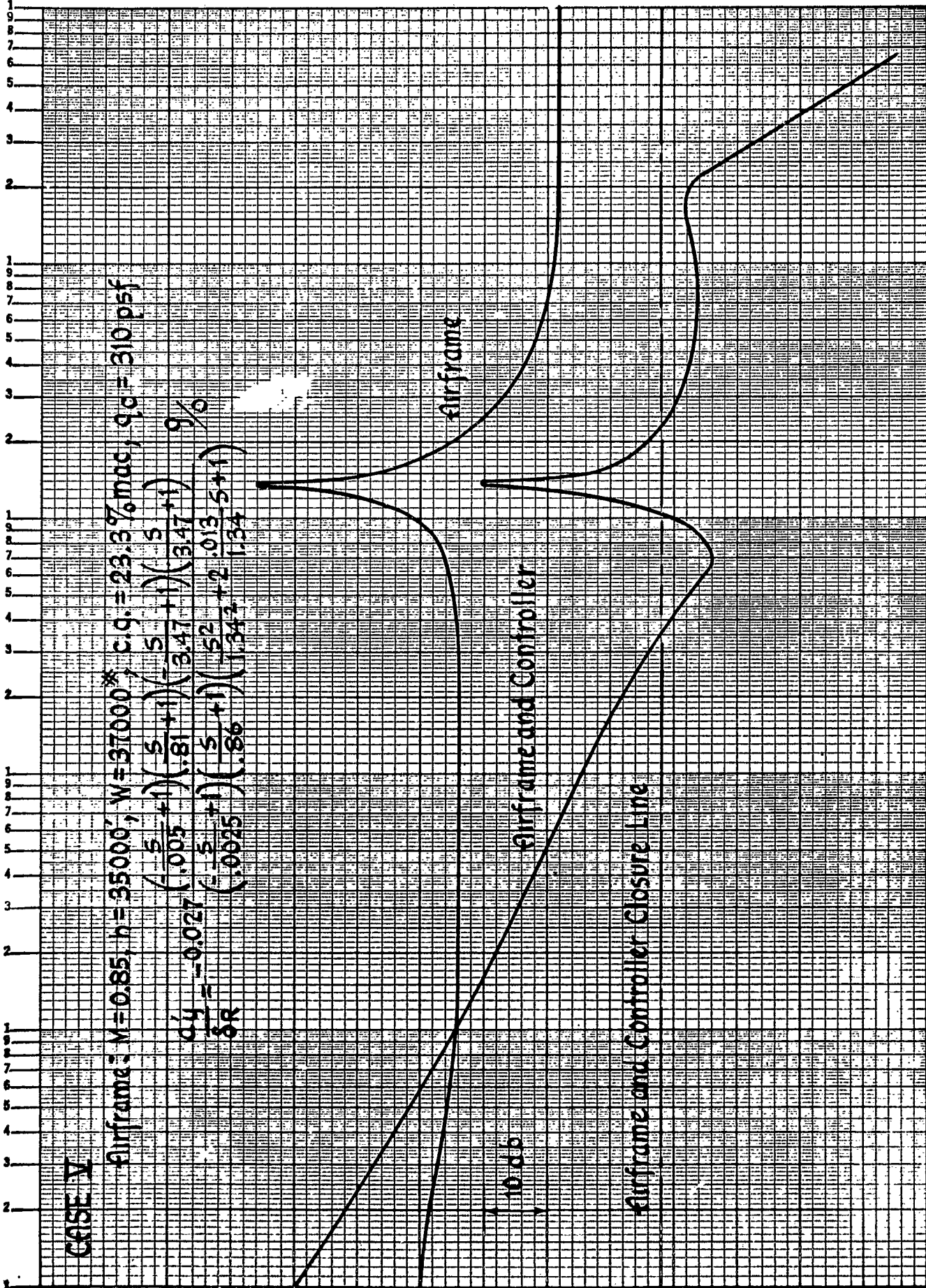
Airframe Phase Angle in Degrees

CASE V

airframe: $M=0.85$, $h=35000'$, $W=37000$ *, $c.g.=23.3\%$ mac, $q_c=310$ psf

$$\frac{\delta y}{\delta R} = -0.027 \left(\frac{.5}{.0025} + 1 \right) \left(\frac{.5}{.81} + 1 \right) \left(\frac{.5}{3.47} + 1 \right) \left(\frac{.5}{3.47} + 1 \right) \left(\frac{.5}{9} \right)$$

$$\frac{\delta R}{\delta R} = \left(\frac{.5}{.0025} + 1 \right) \left(\frac{.5}{.86} + 1 \right) \left(\frac{.52}{1.342} + 2 \right) \left(\frac{.0135}{1.34} + 1 \right)$$



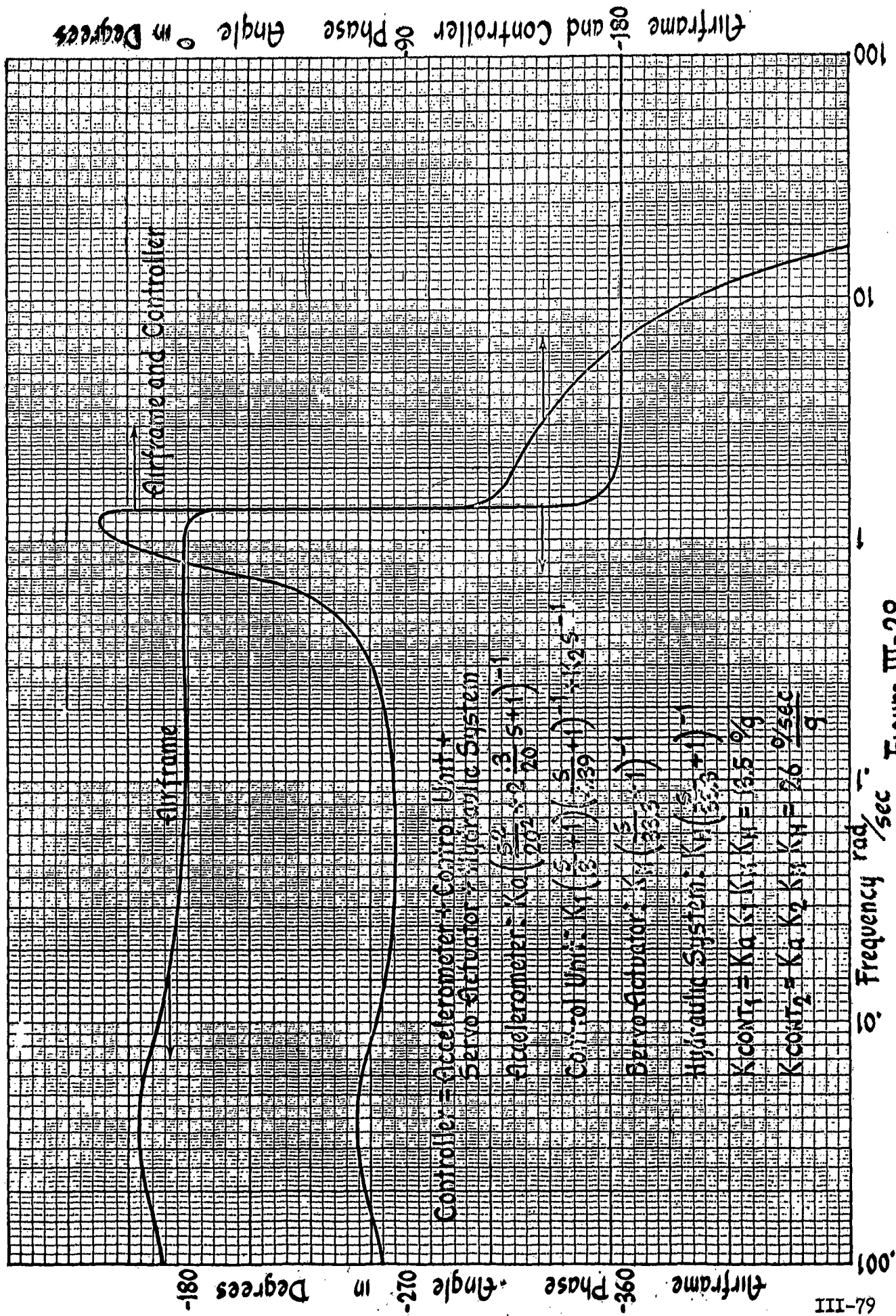


Figure III-28

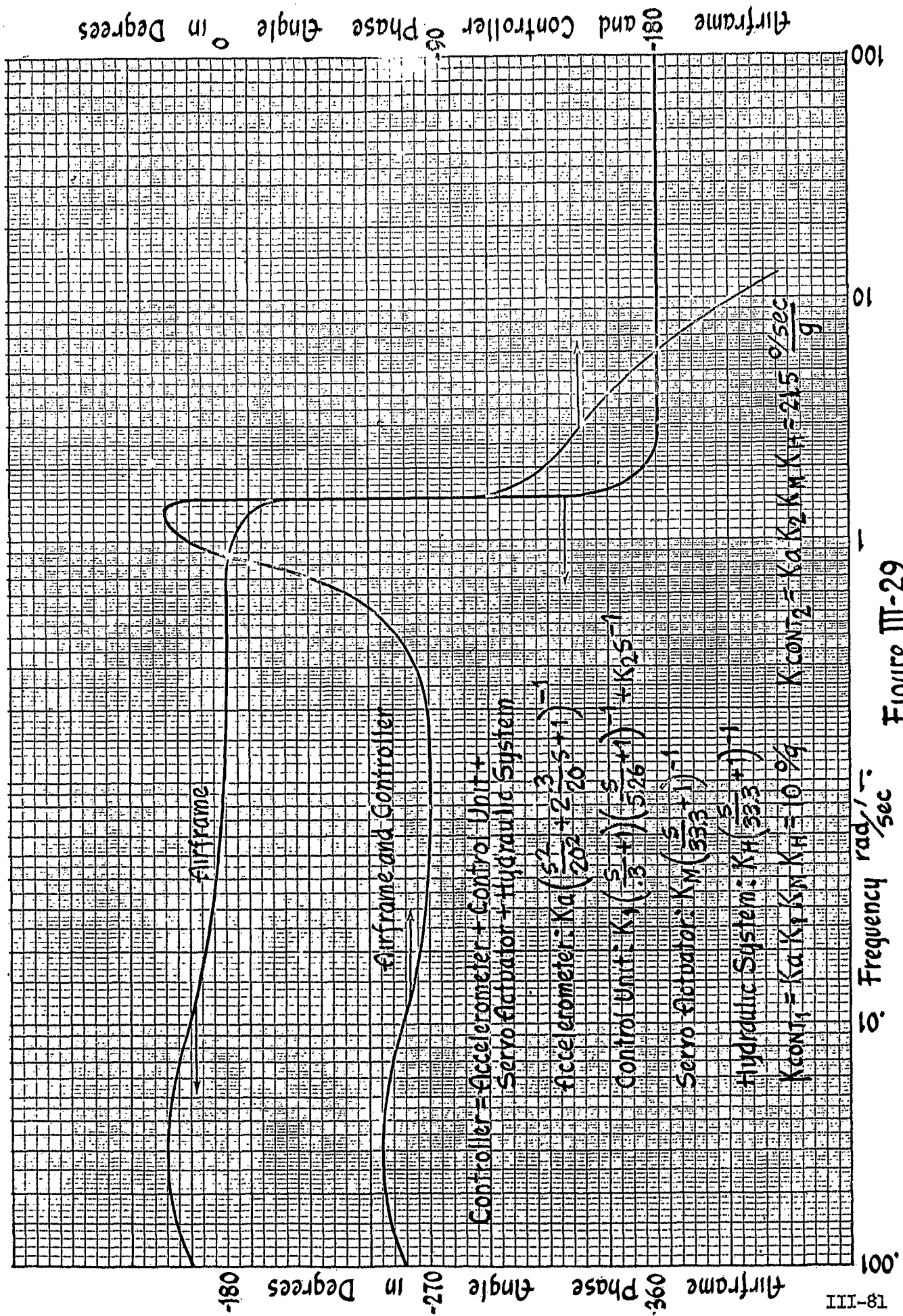
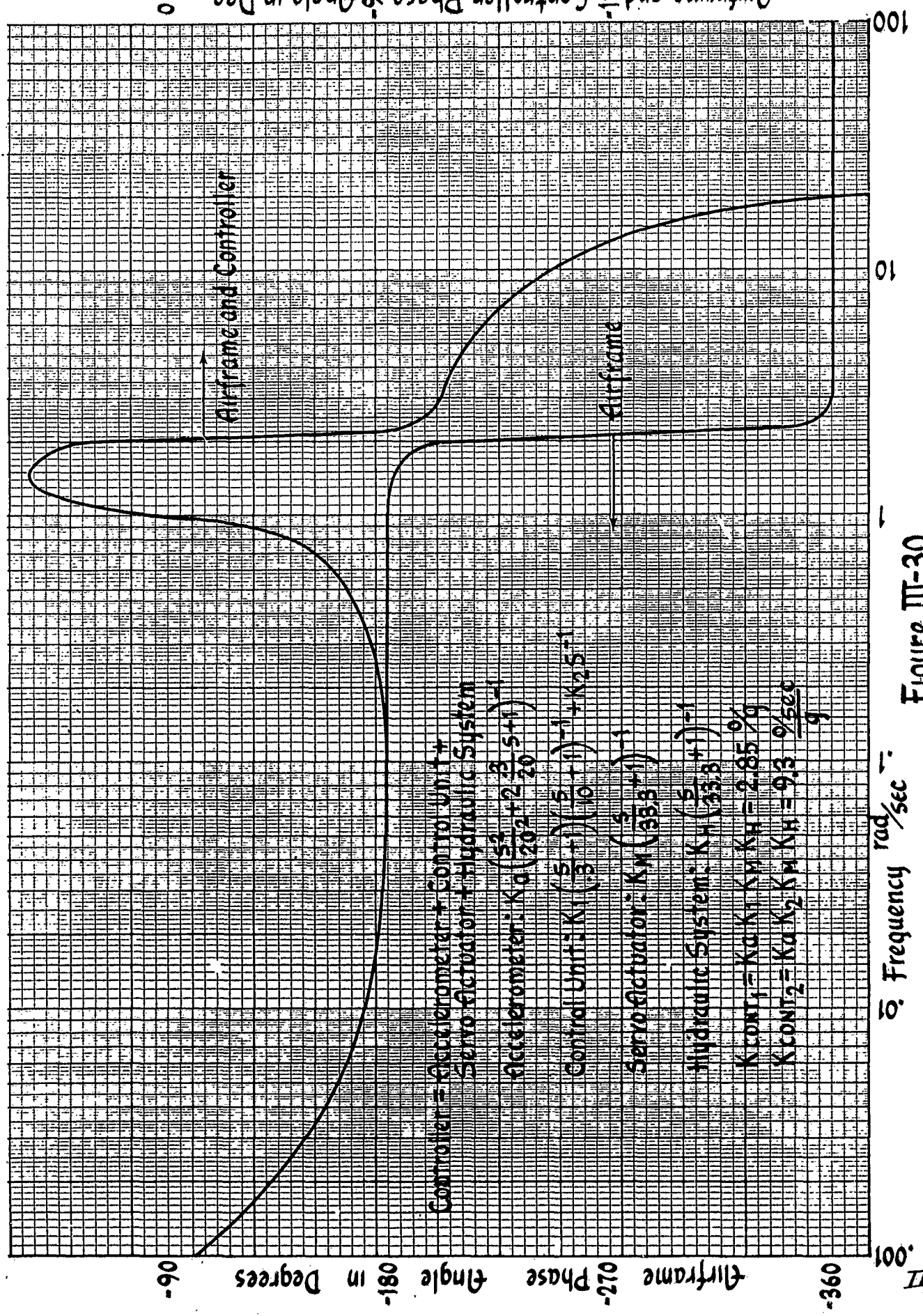


Figure III-29

0

0



Airframe and Controller Phase Angle in Deg. 0

Controller = Accelerometer + Control Unit +
 Servo Actuator + Hydraulic System
 Accelerometer: $K_a \left(\frac{5}{20} + 2 \frac{3}{20} s + 1 \right)^{-1}$
 Control Unit: $K_i \left(\frac{5}{3} + 1 \right) \left(\frac{5}{10} + 1 \right)^{-1} + K_2 s^{-1}$
 Servo Actuator: $K_M \left(\frac{5}{38.3} + 1 \right)^{-1}$
 Hydraulic System: $K_H \left(\frac{5}{35.8} + 1 \right)^{-1}$
 $K_{CONT1} = K_a K_i K_M K_H = 2.85 \frac{\%}{g}$
 $K_{CONT2} = K_a K_2 K_M K_H = 9.3 \frac{\%}{sec}$

Figure III-30

ES-III

Section 3

The first relation in Equations (III-18) assures that any steady state side accelerations will be trimmed out within 12 seconds. The last two relations in Equations (III-18) give a dutch roll damping ratio in the neighborhood of 0.4, a value which is considerably higher than any of those for the basic airframe alone. To verify these observations, the root locus for Condition V is presented in Figure III-31*.

This root locus plot is constructed by keeping the ratio of K_{CONT1} to K_{CONT2} constant (see Equation III-16) while varying K_{CONT2} . This of course means that K_{CONT1} , and K_{CONT2} are both varied to obtain the plot. The ratio used corresponds to the values chosen from Figures III-19 and III-23 for this flight condition or

$$(III-19) \quad \frac{K_{CONT1}}{K_{CONT2}} = \frac{13.5 \text{ SECS}}{26} = 0.52 \text{ SECS.}$$

The figure shows that the dutch roll damping ratio has been increased from 0.013 to 0.39 for the gains chosen. It will also be noted that the damping of the dutch roll mode could be increased by increasing K_{CONT2} (keeping in mind that K_{CONT1} must also be increased to keep the ratio K_{CONT2}/K_{CONT1} constant). Consider a value of K_{CONT2} , which will give the maximum damping for the augmented dutch roll mode. For this condition of $\zeta_{D \text{ MAX}}$, K_{CONT2}

*This condition is chosen because it most closely approaches what may be considered a typical combat condition.

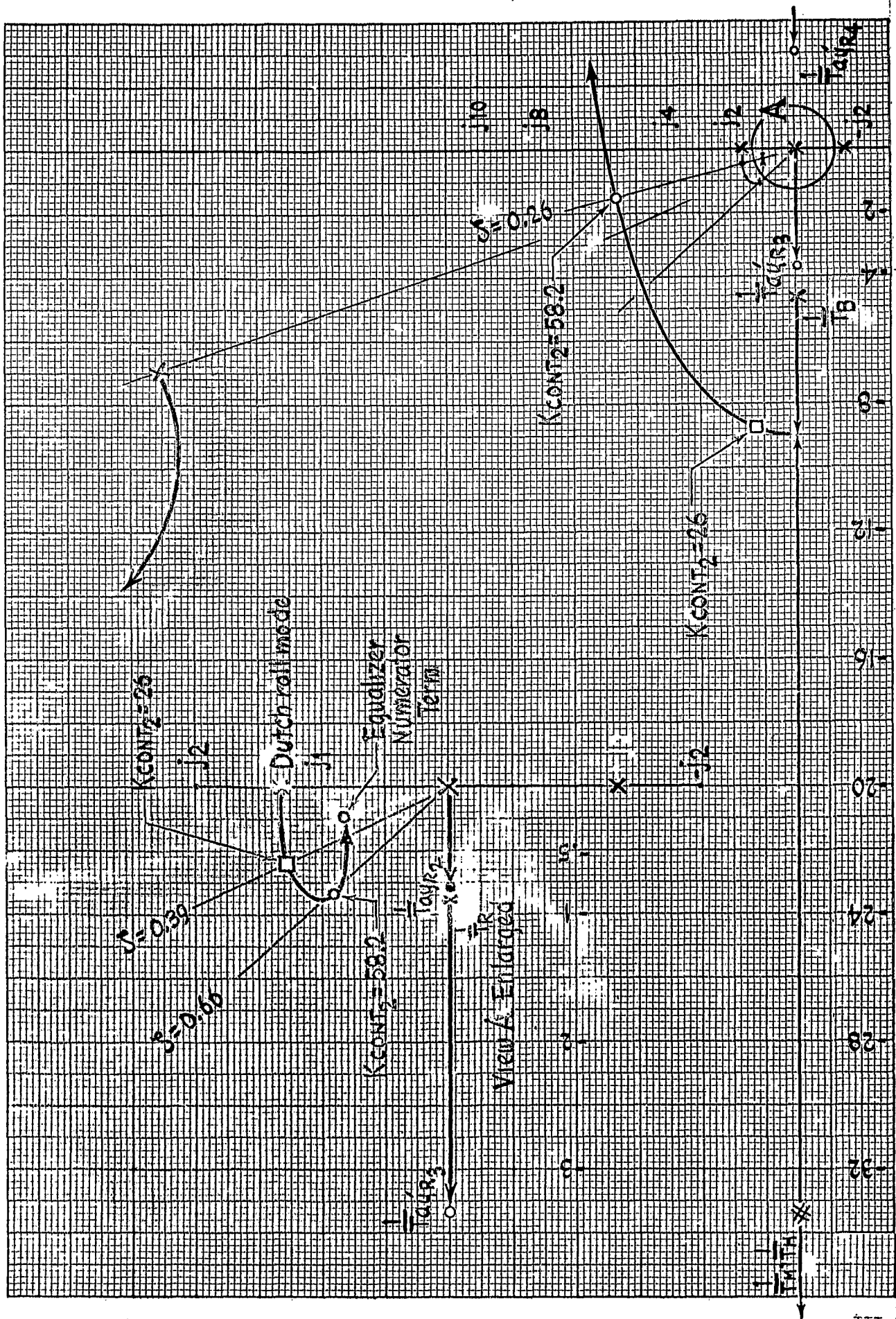


Figure III-31, Case V Root Locus Showing Effects of Varying K_{CONT2}

Section 3

is 58.2. However, with this value for K_{CONT_2} , the mode created by combining the $1/T_B$ and $1/T_H$ roots will be only 0.26 damped.

Furthermore, if the gains for this condition are to be increased, the gains for the other six conditions would probably have to be increased to preserve the desirable mechanization curves, i.e., to preserve the functions $K_{CONT_1} \alpha_{gc}^{-3/2}$ and $K_{CONT_2} \alpha_{gc}^{-1}$. For most of the other six conditions, the augmented dutch roll mode damping is already near a maximum value for the values of K_{CONT_2} and K_{CONT_1} chosen. Raising these gains would not only decrease the damping of the $(1/T_B)-(1/T_H)$ mode, but would also decrease the damping of the augmented dutch roll mode.

Therefore, for the time being, the values of K_{CONT_1} , T_B and K_{CONT_2} given in Figures III-19, III-20, and III-23 will be assumed to be correct. These values lead to the results discussed following Equation (III-18).

The next step in the analysis and synthesis phase of the design procedure consists of an analog computer study to check the validity of the transfer function chosen for the system control unit, and to determine the effects of possible system inherent nonlinearities.

(c) ANALOG COMPUTER STUDIES

The equations used for the analog computer program are the airframe equations given in Chapter II and the sideslip stability augments equations. The airframe equations were given in Chapter II as Equations (II-29). The sideslip stability augments equations used are given by Equations (III-6),

(III-10), and (III-16). The transfer function for the surface actuator is given by Equation (III-11). These equations were mechanized on the analog computer and the test results were recorded by means of a direct inking recording oscillograph.

Figure III-32 shows the response of the basic airframe of Condition V to a pulse rudder input. The poor damping of the dutch roll mode and the divergence of the spiral mode (as shown in the ϕ trace) are clearly evident.

The effect of the lead lag equalizer $K_1 \frac{T_A S + 1}{T_B S + 1}$ on the dynamic response is shown in Figure III-33. For this trace $K_{CONT_1} = 13.5$ (from Figure III-19)* and $T_B = .228$ (from Figure III-20). The dutch roll damping has been improved considerably with the oscillation decaying to negligible values in one cycle. Figure III-34 shows the effect on dutch roll damping, of adding the integration loop. In Figure III-35, the ability of the augments to reduce an out of trim condition is shown. The out of trim condition was simulated by adding a ramp voltage to the voltage representing the rudder deflection.

A comparison of the curves in Figures III-36 and III-34 shows that an increase in K_{CONT_1} and K_{CONT_2} of 25% (with $T_B = .228$) improves the dynamic response characteristics of the system for this particular condition.

*The constants K_1 and K_{TC} shown on the oscillograph records correspond to K_{CONT_2} and K_{CONT_1} respectively.

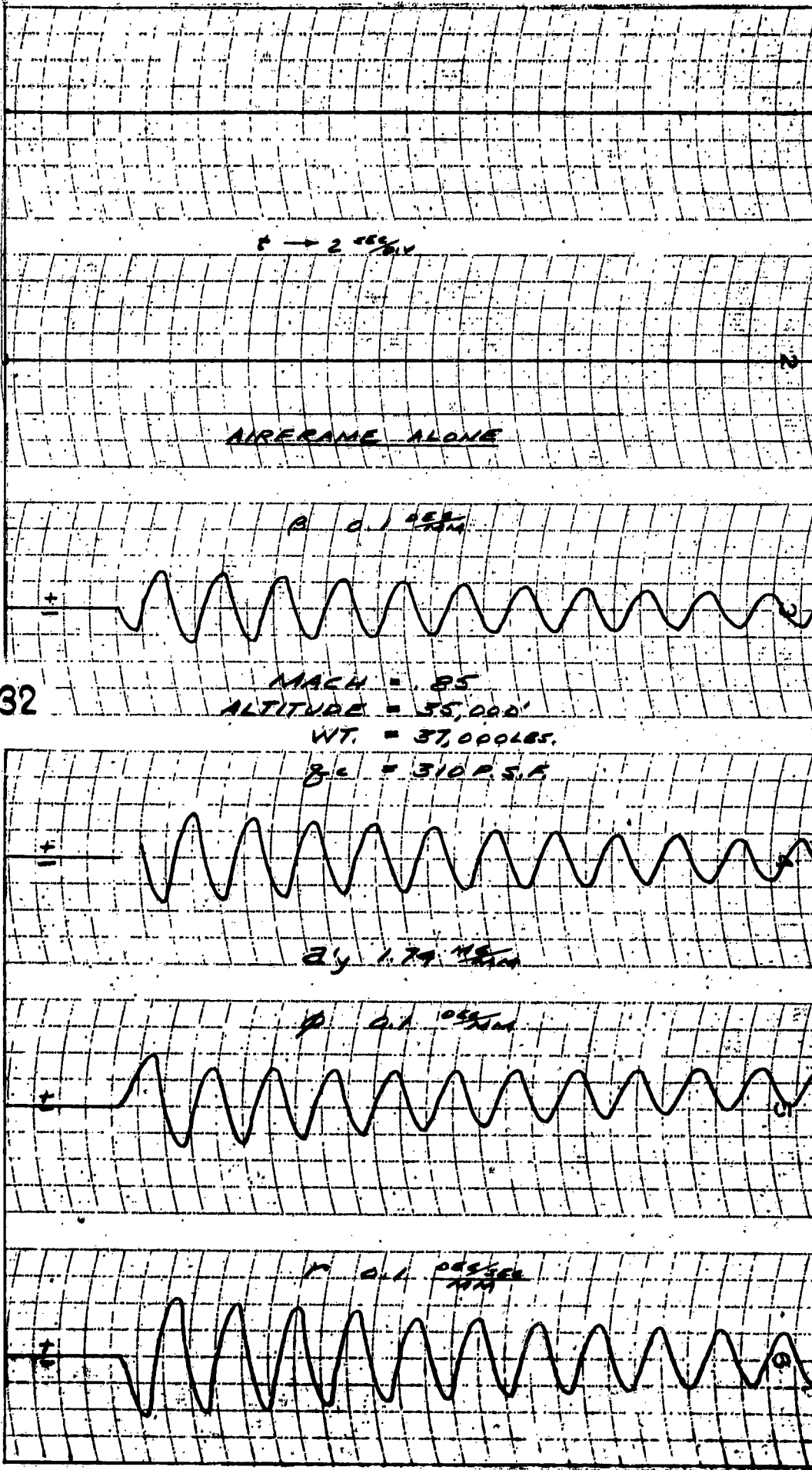


Figure III-32

Case V

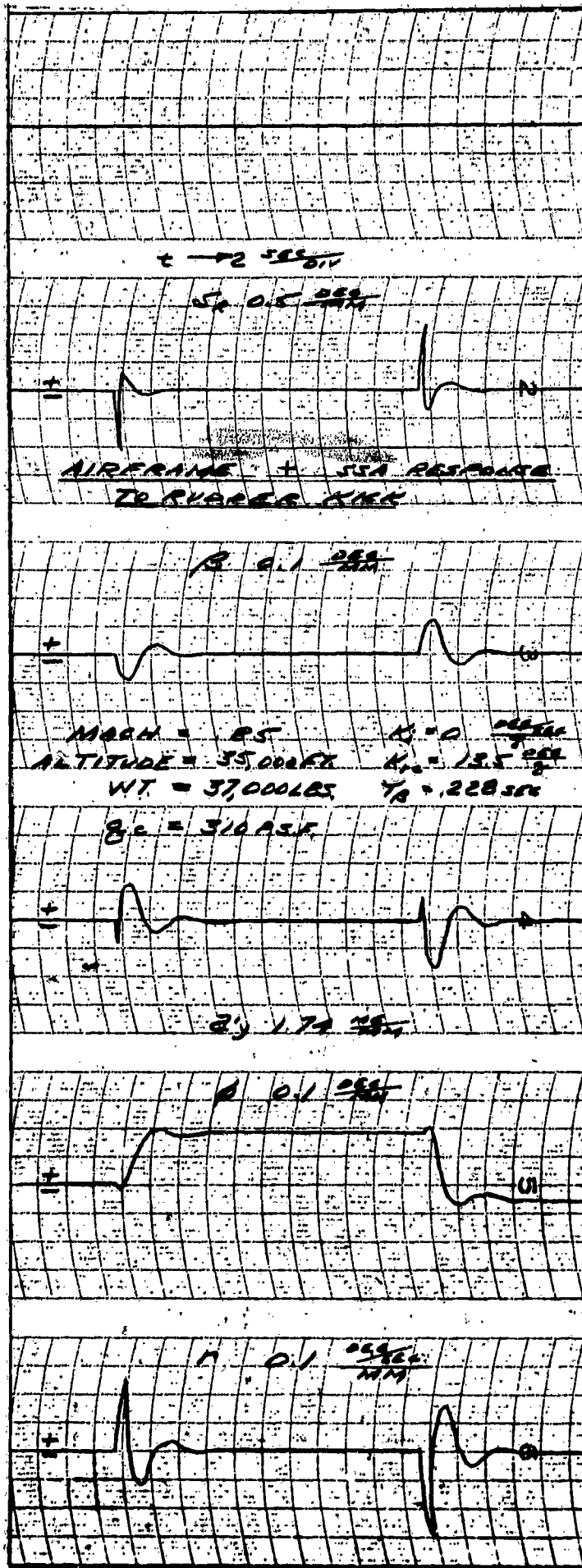
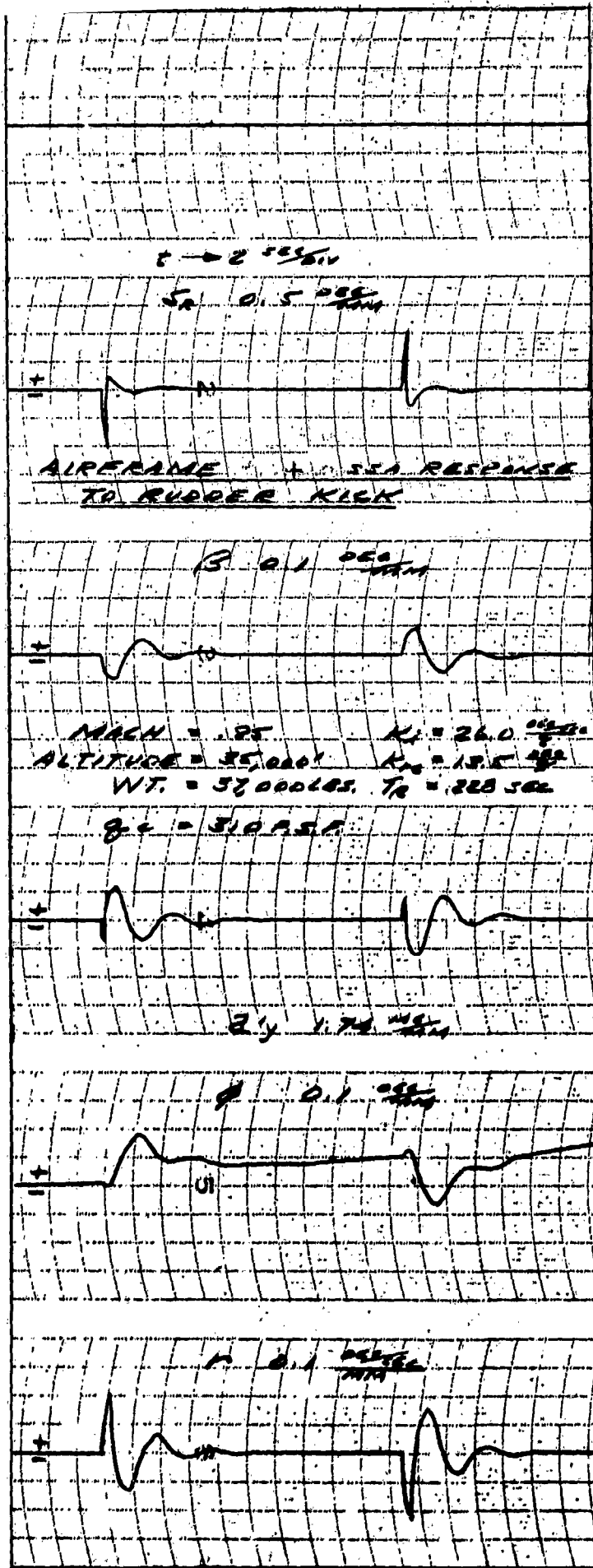


Figure III-33
Case V

Figure III-34
Case V



SENT 0.1 550



c + 2 550V
Sent 0.01 550

AIRFRAME - 1. SEA RESPONSE
TO RAMP OUT-OF-TRIM INPUT

B 0.01 550



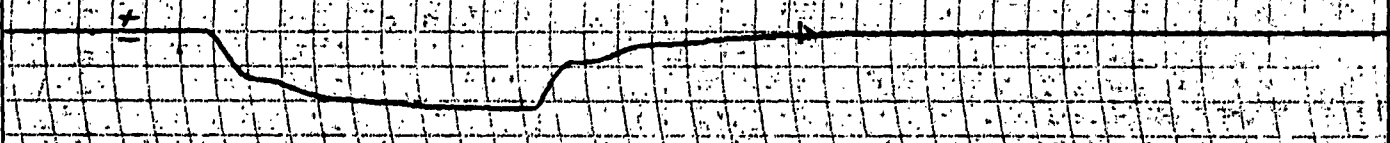
MACH = .85
 ALTITUDE = 35,000'
 WT. = 37,000 LBS.
 $\delta_c = 3.0 \text{ P.S.F.}$

$K_1 = 20.0 \frac{\text{P.S.F.}}{\text{G}}$
 $K_2 = 13.5 \frac{\text{P.S.F.}}{\text{G}}$
 $T_0 = .220 \text{ sec}$

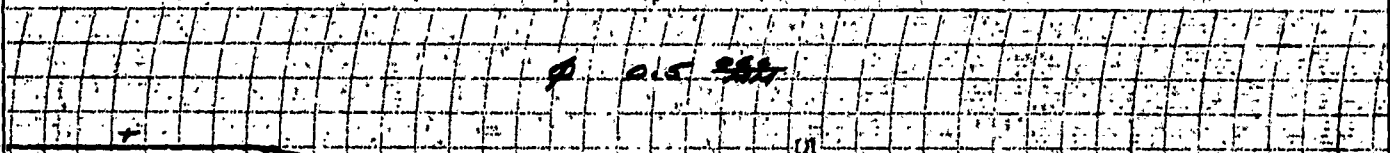
Figure III-35

Case V

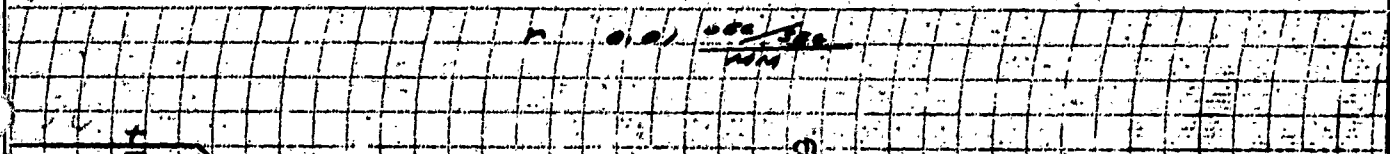
2.1 0.171 550



0 0.15 550



1.1 0.1 0.001 550



Section 3

Computer traces for Condition IV are shown in Figures III-37 through III-41. Again, it will be noted that system performance is improved when K_{CONT_1} and K_{CONT_2} are increased by 25% (e.g. compare Figures III-39 and III-41).

Figures III-42 through III-51 show the computer traces for the other five flight conditions, first for the original values of K_{CONT_1} and K_{CONT_2} and then with these quantities increased by 25%. As a result of these traces, these gains were increased by 25% and are shown for this increase in Figure III-52.

By inserting aileron pulses into the system it was determined experimentally that a simple gain between aileron deflection and rudder deflection would not provide good coordination. By means of a trial and error process, it was found that a one second lag for all flight conditions, with gain varying with flight condition would provide good coordination for aileron turns. Figures III-53 through III-59 show the computer traces for all seven flight conditions. The values for the aileron to rudder gain (K_{Sa}) are given in Table III-5 and plotted in Figure III-60.

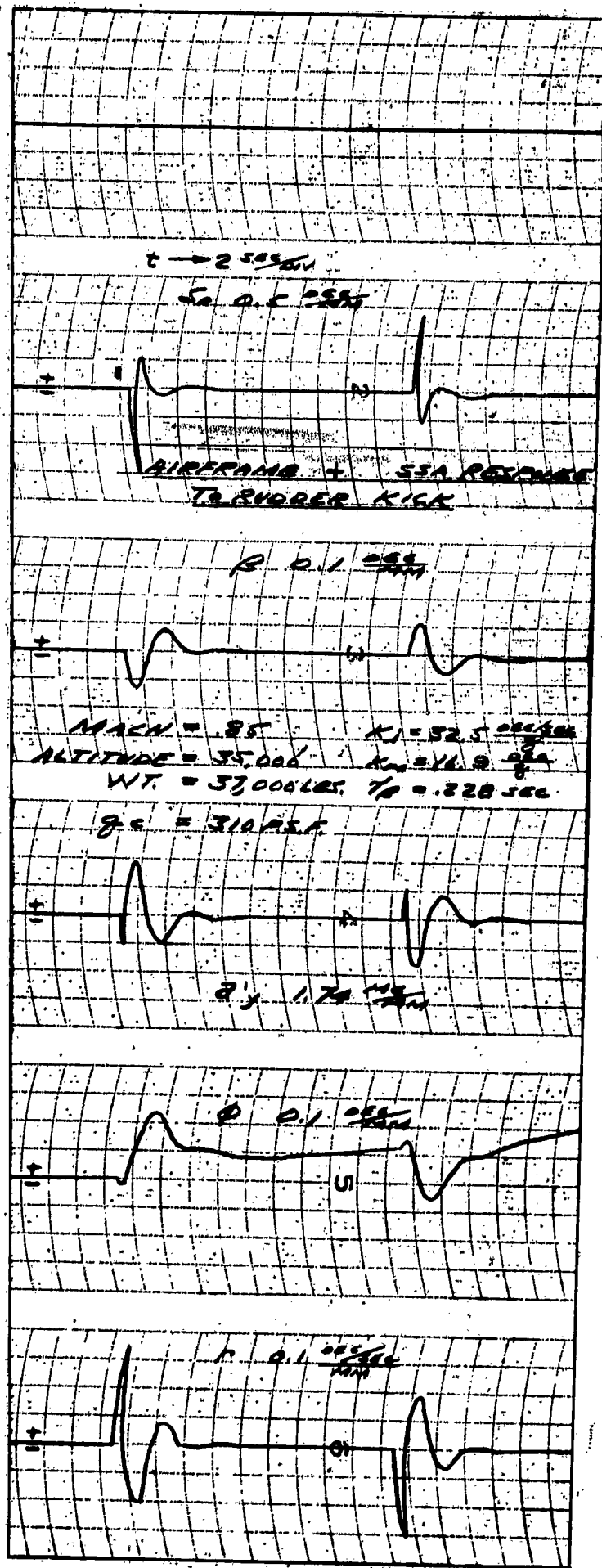


Figure III-36
Case V

Section 3

t → 2 $\frac{SEC}{DIV}$

AIRFRAME ALONE

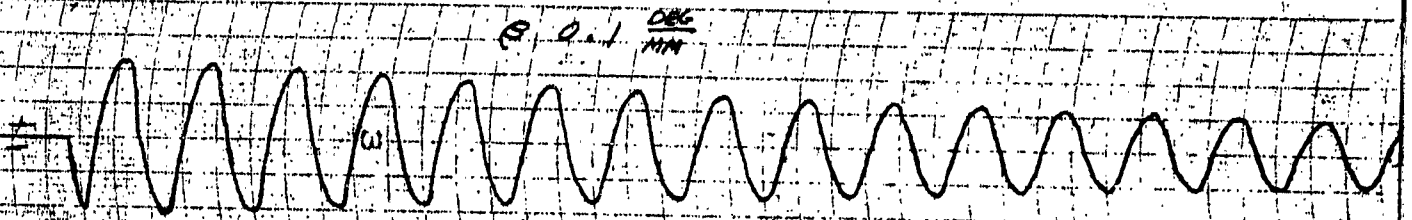
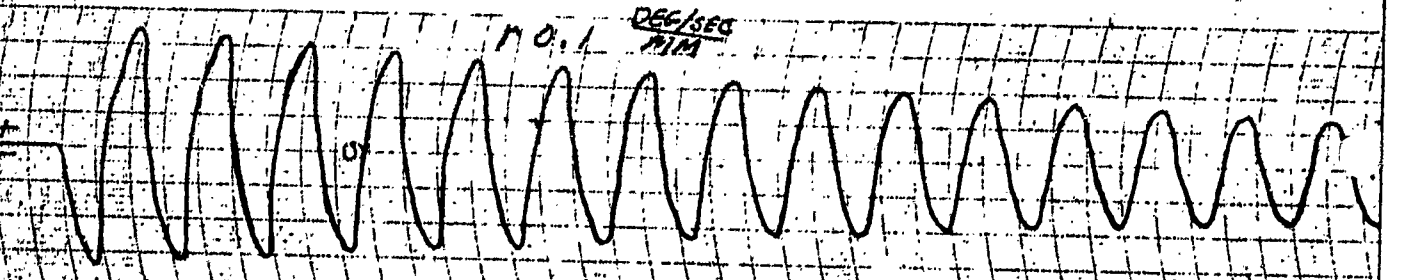
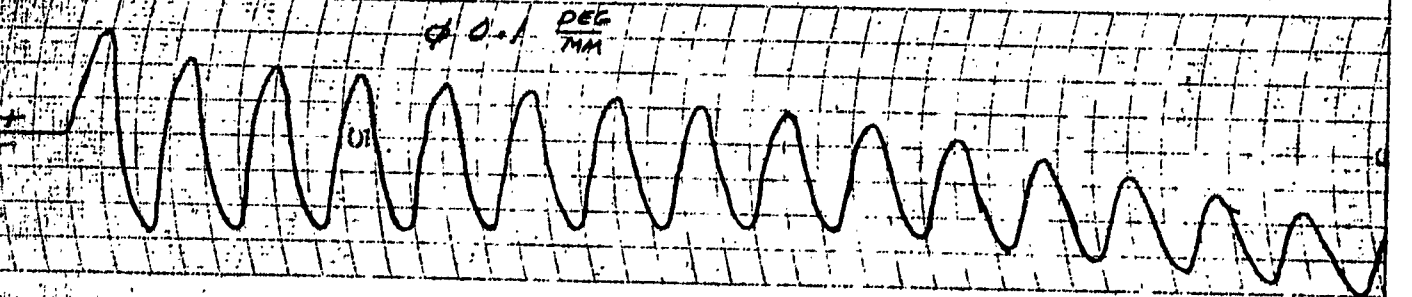
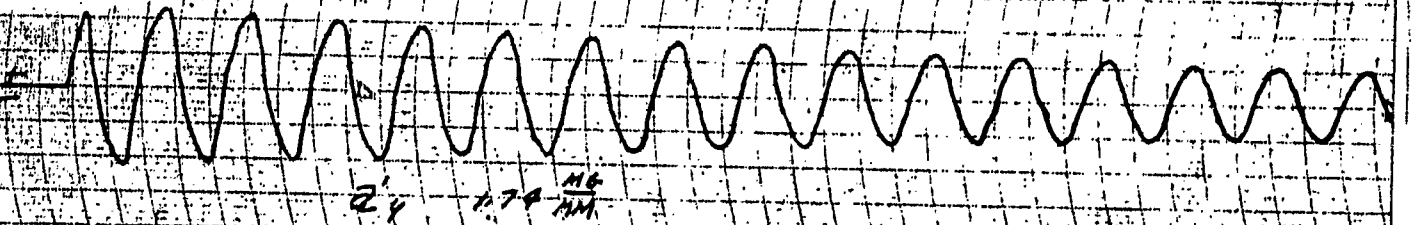


Figure III-37
MACH = .77
ALTITUDE = 35,000 FT
WEIGHT = 37,000 LBS

Case IV
 $\rho = 2.45 \text{ PSF}$



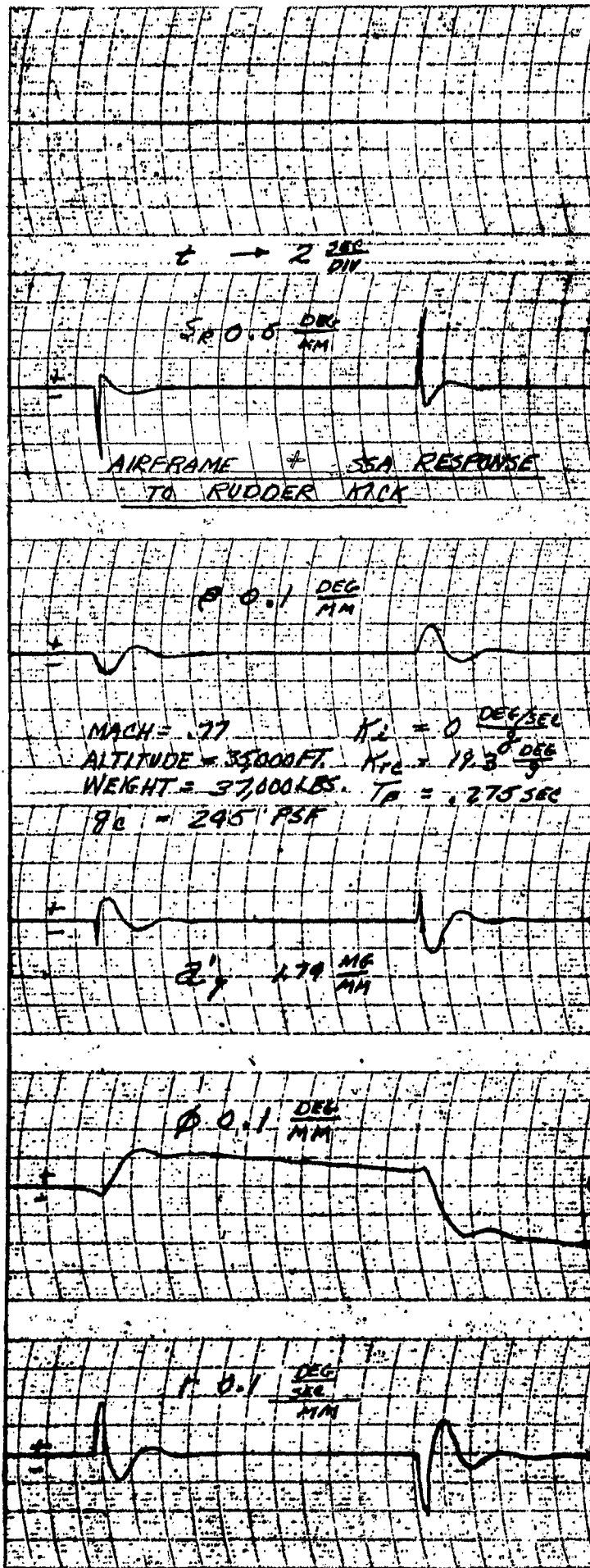
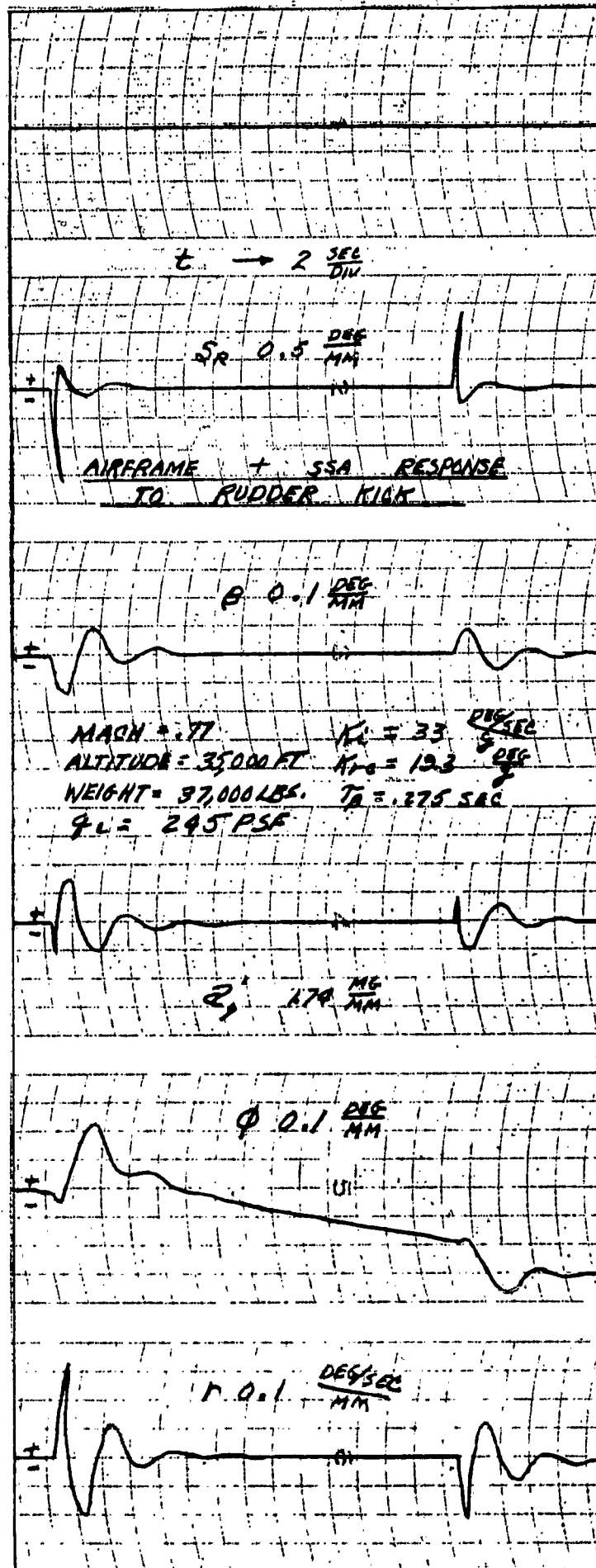


Figure III-38
Case IV

Figure III-39
Case IV



Scale: 0.1 $\frac{DEG}{MM}$

Scale: 2 $\frac{SEC}{DIV}$

Scale: 0.01 $\frac{DEG}{MM}$

AIRFRAME + SSA RESPONSE TO RAMP OUT OF TRIM INPUT

Scale: 0.01 $\frac{DEG}{MM}$

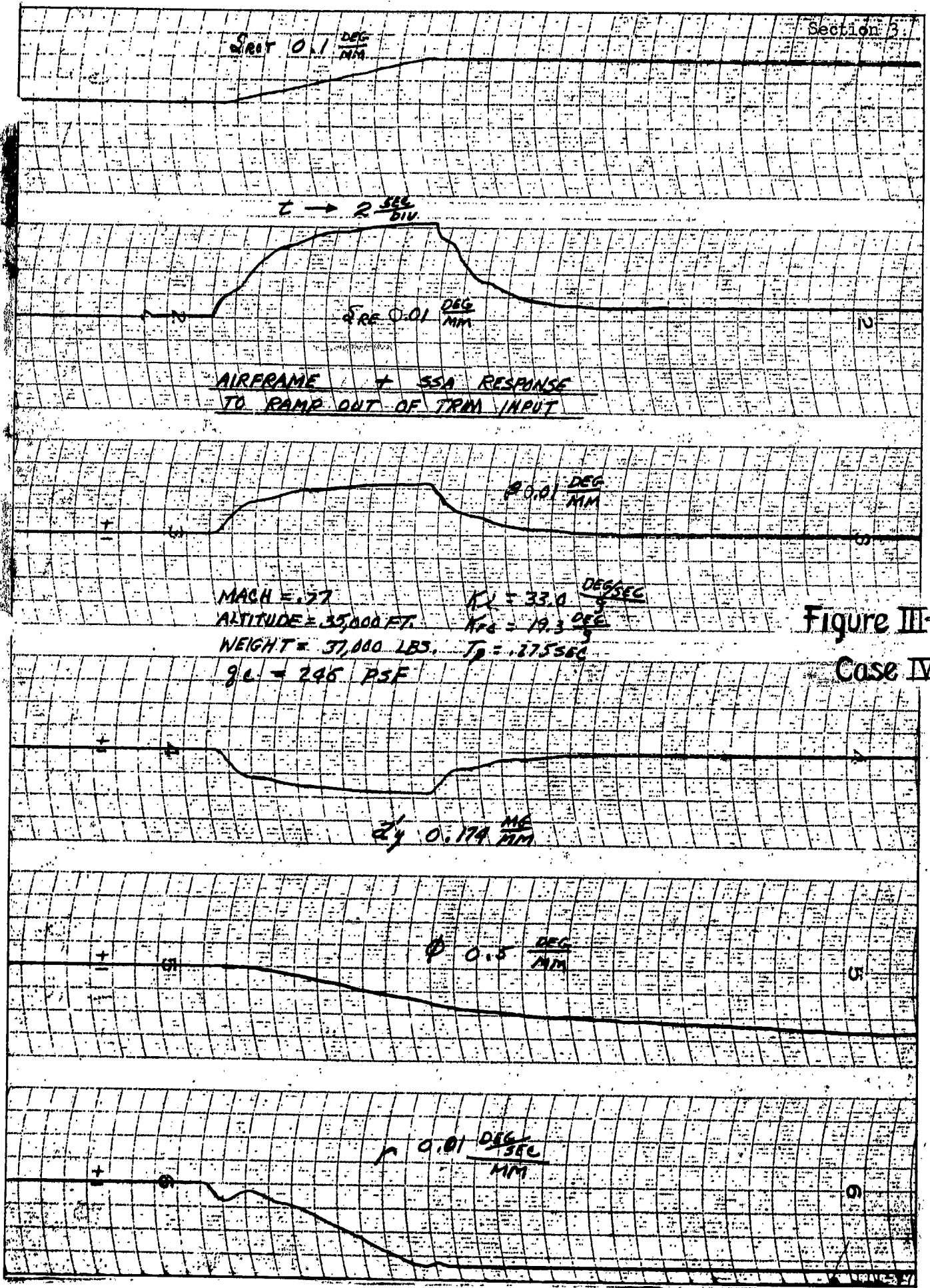
MACH = 0.77 $K_V = 33.0 \frac{DEG}{SEC}$
 ALTITUDE = 35,000 FT. $K_{FC} = 19.3 \frac{DEG}{SEC}$
 WEIGHT = 37,000 LBS. $T_D = 0.275 SEC$
 $q_L = 296 \text{ PSF}$

Figure III-40
Case IV

Scale: 0.174 $\frac{MG}{MM}$

Scale: 0.5 $\frac{DEG}{MM}$

Scale: 0.01 $\frac{DEG}{MM}$



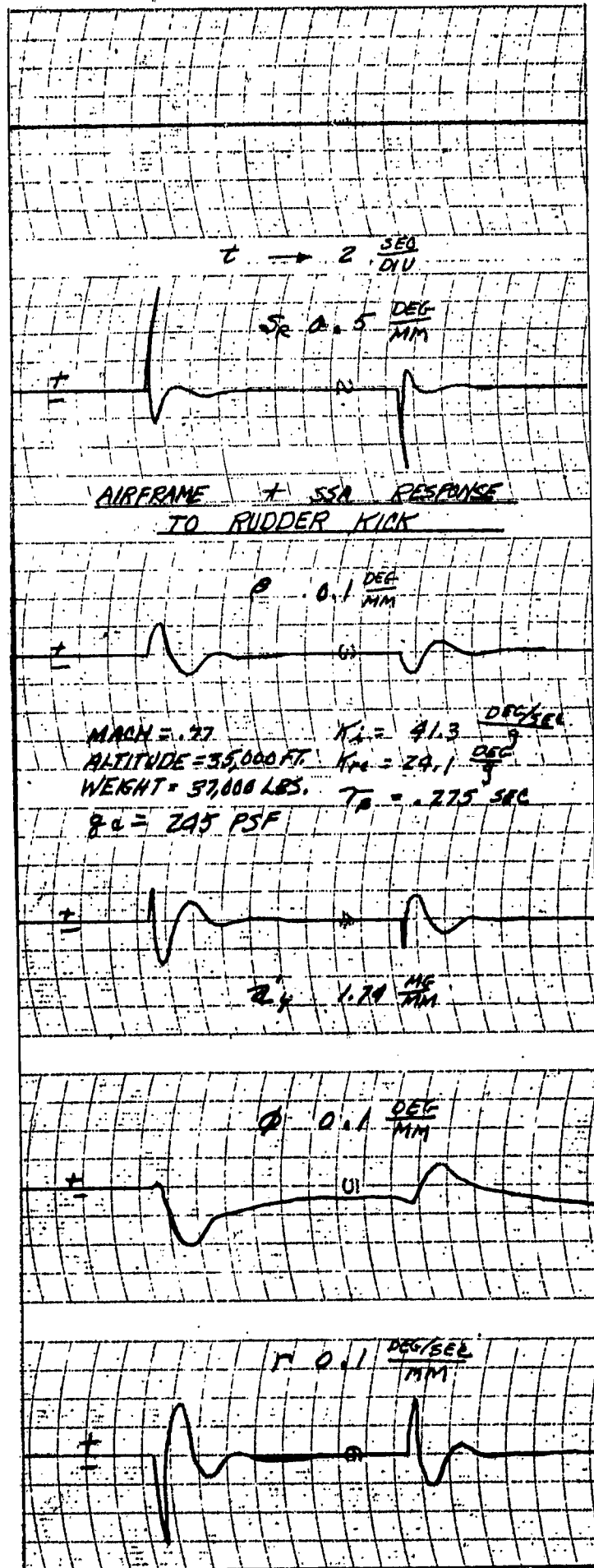
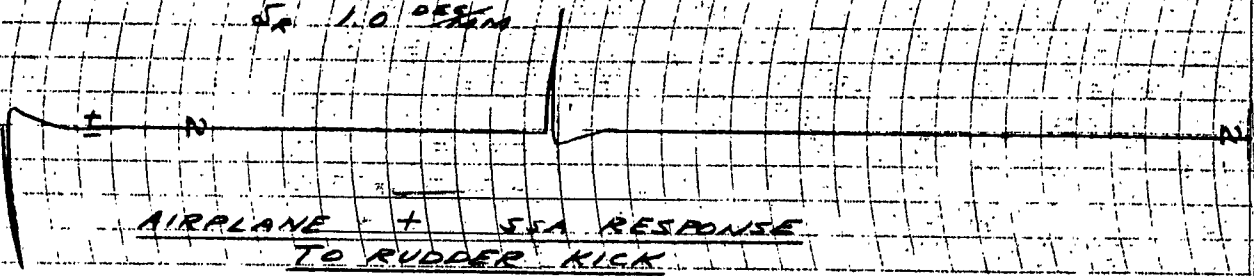


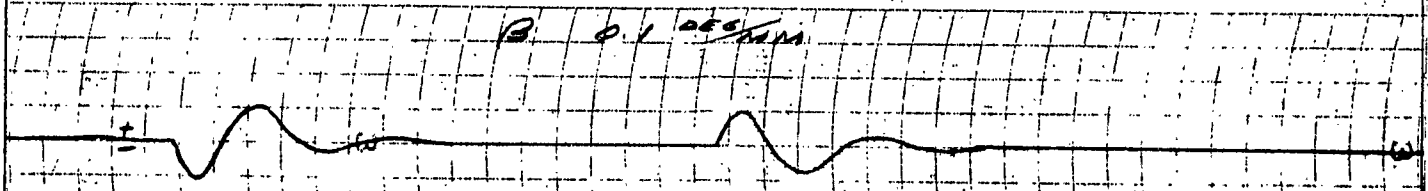
Figure III-41
Case IV

t → 2 SEC/DIV

5x 1.0 DEGREE



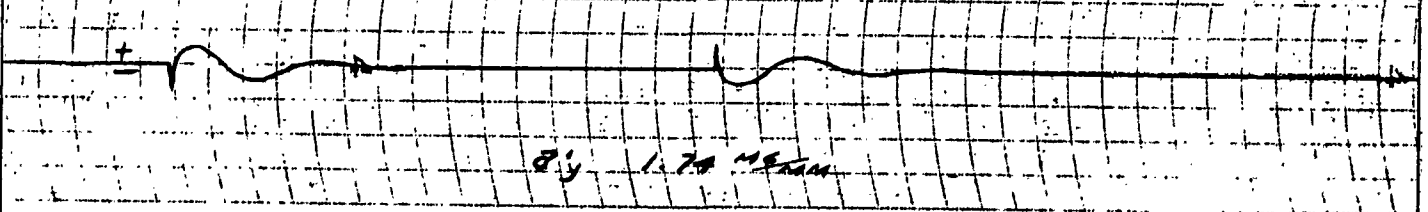
β 0.1 DEGREE



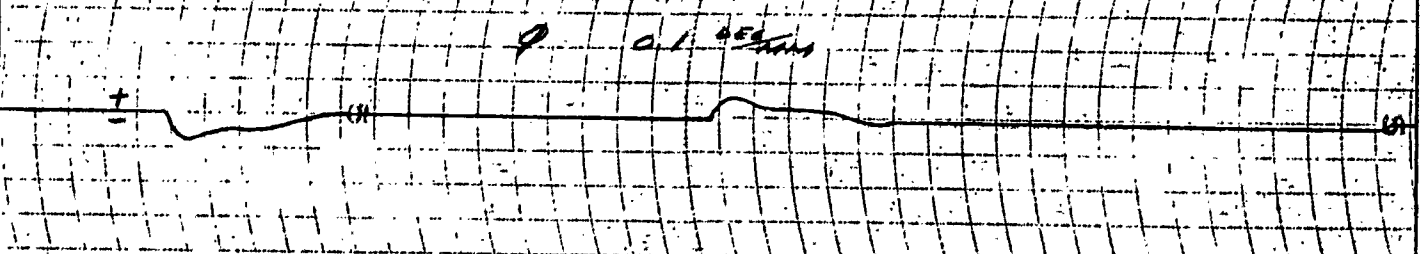
MACH = .26 $K_1 = 96.5 \text{ DEGREE/SEC}$
 ALTITUDE = 5,000' $K_{10} = 92.8 \text{ DEGREE/SEC}$
 WT. = 33,000 LBS. $T_B = .362 \text{ SEC}$
 B.C. = PSPSF

Figure III-42
Case I

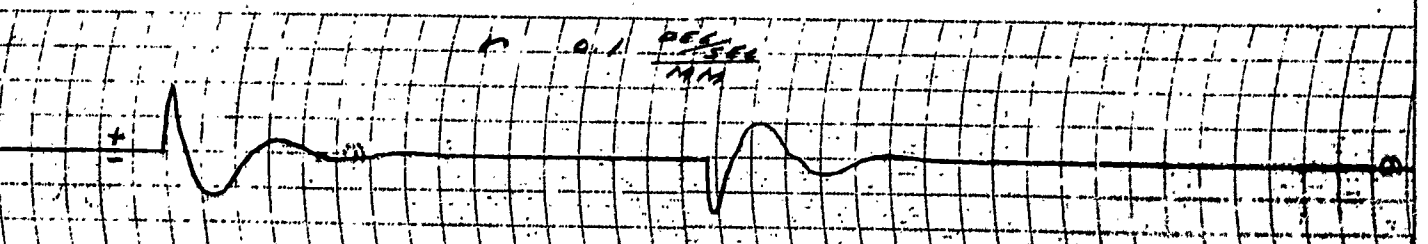
β_y 1.75 DEGREE



φ 0.1 DEGREE



κ 0.1 DEGREE/MM



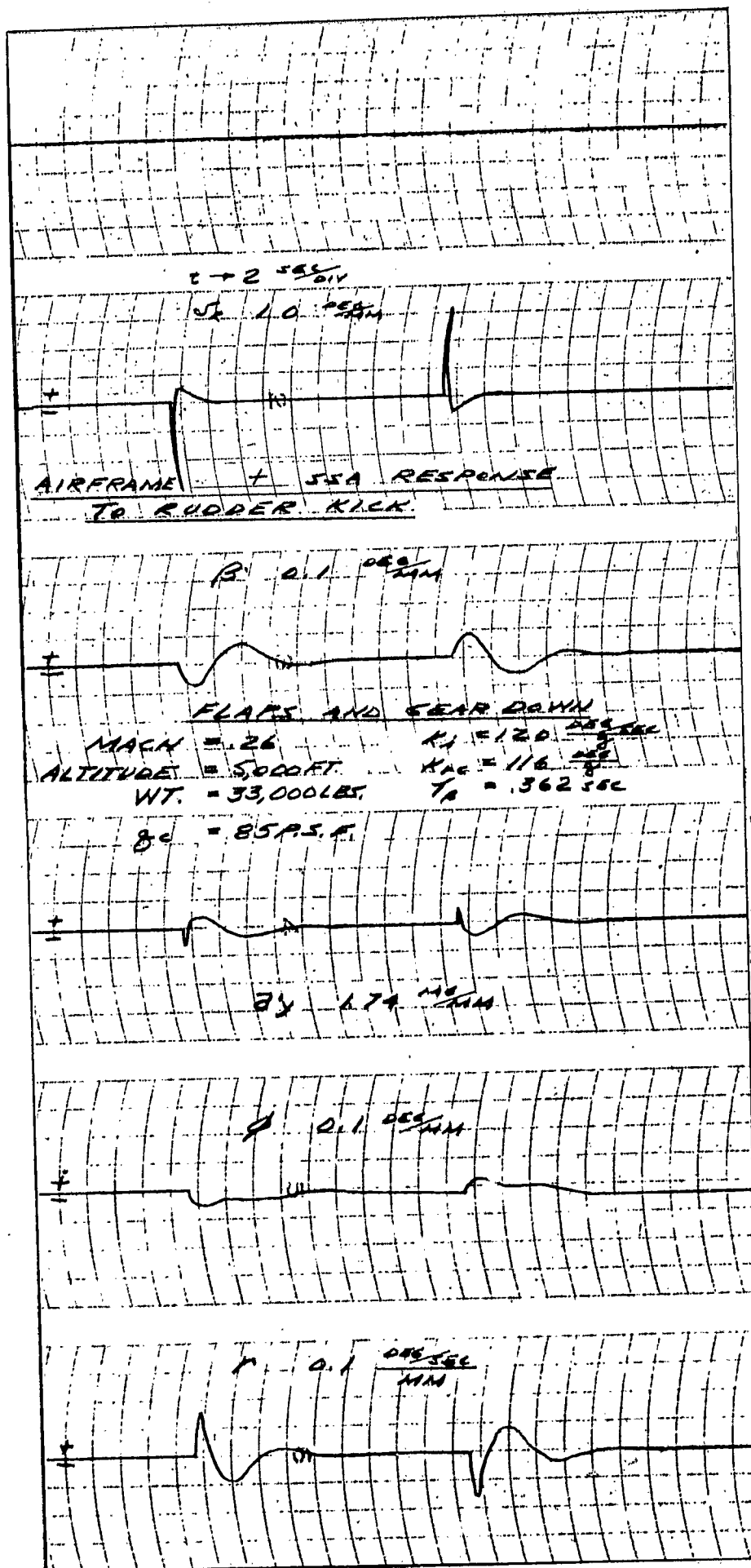


Figure III-43

Case I

MACH = .26 $K_1 = 120 \text{ DEG/SEC}$
 ALTITUDE = 5000 FT. $K_{AC} = 116 \text{ PERCENT}$
 WT. = 33,000 LBS. $T_A = .362 \text{ SEC}$
 $\delta_c = 85 \text{ P.S.F.}$

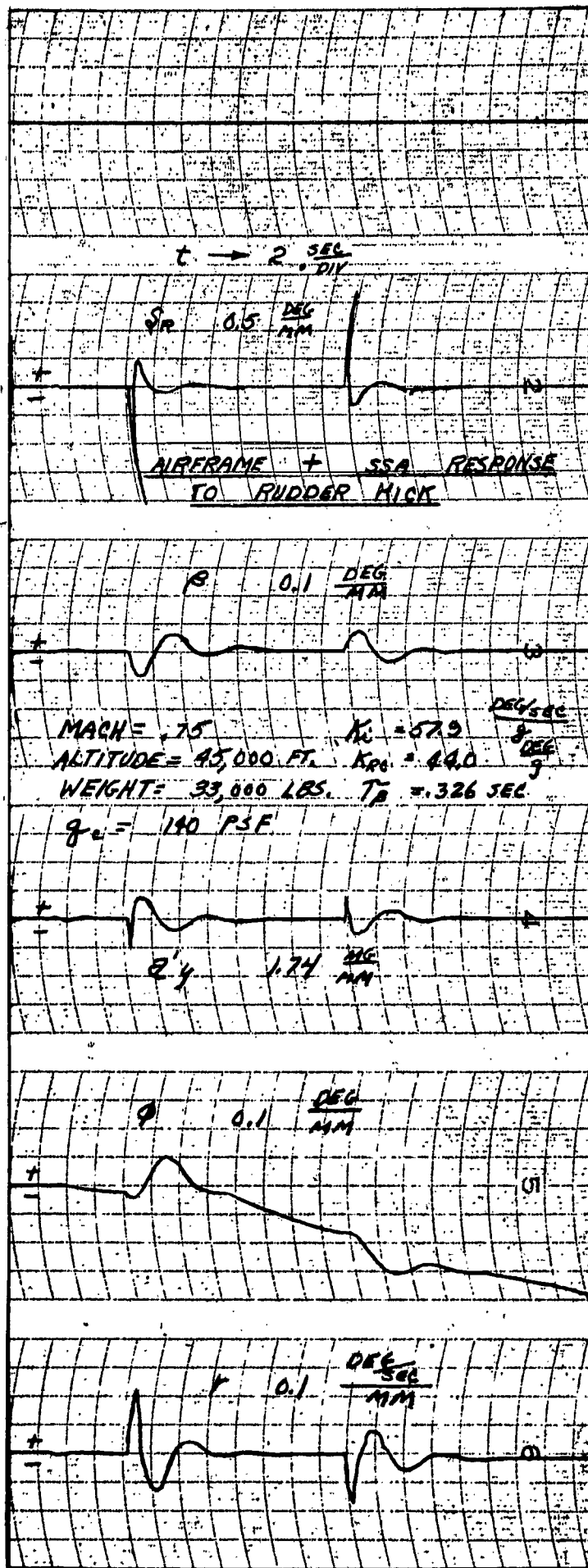


Figure III-44
Case II

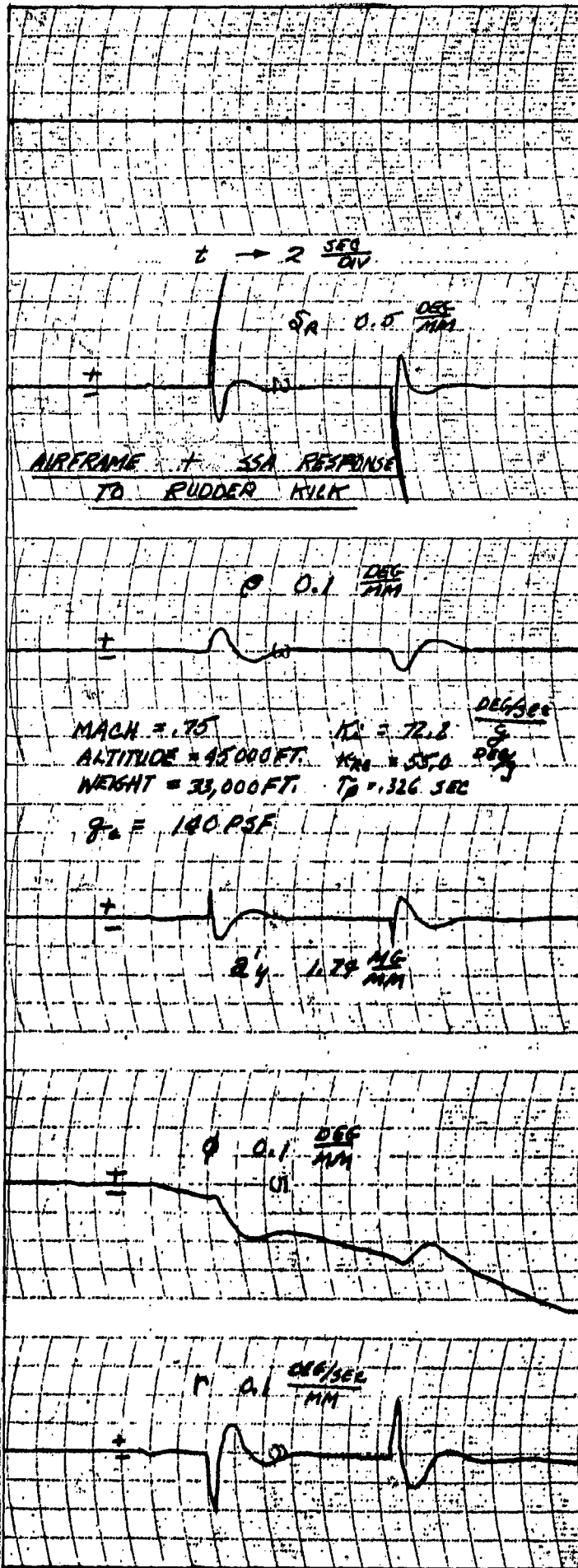


Figure III-45
Case II

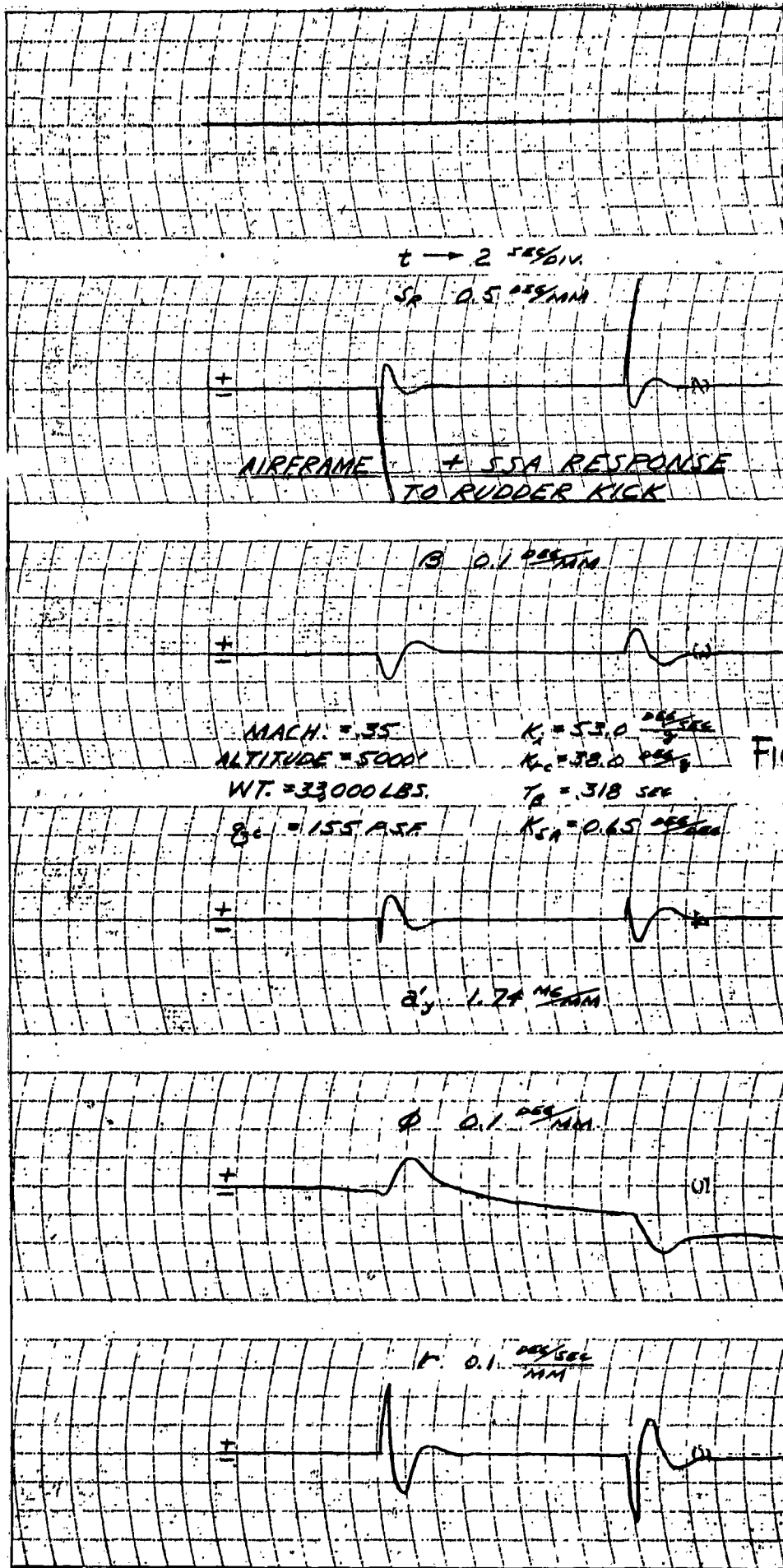


Figure III-46

Case III

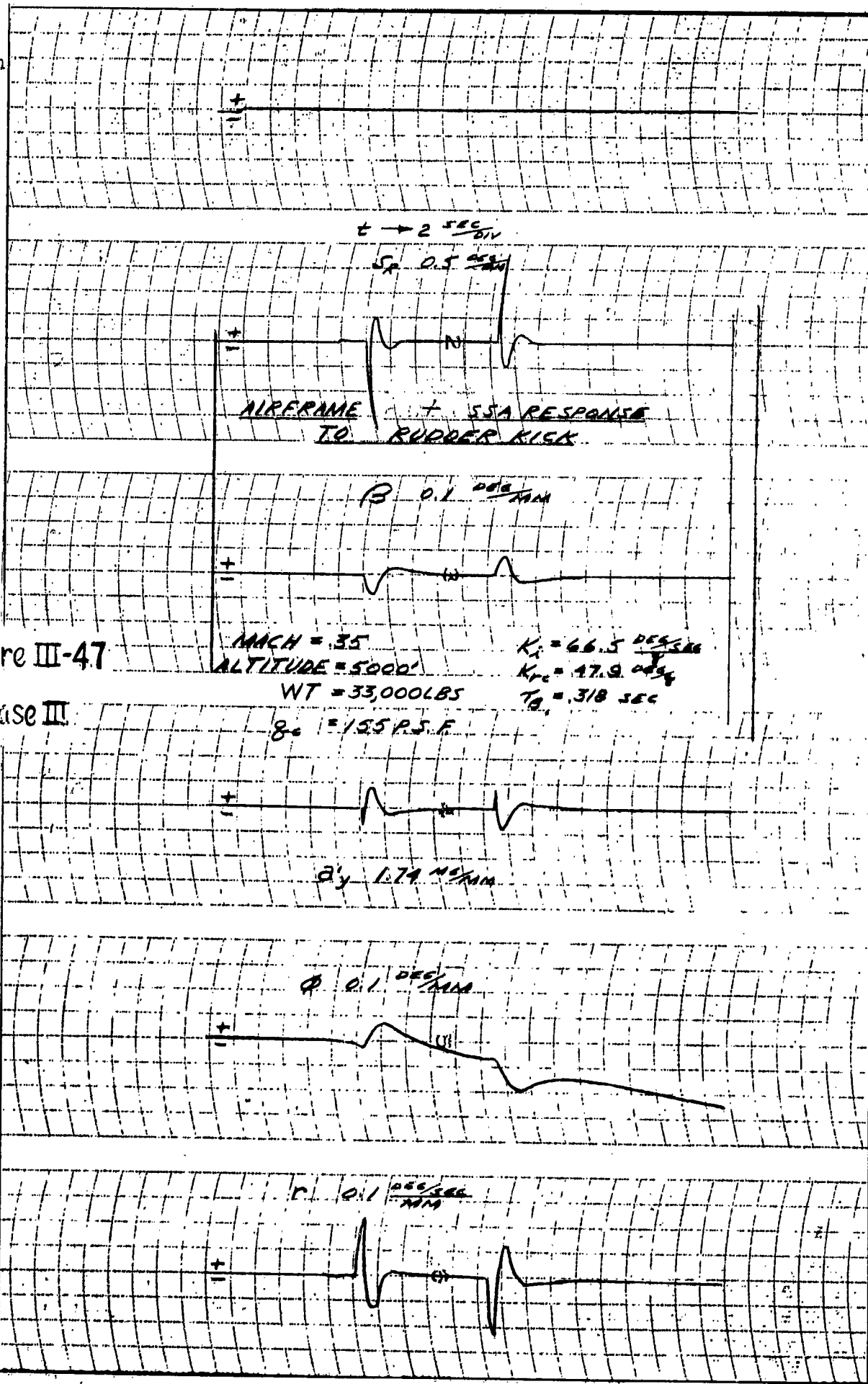


Figure III-47

Case III

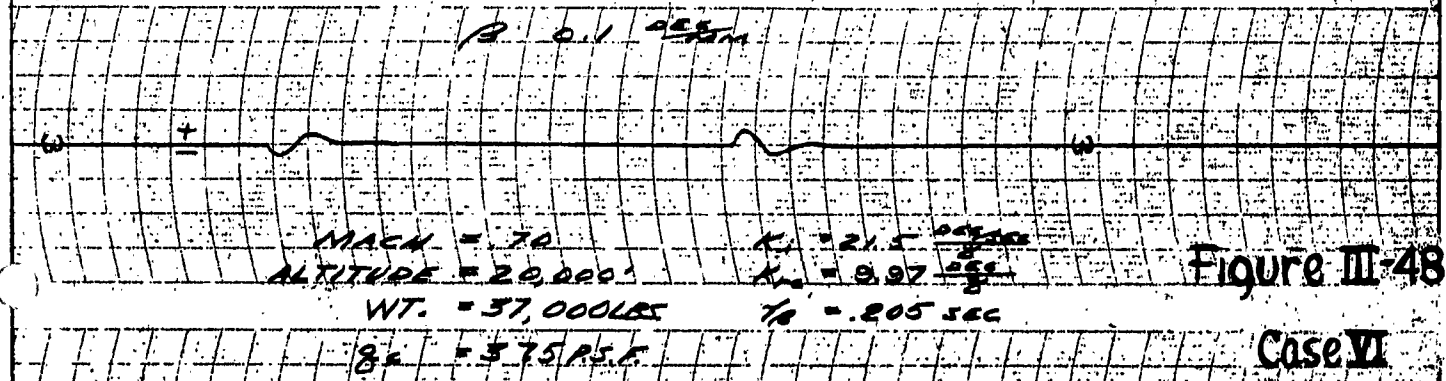
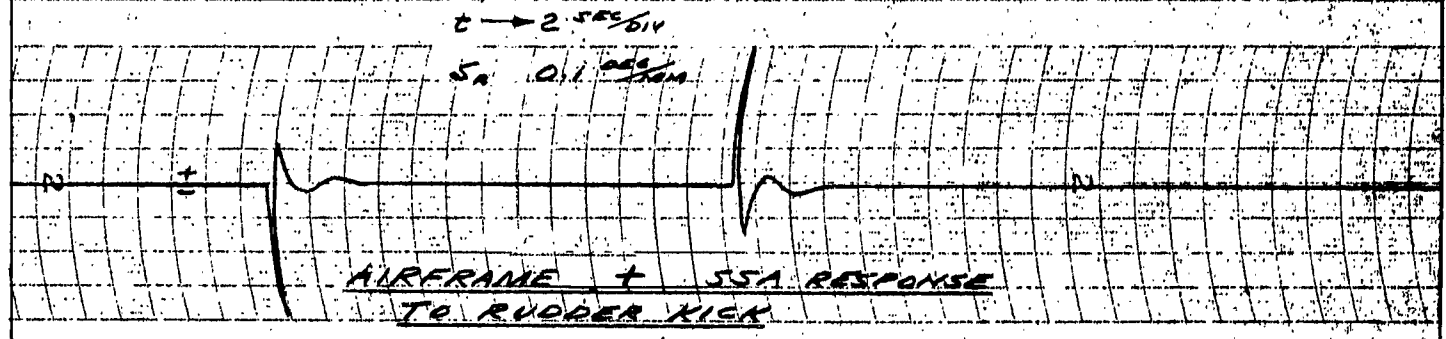
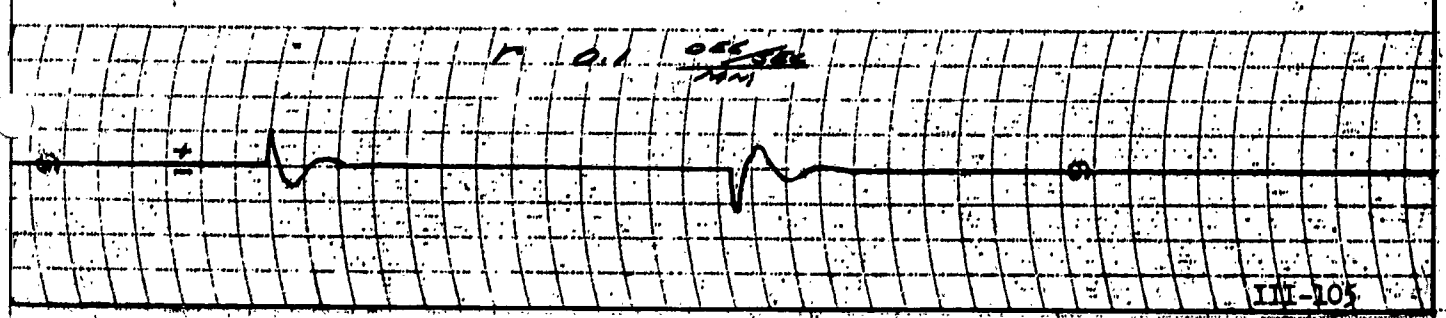
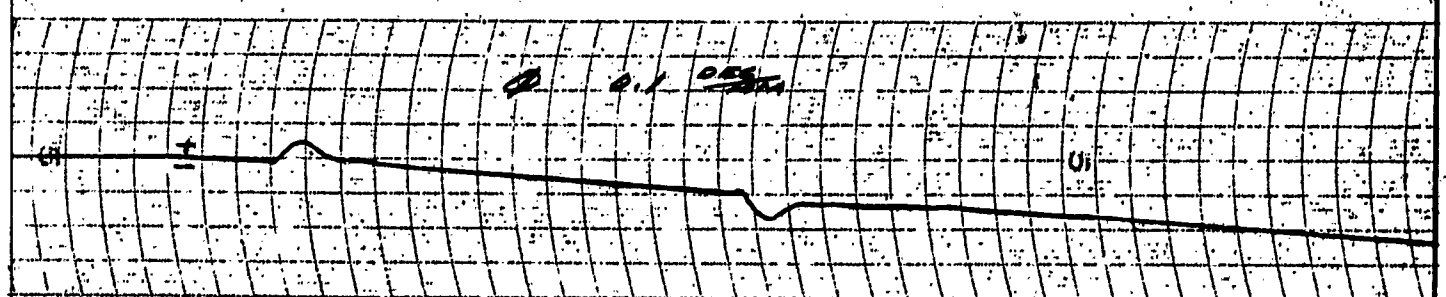


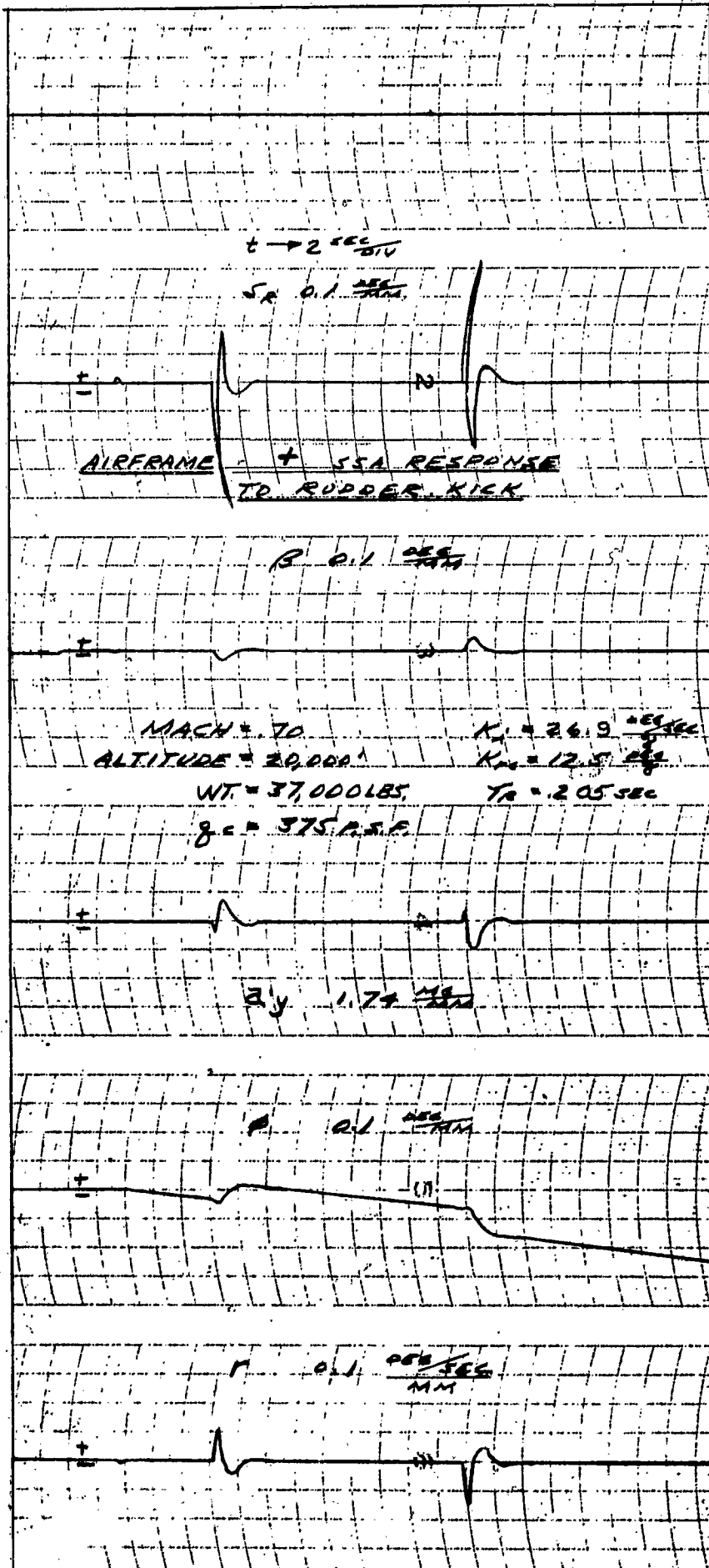
Figure III-48

Case VI



Section 3

Figure III-49
Case VI



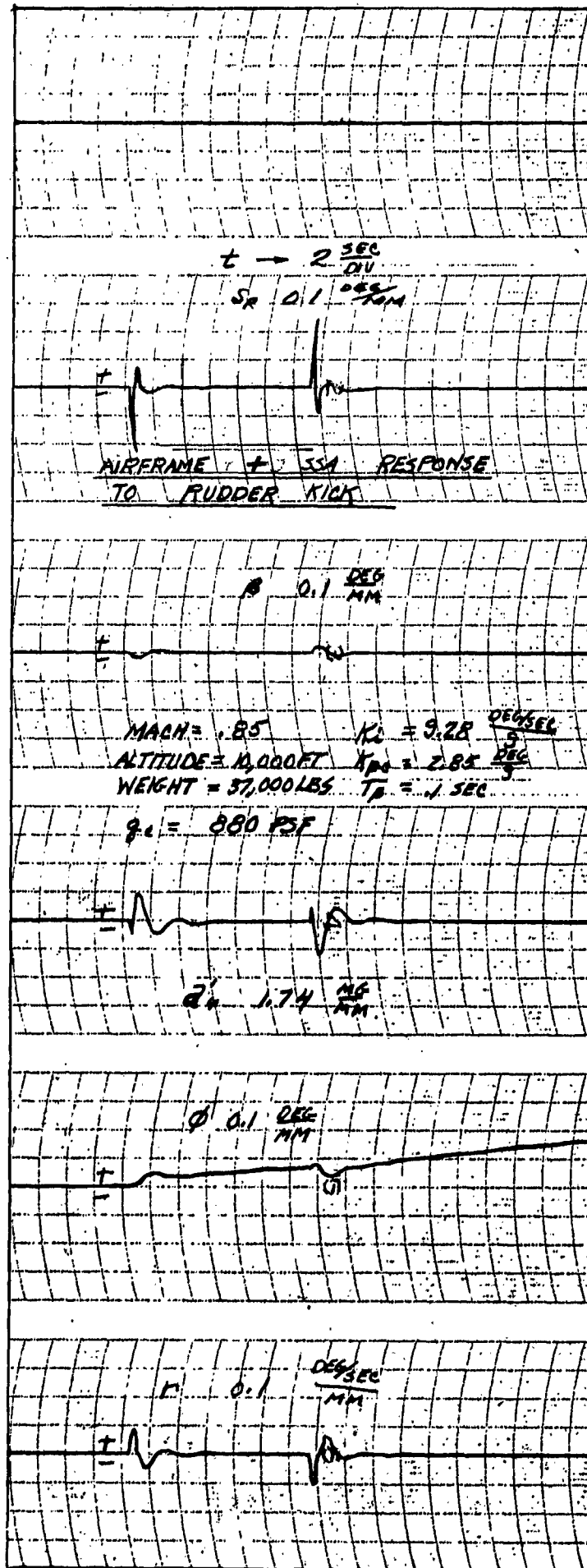
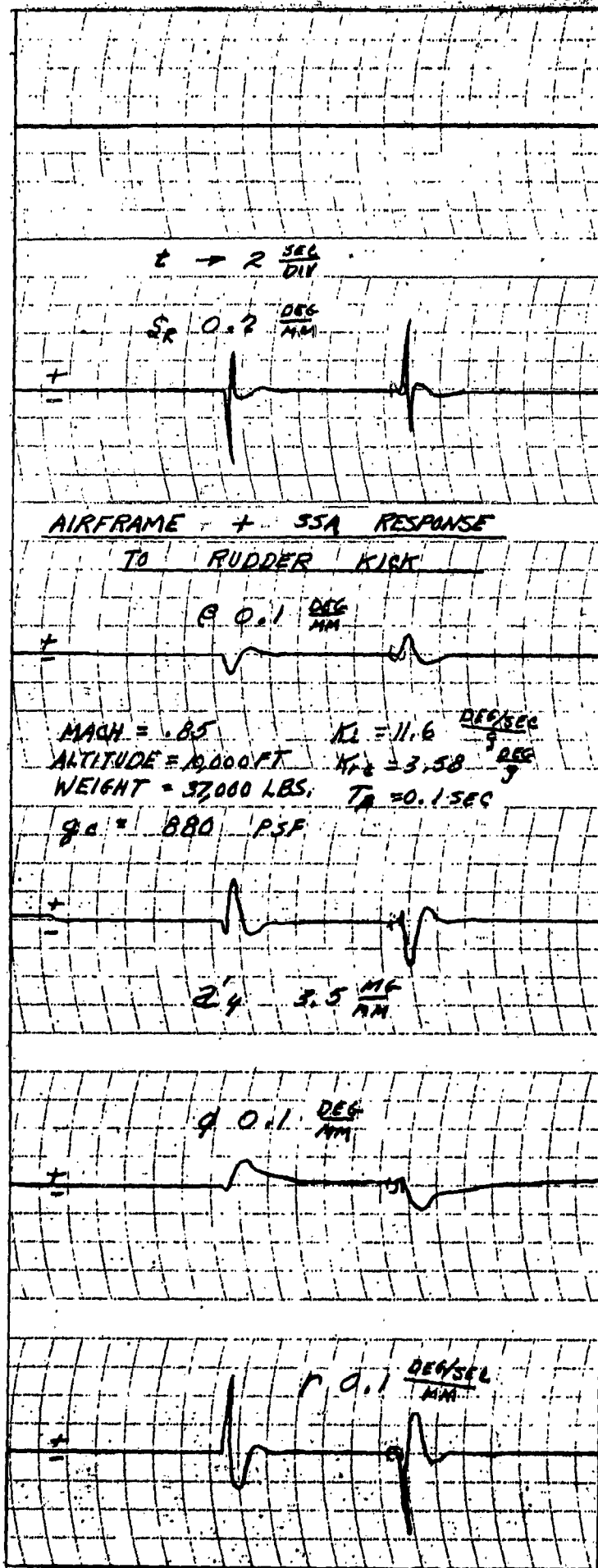


Figure III-50
Case VII

Section 3

Figure III-51
Case VII



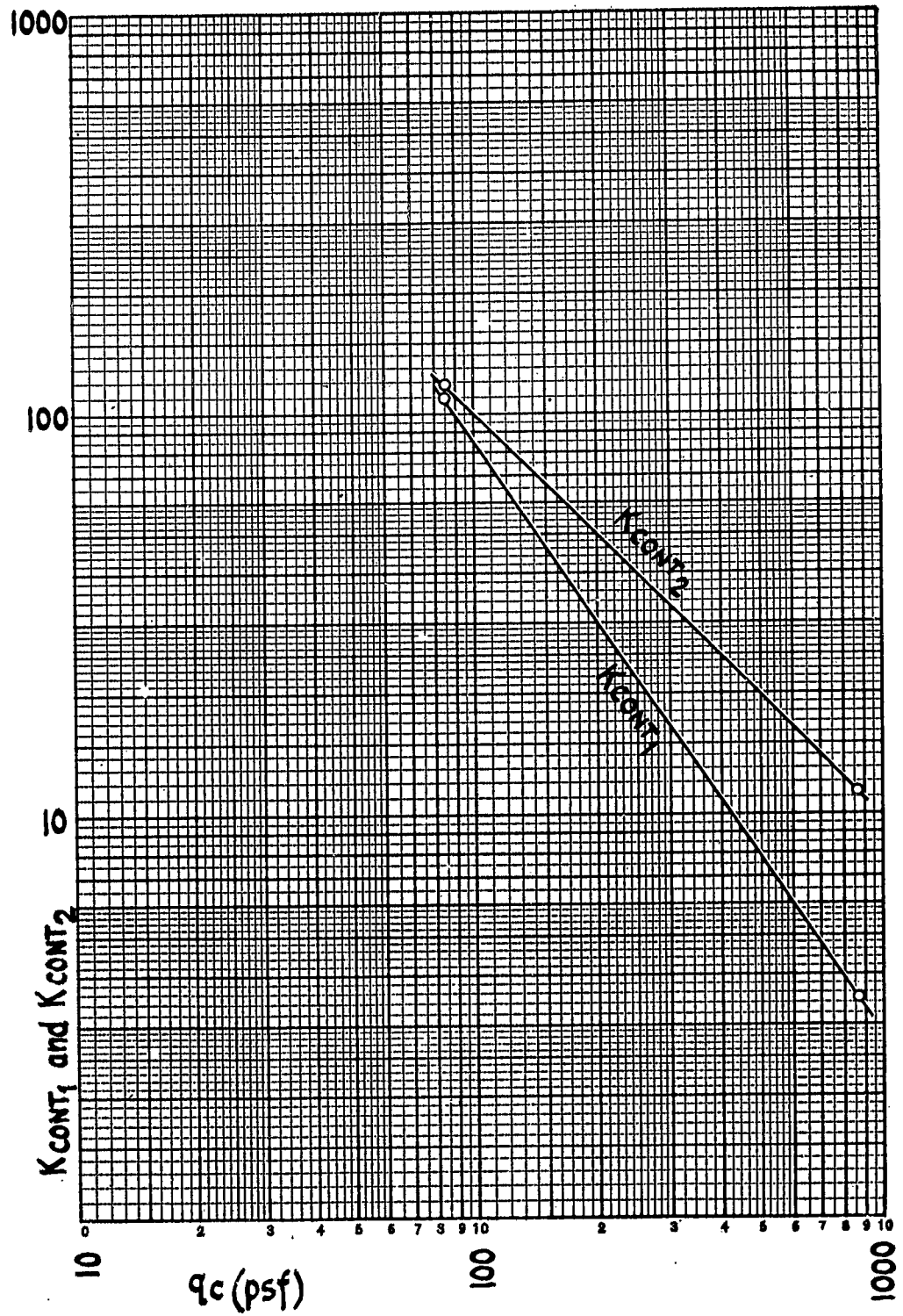


Figure III-52 Readjusted Estimate for K_{cont1} and K_{cont2}

Section 3

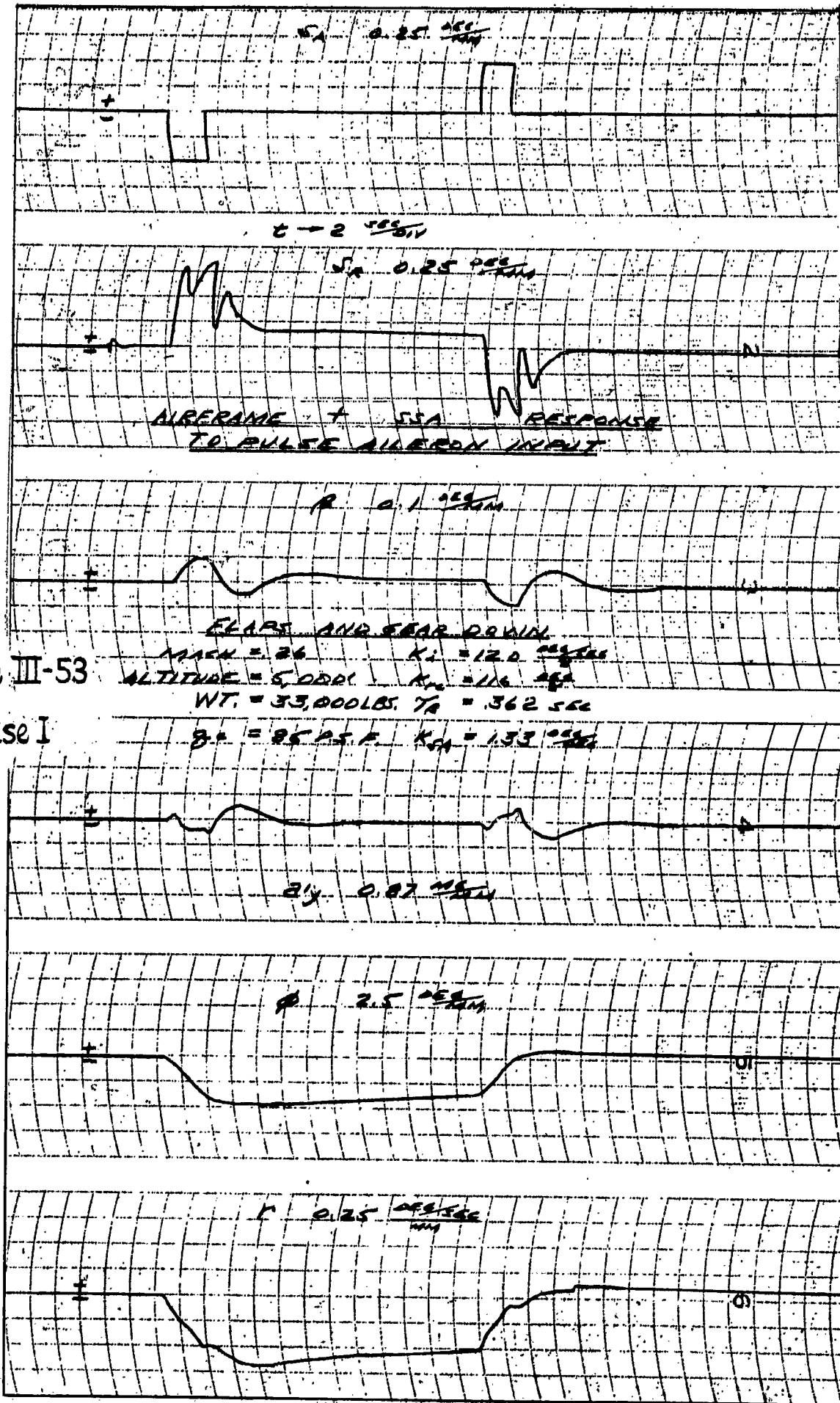


Figure III-53

Case I

$K_1 = 12.0 \frac{deg}{min}$
 $K_2 = 11.6 \frac{deg}{min}$
 $K_3 = 1.33 \frac{deg}{min}$
 $TR = 0.362 \text{ sec}$
 $WT = 33,000 \text{ lbs}$
 $ALTITUDE = 5,000 \text{ ft}$
 $TRACK = 26$

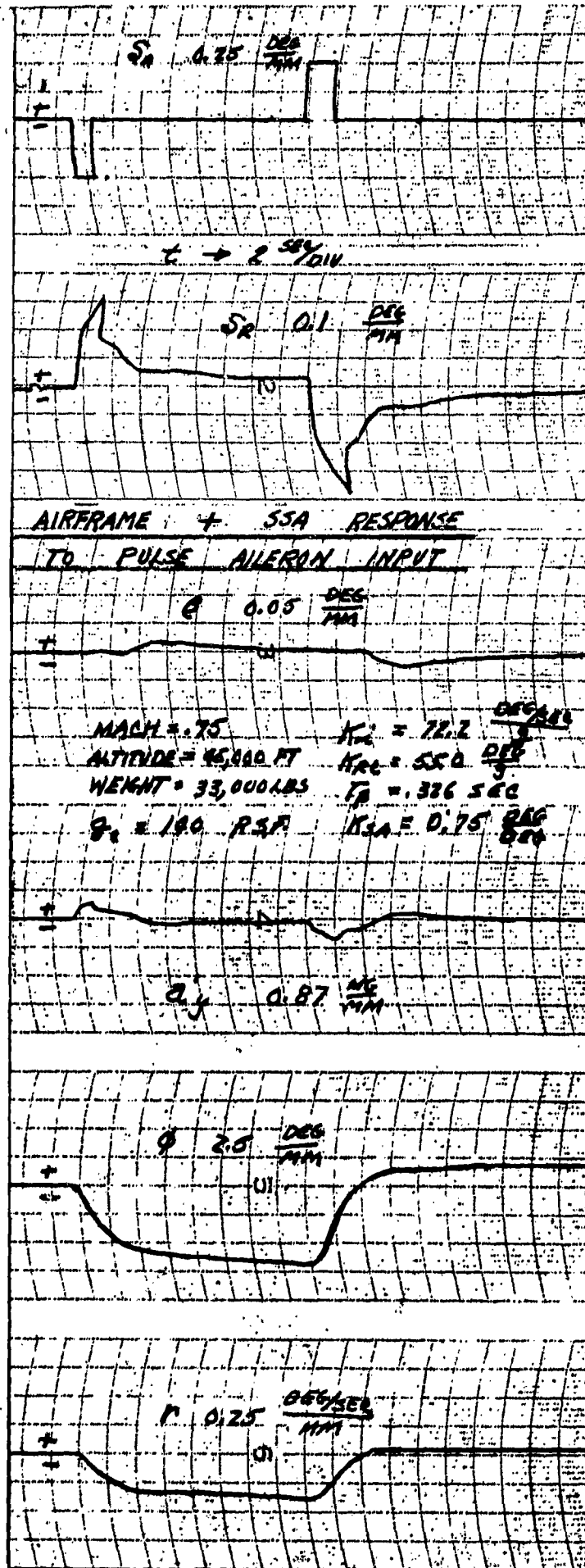


Figure III-54
Case II

Section 3

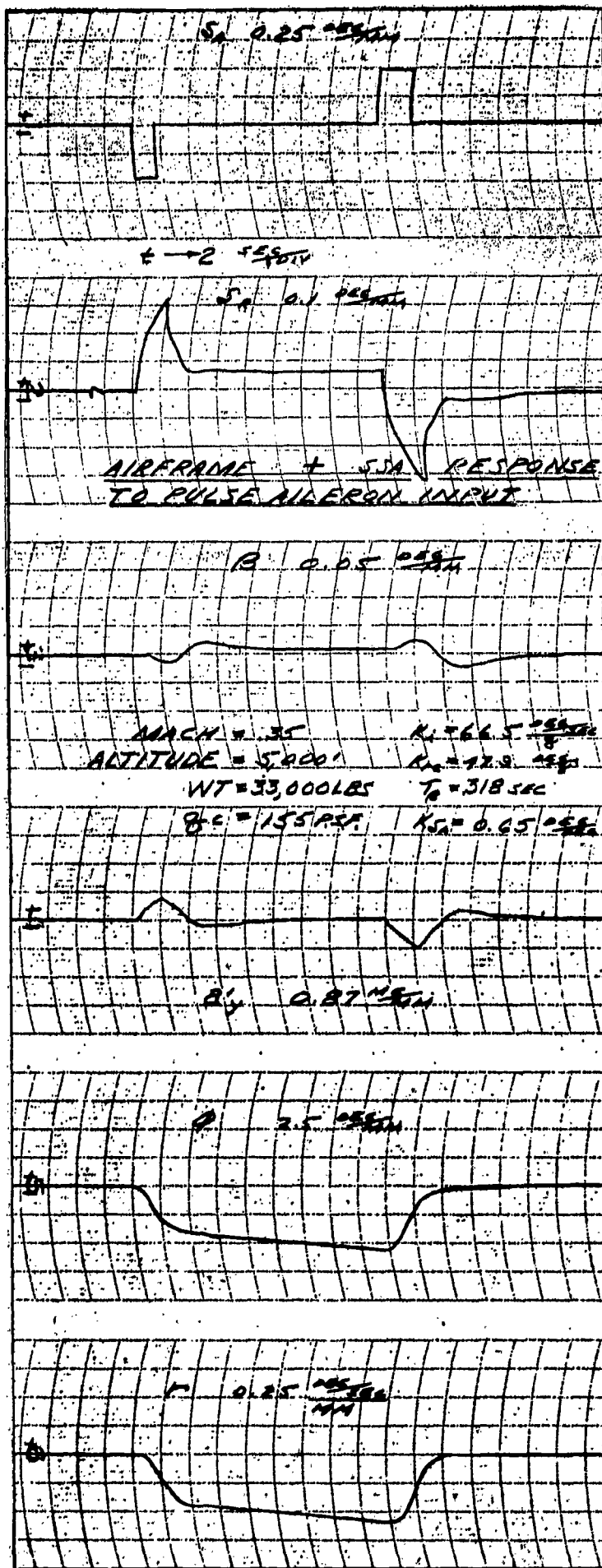


Figure III-55
Case III

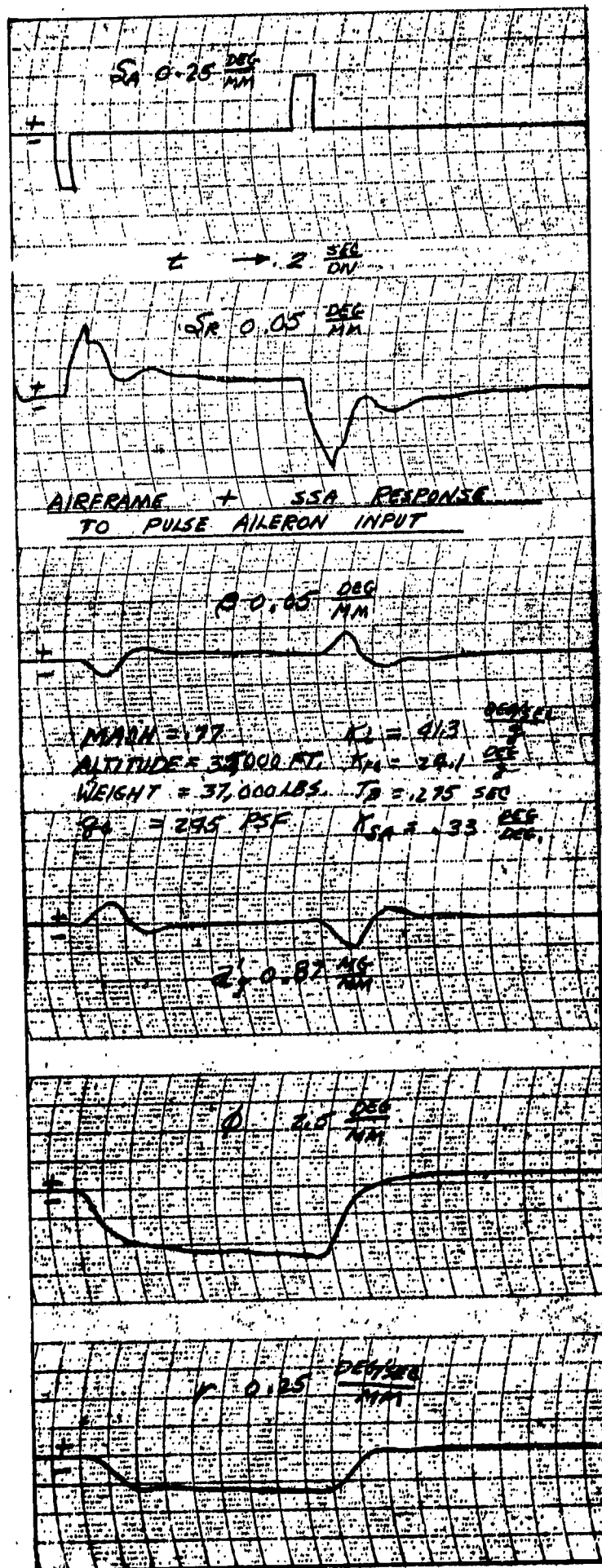
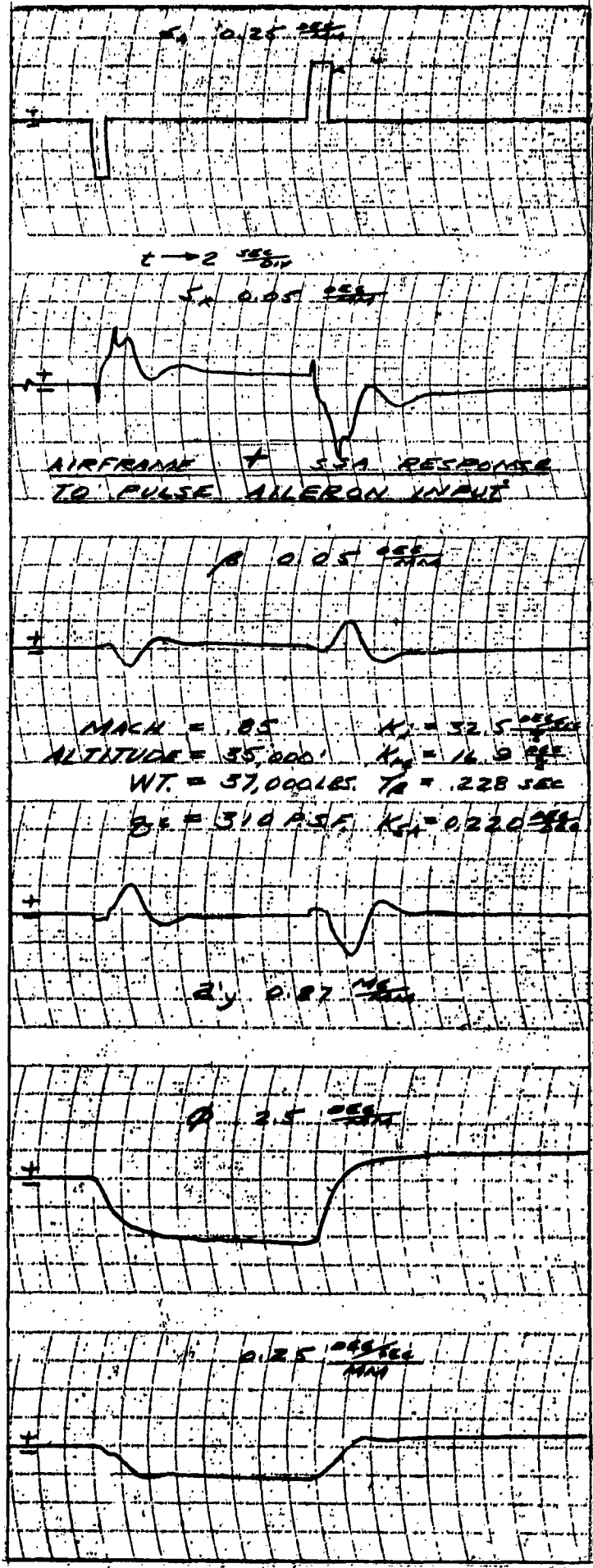


Figure III-56
Case IV

Section 3

Figure III-57
Case V



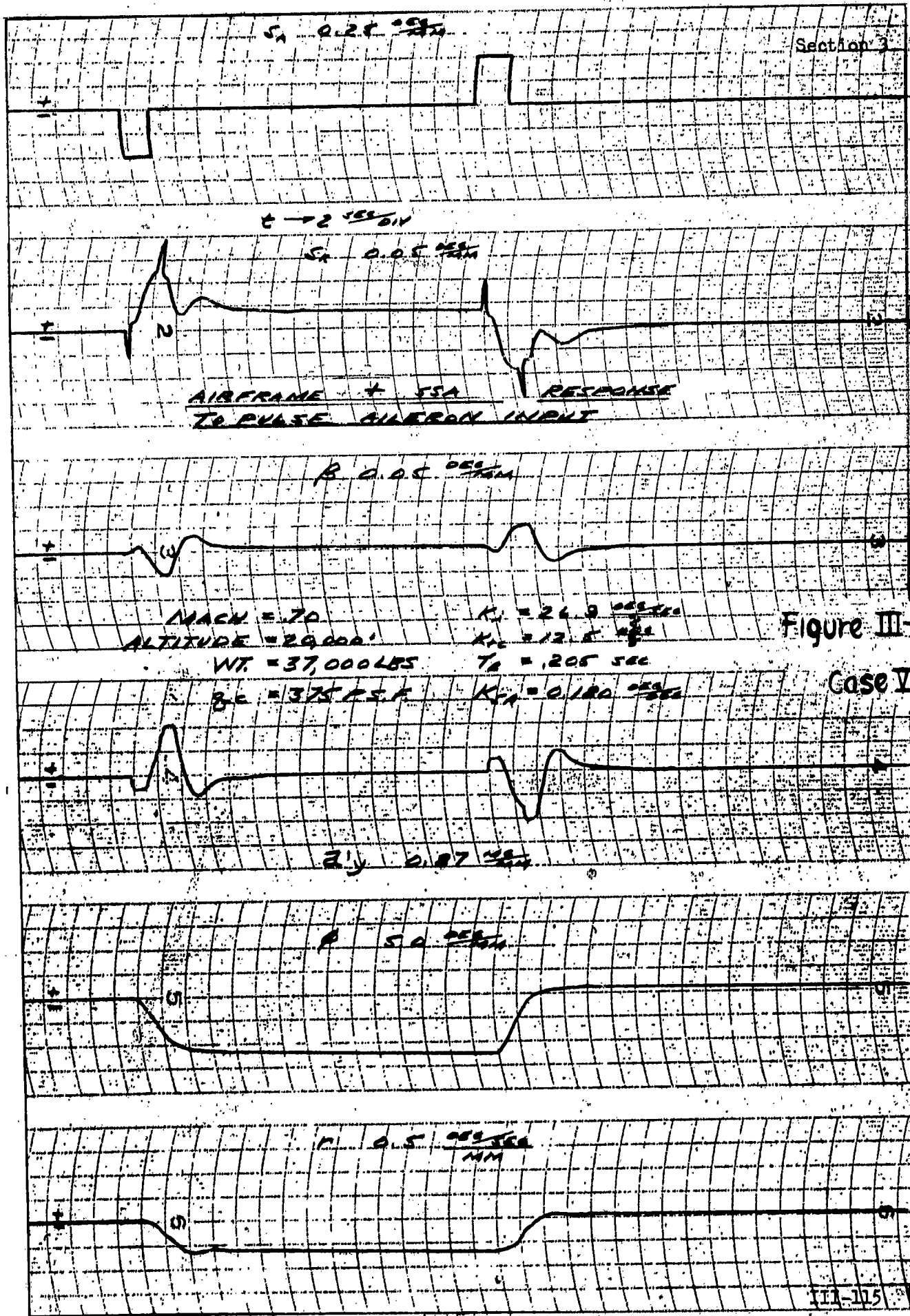


Figure III-58

Case VI

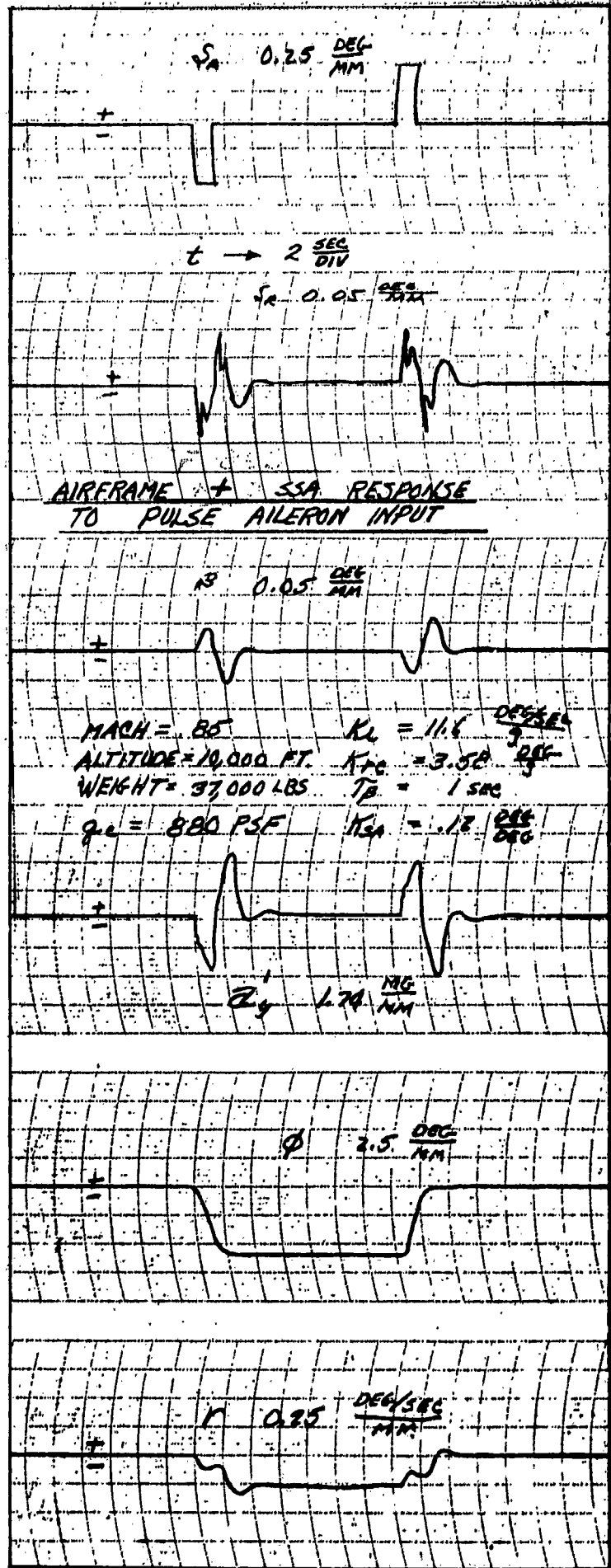


Figure III-59
Case VII

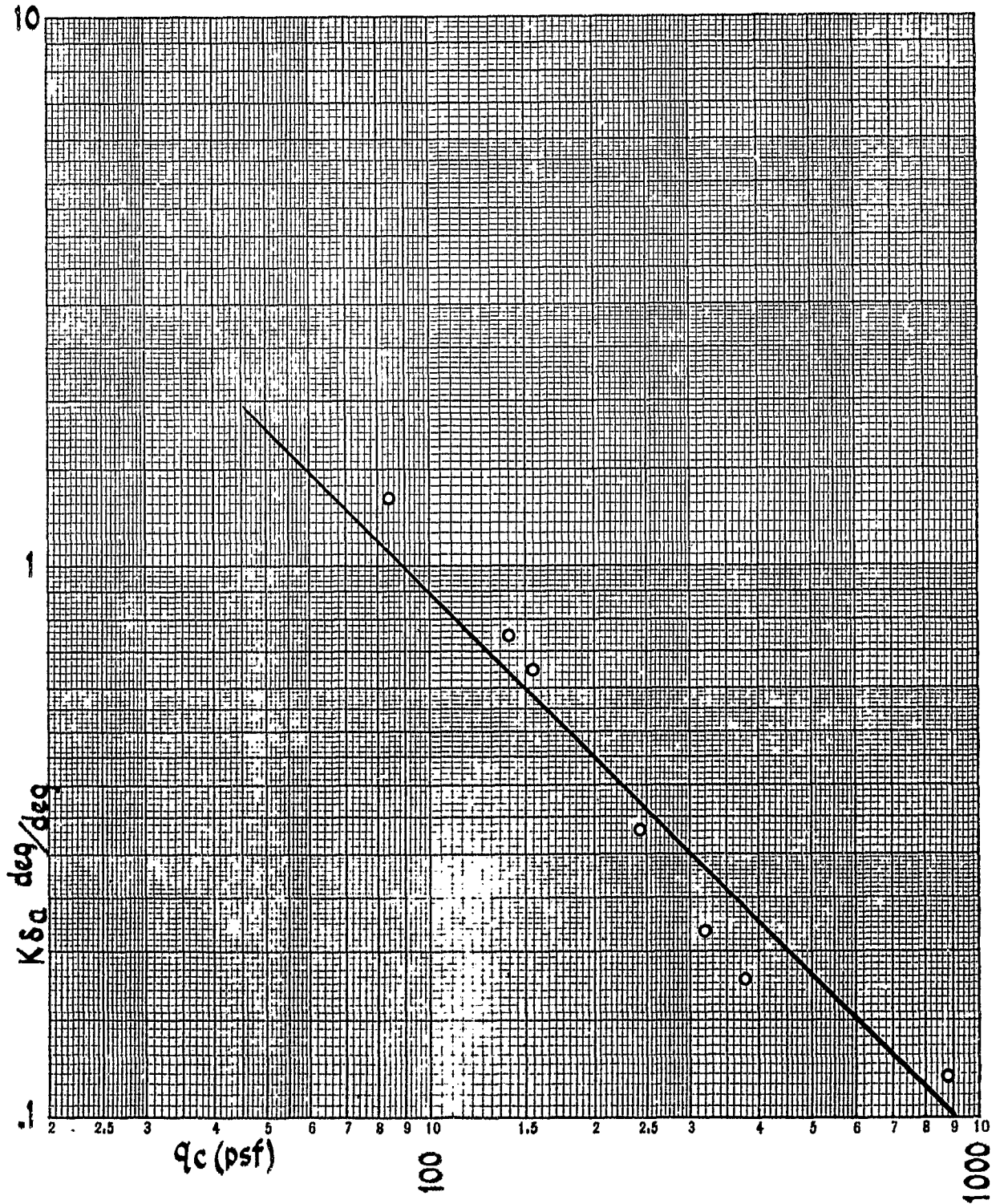


Figure III-60 Preliminary Estimates for K_{sa}

Section 3

CASE	g_c (PSF)	K_{sa} (DEG/DEG)
1	85	1.33
2	140	.75
3	155	.65
4	245	.33
5	310	.22
6	375	.18
7	880	.12

Table III-5 Preliminary Estimates for K_{sa}

The straight line approximation to the points plotted in Figure III-60 corresponds to a g^{-1} curve.

The effects of backlash on system stability were investigated by inserting various amounts of backlash between the controller actuator and the output of the rudder surface actuator. By means of these tests it was concluded that 0.04 degrees of backlash would be unnoticeable to the pilot even though a limit cycle condition exists*. Also the sideslip oscillation is well within system requirements. The computer traces for .04 degree backlash are shown for three flight conditions in Figures III-61 through III-63. Note

*The pilots' sideforce threshold has been experimentally determined to be between the limits of 2 to 20 mg. Although the 2 mg limit is exceeded slightly for one flight condition, it is a condition which exceeds the level flight speed capabilities of the airplane and therefore will seldom be used.

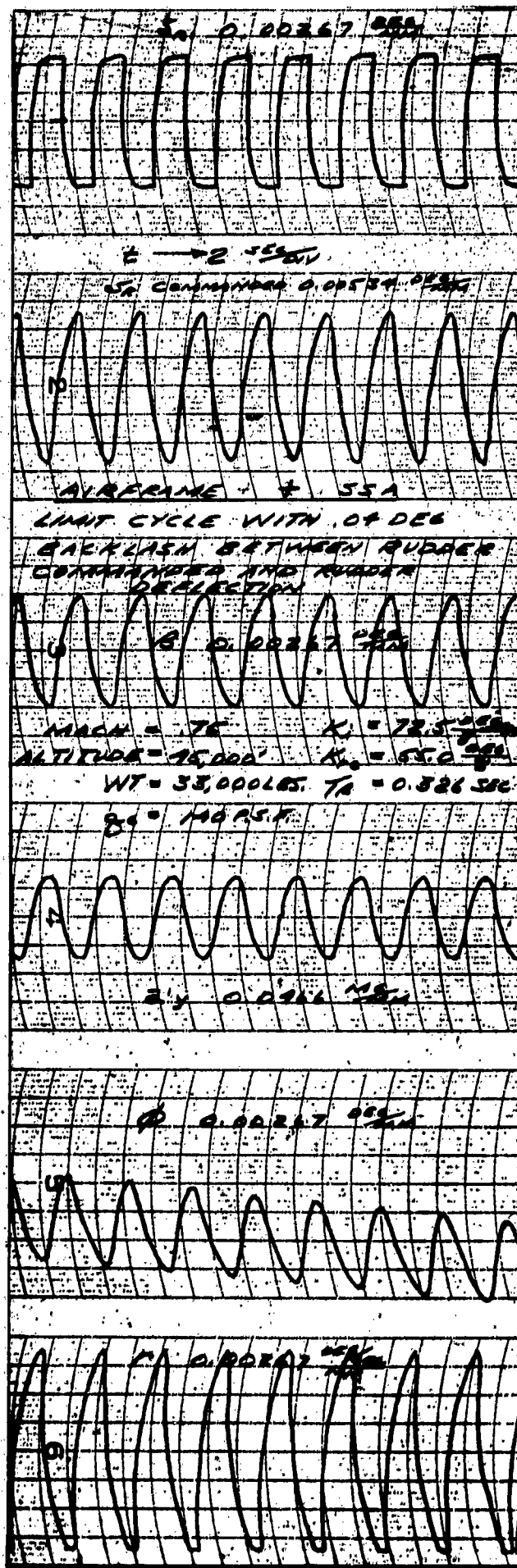
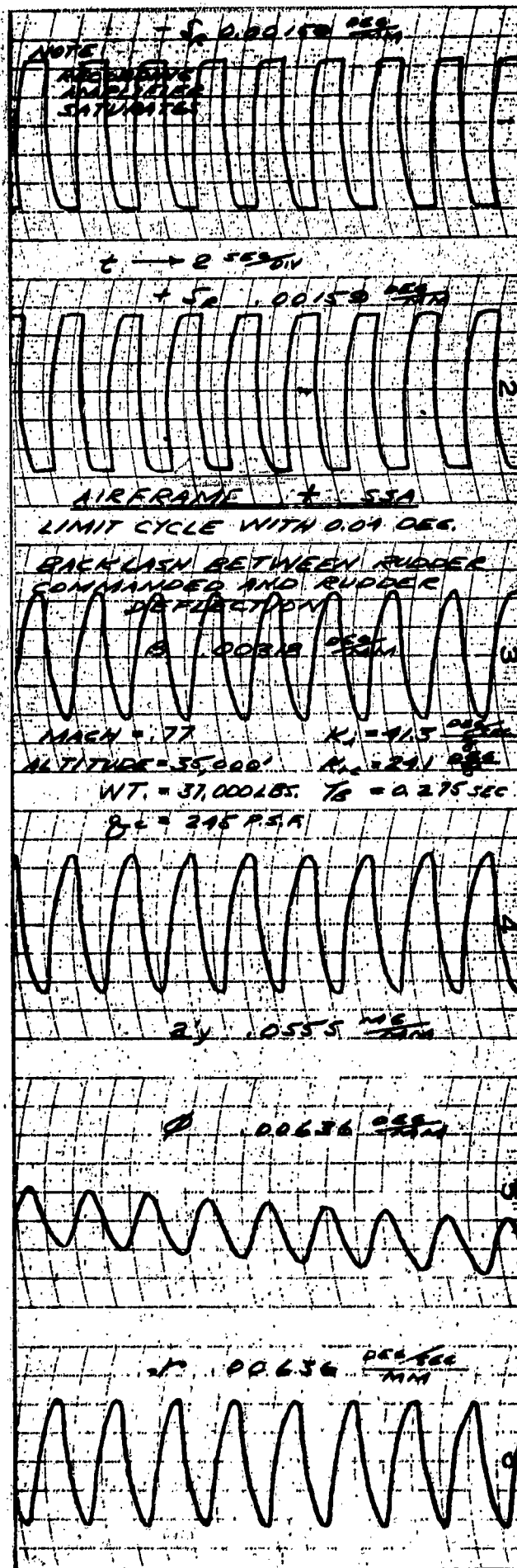


Figure III-61

Case II

Figure III-62
Case IV



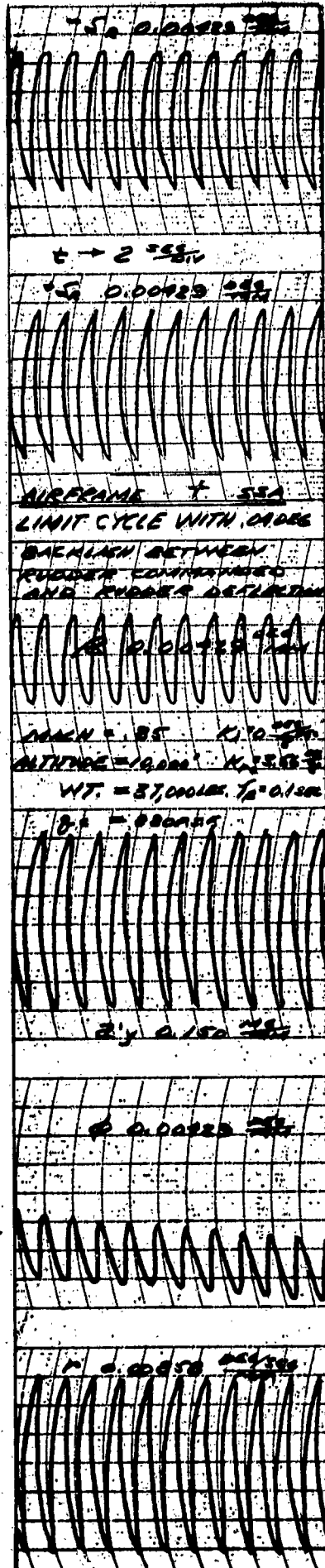


Figure III-63
Case VII

Section 3

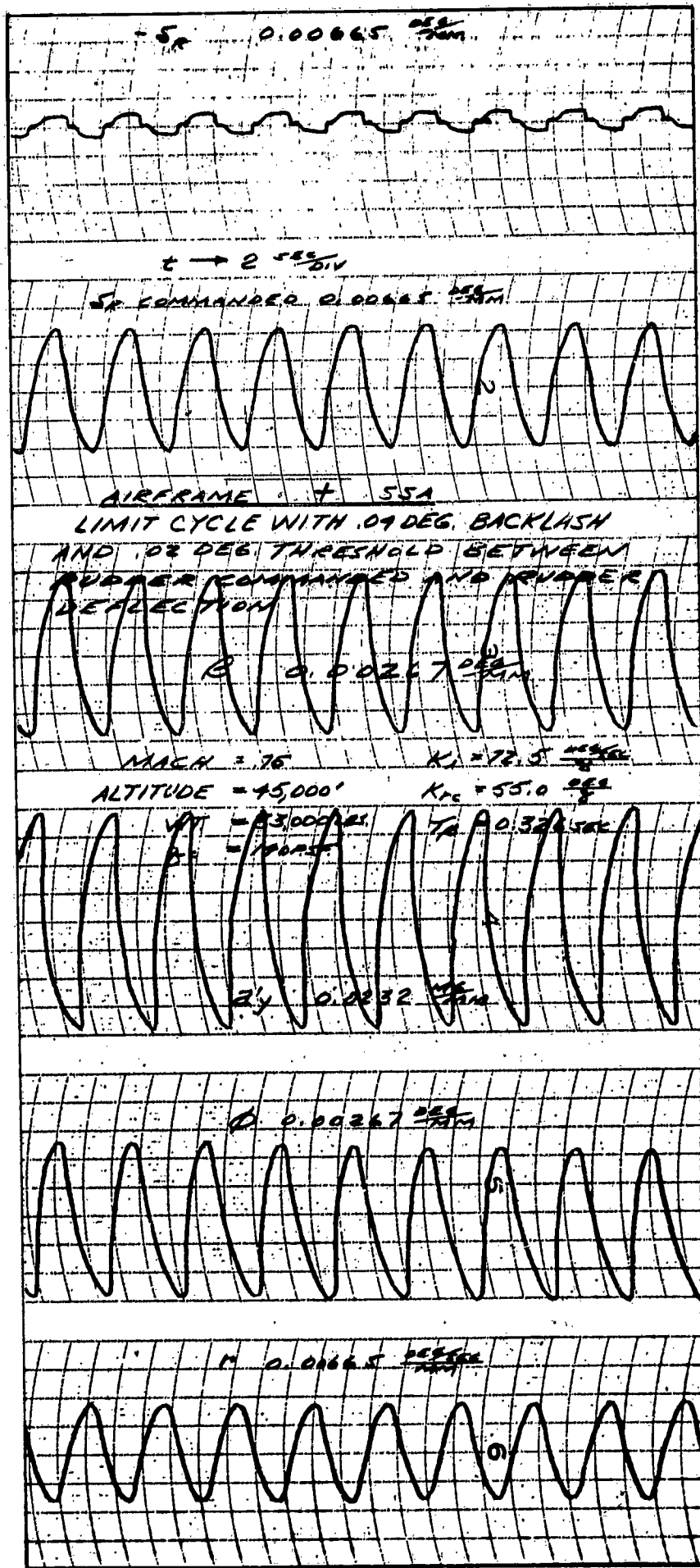


Figure III-64
Case II

that the amplification of the recording device has been increased by a factor varying from 50 to 100 over the previous figures. It will be noted that for this value of backlash $\alpha_{y \max} \approx \pm 2.2 \text{ mg}$ and $\beta \max \approx \pm .03 \text{ deg}$. Figure III-64 shows the effect of .04 degree backlash plus .02 degree threshold between the controller actuator and the surface actuator output. It will be noted that the limit cycle which exists for this condition is still well within the system requirements.

This concludes the analysis and synthesis phase. The results of the study include the system block diagram with all parameters chosen, except the gain from the pilot's trim knob to rudder deflection. The block diagram is shown in Figure III-65.

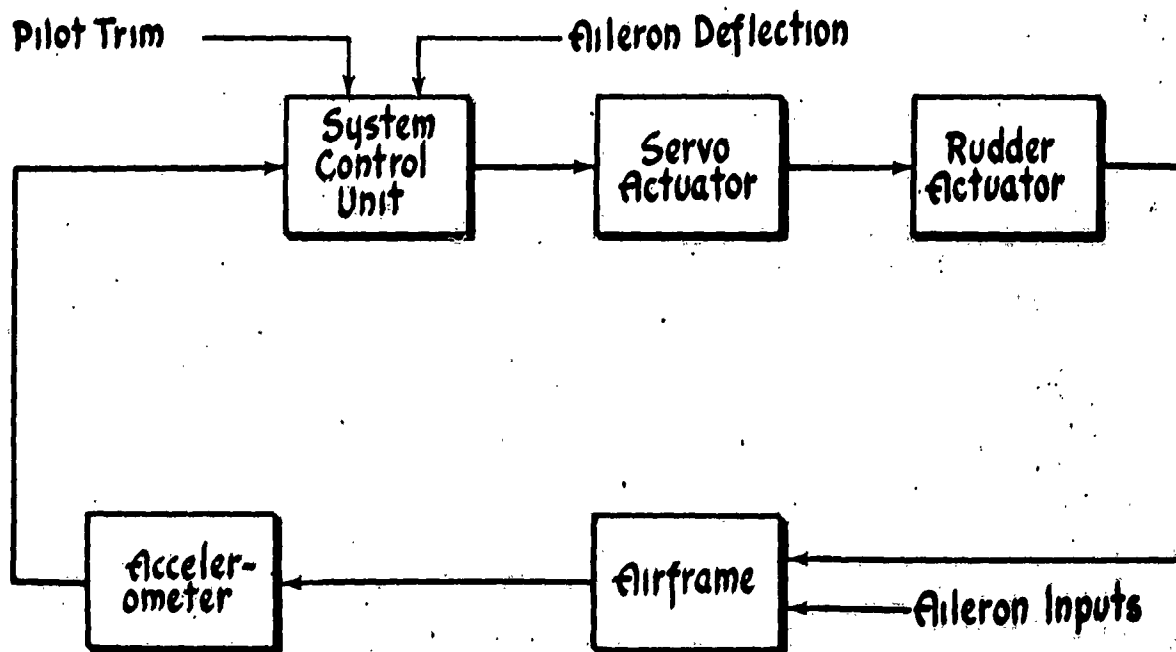


Figure III-65 Block Diagram of Sideslip Stability Augmenter

Section 3

The system control unit transfer functions as derived in the preceding discussion are given by Equations (III-21 and (III-25).

$$(III-21) \frac{\sigma_c}{a'y} = K_2 \frac{\frac{s^2}{\omega_{ne}^2} + 2 \frac{s}{\omega_{ne}} s+1}{s(T_B s+1)}$$

where T_B is given by Figure III-20,

$$(III-22) \omega_{ne} = \sqrt{\frac{K_{CONT2}}{K_{CONT1} T_A}}$$

$$(III-23) S = \frac{\omega_{ne}}{2} \left(\frac{K_{CONT1}}{K_{CONT2}} + T_B \right), \text{ AND } K_{CONT2} \text{ AND } K_{CONT1}$$

are given in Figure III-52. Also,

$$(III-24) K_2 = \frac{K_{CONT2}}{K_M K_H K_A}$$

For aileron inputs the controller transfer function is

$$(III-25) \frac{\sigma_c}{s_a} = \frac{K_3}{s+1}$$

where

$$(III-26) K_3 = \frac{K_{sa}}{K_M K_H}$$

K_{sa} is given in Figure III-60.

The transfer function for pilot trim inputs will be a constant, the gain to be selected later, but should be such as to provide full servo actuator output for approximately full trim pot rotation.

The servo actuator and accelerometer transfer function were selected previously and are given by Equations (III-10) and (III-6) respectively.

(d) SYSTEM TESTS

The remaining phases of the system design procedure which were conducted for the sideslip stability augmentser consisted of open and closed loop bench tests of the developmental model, airplane ground and flight tests of the preproduction model, and airplane ground and flight tests of the production system. The results of the above tests revealed no serious discrepancies in the system configuration which was developed in the analysis and synthesis phase.

CHAPTER IV

SYSTEMS ENGINEERING AND OTHER DESIGN CONSIDERATIONS

SECTION 1 - INTRODUCTION

The purpose of this chapter is to present a discussion of several concepts which facilitate the design of automatic flight control systems. The ideas to be considered are mostly of a non technical nature, however the degree of success of an automatic flight control system depends to a large extent on their application during the design procedure.

A discussion of systems engineering and the advantages of its application to the design of automatic flight control systems is presented in Section 2. Section 3 describes the concept of functional mechanization, while some of the problems associated with the physical installation of the equipment in the aircraft are discussed in Section 4.

SECTION 2 - SYSTEMS ENGINEERING

The present stage of aeronautical development is one in which technological advances in airframe design and similar increases in power plant capabilities are forcing equally rapid developments in allied fields. One of these fields in which rapid developments must of necessity be made is the field of the automatic control of aircraft. Automatic control systems must be integrated in a very special and exacting fashion into the over-all system. The intimate relationship between all the various subsystems, which collectively constitute the over-all system, is such that the design of each subsystem must be based on the consideration of its effects on the operational characteristics of the over-all system.

In order to cope effectively with the problems involved, the concept of systems engineering must direct the coordinated design effort necessary to produce an operationally satisfactory high performance aircraft system. Systems engineering concerns itself with establishing the general requirements for constraining the complete system (consisting of both the controlled and controlling elements or subsystems) to perform in a prescribed manner. The over-all system under consideration here is a piloted aircraft. This, of course, consists of subsystems which are alterable in varying degrees to the control systems designer. Obviously, the human pilot is the primary unalterable subsystem. In addition, as mentioned previously, the basic airframe which is to be controlled is relatively unalterable to the automatic flight control system designer. It is his task to provide control devices which, when operating in the complete system, will result in over-all system operation which meets the customer's requirements.

The procedure discussed in Chapter III, Section 2 is based on the concept of systems engineering. It will be recalled that the procedure begins with the determination of the over-all system requirements. Based on the over-all system requirements, subsystem requirements are derived, and then by means of analysis and synthesis procedures, requirements are established for the individual components which go to make up the subsystems. At the completion of this process, the systems engineer gives consideration to the best method for obtaining components which meet his derived requirements. Existing components are used where no intolerable deterioration in system performance results,

and new components are designed when necessary. This procedure results in the complete integration of all the systems and components involved, thus preventing duplication of equipment. In addition, since by the very nature of his task the systems engineer establishes the requirements for the individual components, he chooses or designs components which will provide optimum system operation, while simultaneously ensuring that the components used are no better than they need to be.

The application of the techniques of systems engineering to the design of automatic flight control systems for piloted aircraft is in its infancy. However, it is mandatory that its application be expanded if future requirements for high performance aircraft are to be met. Systems engineering has been somewhat retarded in the past due to the reluctance of the veteran aircraft controls designer to place full confidence in automatic flight control systems. This reluctance is somewhat understandable, since the controls designer had been using the same techniques successfully for years on airplanes of lesser performance, and in addition, the systems man is treading on what had been the sacred domain of the controls designer. However, future successful designs will result only from the application of systems engineering which requires close coordination between the designers of all the subsystems which go to make up the piloted aircraft.

SECTION 3 - FUNCTIONAL MECHANIZATION

One of the problems which remain after the automatic controls designer has completed his analysis and synthesis is that of obtaining reliable

components to meet his derived requirements. Experience has shown that when newly designed components are used, a large part of the total design time is often spent in debugging these components. This is an expensive and time consuming procedure which makes it very difficult to obtain reliable systems in time to meet the production schedule for new airplanes. In fact, it is not unusual to find the automatic controls designer still attempting to qualify his system after a large portion of the production contract has been delivered to the customer. The problem is becoming more and more acute because the rapid obsolescence of new airplane designs is forcing airframe manufacturers to produce initial flight articles with less and less delay between receipt of a contract and the first flight. The configuration of these new airplanes are such that some means of control in addition to pilot control is mandatory to obtain satisfactory performance. In fact, the trend is toward the use of more automatic control equipment.

At the present time each airframe manufacturer must independently undertake the design of the necessary control equipment for his aircraft. Since new airframe dynamic characteristics are markedly different from those of existing aircraft, the new control system requirements and resulting configuration are also different from existing control systems. As a consequence the procuring agency must assume the development costs of a new flight controller for each airframe model. Even then it is nearly impossible to complete a new development flight controller in time to match the production schedule of a new airplane. Thus the procuring agencies are burdened with great expense and still do not achieve the desired results.

The use of the concept of functional mechanization greatly facilitates the solution of the problem discussed above. As the name implies, functional mechanization is a mechanization according to the function to be performed rather than a grouping of components based solely on physical considerations. The components are unfunctional and are grouped according to the over-all system performance requirements. Each functional sub-assembly such as an amplifier, modulator, matching circuit or power supply is designed as a plug in type unit. Each one of these units undergoes a continual developmental process so that the most current research advances are always reflected in qualified, ready to use components. The components are designed so as to provide the basis for a unified, integrated control system. The procedure operates most efficiently if a limited number of fully developed components are stocked as shelf items. To physically mechanize a controller for a new system, the systems designer needs only to select the proper plug in units, make the necessary couplings and interconnections, and install the complete system for prototype tests. This procedure provides reliable, qualified units at a minimum cost of time and money.

SECTION 4 - OTHER DESIGN CONSIDERATIONS

Although a limited amount of the discussion presented to this point has dealt with physical considerations of the system and components of automatic flight control systems, the bulk of the material has been concerned with methods of obtaining a system which performs in accordance with the detailed requirements. Little consideration has been given to the effects of such factors as the following:

1. The requirements dealing with the physical installation of the equipment in the aircraft
2. The environmental conditions to which the equipment will be subjected
3. Reliability requirements
4. Operation and maintenance requirements

Although their solutions may seem obvious, experience has shown these problems to be more troublesome to the average flight controls designer than the problems associated with analysis and synthesis. It is believed that these problems cause trouble primarily because they are neglected. For this reason the following discussion does not attempt to give detailed solutions to the problems, but only points out their existence.

The requirements dealing with the physical installation of the equipment in the aircraft originate from considerations of the following:

1. Space availability
2. Access provisions
3. Effect of component installations on airframe center of gravity
4. Local environments

Space availability considerations are quite obvious except for those cases where it is important that a component such as an actuator or an accelerometer must be located at a specific point in the aircraft. In this case it behooves one to survey the area of interest at a sufficiently early date to ensure the required space will be available.

Access provisions should be adequate to allow the system to be easily adjusted when installed in the aircraft and to permit removal of components for maintenance.

The characteristics of the local environment at various points in the airframe should be surveyed very carefully before choosing locations for component installations. Conditions of special importance are those due to vibration, temperature, mechanical shock and acceleration. For example, the operation of a motor or a pump may cause severe vibrations in a localized area which would damage certain of the components if they were mounted nearby. Such a condition would require that the component be shock mounted or moved to a more favorable location.

As mentioned previously the military services require that aeronautical equipment be capable of satisfactory operation while being subjected or after being subjected to certain environmental conditions. These requirements are intended to ensure that the equipment will operate satisfactorily under any environmental condition which is likely to be encountered. Conditions for which specific requirements exist are operation while being subjected to high and low temperatures, high humidity, high altitude, vibration and acceleration. In addition, storing the equipment in the presence of fungus or salt spray should not cause damage. Uniform test procedures for establishing that the above requirements are met are given in Reference 19. Components which have passed the tests of Reference 19 in a manner acceptable to the customer are called "qualified" components.

Reliability considerations take on two aspects; first the equipment should be designed to operate satisfactorily without overhaul for a reasonable period of time and second, when the system fails it should "fail safe". A reasonable period of time has been defined as 1000 hours for parts not containing vacuum tubes and 500 hours for vacuum tube replacement. Fail safety considerations require that malfunctions will not make the airplane uncontrollable or cause maneuvers so violent that the airplane suffers structural damage. Malfunctions normally considered in this study are primarily electrical failures such as tubes, open or short circuit or sticking relays, however hydraulic failures such as valve jamming etc., should be considered when applicable.

The problems which arise due to the fact that the equipment will be operated and maintained by personnel not familiar with automatic control theory are often neglected. It is extremely important that automatic flight control systems be designed in a manner conducive to the application of simplified trouble shooting techniques. It is sometimes helpful to include integral trouble shooting circuits in the design of the components. If these are not used, it will probably be mandatory that special test equipment be designed for use in maintaining the system. It has also been found helpful for the system designers to accompany the first few production models into the field for the purpose of indoctrinating military personnel in system operation and maintenance.

Some automatic flight control systems have been considered as unsatisfactory because of neglect of the above problems, even though when operating normally, the systems left little to be desired. Combinations of several of the above problems can be especially troublesome. An example of such a combination occurred for a system in which one component was mounted on a bulkhead beside an air compressor which generated vibrations in excess of the amplitudes for which the automatic flight control equipment was designed. The high level vibration caused rapid deterioration of the potentiometers in the flight control component and this, coupled with the fact that the system was difficult to trouble shoot resulted in the system being inoperative in a large percentage of the airplanes which had been delivered to the customer. The solution to such a problem is, of course, obvious once all the contributing factors have been established. In this particular example, however, several months of intensive investigation were required to determine the factors which caused the problem.

BIBLIOGRAPHY

1. Draper, C. S., "The Control of Flight, Automation in the Air," Engineering, May 27, 1955.
2. Bassett, Preston R., "Instruments and the Control of Flight," Aeronautical Engineering Review, December 1953.
3. Beard, M. Gould, and Percy Halpert, "Automatic Flight Control in Air Transportation," Aeronautical Engineering Review, May 1955.
4. Johnson, Lt. R. L., "Automatic Pilots, Past, Present, and Future," Instruments Branch, Bureau of Aeronautics, BuAer Report (unnumbered), c. 1945.
5. Anast, Capt. James L., USAF, "Automatic Flight Control," Aeronautical Engineering Review, May 1952.
6. Klemen, Alexander; Perry A. Pepper; and Howard A. Wittner, "Longitudinal Stability in Relation to the Use of an Automatic Pilot," NACA Technical Note, TN 666, 1938.
7. Bassett, Preston R., "Development and Principles of the Gyropilot," Instruments, September 1936.
8. Methods of Analysis and Synthesis of Piloted Aircraft Flight Control Systems, prepared by Northrop Aircraft Inc, BuAer Report AE-61-4I, Bureau of Aeronautics, Navy Department, 1952.
9. Dynamics of the Airframe, prepared by Northrop Aircraft Inc., BuAer Report AE-61-4II, Bureau of Aeronautics, Navy Department, 1952.
10. The Human Pilot, prepared by Northrop Aircraft Inc., BuAer Report AE-61-4III, Bureau of Aeronautics, Navy Department, 1954.
11. The Hydraulic System, prepared by Northrop Aircraft Inc., BuAer Report AE-61-4IV, Bureau of Aeronautics, Navy Department, 1953.
12. The Artificial Feel System, prepared by Northrop Aircraft Inc., BuAer Report AE-61-4V, Bureau of Aeronautics, Navy Department, 1953.

13. Handbook Operating and Service Instructions, "Type J-2 Slaved Gyro Magnetic Compass System," U. S. Air Force Technical Order T.O. No. 5 N1-2-4-1, November 1, 1954.
14. Ahrent, William R., "Servomechanisms Practice," McGraw-Hill Book Co., Inc. New York, 1954.
15. "Flying Qualities of Piloted Aircraft," Military Specification MIL-F-8785 (ASG), September 1, 1954.
16. Dawson, John W., Harris, Lawson P., and Swean, Edward A., "Dynamic Response of Two Aircraft-Autopilot System to Horizontal Turn Commands" DACL Report No. 94, Massachusetts Institute of Technology, January 31, 1955.
17. Truxal, John G., "Automatic Feedback Control System Synthesis," McGraw-Hill Book Co., New York, 1955.
18. "Control Systems, Automatic Flight, Aircraft, General Specification for," Military Specification MIL-C-5900 (USAF) March 25, 1955.
19. "Environmental Testing, Aeronautical and Associated Equipment, General Specification for," Military Specification MIL-E-5272A, July 15, 1955.
20. "Specification for Flying Qualities of Piloted Airplanes," Bureau of Aeronautics Specification NAVAER SR-119B, June 1, 1948.
21. "Flying Qualities of Piloted Airplanes," U. S. Air Force Specification No. 1815B, June 1, 1948.
22. Davidson, Martin ed., "The Gyroscope and its Applications," London, Hutchinsons Scientific and Technical Publications (1946).
23. Diemel, R. T., "Mechanics of the Gyroscope," N. Y. The MacMillan Co., (1929).
24. Terry, E. S., "Applied Gyrodynamics," N. Y. John Wiley and Sons, Inc., (1932, 1933).
25. Rowlings, A. L., "The Theory of the Gyroscopic Compass and its Deviations," Ed 2, N. Y. The MacMillan Co., 1944.
26. Weems, William R., "An Introduction to the Study of Gyroscopic Instruments," Department of Aeronautical Engineering Instrumentation Section, Massachusetts Institute of Technology, Cambridge, Mass., January 1948.

27. Roberts, T. R., "Geometrical Cross-Coupling in Rate and Displacement Gyros," Minneapolis-Honeywell Regulator Company Report, AR 2426-R2, March 1951.
28. Becker, Leonard, "Gyro Pickoff Indications at Arbitrary Plane Attitudes," Journal of the Aeronautical Sciences, Vol 18, November 1951.
29. McRuer, D. T. and Askenas, I. L., "Vertical Gyro Relationships," Control Specialists Inc., Inglewood, California, Memo Report No. 5., July 23, 1954.

APPENDIX
EQUATIONS OF THE GYROSCOPE

The development which follows is divided into four sections. The first section presents the derivation of the law of the gyro element. The last three sections develop the equations for gyro pickoff indications, including the effects of geometrical cross coupling for the rate, vertical and directional gyros.

(a) LAW OF THE GYRO ELEMENT

This development has been made somewhat non-rigorous in the belief that the average flight controls engineer is more interested in what the gyro measures than he is in a rigorous explanation of gyro behavior. The reader interested in a rigorous derivation of the law is referred to Reference 26.

Newton's second law states that an applied force acting on a particle will produce a rate of change of linear momentum which is equal to the applied force. In equation form

$$(A-1) \quad F_{app} = \frac{d(mv)}{dt}$$

For a rigid body m is a constant, so

$$(A-2) \quad F_{app} = m \frac{dv}{dt} = ma$$

where the acceleration is referred to inertial space. Although as stated, Newton's second law applies only for a particle, the law also applies for a rigid body, if the force is applied at the center of gravity.

When modified to apply for rotation of a rigid body, Newton's second law states that the torque applied about the center of gravity of a rigid body will produce a rate of change of angular momentum which is equal to the applied torque. Then

$$(A-3) \quad T = \frac{dH}{dt}$$

where

$$(A-4) \quad H = I\omega$$

Since I is constant for a rigid body, Equation (A-3) can be written as

$$(A-5) \quad T = I \frac{d\omega}{dt}$$

It is impractical to proceed further without specifying the axes about which the torque is applied and about which I , ω , and H are measured. This is most easily accomplished by introducing some elementary forms of vector notation.* Referring to Figure A-1, the unit vector i_{ω_s} is

*The reader unfamiliar with elementary vector manipulation is referred to Reference 26.

defined as having the varying direction of the gyro spin axis, but the constant magnitude of unity.* The unit vector $\bar{I}_{\perp \omega_s}$ is perpendicular to \bar{I}_{ω_s} and in the plane defined by \bar{I}_{ω_s} and the torque vector. It will be convenient to utilize the derivative of the unit vector. This is illustrated in Figure A-2, where the notation $\bar{I}(t)$ denotes the position of \bar{I} at time t and $\bar{I}(t+dt)$ the position at time $t+dt$. Since the magnitude of the unit vector is unity, the relationship between $d\bar{I}$ and $d\theta$ can be expressed as:

$$(A-6) \quad d\theta = |d\bar{I}|$$

and

$$(A-7) \quad \frac{d\theta}{dt} = \left| \frac{d\bar{I}}{dt} \right|$$

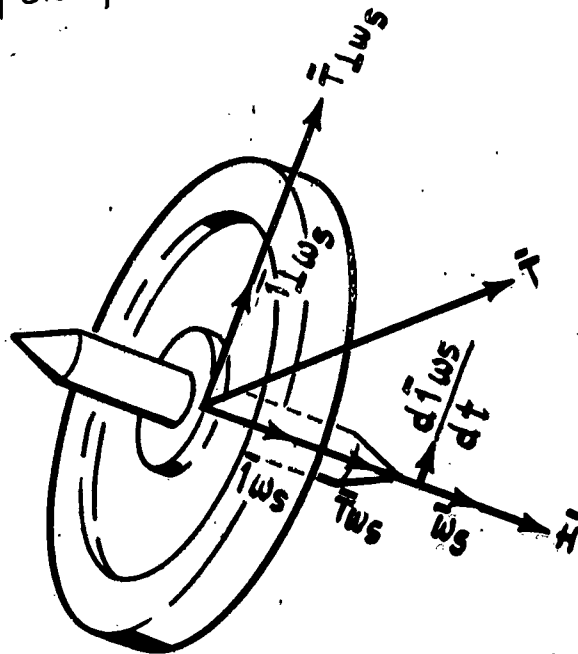


Figure A-1 Vector Notation for Gyro Element

*Vector quantities are indicated by placing a bar over the appropriate symbol.

Thus the magnitude of the time derivative of the unit vector equals its rate of turning, or its angular velocity. The direction of the derivative is the direction in which the tip of the unit vector moves. In vector notation the angular velocity is given by the vector cross product

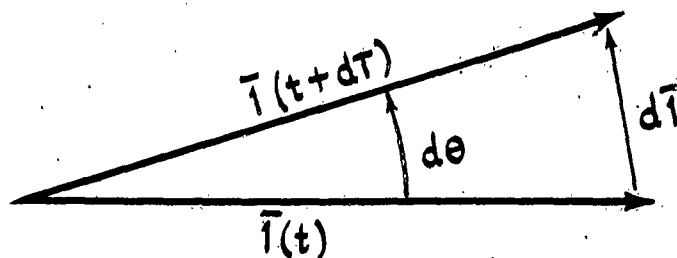


Figure A-2 Derivative of a Unit Vector

$$(A-8) \quad \frac{d\bar{e}}{dt} = \bar{I}\omega_s \times \frac{d\bar{I}\omega_s}{dt}$$

Since for a practical gyro, the rotor is spinning so rapidly about its spin axis that its angular momentum about any other axis is negligible, the gyro angular momentum can be expressed by

$$(A-9) \quad \bar{H} = I_s \bar{\omega}_s$$

where I_s is measured about the spin axis. In terms of the unit vector notation, Equation (A-9) can be written as

$$(A-10) \quad \bar{H} = I_s \omega_s \bar{I}\omega_s$$

Substituting Equation (A-10) into (A-3) results in

$$(A-11) \quad \bar{T} = I_S \frac{d}{dt} (\omega_S \bar{I}_{\omega_S})$$

The rate of change of the spin vector $\omega_S \bar{I}_{\omega_S}$ can be resolved into components as follows

$$(A-12) \quad \frac{d}{dt} (\omega_S \bar{I}_{\omega_S}) = \frac{d\omega_S}{dt} \bar{I}_{\omega_S} + \omega_S \frac{d\bar{I}_{\omega_S}}{dt}$$

Also the torque vector can be resolved into components along axes parallel and perpendicular to \bar{I}_{ω_S} . Then

$$(A-13) \quad \bar{T} = T_{\omega_S} \bar{I}_{\omega_S} + T_{\perp\omega_S} \bar{I}_{\perp\omega_S}$$

Where the subscript $\perp\omega_S$ means "perpendicular to ω_S ". Substituting Equations (A-12) and (A-13) into Equation (A-11) gives

$$(A-14) \quad T_{\omega_S} \bar{I}_{\omega_S} + T_{\perp\omega_S} \bar{I}_{\perp\omega_S} = I_S \left[\frac{d\omega_S}{dt} \bar{I}_{\omega_S} + \omega_S \frac{d\bar{I}_{\omega_S}}{dt} \right]$$

Since it was shown above that the direction of the time rate of change of a unit vector is perpendicular to the unit vector, then $\frac{d\bar{I}_{\omega_s}}{dt}$ can have no component along \bar{I}_{ω_s} . Therefore, Equation (A-14) can be written as two equations as shown by Equations (A-15) and (A-16).

$$(A-15) \quad T_{\omega_s} \bar{I}_{\omega_s} = I_s \frac{d\omega_s}{dt} \bar{I}_{\omega_s}$$

$$(A-16) \quad T_{\perp\omega_s} \bar{I}_{\perp\omega_s} = I_s \omega_s \frac{d\bar{I}_{\omega_s}}{dt}$$

For a flight control application ω_s is so large (greater than 20,000 rpm) that any change due to torque input is negligible. Then Equation (A-15) can be neglected. Equation (A-16) gives the response of the gyro element to a torque applied about an axis perpendicular to the spin vector. It is seen that the response consists of a rotation of the spin vector in a direction such that the tip of the spin vector moves parallel to the torque vector. This rotation is called precession. By Equation (A-8), the rate of precession, $\bar{\omega}_p$, is given by

$$(A-17) \quad \bar{\omega}_p = \bar{I}_{\omega_s} \times \frac{d\bar{I}_{\omega_s}}{dt}$$

Equation (A-17) shows the direction of the $\bar{\omega}_p$ vector to be perpendicular to the plane containing the spin vector and the $\frac{d\bar{I}\omega_s}{dt}$ vector (and therefore the torque vector) with its positive sense determined from the right hand rule by rotating $\bar{I}\omega_s$ into $\frac{d\bar{I}\omega_s}{dt}$.

The inverse of this equation is

$$(A-18) \quad \frac{d\bar{I}\omega_s}{dt} = \bar{\omega}_p \times \bar{I}\omega_s$$

Substituting Equation (A-18) into (A-16) gives

$$(A-19) \quad T_{I\omega_s} \bar{I}_{I\omega_s} = I_s \omega_s (\bar{\omega}_p \times \bar{I}\omega_s)$$

By utilizing Equation (A-9), Equation (A-19) can be written as

$$(A-20) \quad T_{I\omega_s} \bar{I}_{I\omega_s} = \bar{\omega}_p \times \bar{H}$$

In scalar form Equation (A-20) can be written as

$$(A-21) \quad T_{I\omega_s} = \omega_p H$$

with the qualification that ω_s , ω_p , and H are positive in the directions given by Equations (A-9), (A-17), and (A-20). It should be noted that the law of the gyro element is reversible, in that either the precession velocity or the torque may be considered as input or as output.

(b) RATE GYRO INDICATIONS

As discussed in Chapter II, Section 5, the rate gyro has only one degree of freedom. Its input is considered to be precessional velocity, the output being torque which is restrained by some means such as a spring. Rate gyro indications are subject to internal cross coupling errors which arise from the displacement of the gyro element when the gyro is indicating an input rate. The displacement of the gyro element for this condition is shown in Figure A-3. The input reference axis can be considered as the position of the input axis corresponding to zero input rate. The spin reference axis is the position of the spin vector for the same condition. It will be noted that when the gyro is indicating an input angular velocity, the actual input axis is displaced from the reference input axis. The gyro element under this condition responds in accordance with Equation (A-21) to only that component of the input angular velocity vector which lies along the displaced input axis. This component is obviously $\omega_{ir} \cos A_g$, where ω_{ir} is the input angular velocity of the gyro case about the input reference axis and A_g is the deflection of the gimbal from the zero position. In addition, when the gimbal is displaced, the gyro element will respond to a component of an angular velocity input about the spin reference axis. This component is $\omega_{sr} \sin A_g$, where ω_{sr}

is the angular velocity of the case about the spin reference axis. Then the total angular rate about the displaced input axis is given by

$$(A-22) \quad \omega_i = \omega_{ir} \cos A_g + \omega_{sr} \sin A_g$$

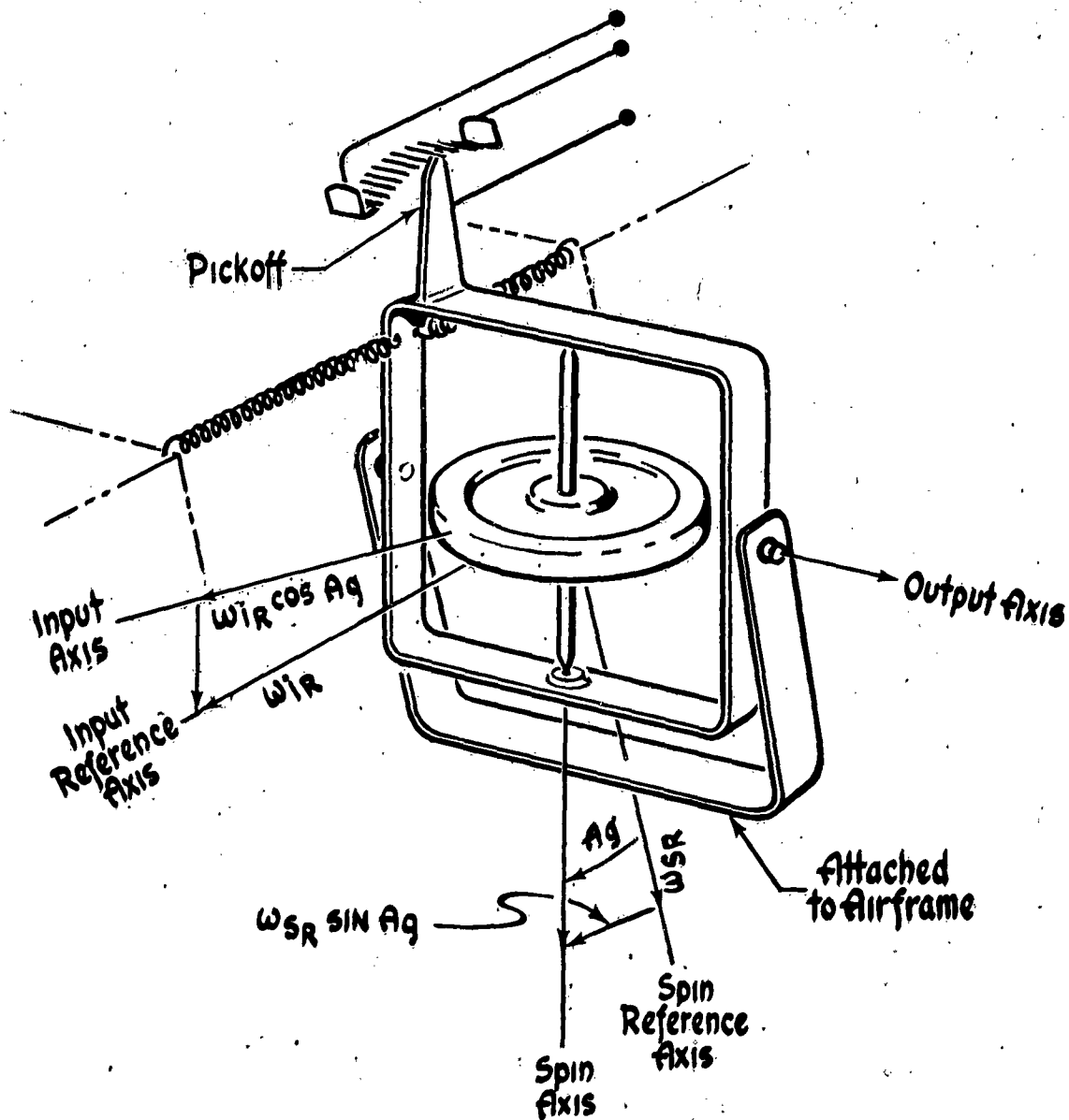


Figure A-3 Rate Gyro Relationships

To determine the effects of rate gyro internal cross coupling, assume a yaw rate gyro to be mounted in an airframe with its input reference axis aligned with the airframe Z axis and its spin reference axis at some arbitrary angle η to the airframe X-axis as shown in Figure A-4.

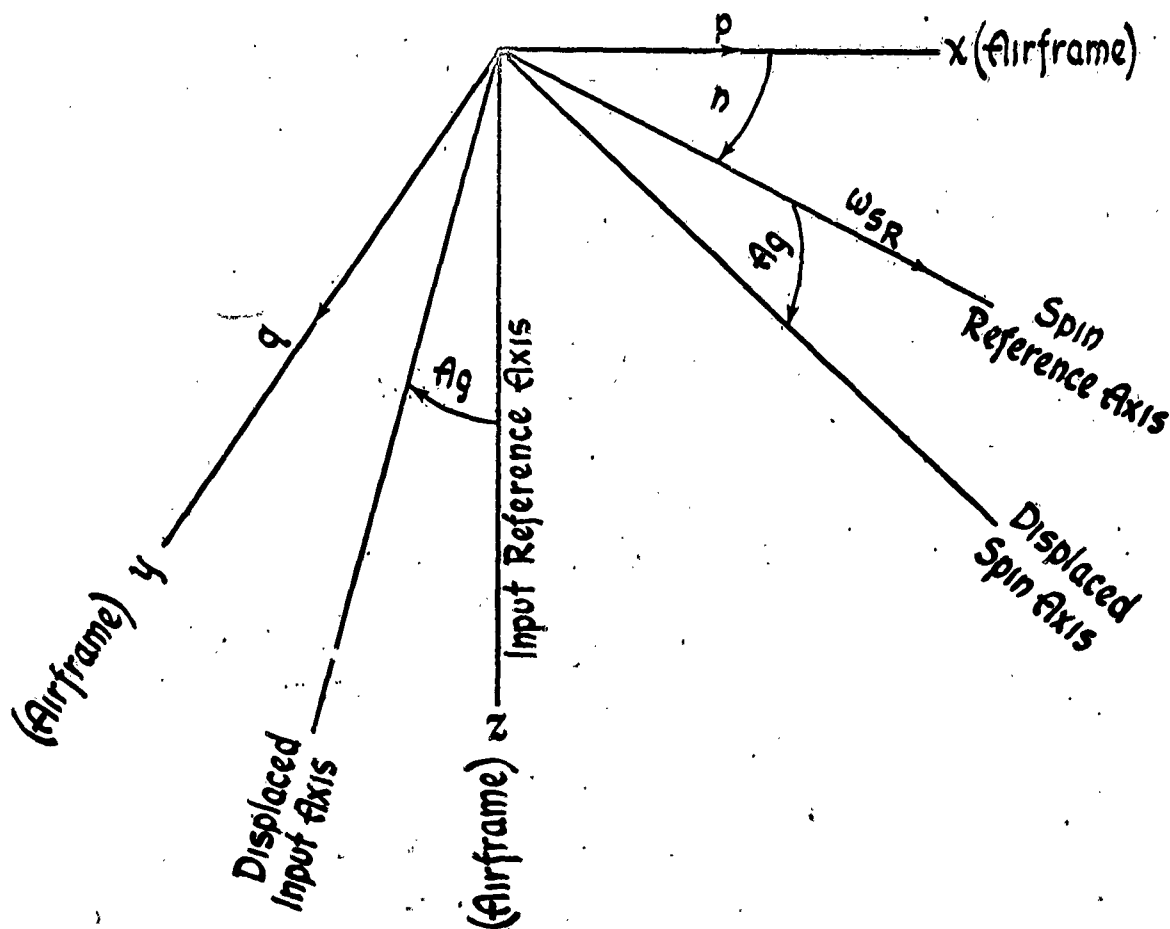


Figure A-4 Yaw Rate Gyro, Arbitrary Orientation

If the airframe is assumed to have rolling and pitching velocities p and q , the components of these velocities about the spin reference axis are given by

$$(A-23) \omega_{sp} = p \cos \eta + q \sin \eta$$

If it is now assumed that the gyro is indicating an input angular rate, the total velocity about the displaced input axis is found by substituting Equation (A-23) into (A-22) (or by direct resolution from Figure A-4) to be

$$(A-24) \omega_{i} = r \cos A_{gr} \pm (p \cos \eta + q \sin \eta) \sin A_{gr}$$

Where the subscript, i denotes yaw rate gyro. The plus or minus sign is used before the bracket because this sign depends on the direction in which the gyro input axis is deflected for a positive yaw rate, which in turn depends on the direction of spin. The minus sign has been assumed in Figure A-4.

The indication of a rate gyro is normally obtained by measuring the angle A_g . In terms of ω_i , A_g is given by

$$(A-25) A_g = \frac{\omega_i H}{K_g}$$

where K_S is the restraining spring constant. In terms of Equation (A-24),

$$(A-26) \quad A_{gr} = \frac{H_r}{K_{sr}} \left[r \cos A_{gr} \pm (p \cos \eta + q \sin \eta) \sin A_{gr} \right]$$

where the subscript r denotes yaw rate gyro, as above.

It is seen that a yaw rate gyro oriented as shown in Figure A-4 does not measure pure yaw rate, but yaw rate plus functions of roll and pitch rates and the angle

η . Since roll rates can be much larger than yaw rate, it is desirable to eliminate the internally cross coupled roll rate component. This can be accomplished by making $\eta = 90^\circ$. Then Equation (A-26) becomes

$$(A-27) \quad A_{gr} = \frac{H_r}{K_{sr}} \left[r \cos A_{gr} \pm q \sin A_{gr} \right]$$

In practice, K_S is adjusted such that A_g is kept small, usually less than 5 degrees. Then to a good approximation,

$$(A-28) \quad \cos A_g = 1, \text{ AND } \sin A_g = A_g$$

Substituting Equation (A-28) into Equation (A-27) results in

$$(A-29) \quad A_{gr} = \frac{H_r}{K_{sr}} \left[r \pm q A_{gr} \right]$$

for the condition in which the spin reference axis is aligned with the airframe Y-axis.

In a similar manner, the indication of a pitch rate gyro oriented to couple yaw rate into pitch rate is given by

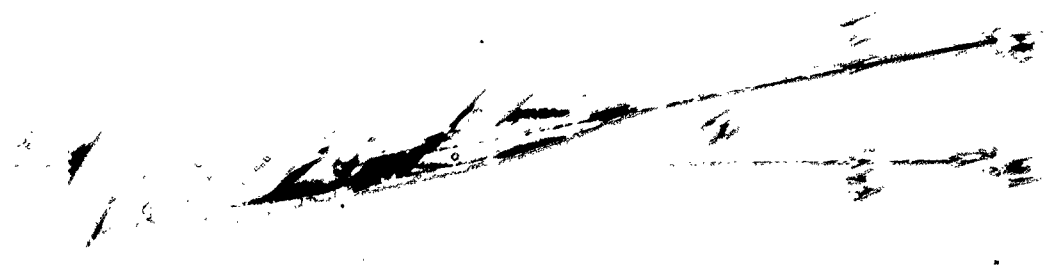
$$(A-30) \quad A_{gq} = \frac{H_q}{K_{sq}} \left[q \pm r A_{gq} \right]$$

where the subscript q denotes pitch rate gyro. For Equation (A-30) the gyro is oriented with its input reference axis aligned with the airframe Y-axis and its spin reference axis along the airframe Z-axis. For a roll rate gyro oriented to couple yaw into roll, the gyro indication is given by

$$(A-31) \quad A_{gp} = \frac{H_p}{K_{sp}} \left[p \pm r A_{gp} \right]$$

In this case the gyro input reference axis would be aligned with the airframe X-axis and the spin reference axis with the airframe Z-axis. Equations (A-29), (A-30), and (A-31) give the rate gyro pick off indications for the orientations assumed including the effect of internal geometrical cross coupling. Other gyro orientations would result in different coupling terms, however, the orientations chosen

[Faint, illegible handwritten text, possibly bleed-through from the reverse side of the page.]



REV 194

1/10/44

WILLIAM S. H. HANDLING OF STABILITY AXES RATES ALONG BODY AXES

here usually provide minimum coupling effects since the relative maximum magnitude of the airframe angular rates are usually in the order of $p \gg q > r$. For this reason it is desirable to eliminate roll coupling wherever possible.

Since the cross coupling term for each of the above cases is directly proportional to gimbal displacement, it is obvious that this effect is reduced when the gimbal angle is kept small.

An effect which must be considered when conducting flight control simulation studies arises when the axes to which the airframe equations are referenced do not coincide with the input reference axes of the rate gyros. This condition is illustrated in Figure A-5 in which it is assumed that three rate gyros are installed with input reference axes aligned with the airframe body axes and that the airframe equations are referred to stability axes. Only the plane of symmetry is shown, since the Y-body and stability axes coincide.

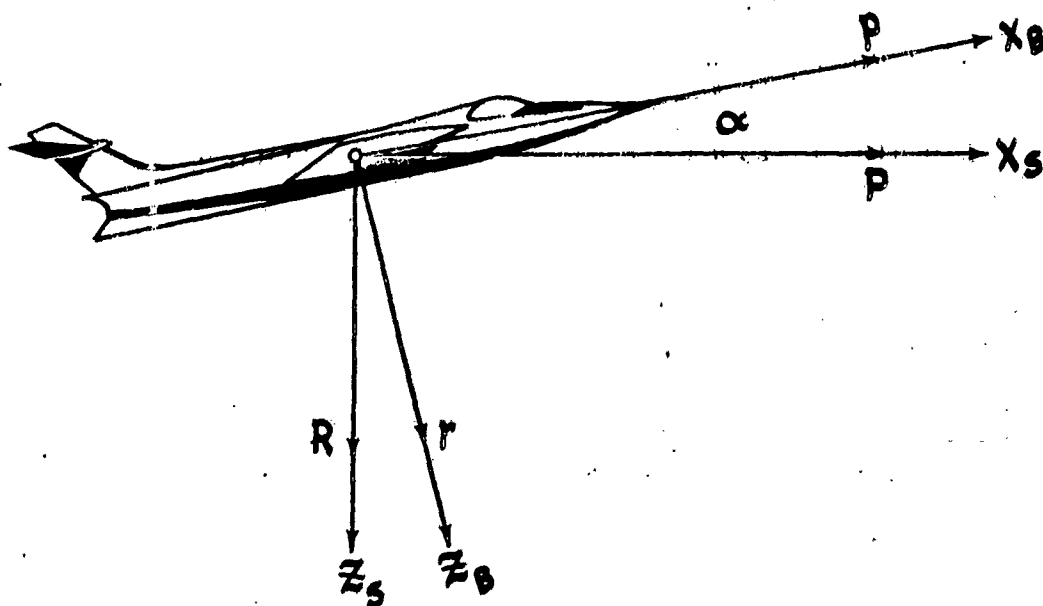


Figure A-5 Resolution of Stability Axes Rates Along Body Axes

From Figure A-5, the angular velocities about the body axes in terms of the angular velocities about the stability axes are given by Equations (A-32).

$$\begin{aligned} p &= P \cos \alpha - R \sin \alpha \\ (A-32) \quad q &= Q \\ r &= R \cos \alpha + P \sin \alpha \end{aligned}$$

When α is small, then $\cos \alpha \approx 1$ and $\sin \alpha \approx \alpha$. Utilizing this approximation, Equations (A-32) are reduced to

$$\begin{aligned} p &\approx P - R\alpha \\ (A-33) \quad q &= Q \\ r &\approx R + P\alpha \end{aligned}$$

Equations (A-33) express what is sometimes called external cross coupling, however it should be remembered that these coupling terms arise only because one chooses to compute angular rates with respect to a set of axes different from those along which the gyros are oriented.

Substituting Equations (A-33) into Equations (A-29), (A-30), and (A-31)

results in

$$\begin{aligned} A_{gp} &= \frac{1}{K_p} [(P - R\alpha) \pm (R + P\alpha) A_{gp}] \\ (A-34) \quad A_{gg} &= \frac{1}{K_g} [\varphi \pm (R + P\alpha) A_{gg}] \\ A_{gr} &= \frac{1}{K_r} [(R + P\alpha) \pm Q A_{gr}] \end{aligned}$$

where $K_p = \frac{K_{sp}}{H_p}$, etc. Neglecting the products αA_{gp} and αA_{gg} ,

and solving for A_g gives the following set of equations.

$$\begin{aligned} A_{gp} &= \frac{P - R\alpha}{K_p \mp R} && \text{ROLL} \\ (A-35) \quad A_{gg} &= \frac{\varphi}{K_g \mp R} && \text{PITCH} \\ A_{gr} &= \frac{R + P\alpha}{K_r \mp Q} && \text{YAW} \end{aligned}$$

Equations (A-35) give rate gyro gimbal deflections in terms of angular velocities about a set of axes displaced from the gyro input reference axes by the angle α , as shown in Figure A-5 for the particular spin reference axes orientations considered. The effects of internal geometrical cross coupling are included.

(c) VERTICAL GYRO INDICATIONS*

A physical description of the vertical gyro is given in Section 5a of Chapter II of this report. It will be recalled that the vertical gyro has two degrees of freedom and that the spin axis is maintained parallel to the average airframe net acceleration vector by means of an erection mechanism which operates very slowly. Since most aircraft spend a large percentage of their time in level, unaccelerated flight, the average net acceleration vector corresponds quite closely to the gravity vector. In this development it is assumed that the gyro spin axis coincides exactly with the gravity vector. The problem of determining vertical gyro indications then resolves itself into that of expressing the geometrical relationships between the inner and outer gimbals, and between the outer gimbal and the airframe in terms of useful airframe quantities. In this section these relationships are first expressed in terms of the airframe attitude (Euler) angles. The relationships are then linearized and the pickoff indications are expressed for small perturbations in terms of the steady state attitude angles and the perturbed airframe angular velocities p , q and r .

*The bulk of the material presented in this section is taken from Reference 29, and is used here with the permission of the authors.

The development which follows is greatly simplified through the use of some elementary forms of vector analysis. The few relationships which are used are stated below. For the reader interested in their derivation, Reference 26 presents a good review of the subject.

\bar{i} , \bar{j} , and \bar{k} are unit vectors directed along the airframe x, y and z body axes respectively (Figure A-8)

\bar{l} , \bar{m} , and \bar{n} are unit vectors directed along the gyro rotor u, v and w axes respectively (Figure A-8)

$\bar{A} \cdot \bar{B}$ is the dot product of the vectors A and B. It is a scalar quantity whose magnitude is the product of A and B and the cosine of the angle between the vectors.

$\bar{A} \times \bar{B}$ is the cross product of the vectors A and B. This operation yields a vector quantity whose magnitude is equal to the product of A and B and the sine of the angle between the vectors. The direction of the cross product is perpendicular to the plane containing A and B, with its positive sense determined by the direction in which a right hand screw would move when rotated in the direction of A into B through an angle less than 180 degrees.

$$\bar{i} \times \bar{j} = \bar{k} = -\bar{j} \times \bar{i}$$

$$\bar{j} \times \bar{k} = \bar{i} = -\bar{k} \times \bar{j}$$

$$\bar{k} \times \bar{i} = \bar{j} = -\bar{i} \times \bar{k}$$

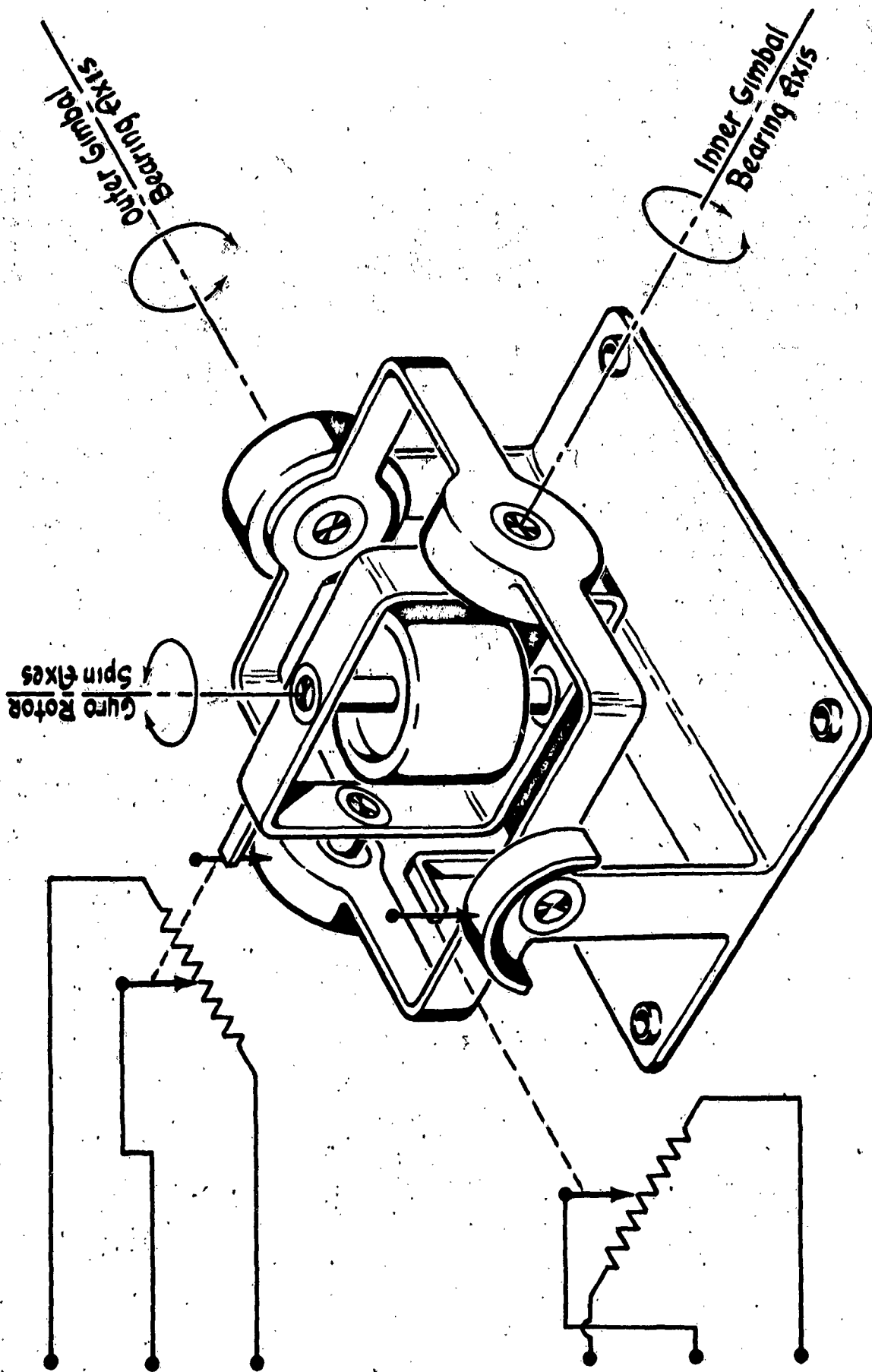


Figure A-6, Case I Vertical Gyro

$$\bar{i} \times \bar{i} = \bar{j} \times \bar{j} = \bar{k} \times \bar{k} = 0$$

$$\bar{i} \cdot \bar{i} = \bar{j} \cdot \bar{j} = \bar{k} \cdot \bar{k} = 1$$

$$\bar{i} \cdot \bar{j} = \bar{j} \cdot \bar{k} = \bar{k} \cdot \bar{i} = 0$$

$$(\bar{A} \times \bar{B}) \cdot \bar{C} = \bar{A} \cdot (\bar{B} \times \bar{C})$$

$$\bar{A} \times (\bar{B} \times \bar{C}) = \bar{B}(\bar{A} \cdot \bar{C}) - \bar{C}(\bar{A} \cdot \bar{B})$$

As is evident from Figure A-6, the outer gimbal bearing axis of a vertical gyro is directed along a fixed line in the aircraft. If the outer gimbal axis is directed more or less along the flight path (an x axis of the airframe) the gyro pickups measure different quantities than those measured if the gyro case is turned 90 degrees to orient the outer gimbal bearing axis along the y axis of the airframe. Therefore, gyro pickoff indications must be derived for two cases:

Case I - the outer gimbal bearing axis is oriented along an airplane x-axis.

Case II- the outer gimbal bearing axis is oriented along an airplane y-axis.

In both cases, the spin axes of the gyro rotor is parallel to the gravity vector.

The relationships between the gravity vector and the airframe axes x, y and z are illustrated in Figure A-7.

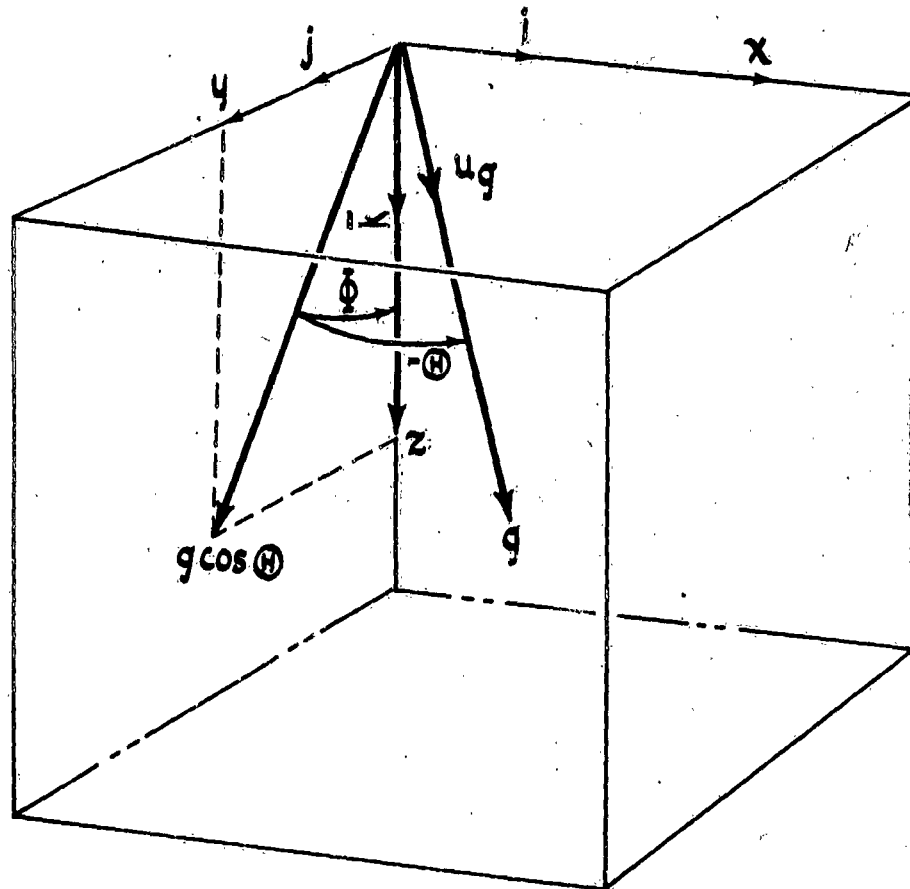


Figure A-7 Gyro Vector Relationships

From Figure A-7, it is seen that a unit vector \bar{u}_g lying along the gravity vector can be expressed as

$$(A-36) \quad \bar{u}_g = \frac{\bar{g}}{|g|} = -\bar{i} \sin \Theta + \bar{j} \cos \Theta \sin \Phi + \bar{k} \cos \Theta \cos \Phi$$

The definitions of the angles Θ and Φ are the same as used in Figure II-2 in Chapter II.

The orientation of the airframe body axes (x, y, z) with respect to the gyro rotor axes (u, v, w) for Case I is shown in Figure A-8.

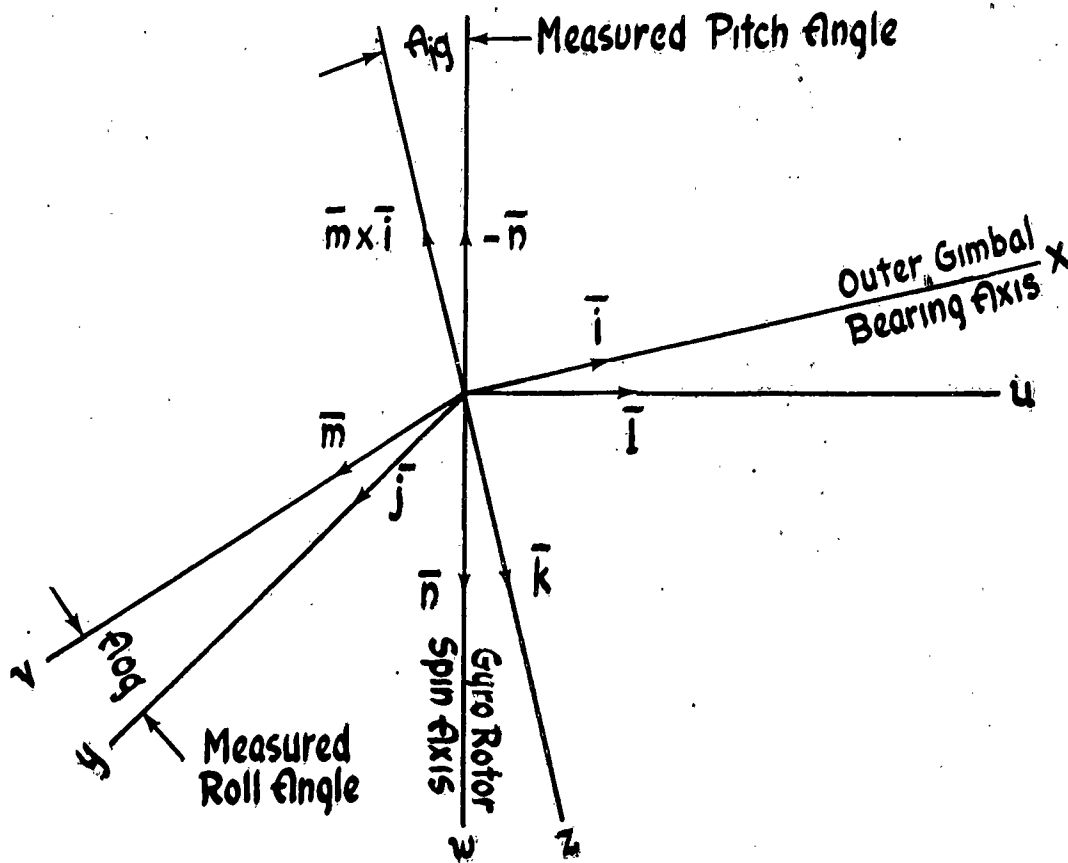


Figure A-8 Vertical Gyro Axis Orientation, Case I

From Figure A-8 the following relationships can be written.

$$(A-37) \quad \cos A_{og} = \bar{m} \cdot \bar{j}$$

Where A_{og} is the angle of the outer gimbal with respect to the airframe. Also

$$(A-38) \quad \cos A_{ig} = +\bar{n} \cdot \frac{(\bar{l} \times \bar{m})}{|\bar{l} \times \bar{m}|}$$

where A_{ig} is the angle of the inner gimbal with respect to the outer gimbal. A third relationship can be written by virtue of gyro construction.

$$(A-39) \quad \bar{m} = \frac{\bar{n} \times \bar{l}}{|\bar{n} \times \bar{l}|}$$

which merely states that the inner gimbal bearing axis is at all times perpendicular to the plane containing the outer gimbal bearing axis and the rotor spin vector. Comparison of Figures A-7 and A-8 reveals a fourth relationship.

$$(A-40) \quad \bar{n} = \bar{u}_g$$

If Equation (A-39) is substituted into Equation (A-37), the result is

$$(A-41) \quad \cos A_{og} = \frac{(\bar{n} \times \bar{i})}{|\bar{n} \times \bar{i}|} \cdot \bar{j}$$

The numerator of Equation (A-41) can be expressed as

$$(A-42) \quad (\bar{n} \times \bar{i}) \cdot \bar{j} = \bar{n} \cdot (\bar{i} \times \bar{j}) = \bar{n} \cdot \bar{k}$$

Equation (A-42) can be written as

$$(A-43) \quad \bar{n} \cdot \bar{k} = \bar{u}_g \cdot \bar{k} = \cos \Theta \cos \Phi$$

Substituting Equation (A-43) into Equation (A-42) results in

$$(A-44) \quad (\bar{n} \times \bar{i}) \cdot \bar{j} = \cos \Theta \cos \Phi$$

To determine the magnitude $|\bar{n} \times \bar{i}|$, the following expression is used

$$(A-45) \quad |\bar{n} \times \bar{i}| = |\bar{u}_g \times \bar{i}| = |\bar{j} \cos \Theta \cos \Phi - \bar{k} \cos \Theta \sin \Phi|$$

The magnitude of Equation (A-45) is

$$(A-46) \quad |\bar{n} \times \bar{i}| = \cos \Theta$$

If Equation (A-41) is now expressed in terms of Equations (A-44) and (A-46), the result is

$$(A-47) \quad \cos A_{og} = \frac{\cos(H) \cos \Phi}{\cos(H)} = \cos \Phi$$

or

$$(A-48) \quad A_{og} = \Phi$$

To determine the expression for the angle of the inner gimbal with respect to the outer gimbal Equation (A-38) can be expressed as

$$(A-49) \quad \cos A_{ig} = +\bar{n} \cdot \frac{\bar{i} \times \bar{m}}{|\bar{i} \times \bar{m}|} = \frac{+\bar{n} \cdot [\bar{i} \times (\bar{n} \times \bar{i})]}{|\bar{i} \times (\bar{n} \times \bar{i})|}$$

by virtue of Equation (A-39).

By means of vector manipulation, the quantity in brackets in the numerator of Equation (A-49) can be simplified as follows:

$$(A-50) \quad \bar{i} \times (\bar{n} \times \bar{i}) = \bar{n}(\bar{i} \cdot \bar{i}) - \bar{i}(\bar{i} \cdot \bar{n}) = \bar{n} - \bar{i}(\bar{i} \cdot \bar{n})$$

Substituting Equation (A-36) into the right hand side of Equation (A-50) results in

$$(A-51) \quad \bar{l} \times (\bar{n} \times \bar{l}) = \bar{j} \cos \Theta \sin \Phi + \bar{k} \cos \Theta \cos \Phi$$

The magnitude of Equation (A-51) is

$$(A-52) \quad |\bar{l} \times (\bar{n} \times \bar{l})| = \cos \Theta$$

The numerator of Equation (A-49) can now be expressed in terms of the Euler angles as the dot product of Equations (A-36) and (A-51). The result is

$$(A-53) \quad + \bar{n} \cdot [\bar{l} \times (\bar{n} \times \bar{l})] = + \cos^2 \Theta$$

Substituting Equations (A-52) and (A-53) into Equation (A-49) results in

$$(A-54) \quad \cos A_{ig} = + \cos \Theta$$

then

$$(A-55) \quad A_{ig} = \Theta$$

In summary, the gyro pickoff indications for a vertical gyro oriented with its outer gimbal bearing axis aligned with the airframe X-axis and with the gyro rotor spin axis aligned with the gravity vector are given in Equations (A-48) and (A-55). These results apply for any combination of Θ and Φ except for the condition of gimbal lock wherein the gyro rotor spin axis is aligned with the outer gimbal bearing axis. For Case I, this corresponds to $\Theta = \pm 90^\circ$. To prevent this occurrence, most vertical gyros are constructed with built in stops which prevent inner gimbal angles (A_{ig}) from exceeding approximately $\pm 85^\circ$.

The orientation of the airframe body axes and the gyro rotor axes for Case II is shown in Figure A-9.

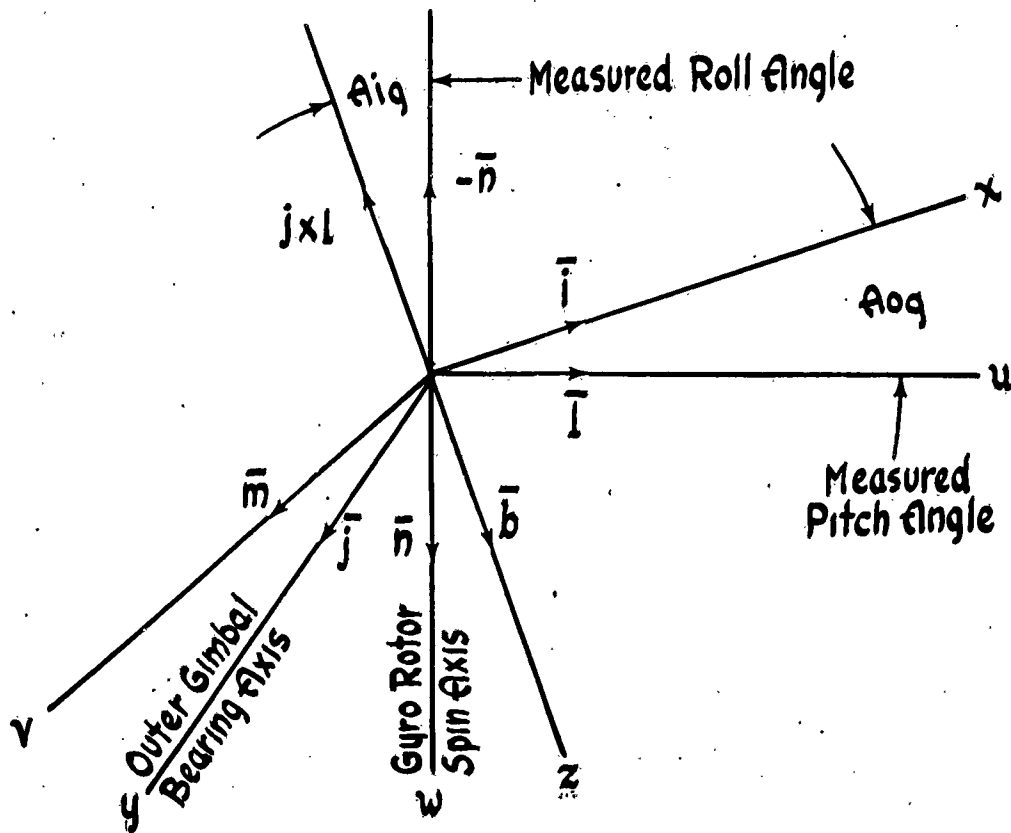


Figure A-9 Vertical Gyro Axis Orientation, Case II

From Figure A-9, the following relationships can be written

$$(A-56) \quad \cos A_{ig} = \frac{-\bar{n} \cdot (\bar{j} \times \bar{l})}{|\bar{j} \times \bar{l}|}$$

$$(A-57) \quad \cos A_{og} = \bar{i} \cdot \bar{l}$$

A third relationship can be written by virtue of gyro construction.

$$(A-58) \quad \bar{l} = \frac{\bar{j} \times \bar{n}}{|\bar{j} \times \bar{n}|}$$

Substituting Equation (A-58) into Equation (A-56) gives

$$(A-59) \quad \cos A_{ig} = \frac{-\bar{n} \cdot [\bar{j} \times (\bar{j} \times \bar{n})]}{|\bar{j} \times (\bar{j} \times \bar{n})|}$$

which can be rearranged to give

$$(A-60) \quad \cos A_{ig} = \frac{-\bar{n} \cdot [\bar{j}(\bar{j} \cdot \bar{n}) - \bar{n}(\bar{j} \cdot \bar{j})]}{|\bar{j}(\bar{j} \cdot \bar{n}) - \bar{n}(\bar{j} \cdot \bar{j})|}$$

The denominator of Equation (A-60) is evaluated by substituting the expression given for \bar{n} in Equation (A-36) and performing the indicated operation. The result is

$$(A-61) \quad |\bar{j}(\bar{j} \cdot \bar{n}) - \bar{n}(\bar{j} \cdot \bar{j})| = |\bar{i} \sin \Theta - \bar{k} \cos \Theta \cos \Phi|$$

which is equivalent to

$$(A-62) \quad \left| \bar{j}(\bar{j} \cdot \bar{n}) - \bar{n}(\bar{j} \cdot \bar{j}) \right| = (\sin^2 \theta + \cos^2 \theta \cos^2 \phi)^{1/2}$$

Utilizing Equations (A-36) and (A-62), the numerator of Equation (A-60) is given by

$$(A-63) \quad -\bar{n} \cdot [\bar{j}(\bar{j} \cdot \bar{n}) - \bar{n}(\bar{j} \cdot \bar{j})] = \sin^2 \theta + \cos^2 \theta \cos^2 \phi$$

When Equations (A-62) and (A-63) are combined, the result is

$$(A-64) \quad \cos A_{ig} = (\sin^2 \theta + \cos^2 \theta \cos^2 \phi)^{1/2}$$

which can be reduced to

$$(A-65) \quad \sin A_{ig} = \cos \theta \sin \phi$$

To determine the outer gimbal pickoff indication, Equation (A-58) is substituted into Equation (A-57). The result is

$$(A-66) \quad \cos A_{og} = \frac{\bar{i} \cdot (\bar{j} \times \bar{n})}{|\bar{j} \times \bar{n}|}$$

The numerator of Equation (A-66) can be written as

$$(A-67) \quad \bar{i} \cdot (\bar{j} \times \bar{n}) = (\bar{i} \times \bar{j}) \cdot \bar{n} = \bar{k} \cdot \bar{n}$$

Substituting Equation (A-36) for \bar{n} gives

$$(A-68) \quad \bar{k} \cdot \bar{n} = \cos \Theta \cos \Phi$$

Substituting for \bar{n} in the denominator of Equation (A-66) gives

$$(A-69) \quad |\bar{j} \times \bar{n}| = |\bar{i} \cos \Theta \cos \Phi + \bar{k} \sin \Theta|$$

which can be written as

$$(A-70) \quad |\bar{j} \times \bar{n}| = (\cos^2 \Theta \cos^2 \Phi + \sin^2 \Theta)^{1/2}$$

When Equations (A-68) and (A-70) are substituted into Equation (A-66),
the result is

$$(A-71) \quad \cos A_{0g} = \frac{\cos \Theta \cos \Phi}{(\cos^2 \Theta \cos^2 \Phi + \sin^2 \Theta)^{1/2}}$$

Equation (A-71) can be rearranged as shown in Equation (A-72)

$$(A-72) \quad \sin A_{og} = \frac{\sin \Theta}{(\cos^2 \Theta \cos^2 \Phi + \sin^2 \Theta)^{1/2}}$$

Equations (A-65) and (A-72) give the gyro pickoff indications for Case II in terms of the Euler angles Θ and Φ . It will be noted that cross coupling effects exist for this gyro orientation, in that both gyro pickoff indications are functions of both Θ and Φ . For this reason, vertical gyros are normally oriented with the outer gimbal bearing axis aligned with the airframe x-axis.

Again, as for Case I, the results are applicable for any combination of Θ and Φ except for the condition of gimbal lock. For the gyro oriented as in Case II, gimbal lock corresponds to $\Phi = \pm 90^\circ$.

To utilize these results in an autopilot simulator, or analog computer study, the Euler angles Θ and Φ must be computed. These angles were given in terms of the aircraft angular rates P , Q , and R as Equations (II-14) in Chapter II which are repeated below.

$$\dot{\Phi} = P + \tan \Theta (Q \sin \Phi + R \cos \Phi)$$

$$(A-73) \quad \dot{\Theta} = Q \cos \Phi - R \sin \Phi$$

(A-73)
CONT.

$$\dot{\Psi} = \frac{R \cos \Phi + \rho \sin \Phi}{\cos H}$$

The third Equation in (A-73) can be ignored unless it is desired to solve for $\dot{\Psi}$. Equations (A-73) can be used in conjunction with either Equations (A-48) and (A-55) or (A-65) and (A-72) to compute vertical gyro pickoff indications, in terms of the airframe angular velocities.

The gyro pickoff equations presented above would normally be used in conjunction with the complete, six degree of freedom airframe equations which were derived in Chapter II. When used with the airframe perturbation equations, the gyro pickoff equations can be linearized. Linearization is only necessary for Case II, since for Case I, gyro pickoff indications are linear even for large angles. For the linear equations, airframe motion is considered as the result of disturbing the airframe from some steady flight condition. Linearization is accomplished by utilizing Assumption 6 of Chapter II which states that all airframe motions from the steady flight condition are assumed small enough so that products and squares of the disturbance angles can be neglected, and their sines are equal to the angles themselves and their cosines are equal to unity.

Thus for Case I,

$$(A-74) \quad A_{og} + Q_{og} = \dot{\Phi}_0 + \dot{\phi}$$

where the \circ subscript indicates steady flight value of the variable and the lower case letters indicate disturbances from the steady flight values. Also for Case I

$$(A-75) \quad A_{iq} + a_{iq} = (\theta)_0 + \theta$$

For Case II, if the relationships

$$(A-76) \quad A_{iq} = A_{iq_0} + a_{iq}, \quad (\theta) = (\theta)_0 + \theta, \quad \text{AND} \quad \bar{\Phi} = \bar{\Phi}_0 + \phi$$

are utilized, Equation A-65 becomes

$$(A-77) \quad \sin(A_{iq_0} + a_{iq}) = [\cos(\theta_0 + \theta)] [\sin(\bar{\Phi}_0 + \phi)]$$

which can be written as

$$(A-78) \quad \sin A_{iq_0} \cos a_{iq} + \cos A_{iq_0} \sin a_{iq} =$$

$$[\cos \theta_0 \cos \theta - \sin \theta_0 \sin \theta] [\sin \bar{\Phi}_0 \cos \phi + \cos \bar{\Phi}_0 \sin \phi]$$

Since the changes from the steady flight condition will be considered small, the following approximations are made

$$(A-79) \quad \cos \alpha_{ig} \approx \cos \theta \approx \cos \phi \approx 1$$

$$\sin \alpha_{ig} \approx \alpha_{ig}, \quad \sin \theta \approx \theta \quad \text{AND} \quad \sin \phi \approx \phi$$

Utilizing Equations (A-79), (A-78) can be reduced to

$$(A-80) \quad \sin \alpha_{ig} + \alpha_{ig} \cos \alpha_{ig} \approx \left[\cos \theta_0 - \theta \sin \theta_0 \right] \left[\sin \phi_0 + \phi \cos \phi_0 \right]$$

If Equation (A-80) is solved for the angle α_{ig} the result is (neglecting the product $\theta \phi$, and recalling that $\sin \alpha_{ig_0} = \cos \theta_0 \sin \phi_0$)

$$(A-81) \quad \alpha_{ig} = - \left[\frac{\sin \theta_0 \sin \phi_0}{\cos \alpha_{ig_0}} \right] \theta + \left[\frac{\cos \theta_0 \cos \phi_0}{\cos \alpha_{ig_0}} \right] \phi$$

If for the steady flight condition chosen, $\phi_0 = 0$, Equation (A-81) is reduced to

$$(A-82) \quad \alpha_{ig} /_{\phi_0=0} = \phi \cos \theta_0$$

Thus for $\bar{\phi}_0 = 0$, the angle α_{ig} is a direct indication of perturbed roll angle, when the gyro is oriented as in Case II.

The linearized expression for the outer gimbal pickoff indication for Case II is developed as follows. Utilizing the approximations of Equation (A-79) in addition to

$$(A-83) \quad \sin \alpha_{og} \approx \alpha_{og} \text{ AND } \cos \alpha_{og} = 1$$

Equation (A-71) can be written as

$$(A-84) \quad \sin (\alpha_{og_0} + \alpha_{og}) = \frac{\sin (\theta_0 + \theta)}{\left[\sin^2 (\theta_0 + \theta) + \cos^2 (\theta_0 + \theta) \cos^2 (\bar{\phi}_0 + \phi) \right]^{1/2}}$$

By means of a rather lengthy but straightforward trigonometric manipulation, Equation (A-84) can be reduced to

$$(A-85) \quad \alpha_{og} = \frac{\theta}{\cos \bar{\phi}_0} - \frac{\sin \bar{\phi}_0}{1 + \cot^2 \theta_0 \cos^2 \bar{\phi}_0} (\theta \tan \bar{\phi}_0 - \phi \cot \theta_0)$$

Although Equation (A-85) appears complicated, it is not difficult to mechanize since all the quantities with zero subscript are constant for a given problem.

If the steady flight condition is chosen such that $\dot{\Phi}_0 = 0$,
Equation (A-85) reduces to

$$(A-86) \quad a_{og} \Big|_{\dot{\Phi}=0} = 0$$

To linearize Equations (A-73), their inverse equations are utilized.
These are given as

$$(A-87) \quad \begin{aligned} P &= \dot{\Phi} - \dot{\Psi} \sin \Theta \\ Q &= \dot{\Theta} \cos \Phi + \dot{\Psi} \sin \Phi \cos \Theta \\ R &= -\dot{\Theta} \sin \Phi + \dot{\Psi} \cos \Phi \cos \Theta \end{aligned}$$

To linearize Equations (A-87), it is assumed that

$$(A-88) \quad P_0 = Q_0 = R_0 = \dot{\Phi}_0 = \dot{\Theta}_0 = \dot{\Psi}_0 = 0$$

Then Equations (A-87) can be written as

$$(A-89) \quad \begin{aligned} p &= \dot{\phi} - \dot{\psi} \sin \Theta_0 \\ q &= \dot{\theta} \cos \Phi_0 + \dot{\psi} \sin \Phi_0 \cos \Theta_0 \\ r &= -\dot{\theta} \sin \Phi_0 + \dot{\psi} \cos \Phi_0 \cos \Theta_0 \end{aligned}$$

where, as before, the zero subscript indicates steady flight value and the lower case letters indicate deviations therefrom. Equations (A-89) can be substituted into the linearized gyro pickoff equations to obtain gyro pick-off indications in terms of aircraft angular rates. For Case I,

$$(A-90) \quad a_{og} = \phi = \int \dot{\phi} dt = \int (p + \dot{\psi} \sin \Theta_0) dt$$

and

$$(A-91) \quad a_{ig} = \theta = \int \dot{\theta} dt = \int \left(\frac{q - \dot{\psi} \sin \bar{\Phi}_0 \cos \Theta_0}{\cos \bar{\Phi}_0} \right) dt$$

To utilize Equations (A-90) and (A-91) it is necessary to compute $\dot{\psi}$. This is obtained by simultaneous solution of Equations (A-89) as

$$(A-92) \quad \dot{\psi} = \frac{r \cos \bar{\Phi}_0 + q \sin \bar{\Phi}_0}{\cos \Theta_0}$$

If for the steady flight condition $\bar{\Phi}_0 = 0$, Equation (A-92) becomes

$$(A-93) \quad \dot{\psi} = \frac{r}{\cos \Theta_0}$$

and Equations (A-90) and (A-91) can be written as

$$(A-94) \quad a_{og} = \int (p + r \text{TAN } \Theta_0) dt$$

$$(A-95) \quad a_{ig} = \int q dt$$

Utilizing Equations (A-89) the linearized gyro pickoff equations for Case II are obtained. Equation (A-81) becomes

$$(A-96) \quad a_{ig} = - \frac{\text{SIN } \Theta_0 \text{ SIN } \Phi_0}{\text{COS } A_{ig_0}} \int \left(\frac{q - \dot{\Psi} \text{ SIN } \Phi_0 \text{ COS } \Theta_0}{\text{COS } \Phi_0} \right) dt$$

$$+ \frac{\text{COS } \Phi_0 \text{ COS } \Theta_0}{\text{COS } A_{ig_0}} \int (p + \dot{\Psi} \text{ SIN } \Theta_0) dt$$

and Equation (A-85) becomes

$$(A-97) \quad a_{og} = \frac{1}{\text{COS } \Phi_0} \int \left(\frac{q - \dot{\Psi} \text{ SIN } \Phi_0 \text{ COS } \Theta_0}{\text{COS } \Phi_0} \right) dt$$

$$- \frac{\text{SIN } \Phi_0}{1 + \text{COT}^2 \Theta_0 \text{ COS}^2 \Phi_0} \left[\text{TAN } \Phi_0 \int \left(\frac{q - \dot{\Psi} \text{ SIN } \Phi_0 \text{ COS } \Theta_0}{\text{COS } \Phi_0} \right) dt \right.$$

$$\left. - \text{COT } \Theta_0 \int (p + \dot{\Psi} \text{ SIN } \Theta_0) dt \right]$$

where, as before, $\dot{\psi}$ is given by Equation (A-92). Again, considerable simplification is effected if the steady flight condition is chosen such that $\dot{\phi}_0 = 0$. Equations (A-96) and (A-97) for this condition become

$$(A-98) \quad A_{ig} = \frac{\cos \Theta_0}{\cos A_{ig_0}} \int (P + r \tan \Theta_0) dt$$

and

$$(A-99) \quad A_{og} = \int q dt$$

The relationships for vertical gyro pickoff indications as derived in this section are summarized in Table A-1.

Table A-1 - Vertical Gyro Pickoff Equations

Case I (outer gimbal axis aligned with airframe X-axis)

$$(A-48) \quad A_{og} = \dot{\phi}$$

$$(A-55) \quad A_{ig} = \Theta$$

Case II (outer gimbal axis aligned with airframe Y-axis)

$$(A-65) \quad \sin A_{ig} = \cos \Theta \sin \dot{\phi}$$

Table A-1 (continued)

$$(A-72) \quad \sin A_{og} = \frac{\sin \theta}{(\cos^2 \theta \cos^2 \phi + \sin^2 \theta)^{1/2}}$$

Linearized Equations

Case I

$$(A-74) \quad \alpha_{og} = \phi$$

$$(A-75) \quad \alpha_{ig} = \theta$$

Case II

$$(A-81) \quad \alpha_{ig} = \left(\frac{\sin \theta_0 \sin \phi_0}{\cos \alpha_{ig_0}} \right) \theta + \left(\frac{\cos \phi_0 \cos \theta_0}{\cos \alpha_{ig_0}} \right) \phi$$

$$(A-85) \quad \alpha_{og} = \frac{\theta}{\cos \phi_0} - \frac{\sin \phi_0}{1 + \cot^2 \theta_0 \cos^2 \phi_0} (\theta \tan \phi_0 - \phi \cot \theta_0)$$

Table A-1 (continued)

Linearized Equations for $\Phi_0 = 0$

Case I

$$(A-74) \quad \dot{q}_{og} = \dot{\phi}$$

$$(A-75) \quad \dot{q}_{ig} = \dot{\theta}$$

Case II

$$(A-82) \quad \dot{q}_{ig} = \frac{\cos \Theta_0}{\cos \Lambda_{ig_0}} \dot{\phi}$$

$$(A-86) \quad \dot{q}_{og} = \dot{\theta}$$

Linearized Equations in terms of the Airframe Angular Rates

Case I

$$(A-90) \quad \dot{q}_{og} = \int (\dot{p} + \dot{\psi} \sin \Theta_0) dt$$

$$(A-91) \quad \dot{q}_{ig} = \int \left(\frac{\dot{q} - \dot{\psi} \sin \Phi_0 \cos \Theta_0}{\cos \Phi_0} \right) dt$$

Table A-1 (continued)

where

$$(A-92) \quad \dot{\psi} = \frac{r \cos \dot{\Phi}_0 + \dot{r} \sin \dot{\Phi}_0}{\cos \Theta_0}$$

Case II

$$(A-96) \quad a_{ig} = -\frac{\sin \Theta_0 \sin \dot{\Phi}_0}{\cos A_{ig0}} \int \left(\frac{\dot{r} - \dot{\psi} \sin \dot{\Phi}_0 \cos \Theta_0}{\cos \dot{\Phi}_0} \right) dt$$

$$+ \left(\frac{\cos \dot{\Phi}_0 \cos \Theta_0}{\cos A_{ig0}} \right) \int (\dot{p} + \dot{\psi} \sin \Theta_0) dt$$

$$(A-97) \quad a_{og} = \frac{1}{\cos \dot{\Phi}_0} \int \left(\frac{\dot{r} - \dot{\psi} \sin \dot{\Phi}_0 \cos \Theta_0}{\cos \dot{\Phi}_0} \right) dt$$

$$- \frac{\sin \dot{\Phi}_0}{1 + \cot^2 \Theta_0 \cos^2 \dot{\Phi}_0} \left[\tan \dot{\Phi}_0 \int \left(\frac{\dot{r} - \dot{\psi} \sin \dot{\Phi}_0 \cos \Theta_0}{\cos \dot{\Phi}_0} \right) dt \right.$$

$$\left. - \cot \Theta_0 \int (\dot{p} + \dot{\psi} \sin \Theta_0) dt \right]$$

Table A-1. (continued)

Linearized equations in terms of the airframe angular rates for $\phi_0 = 0$

Case I

$$(A-94) \quad a_{og} = \int (p + r \tan \theta_0) dt$$

$$(A-95) \quad a_{ig} = \int q dt$$

Case II

$$(A-98) \quad a_{ig} = \frac{\cos \theta_0}{\cos A_{ig0}} \int (p + r \tan \theta_0) dt$$

$$(A-99) \quad a_{og} = \int q dt$$

(d) DIRECTIONAL GYRO INDICATIONS

As indicated in Chapter II, the directional gyro has two degrees of freedom and is oriented with the outer gimbal axis along the airframe Z axis. The gyro rotor spin axis is normally slaved to magnetic north and is maintained in a horizontal plane by an erection mechanism which is slaved to the airframe net acceleration vector. In actual practice the directional gyro only provides correct yaw indications when the outer

gimbal axis is vertical. Therefore, errors are introduced whenever yawing occurs in the presence of any combination of pitch or roll angles.

In this subsection, the directional gyro pickoff indication is derived in terms of the airframe attitude angles Φ , Θ , and Ψ . The resulting expression is then linearized and written in terms of small perturbations about some initial flight condition.

The directional gyro pickoff indication is given by the angular rotation of the outer gimbal with respect to the airframe. Since the inner gimbal bearing axis is rigidly attached to the outer gimbal, it is convenient to measure the directional gyro pickoff indication as the angle between the inner gimbal bearing axis and some reference axis attached to the airframe. For this development it is somewhat arbitrarily assumed that the gyro rotor spin axis orientation for zero pickoff indication is in the plane of symmetry. This assumption simplifies the development which follows, although it in no way reduces its generality. For the chosen zero position of the gyro rotor spin axis, the inner gimbal bearing axis lies along the airframe Y-axis and it is therefore convenient to designate the angle between the inner gimbal bearing axis and the airframe Y-axis as the gyro pickoff indication. This arrangement is shown in Figure A-10.

Equation (A-100) will now be expanded in terms of the airframe attitude angles ϕ , θ , and ψ . To accomplish this, the components of the unit vector \bar{l} along the airframe axes must first be expressed in terms of the angles ϕ , θ , and ψ . This is accomplished through the use of Figure (A-11), in which the gyro rotor axes u and v lie in a horizontal plane, the w axis coincides with the gravity vector, and the x -axis indicates the position of the airframe x -axis.

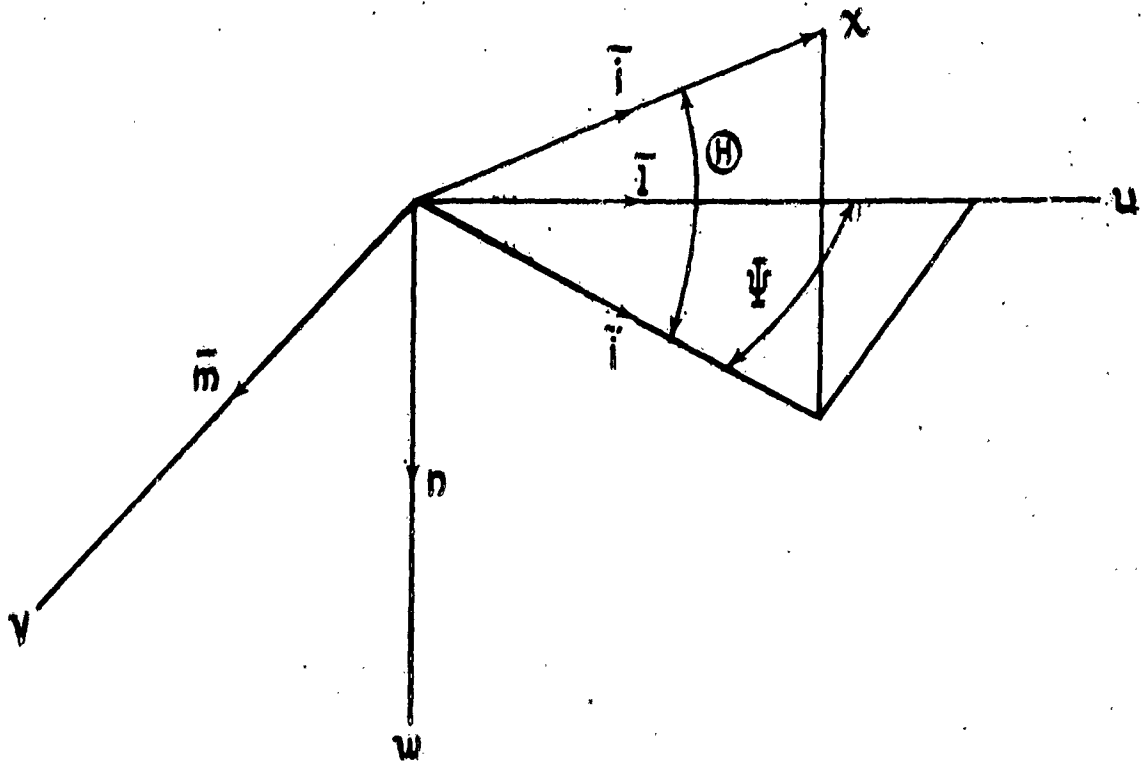


Figure A-11 Directional Gyro Axis Orientation

In Figure A-11, the unit vector \bar{i}' describing the projection of the airframe x-axis on the horizontal plane is given by

$$(A-101) \quad \bar{i}' = (\bar{i} + \bar{n} \sin \Theta) \frac{1}{\cos \Theta}$$

Utilizing Equations (A-36) and (A-40), Equation (A-101) can be expanded to obtain

$$(A-102) \quad \bar{i}' = \bar{i} \cos \Theta + \bar{j} \sin \Theta \sin \Phi + \bar{k} \sin \Theta \cos \Phi$$

The projection of the unit vector \bar{l} on the airframe axes is given by

$$(A-103) \quad \bar{l} = \bar{i} l_x + \bar{j} l_y + \bar{k} l_z$$

Then

$$(A-104) \quad \bar{l} \cdot \bar{i}' = \cos \Phi = l_x \cos \Theta + l_y \sin \Theta \sin \Phi + l_z \sin \Theta \cos \Phi$$

Also

$$(A-105) \quad \bar{l} \cdot \bar{n} = 0 = -l_x \sin \Theta + l_y \cos \Theta \sin \Phi + l_z \cos \Theta \cos \Phi$$

One additional expression is required

$$(A-106) \quad \bar{l} \times \bar{l}' = \bar{n} \sin \Psi$$

Utilizing Equations (A-36), (A-40), and (A-102), Equation (A-106) can be expanded to obtain

$$(A-107) \quad l_y \sin \Theta \cos \Phi - l_z \sin \Theta \sin \Phi = -\sin \Theta \sin \Psi$$

$$-l_x \sin \Theta \cos \Phi + l_z \cos \Theta = \sin \Phi \cos \Theta \sin \Psi$$

$$l_x \sin \Theta \sin \Phi - l_y \cos \Theta = \cos \Phi \cos \Theta \sin \Psi$$

By addition, Equations (A-107) can be combined to form a single equation

$$(A-108) \quad l_x (\sin \Theta \sin \Phi - \sin \Theta \cos \Phi) + l_y (\sin \Theta \cos \Phi - \cos \Theta)$$

$$+ l_z (\cos \Theta - \sin \Theta \sin \Phi)$$

$$= \sin \Psi [\cos \Theta (\sin \Phi + \cos \Phi) - \sin \Theta]$$

The components of the unit vector \bar{l} can now be obtained by simultaneous solution of Equations (A-104), (A-105), and (A-108). The result is:

$$\begin{aligned}
 l_x &= \cos \Psi \cos \Theta \\
 (A-109) \quad l_y &= \sin \Psi \sin \Theta \cos \Phi - \cos \Psi \sin \Phi \\
 l_z &= \sin \Psi \sin \Phi + \cos \Psi \sin \Theta \cos \Phi
 \end{aligned}$$

which in vector form becomes

$$\begin{aligned}
 (A-110) \quad \bar{l} &= \bar{i} \cos \Psi \cos \Theta + \bar{j} (\sin \Psi \sin \Theta \cos \Phi - \cos \Psi \sin \Phi) \\
 &\quad + \bar{k} (\sin \Psi \sin \Phi + \cos \Psi \sin \Theta \cos \Phi)
 \end{aligned}$$

Equation (A-110) can now be used to expand Equation (A-100).

To expand the numerator of Equation (A-100) the operation indicated by the vector cross product $\bar{k} \times \bar{l}$ is first performed. Then

$$(A-111) \quad \bar{k} \times \bar{l} = \begin{vmatrix} \bar{i} & \bar{j} & \bar{k} \\ 0 & 0 & 1 \\ \cos \Psi \cos \Theta & \sin \Psi \sin \Theta \cos \Psi & \sin \Psi \sin \Theta \\ -\cos \Psi \sin \Psi & +\cos \Psi \sin \Theta \cos \Psi & \end{vmatrix}$$

Upon expansion, Equation (A-111) becomes

$$(A-112) \quad \bar{k} \times \bar{l} = \bar{i} (\cos \Psi \sin \Psi - \sin \Psi \sin \Theta \cos \Psi) + \bar{j} (\cos \Psi \cos \Theta)$$

The numerator of Equation (A-100) then becomes

$$(A-113) \quad \bar{j} \cdot (\bar{k} \times \bar{l}) = \cos \Psi \cos \Theta$$

The denominator of Equation (A-100) is given by the absolute value of Equation (A-112). Then

$$(A-114) \quad |\bar{k} \times \bar{l}| = \left[(\cos \Phi \sin \Psi - \sin \Phi \sin \Theta \cos \Psi)^2 + (\cos \Psi \cos \Theta)^2 \right]^{1/2}$$

Utilizing Equations (A-113) and (A-114) Equation (A-100) can be expressed as

$$(A-115) \quad \cos A_{og} = \frac{\cos \Psi \cos \Theta}{\left[(\cos \Phi \sin \Psi - \sin \Phi \sin \Theta \cos \Psi)^2 + (\cos \Psi \cos \Theta)^2 \right]^{1/2}}$$

Equation (A-115) gives the cosine of the directional gyro pickoff angle in terms of the airframe attitude angles Φ , Θ , and Ψ . Equation (A-115) is probably too complex to mechanize on an analog computer. It is valuable however in giving an insight into the type and magnitude of the gimbal errors which exist in directional gyro pickoff indications. To visualize these errors, it is helpful to note the directional gyro pickoff indications for various combinations of airframe attitude angles. Pickoff indications as obtained from Equation (A-115) for several combinations are summarized in Table A-2.

	Actual Attitude	Desired Heading Indication	Actual Heading Indication
1	$\Phi = 0$	$\cos A_{og} = \cos \Psi$	$\cos A_{og} = \frac{\cos \Psi \cos \Theta}{(\sin^2 \Psi + \cos^2 \Psi \cos^2 \Theta)^{1/2}}$
2	$\Theta = 0$	$\tan A_{og} = \tan \Psi$	$\tan A_{og} = \tan \Psi \cos \Phi$
3	$\Psi = 0$	$\cos A_{og} = 1$	$\cos A_{og} = \frac{\cos \Theta}{(\sin^2 \Phi \sin^2 \Theta + \cos^2 \Theta)^{1/2}}$
4	$\Psi = \pm 90^\circ$	$\cos A_{og} = 0$	$\cos A_{og} = 0$
5	$\Phi = \Theta = 0$	$A_{og} = \Psi$	$A_{og} = \Psi$
6	$\Psi = \Phi = 0$	$\cos A_{og} = 1$	$\cos A_{og} = 1$
7	$\Psi = \Theta = 0$	$\cos A_{og} = 1$	$\cos A_{og} = 1$

Table A-2 Directional Gyro Pickoff Indications

It will be noted that correct indications are obtained when $\Psi = \pm 90^\circ$, when $\Phi = \Psi = 0$, when $\Theta = \Psi = 0$, and of course, when $\Phi = \Theta = 0$. Errors are introduced for all other combinations of attitude angles.

Equations (A-115) can be linearized by the same method used in conjunction with the vertical gyro equations. The resulting linear equation

can be used in conjunction with the airframe perturbation equations to study the motion of an airframe under autopilot control for small disturbances from some initial attitude. It will be recalled that linearization is accomplished by assuming that airframe disturbances from the initial attitude are small enough that the cosines of the disturbance angles can be set equal to unity, sines of the angles are equal to the angles themselves, and products of the angles can be neglected.

The linear equation is derived by making the following substitutions in Equation (A-115).

$$\begin{aligned}
 \Phi &= \Phi_0 + \phi \\
 \Theta &= \Theta_0 + \theta \\
 \Psi &= \Psi_0 + \psi \\
 A_{og} &= A_{og_0} + a_{og}
 \end{aligned}
 \tag{A-116}$$

where, as before, the zero subscript designates the initial value and the lower case letters indicate deviations therefrom. When the indicated substitutions are made in Equation (A-115) and the equation is expanded and solved for a_{og} the result is

$$\tag{A-117} \quad a_{og} = \frac{\psi \tan \Phi_0 + \theta \tan \Theta_0 + \frac{D_\phi \phi + D_\theta \theta + D_\psi \psi}{D_1}}{D_2}$$

where

$$D_1 = \cos^2 \Phi_0 \sin^2 \Psi_0 - 2 \sin \Phi_0 \cos \Phi_0 \sin \Theta_0 \sin \Psi_0 \cos \Psi_0 \\ + \sin^2 \Phi_0 \sin^2 \Theta_0 \cos^2 \Psi_0 + \cos^2 \Theta_0 \cos^2 \Psi_0$$

$$D_2 = \sec \Theta_0 \cos \Phi_0 \tan \Psi_0 - \sin \Phi_0 \tan \Theta_0$$

$$D_\phi = \sin \Theta_0 \sin \Psi_0 \cos \Phi_0 (\sin^2 \Phi_0 - \cos^2 \Phi_0) -$$

$$+ \sin \Phi_0 \cos \Phi_0 (\sin^2 \Theta_0 \cos^2 \Psi_0 - \sin^2 \Psi_0)$$

$$D_\theta = -\cos \Theta_0 \cos \Psi_0 (\sin \Phi_0 \cos \Phi_0 \sin \Psi_0 + \cos^2 \Phi_0 \sin \Theta_0 \cos \Psi_0)$$

$$D_\psi = \sin \Psi_0 \cos \Psi_0 (\cos^2 \Phi_0 - \sin^2 \Phi_0 \sin^2 \Theta_0 - \cos^2 \Theta_0)$$

$$+ \sin \Phi_0 \cos \Phi_0 \sin \Theta_0 (\sin^2 \Psi_0 - \cos^2 \Psi_0)$$

It will be noted that Equation (A-117) is linear.

As shown, Equation (A-117) gives the perturbed indication of a directional gyro for an arbitrary initial airframe attitude. Considerable simplification is effected for certain specific initial attitudes. These are summarized in Table A-3.

Attitude Angles	Q_{og}
$\Phi_0 = 0$	$Q_{og} = \psi \cos \Theta + \theta \frac{\sin \Theta_0}{\tan \Phi_0}$ $- \left(\frac{\sin \Theta_0 \cos \Theta_0 \cot \Phi_0}{1 + \cot^2 \Phi_0 \cos^2 \Theta_0} \right) (\phi + \theta \cos \Theta_0 \cot \Phi_0 - \psi \sin \Theta_0)$
$\Theta = 0$	$Q_{og} = \frac{\psi}{\cos \Phi_0} - \frac{\sin \Phi_0}{1 + \tan^2 \Phi_0 \cos^2 \Phi_0} (\phi \tan \Phi_0 + \theta + \psi \tan \Phi_0)$
$\Psi_0 = 0$	$Q_{og} = \frac{\theta}{\sin \Phi_0}$ $- \left(\frac{\cos \Phi_0}{1 + \tan^2 \Theta_0 \sin^2 \Phi_0} \right) (\phi \tan \Theta_0 - \theta \cot \Phi_0 - \psi \sec \Theta_0)$
$\Phi_0 = \pm 90^\circ$	$Q_{og} = \psi$
$\Phi_0 = \Theta_0 = 0$	$Q_{og} = \psi$
$\Psi_0 = \Phi_0 = 0$	$Q_{og} = \psi (\csc \Theta_0 + \tan \Theta_0) - \phi \tan \Theta_0$
$\Psi_0 = \Theta_0 = 0$	$Q_{og} = \psi \cos \Phi_0 - \theta \cos \Phi_0 \cot \Phi_0$

Table A-3 Linearized Directional Gyro Equations

INDEX

- Accelerometers, general discussion of, II-105
- Accelerometer threshold, determination of, III-43
- Actuators, Controller, III-119
 - Electrohydraulic, III-126
 - Electromechanical, III-123
- Aerodynamic data, presentation of, II-16
- Airframe
 - Axis Systems, II-5
 - Equations of Motion, Complete, II-4
 - Equations of Motion, perturbation, II-22
 - General, II-2
 - Motions in transonic flight, II-37
 - Motions, lateral, II-48
 - Motions, longitudinal, II-37
 - Output and actuating quantities, II-31
 - Transfer function, lateral, II-45
 - Transfer functions, longitudinal, II-34
- Alterability of control system elements, III-6
- Analog computers, use of III-4, III-10, III-86
- Analysis and Synthesis, III-5, III-32
- Analysis, preliminary, III-1, III-31
- Bibliography, (following III-9)
- Bode plot analysis, example of use of, III-52
- Components of automatic flight control systems, II-1
- Controlled element characteristics, determination of, III-4

Design methods, III-1

Design problem, example, III-31

Design procedure, III-1

Equivalent stability derivative approach, II-60

Euler angles, II-11

Factors, lateral transfer function, II-47

Factors, longitudinal transfer function, II-36

Flow, local, direction detectors, II-113

Flow, local, magnitude detectors, II-114

Functional mechanization, III-3

Gyro element, derivation of law of, A-1

Gyros, general discussion of, II-93

- Directional, II-100
- Rate, II-100
- Vertical, II-96

Gyro pickoff indications, derivation of equations for

- Directional, A-44
- Rate, A-8
- Vertical, A-17
- Vertical, summary of equations for, A-40

History of automatic flight control, I-1

Human pilot, II-75

Inspection test procedures, III-24

Installation problems, automatic control equipment, III-6

Loads, servo actuator II-80, II-81, II-84

Parallel connection, servo actuator, II-80

Percussion, center of, III-35

Prototype system, III-12

Requirements, determination of

Root locus analysis, example of use of, III-52

Sensing elements, summary of, II-117

Sensors, II-92

Series connection, servo actuator, II-81

Specifications, III-1

Stability augmenters, I-8, III-31

Stability derivative, II-20

Stability derivatives, variation of, II-66

Surface control system, II-79

System controller, II-118

Systems engineering, IV-1

Testing

- Airplane ground, III-23
- Component, III-14
- Flight, III-25
- Production system, III-27
- Prototype system, III-13

Test stand, control system, III-15